

Variability of biofilm formation in
Candida glabrata and *Candida parapsilosis* and its
consequences on the infection process

Dissertation

In partial fulfillment of the requirements for the degree

“Doctor of Philosophy (PhD)”

at the Georg-August-Universität Göttingen

within the “Biology” Doctoral program

at the Georg-August University School of Science (GAUSS)



submitted by

Emilia Gómez Molero

born in

Albacete, Spain

Göttingen, 2019

To my Family

*“Todo hombre puede ser, si se lo propone,
el escultor de su propio cerebro”*

Dr. Santiago Ramón y Cajal (1852-1934)

Supervisors:

Dr. rer. nat. Oliver Bader (Main Supervisor)
(Institute for Medical Microbiology, Department of Medical Microbiology, University Medical Center Göttingen)

Prof. Dr. med. Michael Weig (Second Supervisor)
(Institute for Medical Microbiology, Department of Medical Microbiology, University Medical Center Göttingen)

Members of the Thesis Committee:

Prof. Dr. med. Uwe Groß
(Institute for Medical Microbiology, Department of Medical Microbiology, University Medical Center Göttingen)

Prof. Dr. Gerhard Braus
(Institute for Microbiology and Genetics, Department of Molecular Microbiology and Genetics, University Göttingen)

Dr. rer. nat. Oliver Bader (Supervisor)
(Institute for Medical Microbiology, Department of Medical Microbiology, University Medical Center Göttingen)

Members of the Examination Board:

Prof. Dr. med. Uwe Groß (1st Reviewer)
(Institute for Medical Microbiology, Department of Medical Microbiology, University Medical Center Göttingen)

Prof. Dr. Gerhard Braus (2nd Reviewer)
(Institute for Microbiology and Genetics, Department of Molecular Microbiology and Genetics, University Göttingen)

Further Members of the Examination Board:

Prof. Dr. rer. nat. Carsten G. K. Lüder
(Institute for Medical Microbiology, Department of Medical Microbiology, University Medical Center Göttingen)

PD Dr. Michael Hoppert
(Institute for Microbiology and Genetics, Department of General Microbiology, University Göttingen)

Prof. Dr. Fabian Commichau
(Institute for Microbiology and Genetics, Department of General Microbiology, University Göttingen)

Prof. Dr. Kai Heimel
(Institute for Microbiology and Genetics, Department of Molecular Microbiology and Genetics, University Göttingen)

Date of Disputation:

TABLE OF CONTENTS

TABLE OF CONTENTS.....	III
ACKNOWLEDGEMENTS	VII
LIST OF TABLES	XI
LIST OF FIGURES.....	XII
LIST OF ABBREVIATIONS	XV
ABSTRACT	XX
1. INTRODUCTION	1
1.1 Epidemiology of <i>Candida spp.</i>	1
1.2 Features and phylogeny of the genus <i>Candida</i>	5
1.3 <i>C. albicans</i> infections and host-pathogen interactions	7
1.4 <i>Candida</i> biofilms.....	10
1.5 The fungal cell wall.....	13
1.6 <i>Candida spp.</i> cell wall proteins (CWP)	14
1.7 GPI-anchored Cell Wall proteins (adhesins)	15
1.8 <i>Candida glabrata</i>	18
1.8.1 <i>Candida glabrata</i> cell wall proteins	20
1.9 <i>Candida parapsilosis</i>	21
1.9.1 <i>Candida parapsilosis</i> cell wall proteins	22
1.10 <i>Candida</i> species interaction in host invasion.....	23
1.11 Aims of the study	25
2. MATERIALS AND METHODS.....	26
2.1 Materials	26
2.1.1 Synthetic oligonucleotides	30
2.1.2 <i>Candida spp.</i> clinical isolates.....	30
2.1.3 <i>Candida spp.</i> reference strains	31
2.2 Methods	32
2.2.1 Routine diagnostic procedures	32
2.2.2 <i>Candida spp.</i> strain maintenance and growth conditions	32
2.2.3 MALDI-TOF analyses species-identification	33
2.2.4 <i>C. glabrata</i> biofilm formation capacity to polystyrol.....	33
2.2.5 <i>C. glabrata</i> biofilm formation capacity to silicone elastomers.....	35

2.2.6	<i>C. parapsilosis</i> biofilm formation capacity to polystyrol.....	36
2.2.7	Antifungal susceptibility test.....	38
2.2.8	Agar invasion capacity.....	39
2.2.9	Optical and phase-contrast microscopy	39
2.2.10	Sedimentation assay of clinical morphotypes	40
2.2.11	Electrophoretic karyotyping of colony morphotypes	40
2.2.12	Genomic DNA isolation	41
2.2.13	Polymerase chain reaction analyses of adhesin-encoding genes in clinical morphotypes	42
2.2.14	DNA Sanger sequencing	43
2.2.15	<i>Candida</i> cell wall isolation.....	43
2.2.16	<i>Candida spp.</i> genome sequencing analyses.....	44
2.2.17	<i>In vivo</i> infection analyses. <i>Galleria mellonella</i> animal model.....	44
2.2.18	<i>C. albicans</i> and <i>C. glabrata</i> identification from patient blood cultures	45
2.2.19	<i>C. albicans</i> and <i>C. glabrata</i> interaction under phase-contrast microscopy.....	45
3.	RESULTS	47
3.1	Genomic plasticity enhances phenotypic diversity in <i>Candida glabrata</i> clinical isolates from different clades	47
3.1.1	Changes in the genome of hyper-biofilm-forming <i>C. glabrata</i> isolates	47
3.1.2	Genomic changes between time-resolved <i>C. glabrata</i> isolates	53
3.2	Phenotypic variability in <i>C. glabrata</i> clinical isolates correlates with variations in cell wall proteome and infection-relevant parameters.....	55
3.2.1	Biofilm formation capacity to polystyrol of a large <i>C. glabrata</i> clinical strain collection	58
3.2.2	Virulence of <i>C. glabrata</i> isolates in the <i>Galleria mellonella</i> model	59
3.2.3	Variations in <i>C. glabrata</i> biofilm formation capacity to silicone elastomers	62
3.2.4	Different adhesins are present in hyper biofilm-forming clinical isolates.....	64
3.2.5	Hyper biofilm-forming <i>C. glabrata</i> clinical isolates' adherence to <i>C. albicans</i>	69
3.2.6	<i>C. albicans</i> and <i>C. glabrata</i> mixed culture analysis.....	71
3.3	Pheno- and genotypic analyses of <i>Candida parapsilosis</i> clinical isolates	76
3.3.1	Establishing a classification reference	76

3.4	<i>Candida parapsilosis</i> polymorphism drives differences at morphological and genotypic level in isolates from a single patient.....	80
3.4.1	The five clinical isolates are distributed into three different genetic categories....	87
3.4.2	Isolates strongly vary in their adhesion genes.....	89
3.5	<i>Candida parapsilosis</i> phenotypic cell surface variations correlate with differences at a proteomic level among isolates from a clinical strain collection.....	91
3.5.1	<i>C. parapsilosis</i> isolates present variations in antifungal susceptibility based on the biofilm formation capacity to abiotic surfaces	95
3.5.2	Morphotype generally predetermines other phenotypic properties in <i>C. parapsilosis</i> clinical isolates	98
3.5.3	Biofilm formation capacity on silicone.....	104
3.5.4	Sedimentation rates differ between colony morphotypes	105
3.5.5	Clinical <i>C. parapsilosis</i> isolates show virulence differences.....	106
3.5.6	Differences in the cell wall proteome among clinical isolates.....	108
4.	DISCUSSION.....	114
5.	CONCLUSION	134
6.	BIBLIOGRAPHY	136
7.	APPENDIX.....	156
	Distinct sets of strains used in this study.....	156
	CURRICULUM VITAE.....	163

AFFIDAVIT

Here I declare that my doctoral thesis entitled

“Variability of biofilm formation in *Candida glabrata* and *Candida parapsilosis* and its consequences on the infection process”

has been written independently and with no other sources and aids than quoted.

Emilia Gómez Molero
Göttingen, June 2019

ACKNOWLEDGEMENTS

I would express my thanks to the supervisors, collaborators, all my friends and family that help me along this process to submit my doctoral thesis today.

First, I really would like to thank my supervisor Dr. Oliver Bader for his excellent supervision. This thesis is ready thanks to him and this is half yours. I would like to remark his help along these years and his immense patient and support. You trusted me from the beginning and you showed me how important is working hard for the research you want to do, I will never forget it. Thank you so much for your guidance, for all the suggestions about the project and for all the advices and recommendations I received from you. Oli, I know it was hard time and you know me so well, but we fight for it together and finally, we get it. Thank you so much for making me feel like home, I will always remember it because this was really important for me!, DANKE, OLI.

I would also like to thank Prof. Dr. med. Uwe Gross and Prof. Dr. med. Michael Weig for giving me the opportunity to come to Göttingen and do my PhD in this institute, as well as for the great advices and their perfect supervision along the project, seminars and conferences, thank you very much. I would like to thank prof. Dr. Gerhard Braus for his guidance in all the progress reports and the suggestions to improve my research. It was really helpful and necessary to strength the weak points of the project.

I would also like to thank our collaborators: Henk L. Dekker (University of Amsterdam, Amsterdam, The Netherlands), Dr. Attila Gácsér, Dr. Tibor Nemeth (University of Szeged, Szeged, Hungary), Dr. Toni Gabaldón Estevan, Ester Saus, Ewa Ksiezopolska (CRG, Barcelona, Spain), Dr. Guillermo Quindós Andrés, Iker de La Pinta (UPV/EHU, Bilbao, Spain), and Anna Dudakova (UMG, Göttingen, Germany). They provide us the *C. glabrata* and *C. parapsilosis* MS/MS analyses, the genome sequence analyses, the virulence assays outcome, the preformed biofilm analyses and the supervision and information regarding clinical data, respectively. Thank you for letting us being part of your research projects, for your collaborations and suggestions along these years. I would like to mention your contribution along paper writing process. Thanks a lot for your help, you complete the studies we performed with an excellent feedback and contribution. Without your help, this work would not be possible.

Epecially, I would like to thank our collaborator Dr. Piet de Groot (CRIB, Albacete, Spain). Thank you for providing us the proteomic analyses and be part of the project. Piet, for you I am now here, thank you for giving me the opportunity when nobody did, you help me to enter again in contact with lab research and of course, you help me to improve my knowledge in mycology. Bit by bit I was recovering my confidence again and this let me the opportunity to come to Göttingen. You know that I will be always grateful for your generous contribution and help. Dank Je!, Thanks a lot Piet and Ana.

I would also like to thank to all my colleagues because there are many people who contribute to this. First, to my lab mates, I want to express my thanks to Agnieszka Goreztki, Yvonne Laukat, Benjamin (Benni) Sahlke, Nina Gerken, and Ichsan thank you all, I think half of this thesis is due to your help. I would like to thank my colleagues, especially, Pia Sternisek (I will miss you a lot, amazing Pia we are a perfect team), Sabrina Minatelli (Gracias, Gracias y Gracias por todo), Julian Schwanbeck (million thanks for all your patient, support and help with all the computer software's and programs I used, Danke Julian!). I also would like to mention Mathias Emele, Anastasia Lübke, Katrin Gunka (I missed you) and Roswitha Nast (Rosi and Felix, thanks a lot for everything since I came to Göttingen, I will never forget) with you all these years and the distance to my home was smaller. I would like to thank every Lab mate (Sabine Ceramella, Felix Joppe, Marcel te Vrügt), PIs (Prof. Carsten Lüder, Wolfgang Bohne and Raimond Lugert) and Staff member of the Institute for Medical Microbiology, Ruth, Maik, Marco...You have all made me feel at home here!.

I would also like to thank the organizers of the Marie Curie Initial training network fellowship to give me the opportunity to do my PhD in an interdisciplinary and multicultural working team. They let me the opportunity to get in contact with different new techniques, different working groups in Europe and being part of an amazing group of people. I would also like to mention my two supervisors within the consortium Dr. Attila Gácsér and Prof. Julian Naglik, thank you so much for your help and guidance along these three years. THANK YOU ImResFun consortium and thank you all guys, for the conferences and meetings we shared together.

Last, but not least, I would like to thank my colleagues of the Regional Center for Biomedical Research (CRIB, Albacete, Spain): Jose I., Elena, Jesús, Albert, Manu, Ana and Pablo. Thanks a lot for the amazing time we shared, for all your help, support and your friendship, muchísimas gracias a todos.

I would like to thank my five friends since childhood, for all the moments we spent together. THANKS, GIRLS. Especially, I'd like to mention Gracia Honrubia, María Lahoz and Pilar López for always cheer me up during these years, encouraging me to continue working hard. I really appreciate it, thanks a lot.

Finally, I would like to thank my family Joaquín, María Cruz and Victoria; I don't know how I would face these years without your help. You always trust on me, does not matter the distance, thanks a lot for your patience and effort (Papá, mamá, muchas gracias). Vito, you've shown me how to keep going and fight for your ideas and your dreams, you are the best example for me, thank you. Finally, I really want to mention my partner Eduardo, together with my family you have helped me to make it works. You were close to me in the distance, you always have a smile, cheering me up and relying on me, ALWAYS. *GRACIAS POR TODO, OS QUIERO.*

Thank you all, Gracias

PUBLICATIONS

Original Publications:

Carreté L, Ksiezopolska E, Gómez-Molero E, Angoulvant A, Bader O, Fairhead C, Gabaldón T. (2019). Genome Comparisons of *Candida glabrata* Serial Clinical Isolates Reveal Patterns of Genetic Variation in Infecting Clonal Populations. *Front. Microbiol.* 10:112.

Carreté L, Ksiezopolska E, Pegueroles C, Gómez-Molero E, Saus E, Iraola S, Loska D, Bader O, Fairhead C, Gabaldón T. (2018). Patterns of genomic variation in the opportunistic pathogen *Candida glabrata* suggest the existence of mating and a secondary association to the human host. *Current biology.* 28:15-27.

Gómez-Molero E, Dekker H.L, de Boer A.D, de Groot P.W.J. (2016). Identification of secreted *Candida* Proteins Using Mass Spectrometry. *Methods. Mol. Biol.* 1356:79-94.

Gómez-Molero E, de Boer A.D, Dekker H.L, Moreno-Martínez A, Kraneveld EA, Ichsan, Chauhan N, Weig M, de Soet J.J, de Koster C.G, Bader O, de Groot P.W.J. (2015). Proteomic analysis of hyperadhesive *Candida glabrata* clinical isolates reveals a core wall proteome and differential incorporation of adhesins. *FEMSYR.* 15(8).

Publications under revision:

Gómez-Molero E, De-la-Pinta I, Groß U, Weig M, Quindós G, de Groot P, Bader O. (2019). Influence of *C. parapsilosis* biofilm formation on antifungal drug susceptibility. *J. Clin. Microbiol.* [submitted].

Gómez-Molero E, Willis J.R, Dudakova A, Carreté L, Weig M, Groß U, Gácsér A, Gabaldón T, Bader O. (2019). Phenotypic variability denotes coinfection with three independent *C. parapsilosis* lineages. *Clin. Microbiol. Infect.* [submitted].

Publications in Preparation:

Gómez-Molero E, Moreno-Martínez A, Dekker H.L, Németh T, Groß U, Weig M, Gácsér A, Bader O, de Groot P.W.J. (2019). Differential incorporation of cell wall adhesins in biofilm-forming *Candida parapsilosis* clinical isolates. [manuscript in preparation].

Wojak KP, Ungermann GF, Ichsan, Gómez-Molero E, et al. Host age and denture wearing are independent factors contributing to oral colonization with *Candida glabrata*. [manuscript in preparation].

Authors	Publication and Journal	Contribution
<u>Gómez-Molero E</u> , De-la-Pinta I, Groß U, Weig M, Quindós G, de Groot P, Bader O.	Influence of <i>C. parapsilosis</i> biofilm formation on antifungal drug susceptibility. (2019). J Clin. Microbiol. [submitted]	Designed and performed experiments, conducted phenotypic and antifungal susceptibility analyses, evaluated and interpreted laboratory data, wrote manuscript and study preparation <u>Preformed biofilms</u> : UPV/EHU, Bilbao, Spain
<u>Gómez-Molero E</u> , Willis J.R, Dudakova A, Carreté L, Weig M, Groß U, Gácsér A, Gabaldón T, Bader O.	Phenotypic variability denotes coinfection with three independent <i>C. parapsilosis</i> lineages. (2019). Clin. Microbiol. Infect [submitted]	Designed and performed phenotypic, molecular and antifungal susceptibility analyses, evaluated and interpreted laboratory data, wrote manuscript and study preparation <u>Genome sequence analyses</u> : CRG, Barcelona, Spain <u>Coordinated routine diagnostics and added clinical data</u> : UMG, Göttingen, Germany
Carreté L, Ksiezopolska E, <u>Gómez-Molero E</u> , Angoulvant A, Bader O, Fairhead C, Gabaldón T.	Genome Comparisons of <i>Candida glabrata</i> Serial Clinical Isolates Reveal Patterns of Genetic Variation in Infecting Clonal Populations. (2019). Front. Microbiol. 10:112.	Performed phenotypic and antifungal susceptibility test analyses of selected clinical isolates (UMG, Göttingen)
Carreté L, Ksiezopolska E, Pegueroles C, <u>Gómez-Molero E</u> , Saus E, Iraola S, Loska D, Bader O, Fairhead C, Gabaldón T.	Patterns of genomic variation in the opportunistic pathogen <i>Candida glabrata</i> suggest the existence of mating and a secondary association to the human host. (2018). Current biology. 28:15-27	Performed phenotypic , karyotypic and antifungal susceptibility experiments, analyzed and interpreted data (UMG, Göttingen)
<u>Gómez-Molero E</u> , Moreno-Martínez A, Dekker H.L, Németh T, Groß U, Weig M, Gácsér A, Bader O, de Groot P.W.J.	Differential incorporation of cell wall adhesins in biofilm-forming <i>Candida parapsilosis</i> clinical isolates. (2019). [In preparation]	Designed and performed experiments, evaluated and interpreted laboratory data, wrote manuscript and study preparation <u>Proteomic analyses</u> : CRIB, Albacete, Spain <u>Virulence assays</u> : University of Szeged, Szeged, Hungary

LIST OF TABLES

Table 1. Chemicals and disposables used in this study.....	26
Table 2. Media used in this study.....	28
Table 3. Solutions used in this study.....	29
Table 4. Solutions used in this study.....	29
Table 5. oligonucleotides used for PCR amplification.....	30
Table 6. List of <i>C. parapsilosis</i> reference strains used in this study.....	31
Table 7. List of <i>C. glabrata</i> reference strains used in this study.....	31
Table 8. List of <i>C. albicans</i> reference strains used in this study.....	31
Table 9. Description of antimycotic dilutions used in antifungal susceptibility test.....	38
Table 10. Distribution of MIC values of the eight antifungal drugs in the total number of isolates and selected multi resistant clinical isolates.	50
Table 11. Virulence capacity of <i>C. glabrata</i> isolates stratified by adherence capacity and site of isolation.....	61
Table 12. Variable proteome of selected hyper biofilm-forming isolates under biofilm conditions in this study.....	67
Table 13. Core proteome of selected hyper biofilm-forming isolates under biofilm conditions in this study.....	68
Table 14. Percentage of <i>Candida spp.</i> interaction between selected <i>C. glabrata</i> clinical isolates and GFP-SC5314 <i>C. albicans</i> reference strain.....	71
Table 15. Frequency of <i>C. glabrata</i> and <i>C. albicans</i> infections (n = 15532) per source of isolation.....	72
Table 16. <i>C. glabrata</i> blood cultures identification in CHROMagar.....	73
Table 17. <i>C. parapsilosis</i> colonies morphology identification key chart.....	80
Table 18. Summary of clinically relevant properties in <i>C. parapsilosis</i> colony morphotypes.....	86
Table 19. Percentage of Single Nucleotides Polymorphisms (SNPs) similarity between five clinical isolates.....	88
Table 20. Antifungal susceptibility test of the morphotypic switches (smooth<>crepe<>concentric) of nine selected <i>C. parapsilosis</i> isolates.....	100
Table 21. Summary of proteomic analyses using seven of the selected <i>C. parapsilosis</i> clinical isolates.....	110

LIST OF FIGURES

Figure 1. <i>Candida spp.</i> phylogenetic tree.....	6
Figure 2. Schematic overview of <i>C. albicans</i> tissue invasion.	8
Figure 3. Biofilm formation on biotic and abiotic surfaces in <i>C. albicans</i> (modified from Chandra <i>et al.</i> , 2008).....	12
Figure 4. Schematic <i>Candida spp.</i> cell wall model	14
Figure 5. Cell wall GPI-anchored proteins (adhesins) general structure, adapted from ten Cate <i>et al.</i> , 2009; de Groot <i>et al.</i> , 2013	15
Figure 6. Adhesin-like cell wall proteins secretion and cell wall attachment process	16
Figure 7. <i>C. glabrata</i> morphology	18
Figure 8. <i>C. glabrata</i> biofilm <i>in vitro</i> schematic model.....	19
Figure 9. Chromosomal distribution of putative <i>C. glabrata</i> adhesins-encoding genes	21
Figure 10. <i>C. parapsilosis</i> CDC 317 morphology.....	21
Figure 11. <i>C. parapsilosis in vitro</i> schematic model	22
Figure 12. Schematic <i>C. glabrata</i> biofilm formation to polystyrol.....	34
Figure 13. Schematic <i>C. glabrata</i> biofilm formation to silicone.	36
Figure 14. Schematic <i>C. parapsilosis</i> biofilm formation capacity to polystyrol	37
Figure 15. Electrophoretic karyotyping of <i>C. glabrata</i> clinical isolates divided in 7 different clades.....	48
Figure 16. Biofilm formation capacity to polystyrol of thirty-three clinical isolates	52
Figure 17. <i>C. glabrata</i> phenotypic analyses of three clonal clinical isolates	54
Figure 18. Cell aggregation capacity of selected biofilm-forming <i>C. glabrata</i> clinical isolates under planktonic and biofilm conditions	55
Figure 19. Biofilm formation analyses of eight selected clinical isolates + CBS-138	56
Figure 20. Cell surface analyses of reference isolates	57
Figure 21. <i>C. glabrata</i> clinical isolates stratified according to body sites of isolation and quantitative biofilm formation capacity to polystyrol.....	58
Figure 22. Kaplan-Meier <i>G. mellonella</i> survival curves infected with 77 <i>C. glabrata</i> clinical isolates + CBS-138 classified attending to their biofilm formation capacity	60
Figure 23. <i>C. glabrata</i> correlation analyses between virulence capacity and adherence to polystyrol.....	62

Figure 24. Correlation between biofilm formation capacity to silicone and polystyrol from 115 selected <i>C. glabrata</i> clinical isolates	63
Figure 25. Biofilm formation capacity to abiotic surfaces of selected thirty-two <i>C. glabrata</i> clinical isolates.....	64
Figure 26. <i>C. glabrata</i> : <i>C. albicans</i> -GFP-SC5314 interaction <i>In vitro</i> model	70
Figure 27. General distribution of single and mixed <i>Candida spp.</i> infections caused by <i>C. albicans</i> and <i>C. glabrata</i>	73
Figure 28. <i>C. albicans</i> and <i>C. glabrata</i> identification from infected-patient's blood cultures	75
Figure 29. Morphogenic switching in a <i>C. parapsilosis</i> non-biofilm forming clinical isolate (PEU582).....	76
Figure 30. General characterization of <i>C. parapsilosis</i> cell-related properties.....	78
Figure 31. Classification references of <i>C. parapsilosis</i> colony morphologies on SAB's and Phloxine B agar produced in this work.....	79
Figure 32. Colony morphology in routine culture.....	81
Figure 33. Morphological variations between clinical morphotypes. Top row: colony morphology on Phloxine B agar. Bottom row: cell shape and cell aggregation at 100X magnification in phase-contrast.	83
Figure 34. Biofilm formation-related phenotypes	84
Figure 35. Genome sequencing analyses.	88
Figure 36. <i>C. parapsilosis</i> adhesin-encoding genes analyses.	90
Figure 37. Colony morphology on SAB agar.....	91
Figure 38. <i>C. parapsilosis</i> clinical isolates distribution.....	92
Figure 39. Clinical isolates biofilm formation capacity	93
Figure 40. Correlation between agar invasion and biofilm formation capacity.	95
Figure 41. Drug susceptibility test of one hundred eighteen clinical isolates + 2 reference strains (CDC 317, ATCC 22019).....	97
Figure 42. Morphologic variation of nine <i>C. parapsilosis</i> isolates on SAB agar plates.	99
Figure 43. Electrophoretic karyotyping of <i>C. parapsilosis</i> PEU468 morphotypes.	101
Figure 44. Phenotypic and morphological differences in nine <i>C. parapsilosis</i> clinical isolates.	103

Figure 45. *C. parapsilosis* biofilm formation to polystyrol and silicone from a clinical isolates strain collection.105

Figure 46. *C. parapsilosis* sedimentation capacity between different clinical morphotypes.106

Figure 47. *Galleria mellonella* infection animal model. Survival curves.....107

LIST OF ABBREVIATIONS

5FC	Flucytosine/5-Fluorocytosine
Abs.	Absorbance
ANI	Anidulafungin
AFM	Atomic force microscopy
AM3	Antibiotic medium 3
AMB	Amphotericin B
AMP	Ampicillin
approx.	Approximately
Asn	Asparagine
ATCC®	American type cell culture
Awp	Adhesin wall protein
BF	Biofilm
bp (s)	Base pair(s)
bsc	Blood smooth colony
α-CHCA	α-cyano-4-hydroxycinnamic acid
°C	Degree Celsius
<i>C. a</i>	<i>Candida albicans</i>
<i>C. g</i>	<i>Candida glabrata</i>
<i>C. p</i>	<i>Candida parapsilosis</i>
CAC	CHROMagar <i>Candida</i>
CAS	Caspofungin
CBS	Centraalbureau Voor Schimmelcultures
CBS-KNAW	Centraalbureau Voor Schimmelcultures and Royal Netherlands Academy of Arts and Sciences
CHEF	Contour-clamped homogeneous electric field electrophoresis
cm	Centimeter
CMA	Corn meal agar
cn	Concentric
cn-crt	Concentric-crater
cn-cr	Concentric-crepe
cr	Crepe
CRIB	Regional Center for Biomedical Research
CRG	Centre for Genomic Regulation
crt	Crater
CV	Crystal violet
CW	Cell wall
CWP	Cell wall protein
d	Derby morphotype
DNA	Deoxyribonucleic acid
ddH ₂ O	Bidistilled water
DMSO	Dimethylsulfoxid

DNA	Deoxyribonucleic acid
dNTP	Deoxynucleosidtriphosphate
DSMZ	German Collection of Microorganisms and Cell Cultures
ECM	Extracellular matrix
EDTA	Ethylenediaminetetraacetic acid
Efg/1	Enhanced filamentous growth protein 1
EGFP	Enhanced green fluorescent protein
Epa	Epithelial adhesin protein
EPS	Extracellular polymeric substance
<i>ERG11</i>	Lanosterol 14-alpha-demethylase
ER	Endoplasmic reticulum
<i>et al.</i>	And others (<i>et alii</i>)
EtOH	Ethanol
EUCAST	European Committee on Antimicrobial Susceptibility Testing
F/fwd.	Forward
Fig.	Figure
FISH	Fluorescence in-situ hybridization
FLU	Fluconazole
g	Gram
GA	Illumina Genome Analyzer IIx
GFP	Green fluorescent protein
GC	Guanine/cytosine
GI	Gastrointestinal
GPI	Glycophosphatidylinositol
GUT	Gastrointestinally-Induced Transition
h	Hour
H/HBF	High biofilm-forming
HS	HiSeq
I/IBF	Intermediate biofilm-forming
IC	Invasive candidiasis
ICU	Intensive care unit
IL-4	Interleukin (inflammatory cytokines)-4
IL-12	Interleukin (inflammatory cytokines)-12
ISA	Isavuconazole
ITC	Itraconazole
JCM	Japan Collection of Microorganisms
Kb (s)	Kilo base(s)
KCl	Potassium chloride
KHPO ₄	Hydrogen phosphate ion (2-)
L/LBF	Low biofilm-forming
l	Liter
L-M	Low-medium
LC-MC	Liquid chromatography–mass spectrometry

M	mannose
M-H	medium-high
MALDI	Matrix Assisted Laser Desorption Ionization
mbp	Megabase pair(s)
β-ME	β -mercaptoethanol
MetOH	Methanol
mg	Milligram
mg/ml	Milligram per milliliter
MIC/MIC50	Minimum inhibitory concentration with a 50% of inhibition
MICA	Micafungin
min	Minutes
ml	Milliliter
mm	Millimeter
mM	Millimolar
mQ	Milli-Q water®, ultrapure laboratory Grade water
<i>MRR1</i>	Regulator of MDR1 transcription
MS	Mass spectrometry
m/s	Meter per second
mt	Mitochondrial
μg	Microgram
μl	Microliter
μm	Micrometer
μM	Micromolar
μg/μl	Microgram per microliter
n	Number of replicates
n.d/ND	Undetermined
NaCl	Sodium chloride
NaCl _{physiol}	Physiological NaCl
Na ₂ HPO ₄	Sodium hydrogen phosphate
NCAC	Non- <i>Candida albicans Candida</i> species
NCBI	National Centre of Biotechnology
ncc	Nose crepe colony
NITE-BRC/NBRC	National Institute of Technology and Evaluation
nm	Nanometer
NMR	Nuclear magnetic resonance
NRRL (ARS)	Agricultural Research Service Culture Collection
nsc	Nose smooth colony
OD	Optical density
OI	Origin isolate
OPC	Oropharyngeal candidiasis
ON	Overnight

ORF	Open reading frame
OTL	On-target lysis
PAMPs	Pathogen-associated molecular patterns
PA14	Anthrax protective antigen
PBS	Phosphate buffered saline
PCR	Polymerase chain reaction
PFGE	Pulsed-field gel electrophoresis
pH	Preponderance of hydrogen ions
pmol	Pico molar
PM	Plasma membrane
PNA	Peptide nucleic acid
POS	Posaconazole
PRRs	Pattern recognition receptors
PWP	Protective antigen wall proteins
R	Regular
R/rev.	Reverse
RAP1	Repressor activator protein
PCR-RFLP	Restriction fragment length polymorphism
RNA	Ribonucleic acid
RNase	Ribonuclease
rRNA	Ribosomal ribonucleic acid
rDNA	Ribosomal deoxyribonucleic acid
rpm	Rounds per minute
RPMI 1640	Roswell Park Memorial Institute 1640
RT	Room temperature
s	Smooth
S	Spider
s-cn	Smooth-concentric morphotype
s-g	Smooth-glossy morphotype
s-m	Smooth-matte morphotype
sn-wr-cr	Snowball-wrinkled-crepe
SAB agar	Sabouraud agar
Sap	Secreted aspartyl proteinases
SD	Standard deviation
SDA	Sabouraud dextrose agar
SDS	Sodium dodecyl sulfate
sec.	Seconds
Ser/S	Serine
SIR	Silent information regulator
sn	Snowball
<i>Spp.</i>	Species
SZMC	Szeged Microbiology Collection
t	Time
TAE	Tris-acetate-EDTA
<i>Taq.</i>	<i>Thermus aquaticus</i>

tcc	Tracheal crepe colony
Thr/T	Threonine
TOF	Time of flight
Tris	Tris-(hydroxymethyl)-aminoethan
Tris-HCl	Tris hydrochloride
tsc	Tracheal smooth colony
TRR	Tandem repeat region
UMG	University Medical Centre Göttingen
v	Volts
V-H	Very-high
VOR	Voriconazole
v/v	Volume per volume
VVC	Vulvovaginitis candidiasis
WGD	Whole genome duplication
wr	Wrinkled
WT	Wild type
w/v	Weight per volume
YOLT	Yeast on-target lysis
YPD	Yeast extract peptone dextrose

ABSTRACT

The prevalence of *Candida* species has increased in the last two decades, becoming the third to fourth most common cause of infections in hospitals. In general, *Candida spp.* are opportunistic pathogens found as commensals in the Gastrointestinal Tract (GI), the oral cavity, oral mucosa, vagina, or skin, without causing any symptoms or pathology. When the immune system is altered (e.g. T-cell deficiencies in immunocompromised patients), a preliminary colonization process of the skin or mucosa (superficial candidiasis) may progress to life-threatening invasive candidiasis, sepsis, and eventually to death. Invasive Candidiasis (IC) has become a serious problem in the last years, affecting young and elderly population. *Candida albicans* is the most frequent cause of invasive candidiasis globally, but over the last decades non-*Candida albicans Candida* (NCAC) species have become more medically relevant. *Candida spp.* are able to exist inside the human host displaying different pathogenicity and antifungal drug resistance strategies. Most microbes, including NCAC species, usually constitute microbial communities encased in an extracellular polymeric substance forming biofilms on abiotic and biotic surfaces. *Candida glabrata* and *Candida parapsilosis* are the two most common causes of NCAC infections. Their relevance have been attributed to the ability to form biofilms on abiotic surfaces and the increased multidrug resistance capacity, together leading to different levels of pathogenicity. Both species display superficial, mucosal and systemic infections associated with abiotic devices, presenting clear morphologic and phenotypic differences between them. *C. glabrata* and *C. parapsilosis* belong to two different *Candida* clades, presenting differences at genomic and pathogenic level. The fungal cell wall is the outermost layer involved in host-pathogen recognition, cell structure, permeability, protection and virulence and the phylogenetic distance between both species is reflected by variations in cell wall composition including its proteome.

In this study, we performed phenotypic and morphological analyses of two *C. glabrata* and *C. parapsilosis* clinical strain collections, to decipher how phenotypic and morphological differences will predetermine genome and cell wall proteome as a pathogenic strategy during host infection. Based on previous studies (de Groot *et al.*, 2008 and Gabaldón *et al.* 2016), MS/MS analyses and Illumina genome sequence analyses of selected *C. glabrata* and

C. parapsilosis clinical isolates will provide more information regarding cell wall constituents and genomic differences within NCAC clinical isolates.

A high variability in phenotypic properties between isolates were found. In this study, we observed that *C. glabrata* showed a positive correlation between biofilm formation capacity, cell aggregation and cell sedimentation. In case of *C. parapsilosis*, biofilm formation capacity on abiotic surfaces was influenced by the colony morphotype. *C. glabrata* and *C. parapsilosis* proteome is highly variable and it has been divided in a core proteome and a unique variable proteome. Differences in the number of adhesins identified in the cell wall positively correlate with adhesion. Here, we observed that *C. glabrata* cell wall adhesins enable the co-interaction with *C. albicans* hyphae facilitating epithelia invasion. Differences in the variable proteome may also elucidate a high immunogenic heterogeneity as a possible host-defense mechanism. In *C. parapsilosis*, an increased number of adhesins identified in the cell wall correlates with “rough” and high biofilm-forming morphotypes. *C. parapsilosis* rough morphotypes presented azoles’ and caspofungin reduced-susceptibility, nevertheless, EUCAST-based antifungal susceptibility testing in the collection was not able to predict these variations. Rough morphologies in patient’s culture would be an indicator of biofilm’s presence to start echinocandins therapeutic treatment.

Our studies proposed that phenotypic variations in *C. glabrata* and *C. parapsilosis* clinical isolates will predetermine differences at genomic and proteomic level. A reduced number of adhesins in the wall correlates with low biofilm-forming (LBF) isolates and high virulence capacity indicating that these morphologies will easily disseminate trough the bloodstream.

Genome sequence analyses of selected *C. glabrata* isolates confirm the presence of deletions and duplications of cell wall adhesin-encoding genes as an important adaptive mechanism moving on from colonization to infection and dissemination.

1. INTRODUCTION

1.1 Epidemiology of *Candida spp.*

The prevalence of *Candida* species has increased in the last two decades becoming the third to fourth most common cause of infection in hospitals (reviewed by Pappas *et al.*, 2018). In general, *Candida spp.* are opportunistic pathogens found as commensals in the gastrointestinal tract (GI), the oral cavity, oral mucosa, vagina, or skin, without causing any symptoms or pathology. Several factors such as abdominal surgeries, malignant neoplasms, corticoid steroid use, and chemotherapeutic treatment can lead to higher risks of infection (Quindós, 2014). Patients with diabetes mellitus (Lamster *et al.*, 2008), or the use of non-sterile medical devices together with preceding bacterial infections, are potential candidates to suffer from *Candida* pathologies (Percival *et al.*, 2014). When the immune system is altered (e.g. T-cell deficiencies in immunocompromised patients), a preliminary colonization process of the skin or mucosa (superficial candidiasis) may progress to life-threatening invasive candidiasis, sepsis, and eventually to death (reviewed by Nobile and Johnson, 2015). Invasive candidiasis (IC) has become a serious problem in the last years affecting young population and adults. As an example, *Candida albicans* is the main species involved in Vulvovaginitis Candidiasis (VVC) or Oral-Pharangeal Candidiasis (OPC), affecting a high percentage of healthy women (~ 80%) and immunosuppressed or terminally ill patients, respectively (reviewed by Kim and Sudbery, 2011).

Recent epidemiological studies have confirmed a high percentage (~ 50%) of a thirty-day mortality (~8-30 days) remarking the importance of the host's health conditions. Nevertheless, fast diagnosis has been crucial to reduce early-phase mortality (0-7 days) in IC (Puig-Asensio *et al.*, 2014). Since the last decade, there are several studies on *Candida* infections in hospitals and Intensive Care Units (ICU) that analyse the frequency of patients with candidemia and the use of antifungals therapies. Studies conducted in the United States on candidemia episodes between 1992 and 2011 have indicated that it is still associated with high mortality rates especially in elderly population ≥ 65 years old (Cleveland *et al.*, 2012). A complementary study in the U.S has reported an increase of ~6.000 patients diagnosed with *Candida* infections between 2000 and 2005. Also the

INTRODUCTION

incidence of hospitalization was higher in adults (45-85 years old) than in young patients (18-44 years old) in the year 2000 (Zilberberg *et al.*, 2008).

Other studies have outlined *C. albicans*, *C. glabrata*, *C. parapsilosis*, *C. tropicalis*, and *C. krusei* as the most frequent causes of candidemia in the United States: epidemiological data from the 1980s marked a high frequency of IC due to *C. albicans*. According to several antifungal surveillance studies (e.g. the ARTEMIS study) performed between 1997 and 2007, *C. albicans* was still the most frequent cause of fungemia (62%) all over the world (reviewed by (Pfaller and Diekema, 2007; Pfaller *et al.*, 2006) this proportion has fluctuated over time, decreasing in the last decade in favour of non-*Candida albicans* *Candida* species (NCAC). The percentage of patients infected by *C. albicans* was clearly reduced in 2011 (11% reduction) and has been surpassed by *C. glabrata* (~15% increase in 2011) and *C. parapsilosis* (~5 % increase in 2010) (Lockhart *et al.*, 2012; Lyon *et al.*, 2010; Pfaller *et al.*, 2010).

In Europe, the distribution has supported that *C. albicans* (56%) is the most prevalent cause of candidemia followed by *C. glabrata*, *C. parapsilosis*, and *C. tropicalis*. In agreement with this, the most prevalent single *Candida spp.* reported overall was also *C. albicans*, albeit the distribution of NCAC species varies between countries (Tortorano *et al.*, 2004). For instance, *C. glabrata* infections are more frequent in Northern Europe and the U.S. (13.2% and 29% respectively), while *C. parapsilosis* is more prevalent in South America or Spain. There are several hypotheses regarding these divergences such as climate differences, hospital hygiene, and improper use of antimycotic treatments (reviewed by Guinea, 2014). A review by (Ruhnke, 2014) has indicated that approximately around 4 thousand cases of Candidemia in Intensive Care Units of German hospitals (ICU) were described in 2008. The prevalence was ~ 5 patients per 100 000 inhabitants, this frequency was quite similar to the values for invasive candidiasis (IC). Several studies performed along the country in ICU's corroborated that the percentage of *C. albicans* compared with non-*Candida albicans* *Candida* species was approximately 30 % higher (Meyer *et al.*, 2013; Tragiannidis *et al.*, 2012).

Divergences in *Candida spp.* patient's distribution have been remarked; while *Candida tropicalis*, *Candida krusei* and *C. glabrata* frequently colonized and infect elderly patients, *C. parapsilosis* is frequently found in children (reviewed by Quindós, 2014; Trofa *et al.*, 2008). In *C. parapsilosis*, the presence of candidemia in infants is approximately 15 %

INTRODUCTION

more frequent than in adults (reviewed by Yapar, 2014). *C. parapsilosis* is considered an extended moderately non-pathogenic fungus frequently found as associated nosocomial infection due to the use of medical devices (reviewed by Jahagirdar *et al.*, 2018). In 2004, Pfaller and Diekema published an epidemiological study along ten years focused on the prevalence of Bloodstream Infections (BSI) ranking *C. parapsilosis* as the third most common cause of septicemia appearing, in some situations, as a secondary infection (Patel *et al.*, 2000).

Conversely, *C. glabrata* is known to be commonly present in elderly and neutropenic patients (Bodey *et al.*, 2002; Malani *et al.*, 2011). The incidence of *C. glabrata* has been increased in the last years, becoming the second most prevalent *Candida* pathogen in nosocomial infections affected by the dose of antibiotic administered, the immune system of the patient, as well as the period of hospitalization (reviewed by Rodrigues *et al.*, 2014). *C. glabrata* infections frequently increment with the age of the patient (Krcmery and Barnes, 2002), and has raised the frequency in the oral cavity due to a remarkable ability to adhere to denture-surfaces (Li *et al.*, 2007; Rodrigues *et al.*, 2017). Compared with another NCAC species is quite usual to find it coupled with *C. albicans* in oral candidiasis (reviewed by Rodrigues *et al.*, 2017).

Studies performed by Pappas and McCarty have shown that the antifungals administered, the age of the patient and the ability to recover from bloodstream infections varies between adults and young population in the different *Candida spp.* (McCarty and Pappas, 2016; Pappas *et al.*, 2003). The uncontrolled administration of antibacterials decreases bacterial communities and promoting fungal pathologies. Broad spectrum antibiotics have usually altered the gut microbiota disrupting the colonization resistance facilitating *Candida spp.* be part in a long term colonization process (Erb Downward *et al.*, 2013; Hill *et al.*, 2015). Although resistance to more than one antifungal drug of different substance classes is still infrequent, multidrug resistance have increased in the last years including some novel species such as *Candida auris* (Arendrup and Patterson, 2017). The lacking development of new antifungal agents in the last decades, the extensive use of antibiotics, and increasing long-term hospitalization have constrained the use of antifungal drugs, as well as lead to an alteration in the susceptibility rates. Knowing the limitation of antifungals therapies, azoles are still the most frequent antimycotic drugs used. The high availability, the oral administration and a broad knowledge of the therapy effect on

INTRODUCTION

patients makes FLU the most administered antifungal currently. FLU inhibits lanosterol 14- α -demethylase (*ERG11*) essential for the *Candida* membrane biosynthesis (Pfaller *et al.*, 2010). The level of azole resistance in *Candida* species have varied depending on the type of infection and the species of study (reviewed by Whaley *et al.*, 2016). The clinical resilience against FLU has also increased through the appearance of other *Candida spp.* Principally, *Candida* isolates are still susceptible to liposomal amphotericin B (AMB) and mostly to echinocandins (CAS and MICA), although recent data suggest that therapies against *C. glabrata* and *C. krusei* may require high doses of echinocandins (Kuhn *et al.*, 2002). In particular, *C. glabrata* is quite special showing a Minimal Inhibitory Concentration (MIC) of 64 $\mu\text{g/ml}$ towards FLU. The decreased susceptibility of *C. glabrata* to antifungal drugs seems to be attributable to the long-period treatments and some specific properties as haploidy. The absence of reaction against azoles has promoted the use of novel antifungal agents as echinocandins inhibiting the synthesis of β -1, 3-glucan (Cleveland *et al.*, 2012; Lockhart *et al.*, 2011; Pfaller *et al.*, 2012). In the last fifteen years has been reported *C. glabrata* susceptibility against the semisynthetic echinocandin ANI (Pfaller *et al.*, 2005), as well as, *C. glabrata* susceptibility against VOR which has risen in certain European and Latin American countries (Pfaller *et al.*, 2004).

In contrast, susceptibility against echinocandins (ANI, MICA and CAS) and azoles (especially FLU) has decreased in the last decade in the *C. parapsilosis* complex, although it is clearly strain dependent (reviewed by Neji *et al.*, 2017; Pfaller *et al.*, 2004). This is in particular the case for CAS and ANI in *C. parapsilosis sensu stricto* (van Asbeck *et al.*, 2008). The depletion of FLU susceptibility in *C. parapsilosis* clinical isolates has been related with a point mutation in the *ERG11* and an upregulation of the *MRR1* transcription factor. The procedure of reduced azole's susceptibility in *C. parapsilosis* is similar to the one described for *C. albicans* (Silva *et al.*, 2011).

A shift in *Candida spp.* frequency is also evident, and invasive candidiasis due to *C. albicans* has been surpassed by *C. glabrata*, *C. parapsilosis* including the emergence of the recent multidrug-resistant *C. auris* (Lamoth *et al.*, 2018). Therefore, a reliable characterization using novel techniques as PCR-RFLP, Sanger-sequencing (Cornet *et al.*, 2011), T2 magnetic resonance (Zervou *et al.*, 2017) and MALDI-TOF MS systems for species-determination (Bader *et al.*, 2011) are crucial prerequisites for an early and adequate *Candida*-infection treatment. Additionally, the identification of yeast-specific virulence factors as adherence

INTRODUCTION

capacity, biofilm formation and production of hydrolytic enzymes will facilitate the development of antifungal therapies against particular *Candida spp.* (Schaller *et al.*, 2005).

1.2 Features and phylogeny of the genus *Candida*

Yeasts of the *Candida* genus were first described as *Oidium albicans* by Robin in 1853. Originally, they were included in a different group encompassing most Ascomycetes in the imperfect stage causing fruit infections (“powdery mold”) far related to the “thrush” or pathogenic fungi (Ainsworth and Austwick, 1955). In 1923, they were grouped into the genus *Candida* (Berkhout, 1923) still used today. Former reviews from the end of the 19th to the beginning of the 20th century have included the first studies regarding *Candida* in-situ isolated from patients (Martin and Jones, 1940). In 1954, *Candida spp.* were admitted as generic name in the classification system (Roger *et al.*, 1953) and incorporated into the kingdom Fungi, division Ascomycota, order Saccharomycetales, and family Saccharomycetaceae (reviewed by Barnett, 2004).

Today, the name *Candida* is known to be quite broad and heterogeneous, comprising more than 150 species of which only around 12% have clinical relevance (Odds, 1988; Schauer and Hanschke, 1999). The most representative one is *C. albicans* (Robin (Berkhout), 1923) described as the primary opportunistic fungal pathogen causing bloodstream infections in population with a permanently weakened immune system. The *Candida* clade has been described as extremely diverse including several species close to the basidiomycetes as well as imperfect yeasts able to develop pseudohyphae or only yeast morphologies. They are characterized attending to their capability to use carbon sources, the ability to ferment (Shepherd *et al.*, 1985), their clinical relevance, reproduction, colony-morphology shape, and level of pathogenicity (reviewed by Fitzpatrick *et al.*, 2010; Hull *et al.*, 2000; McCullough *et al.*, 1996).

Fitzpatrick *et al.* (2006) performed a fungal phylogenetic analysis based on genome sequences reorganizing the Saccharomycotina subdivision. In 2012, Kurtzman and collaborators studied the characterization of *Candida* in the subphylum Saccharomycotina including *Saccharomyces* and *Arxula*. This subphylum was then classified as monophyletic, which was confirmed based on differences in ribosomal DNA (rDNA) (Kurtzman and Robnett, 2013).

INTRODUCTION

This subphylum is divided into the monophyletic CTG clade and the whole genome duplication (WGD) subclade (Figure 1A). The majority of pathogenic *Candida* species were classified in the CTG clade underlying as main characteristic the translation of the CUG codon into serine rather than leucine in the standard genetic code. *C. parapsilosis* is phylogenetically more closely related to *C. albicans*, *C. tropicalis*, and *C. dubliniensis* coming from the same branch of the CTG clade with no apparent sexual cycle and differing from *C. guilliermondii*, (sexual cycle described), *Candida lusitaniae* and *Debaryomyces hansenii* on the number of alleles per chromosome (reviewed by Santos *et al.*, 2011).

Contrary, a unique WGD subclade is constituted by the *Nakaseomyces* genus (Kurtzman and Robnett, 2003) including the *glabrata* group. Inside the group, it has been distinguished the pathogenic *C. glabrata* as a close relative of Baker's yeast together with *Candida bracarensis* (Correia *et al.*, 2006), *Candida nivariensis* (Alcoba-Flórez *et al.*, 2005) and *Nakaseomyces (Kluyveromyces) delphensis* (Dujon *et al.*, 2004; Gabaldón *et al.*, 2013a), (Figure 1B).

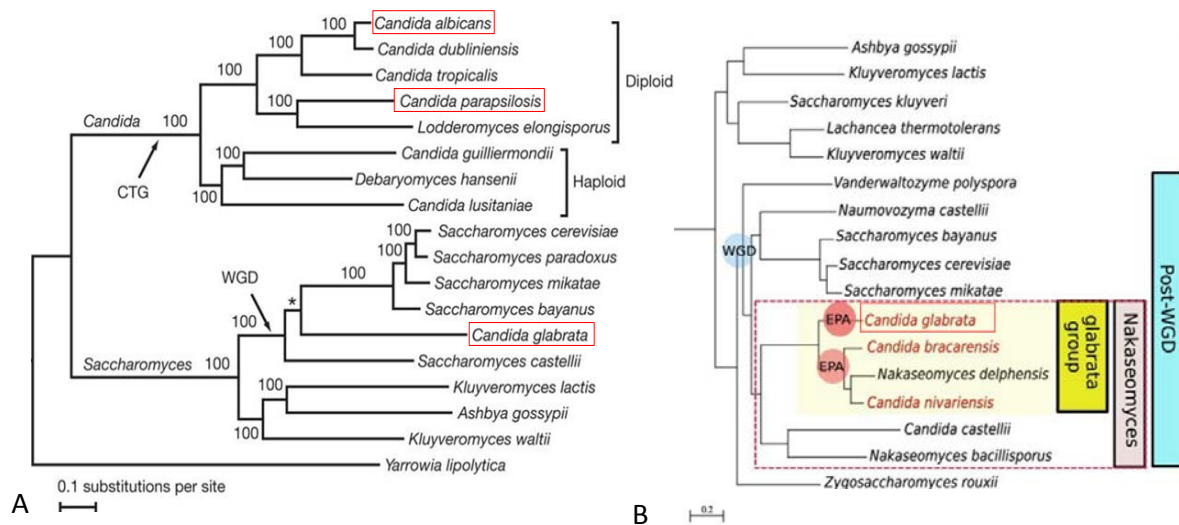


Figure 1. *Candida spp.* phylogenetic tree (modified from Butler *et al.*, 2009; Gabaldón and Carreté, 2016). (A) Phylogenetic representation of the *Candida* and *Saccharomyces* clades into the Saccharomycotina subdivision. Red boldfaced squares represent the location and phylogenetic distance of the three species of interest in our study (*C. albicans*, *C. glabrata* and *C. parapsilosis*). (B) Diagram of the *Saccharomyces* clade including the WGD subclade that contains the *glabrata* group. In red are indicated the three *Candida* species with identified Epithelia Adhesin Proteins (EPA).

In this study, we refer to *C. glabrata* and *C. parapsilosis* as the main NCAC species of interest. Initially, *C. glabrata* was described as *Torulopsis glabrata* (Anderson) by Lodder and de Vries in 1938 and lately, in the 1980s, was classified in the genus *Candida* as

INTRODUCTION

C. glabrata (Yarrow and Meyer, 1978). This change in the phylogenetic classification pointed at the pathogenicity of *C. glabrata* rather than the absence of pseudohyphae and hyphae formation (reviewed by Rodrigues *et al.*, 2017). The above mentioned WGD clade encompassed species with duplication in the genome, placing *C. glabrata* close to *Saccharomyces castellii* in the basal part of the tree (Fitzpatrick *et al.*, 2006; Butler *et al.*, 2009).

Similarly, *C. parapsilosis* was originally described by Ashford in 1928 as *Monilia parapsilosis* and the type strain (ATCC 22019) was reassigned four years later as *C. parapsilosis* by Langeron and Talice, 1932. In the first descriptions, *C. parapsilosis* was considered as a minor pathogen with no remarkable clinical pathogenicity (reviewed by van Asbeck *et al.*, 2009).

Butler *et al.* (2009) has remarked a high diversity in genome size, GC content and levels of ploidy between *Candida*-clade species. Species from the same subclade have no clear variation in the number of protein-encoding genes; and pathogenicity correlates with specie-modifications of certain cell-wall protein families and enrichment of virulence-encoding genes.

In contrast, the *Saccharomyces* clade does not present an elevated number of virulence-factors, highlighting some specific glycosylphosphatidylinositol-linked aspartyl proteases or phospholipases implied in *C. glabrata* pathogenicity (Kaur *et al.*, 2007).

Nevertheless, Gabaldón and colleagues have reported that *C. nivariensis*, *C. bracarensis* and *C. glabrata* are considered pathogenic species which present between 9 to 18 EPA-encoding genes respectively (reviewed by Gabaldón and Carreté, 2016) and only one EPA gene was shown up in the non-pathogenic *N. delphensis*.

Therefore, phylogenetic analyses comparing *C. albicans*, *C. glabrata* and *C. parapsilosis* have shown diversity between them, pointing that new virulence factors have emerged along the evolution process (reviewed by Gabaldón *et al.*, 2016).

1.3 *C. albicans* infections and host-pathogen interactions

Together with *Saccharomyces cerevisiae*, *C. albicans* is the best investigated yeast that has been used as a classic study model for pathogenicity over the last decades. It is considered as diploid, imperfect, unicellular fungus able to form germ tubes and true hyphae when

INTRODUCTION

cells are incubated at 37 °C. It is commensal yeast without symptomatology becoming harmless when the yeast-host balance is affected by different situations triggering a broad spectrum of human diseases (Figure 2).

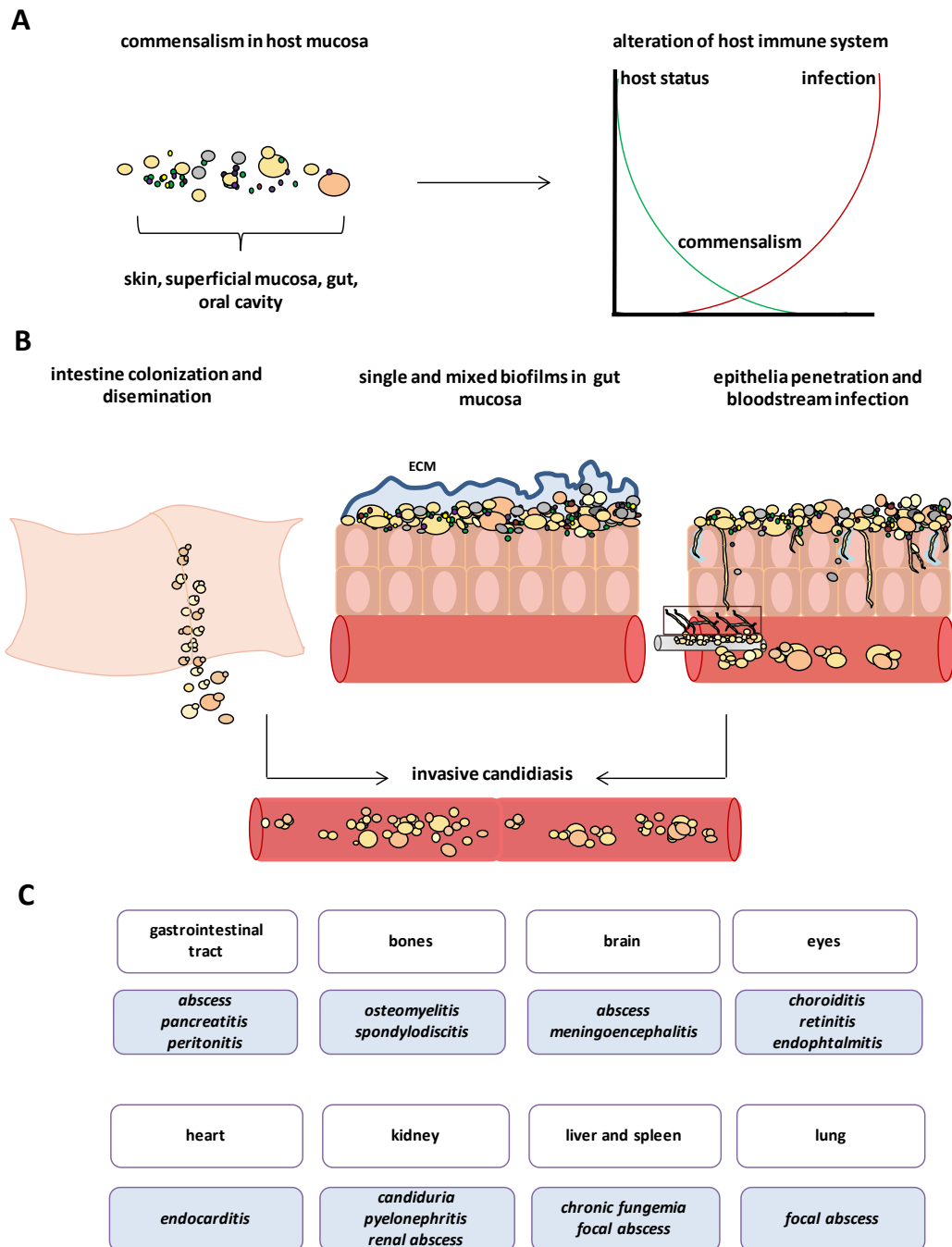


Figure 2. Schematic overview of *C. albicans* tissue invasion. (A) Commensalism and alteration of the host immune system. (B, left) *Candida* colonization and dissemination in the gastrointestinal tract. (B, middle) Biofilm formation on epithelia surfaces and indwelling devices with the extracellular polymeric matrix (ECM). (B, right) yeast and hyphae penetration through the epithelia leading to bloodstream infections, Invasive Candidiasis (IC). (C) Frequent host-sources affected by *Candida spp.* and their respective diseases (adapted from (Pappas *et al.*, 2018)).

INTRODUCTION

Cell morphogenesis has been described as a crucial step during the colonization and invasion process (Whiteway and Bachewich, 2007). As a polymorphic fungus, *C. albicans* can be present as round yeast cells, pseudohyphae form linked to the mother cell, true hyphae with real septum and chlamydospores (reviewed by Sudbery *et al.*, 2004; Kim and Sudbery, 2011). Originally, *C. albicans* yeast cells were considered to constitute a non-invasive stage only involved in commensalism, whereas true hyphae were known as key structures during epithelia penetration (invasion). Recently, functional plasticity in *C. albicans* has increased its relevance, attending to a variety of new cell types that reports different *in vitro* and *in vivo* properties. The “white-opaque” switch (Slutsky *et al.*, 1985; Slutsky *et al.*, 1987) is triggered by several factors that facilitate the transition between morphologies such as change in temperature (30°C to 37°C), pH (pH 4 to 7), or media. Other ellipsoid cell types (opaque, grey and GUT), in addition to the standard “white-yeast” form, show morphological differences as well as infective variability during yeast-host interaction (reviewed by Noble *et al.*, 2017).

An abundant number of cell wall proteins (Als1, Als3, Hwp1), transcription factors (Efg1), secreted enzymes (Sap family) and the only recently discovered cytolytic peptide toxin Candidalysin (Moyes *et al.*, 2016) are crucial virulence attributes for *C. albicans* infection (reviewed by Jacobsen and Hube, 2017). Concisely, *C. parapsilosis*, extracellular lipases have been pointed as one of the most determinant factors in the host-infection process (reviewed by Toth *et al.*, 2017).

The expression of essential CWP encoding-genes in case of *C. albicans* (*HWP1*, *HYR1*, *ALS3*) are clearly up-regulated during yeast-hyphae switch. To corroborate the importance of morphogenesis in the infection process, mutants of hyphae-induced proteins have shown an alteration in hyphae formation which consequently affects the cell wall constituents and the pathogenicity (Lo *et al.*, 1997; Zheng *et al.*, 2007). Several genetic and environmental factors are involved in morphology-switching affecting hyphae development and *in vivo* biofilm formation (reviewed by Kim and Sudbery, 2011) *Candida* morphotype has also affected the host immune system recognition, for example, yeast cells and hyphae form, present different recognition receptors which (IL12 and IL4 respectively) will activate alternative inflammatory pathways during host response (reviewed by Gow *et al.*, 2012).

1.4 *Candida* biofilms

Biofilms are microbial communities encased in a matrix of extracellular polymeric substances distinguishing themselves from the free floating cells (reviewed by Costerton *et al.*, 1999; Harriott and Noverr, 2011). Approximately, 80 % of the microorganisms live as biofilms, (reviewed by d'Enfert and Janbon, 2016) mostly in endothelial cells and mucosa (e.g. host tissues, tooth surfaces, respiratory tract, urinary tract and eyes) (reviewed by (Mukherjee *et al.*, 2005). The ability of *Candida* cells to adhere to host surfaces (Figure 3A) and abiotic medical devices (such as indwelling catheters, pacemakers, dental prosthesis, contact lenses, or artificial joints) is defined, among others, by their cell wall composition (Hawser and Douglas, 1995; Hawser, 1996a; Hawser, 1996b; Baillie and Douglas, 1999). A combination of cell wall proteins and transcriptional factors regulate the attachment of *Candida* cells to different surfaces such as polymethylmethacrylate, elastomers, as well as host surfaces (Nobile *et al.*, 2006; Chandra *et al.*, 2008; Finkel *et al.*, 2012). *Candida* biofilms are a combination of different cell stages or morphologies such as round blastospores, pseudohyphae, and hyphae depending on the number and species involved. As defined by (Baillie and Douglas, 1999; Nobile *et al.*, 2009), biofilm formation on host tissues is generally divided into three main stages (Figure 3B), remarking the importance of the cell morphology and the composition of the matrix on the establishment of the biofilm. The initial phase (early) occurs during the first 11 hours, including the attachment and aggregation of spherical cells along the surface. Afterwards, the secondary stage (intermediate) during the following 12-30 hours, remark the primary development of the Extracellular Matrix (ECM/EPS) containing glycoproteins, carbohydrates, lipids and nucleic acids. The largest proportion of polysaccharides is mainly constituted by glucose and mannose, this polymeric substance is secreted by *Candida* and host cells previously incorporated into the microbial community. The ECM covers the whole surface of the biofilm as a superficial and complex layer embracing the total number of cells conferring a defence mechanism (Nett *et al.*, 2015). The final phase (mature) comprises a heterogeneous and stratified distribution of microcolony aggregates embedded in the matrix where the hyphae of filamentous species create a stable architecture (Chandra *et al.*, 2001; Zarnowski *et al.*, 2014). The maturation stage can be extended for 38-72 h. After

INTRODUCTION

this, the non-adherent daughter cells disperse and invade the tissues and bloodstream (reviewed by Cavalheiro and Teixeira, 2018).

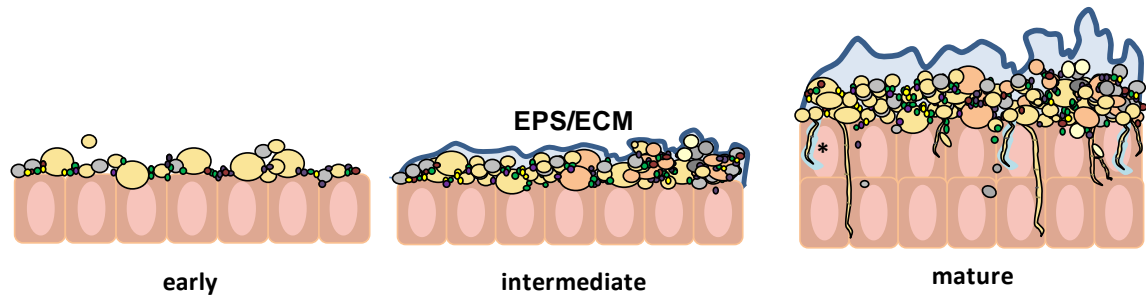
In fungal biofilms, usually *C. albicans* is present as one of the most frequent *Candida* species. Many clinical studies about interactions between *C. albicans* with other microorganisms have been reported in the last years. *C. albicans* could be easily found in dental prosthesis and oral mucosa in combination with different *Streptococcus* species (Nobbs *et al.*, 2010). Moreover, it can be a dual colonizer of epidermis, skin injuries and medical devices together with *Pseudomonas aeruginosa* and *Staphylococcus epidermidis* (Jack *et al.*, 2015; Lindsay *et al.*, 2014). Dual biofilms generally increase (excluding *Lactobacillus spp.*) the capacity to adhere and colonize host surfaces just like the defence against antifungals drugs and host immune response (reviewed by Peleg *et al.*, 2010).

Remarkably, fungal biofilms offer less susceptibility against the four major antifungals currently used such as azoles, polyenes, echinocandins or/and nucleosides (Fox *et al.*, 2015).

Ramage *et al.* (2002) reviewed that the consistency of the biofilm microbial community (mainly sessile cells) and the polymeric matrix are not the only factors involved in antifungal resistance. They underlined that, at least, two transmembrane efflux pumps (ABC and MSF transporters) located in the plasma membrane, seem to be involved in the process.

A recent study from Uppuluri *et al.* (2018) in *C. albicans* has introduced a new concept based on biofilm propagation from independent “free-floating” cells differing from planktonic in their composition and functionality . They are “dispersed” from the outer-hyphal layer of the biofilms and constitute novel targets for the development of antifungal drugs.

A- general model of multi-species biofilm attachment to human epithelia



B- *in vitro* schematic model of biofilm formation to different medical devices

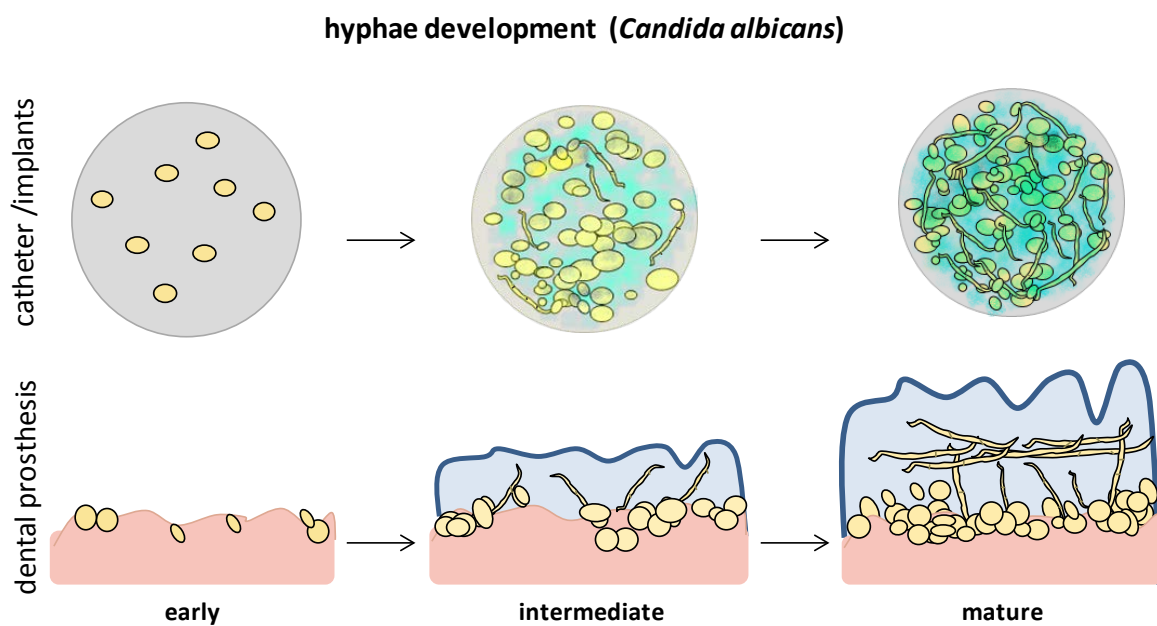


Figure 3. Biofilm formation on biotic and abiotic surfaces in *C. albicans* (modified from Chandra *et al.*, 2008). (A) General schematic model of mixed biofilms in human surfaces. Yellow big spheres represented *C. albicans* yeast cells in early and intermediate stages, grey and orange big spheres represented other possible *Candida spp.* cells together with *C. albicans*. Small green, red and purple spheres indicated different bacteria species together with *C. albicans* (mixed biofilms) included in the EPS/ECM. * cytolysin (Candidalysin) (Moyes *et al.*, 2016). (B) *In vitro* model of putative biofilm formation process on catheters and prosthesis. Biofilms are divided in three main stages: early (11h.) represented by yeast cells (yellow), intermediate (12-30 h.) represented by yeast and incipient hyphae forms and mature phase (38-72 h.), yeast and developed hyphae (yellow) covered by the ECM.

1.5 The fungal cell wall

The cell wall is the outermost part of *Candida spp.* that confers stability and rigidity as well as protection. It is defined as a fungal exoskeleton and a matrix in contact with host surfaces. The constituents of the cell wall are essential during the colonization process and invasion. The cell wall plays an important role in terms of pathogenicity and is therefore also a target for the development of antifungals treatments (Klis *et al.*, 2001). Both, the external cell surface structures and the components of the inner layers are part of the cell wall pathogen-associated molecular patterns (PAMPs) which are recognized by the host innate immune system (reviewed by Jouault *et al.*, 2009).

C. albicans cell wall has been studied for long time together with *S. cerevisiae*, differing on baker yeast's cell wall in the amount of glucans (20 % higher in yeast form) and the reduction of mannoproteins content (10 % less than *S. cerevisiae*). Approximately, the 90 % of the total mass is made up of carbohydrates followed by proteins and lipids. It is generally divided in two fractions, the unified inner part in contact with the plasma membrane that especially contains chitin and glucans (50-60%), and a thicker heterogeneous layer with covalently bound mannoproteins (Figure 4) with direct contact to the host surface (reviewed by Klis *et al.*, 2009).

The internal cell wall layer presents mainly β -1, 3-glucans linked to β -1, 6 glucans and chitin (Klis *et al.*, 2001). Approximately a 35-40 % of the total dry mass of yeast cell wall is comprised by cell wall proteins (CWPs) which are also classified into two different categories based on location and structure. It can be distinguished a first group of GPI-CWPs connected to the network of polysaccharides in the inner cell wall and a second groups including unbound proteins (reviewed by Chaffin, 2008).

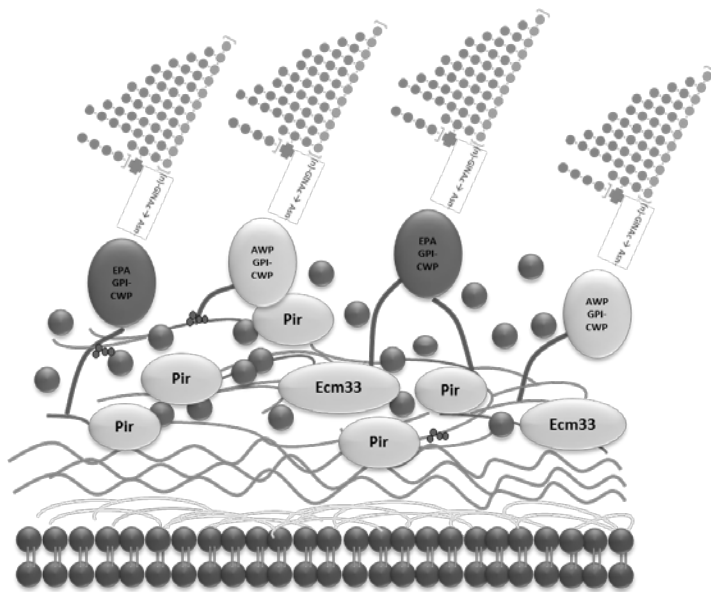


Figure 4. Schematic *Candida spp.* cell wall model. Top, outer part of the cell wall composed by chains of mannans linked to the proteins by an asparagine residue (Asn). Middle, cell wall proteins (GPI-CWP (adhesins), Ecm33 and Pir proteins) linked to β -1, 3-glucans, β -1, 6 glucans and chitin (light grey). Bottom, plasma membrane

1.6 *Candida spp.* cell wall proteins (CWP)

In the last years the development of bioinformatics programs and the improvement of sequencing techniques has promoted that several laboratories design different strategies to calculate algorithms which analyse the whole *Candida* genome to find expected adhesin-like encoding genes. These implements are essential to predict CWPs including GPI-anchored CWPs (De Groot *et al.*, 2003; Eisenhaber *et al.*, 2004). As an example, the program FungalRV has been used to predict putative adhesins-encoding genes in *C. albicans* (Chaudhuri *et al.*, 2011).

The cell wall proteins are involved in protein-protein attachment, yeast-microbe linkage and host-pathogen interaction. As it has been mentioned before, the proteins are classified depending on their structure and location. Within the covalently CWP proteins, two different types have been characterized. The glycosphosphatidylinositol (GPI)-anchored proteins are mainly located in the outer part of the cell wall (Verstrepen and Klis, 2006; Hoyer *et al.*, 2008; Zupancic *et al.*, 2008) linked with the β -1, 3 glucans by β -1, 6 glucans (reviewed by Chaffin, 2008). In case of proteins with internal repeats (Pir proteins), it has been found covalently attached to the plasma membrane via alkali-sensitive connectors (reviewed by Ruiz-Herrera *et al.*, 2006). According to studies performed by de Groot and

INTRODUCTION

colleagues, proteomic analyses of *C. albicans* cell wall have exhibited new surface proteins classified in four different groups including carbohydrate-active enzymes, adhesins, putative flocculins (Pga24p) and superoxide dismutases (de Groot *et al.*, 2004).

In contrast, the *Candida* cell surface presents several unbound proteins that can be found either in the cell wall or in the supernatant (Bgl2p) as well as secreted proteins like the Cht3p and Pra1p. Proteins like the Ecm33 and the aspartyl proteases Sap9 and Sap10 that has been found as a transit protein which can be present, at the same time, in the membrane and the cell wall (reviewed by Chaffin, 2008).

1.7 GPI-anchored Cell Wall proteins (adhesins)

As it has been mentioned before, the GPI-anchored CWP proteins are defined as adhesins which are mainly situated in the outer layer of the cell wall. These adhesins are secreted via Golgi apparatus and their elementary structure consists on a C-terminal part defined as a low complexity domain containing tandem repeat regions (TRRs) rich in serine and threonine (Ser/Thr) residues linked to the endoplasmic reticulum (ER) membrane by glycosylphosphatidylinositol linkage (GPI-anchor). The N-terminus part or high complexity domain presents a signal peptide involved in the secretion process and confers the adhesion-binding specificity to different host surfaces (Figure 5). The glycosylation of the proteins increase the molecular mass of them which contains a signal peptide that is going to be removed in the mature structure (Nather and Munro, 2008; de Groot *et al.*, 2013).

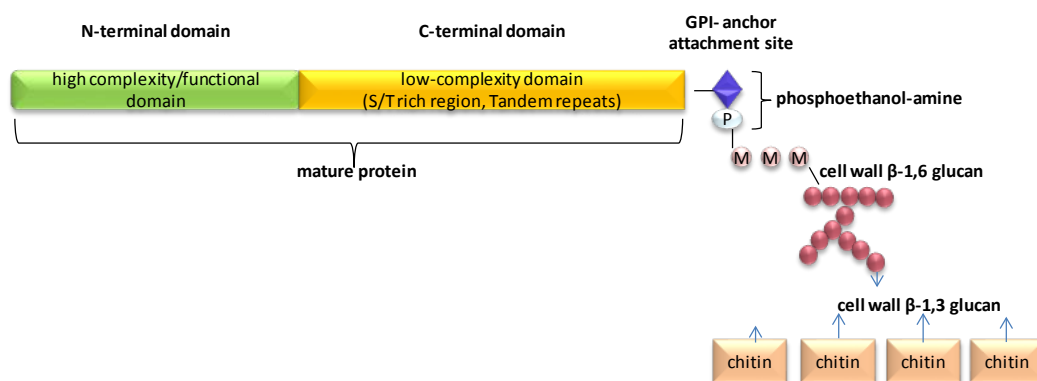


Figure 5. Cell wall GPI-anchored proteins (adhesins) general structure, adapted from ten Cate *et al.*, 2009; de Groot *et al.*, 2013. Mature adhesins are divided in two main parts, N-terminal domain (green) and C-terminal domain (yellow) linked to the cell-wall *Candida* glucans by a GPI-anchor site containing a large number of TRRs.

INTRODUCTION

The mature structure of the adhesins is characterized by the absence of the signal peptide and the high N- and O-protein glycosylation during the transfer to the cell wall (Figure 6). The highly glycosylated mannan-network is located in the outer part of the cell wall direct contact with the host-recognition structures (PRRs). Novel techniques have been developed to extensively analyse adhesin structures, these new strategies include binding-domain crystallization, mutagenesis, atomic force microscopy (AFM) and nuclear magnetic resonance (NMR) (Ielasi *et al.*, 2012; Beaussart *et al.*, 2012).

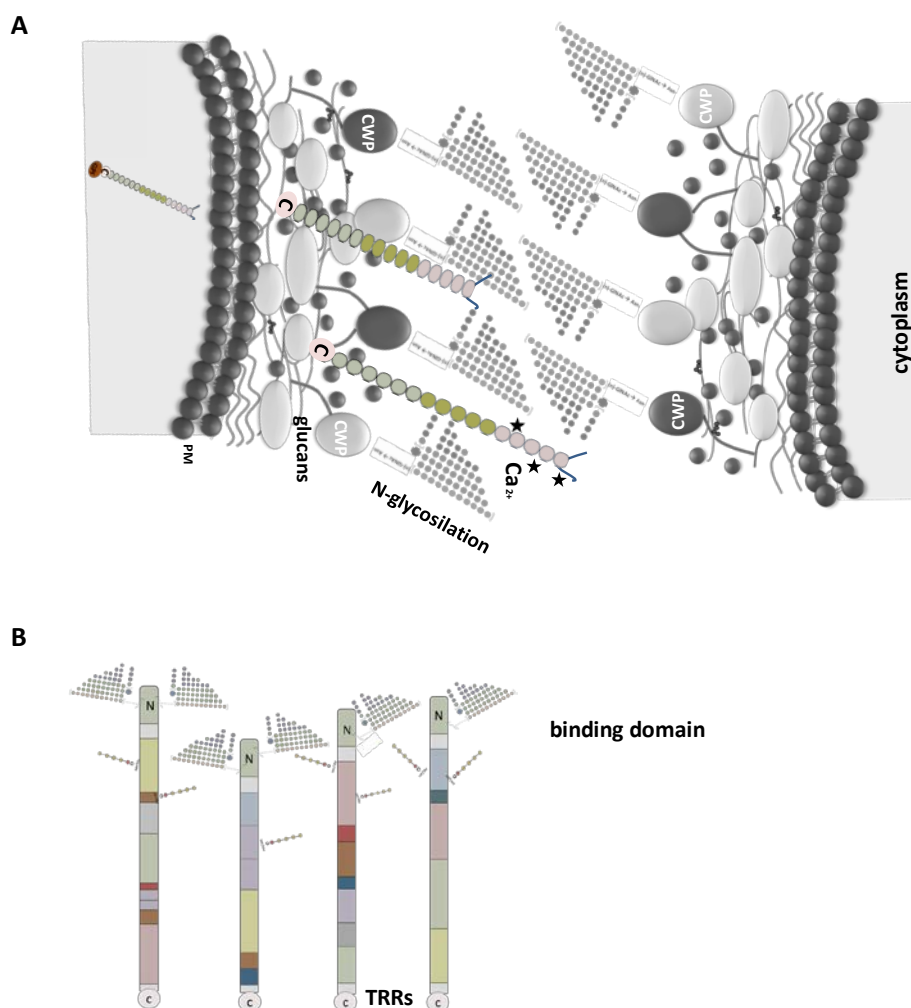


Figure 6. Adhesin-like cell wall proteins secretion and cell wall attachment process. (A) Structure of adhesin-protein secreted via endoplasmic reticulum and Golgi apparatus containing GPI anchor (orange). Signal peptides removal and protein's glycosylation take place along the secretory pathway. In the membrane the GPI anchor is cleaved from the mature protein. Protein is stabilized with Ca²⁺ via O-glycosylated chains and integrated into the cell wall via glucans (reviewed by Verstreppe and Klis, 2006). (B) Mature adhesin scheme constituted by N-terminal binding domain (green), C-terminal anchoring domain (light pink), TRRs (Tandem Repeats Regions) in colours, and protein "branches" constituted by N-mannans and O-mannans. Adhesins presented different sizes depending on the length of the TRRs.

INTRODUCTION

C. albicans adhesins has been investigated for long time. They have been distributed into three families including the deeply analysed Als family, the Hwp family and the Iff/hyr that has been described in CTG-clade *Candida* species, in contrast, these adhesins has not been detected in *C. glabrata* (Jackson *et al.*, 2009; Butler *et al.*, 2009; Boisramé *et al.*, 2011).

Als family: The agglutinin-like-sequence (Als) CWP family was the earliest CWP described in *C. albicans* divided in three subfamilies attending to the low complexity C-domain (tandem repeats domain) and they are implicated in adhesion to host surfaces. Differences between the subfamilies depend on the repeat region (reviewed by Hoyer, 2001). The majority of the adhesins genes are located in telomeric regions of the chromosomes 3, 6 and R (Hoyer *et al.*, 1995; Hoyer *et al.*, 1998a; Hoyer and Hecht, 2001).

There is a broad variation between *ALS* genes among isolates and there are influenced by media composition (Als1), morphogenesis process (Als3 and Als8) and growth parameters (Als4) (Hoyer *et al.*, 1995; Hoyer *et al.*, 1998a; Hoyer *et al.*, 1998b; Hoyer and Hecht, 2000). They are homogeneously distributed along the cell wall (Kapteyn *et al.*, 2000) connected with the β -1, 6-glucan. The *ALS* genes are also presented in *C. dubliniensis* (reviewed by Hoyer *et al.*, 2001). Complementary studies have asserted the presence of *ALS* encoding-genes in several NCAC species as *C. dubliniensis*, *C. tropicalis* and *C. parapsilosis*. It has been detected a strong variability between *ALS* genes along isolates, for example, the size of the adhesins fluctuate between strains, which mean that the divergence in the number of repeats is a key point in the attachment to the host (Hoyer and Hecht, 2001). The Als-adhesins have been also differentiated attending to their functionality in the pathogenic process, for example, Als1, Als2, Als3, Als4 and Als9 are involved in the adherence to epithelia and endothelial cells as well as laminin, fibronectin, and collagen (Als3). The members of Als family take part in the attachment of *Candida* cells to abiotic devices (glass, silicone-elastomers and acrylic methacrylate). In contrast, deletion mutants of Als5, Als6 and Als7 (Hoyer and Hecht, 2000) have increased their capacity to adhere to host tissues and have usually been identified in biofilms due to their aggregation capacity. Als1, Als3 (hyphae specific) and Als5 cell wall proteins present amyloid structures able to aggregate between them increasing the adherence in *Candida-Candida* interaction or *Candida*-bacteria (Otoo *et al.*, 2008; Nobbs *et al.*, 2010).

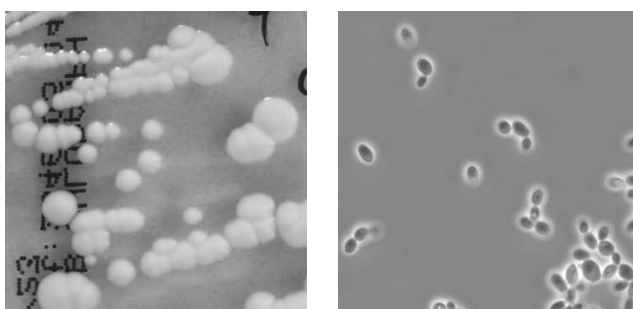
INTRODUCTION

Hwp1 family: the adhesins included in this family are expressed under hyphae morphology such as Hwp1, Hwp2/Pga8 (hyphal wall protein) and Rbt1 (repressed by Uup1). They are involved in abiotic biofilm formation to polystyrol (Hwp1 and Eap1/Pga47) and silicone (Hwp2/Pga8), in biotic attachment to oral mucosa and epithelia, and they are also implicated in mating process (Nobile *et al.*, 2008; Ene and Bennett, 2009).

Iff/Hyr family: to date, it is constituted by adhesins mostly express in the hyphae form as the other two families (hyphally uprergulated proteins) highlighting Hyr1, that controls host-immune cell destruction, and the iff subfamily needed for adherence to epithelia and cell surface maintenance (reviewed by de Groot *et al.*, 2013).

1.8 *Candida glabrata*

C. glabrata was described as imperfect non-dimorphic yeast (2.5 to 4.5 X 4.6 μ m) that usually grows as blastoconidia (37°C) producing small, round and glossy-creamy colonies without mycelia development (Sinnott *et al.*, 1987 and Kwon-Chung and Bennett, 1992). It can be identify in selective CHROMagar as round creamy green colonies but is nearly impossible to differentiate from other *Candida* species on Sabouraud-Dextrose-Agar (SDA) plates, unless for the small size (Figure 7). *C. glabrata* ovoid cells forms small chains connected to each other by multilateral buds (Saballs *et al.*, 2000). It is haploid yeast that does not have the ability to produce capsules and no sexual spores have been described.



Candida glabrata CBS-138

Figure 7. *C. glabrata* morphology. Left, colony phenotype on Sabouraud's agar. Right, round yeast cells in YPD liquid culture.

Unless is still under investigation, some virulence factors are decisive for *C. glabrata* pathogenicity. Among them, we can underline the adherence to surfaces, the formation of biofilms and a remarkable number of cell wall proteins (reviewed by López-Fuentes *et al.*,

INTRODUCTION

2018). It has been also highlighted the importance of surface glycoproteins controlled by SIR and *RAP1* subtelomeric silencing (De Las Peñas *et al.*, 2003). Furthermore, it has been remarked the resistance to oxidative stress (reviewed by Vale-Silva and Sanglard, 2015) and the recently described CgDtr1 which has been involved in *Galleria mellonella* virulence (Romão *et al.*, 2017).

Contrary to *C. albicans*, the ability to only form budding cells, allows *C. glabrata* to create a compact microbial community constituted by yeast and ECM (Kucharíková *et al.*, 2015) that behaves as a perfect deposit for consecutive infections.

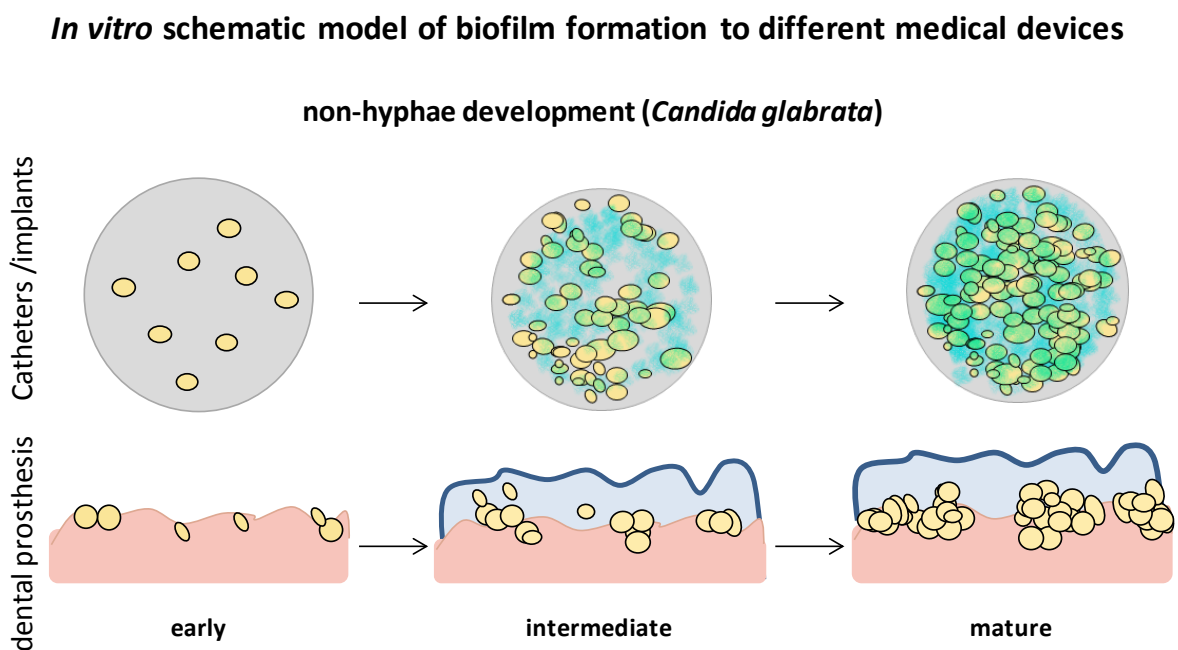


Figure 8. *C. glabrata* biofilm *in vitro* schematic model. Top row: *C. glabrata* biofilm formation in catheters (elastomers). Bottom row: biofilm formation capacity to acrylic dental prosthesis. Both procedures are divided in three major steps (early, intermediate and mature). In blue, extracellular matrix (ECM).

Little is known about *C. glabrata* biofilm composition excluding the ability to form dense communities divided into defined multilayers constituted by proteins, β -1, 3-glucans as well as ergosterol in the matrix (Nett *et al.*, 2007; Silva *et al.*, 2009). *C. glabrata* is able to form compact biofilms (Figure 8) in different biotic and/or abiotic materials used in nosocomial environments like silicone elastomers, polyvinyl, polystyrol (reviewed by Tournu and Van Dijck, 2012) or dental acrylic resins (Pathak *et al.*, 2012). Currently, the majority of the biofilm formation tests have been performed *in vitro* using this medical devices (catheters, dentures) or standard materials (polystyrol) with hydrophobic surfaces.

INTRODUCTION

As it has been addressed by (El-Kirat-Chatel *et al.*, 2015), the adherence capacity of *C. glabrata* cells to negatively charged surfaces is higher compared to hydrophilic areas (Hazen *et al.*, 1986; Luo and Samaranayake, 2002). *C. glabrata* biofilms display certain resistance against azoles and polyenes but are still susceptible to echinocandins (Seidler *et al.*, 2006; Kuchariková *et al.*, 2015).

1.8.1 *Candida glabrata* cell wall proteins

(Desai *et al.*, 2011) indicated that *C. glabrata* genome contains more than 300 specific genes that are still not totally characterized but may influence in its virulence capacity.

This assumption was subsequently investigated by Weig *et al.* (2004) and de Groot *et al.* (2008) showing that *C. glabrata* presents 67 sequences adhesion-specific in the cell wall of the type strain CBS-138. These are grouped in seven subfamilies attending to the binding domain, nevertheless, the function and role during fungal infections is still not well characterized for all. As it is shown in Figure 9, the adhesin-encoding genes are, in large part, present in the telomeric regions and controlled by subtelomeric silencing (Reviewed by De Las Peñas *et al.*, 2015). These genes have high tendency to present homologous recombination as well as gene rearrangements. The first two families differentiated in *C. glabrata* are the Epa family (epithelial adhesins) and the Pwp family (protective antigen wall proteins). Both families present the lectin binding domain PA14 (anthrax protective antigen).

The Epa family (17 members) is a really well characterized adhesin group involved in host-epithelia attachment (Cormack *et al.*, 1999; Zupancic *et al.*, 2008). According to the review of Timmermans *et al.* (2018), *C. glabrata* adhesins are classified in three different categories depending on their functionality: adhesins present in planktonic cells, adhesins involved in adherence and colonization and adhesins identified in biofilms.

Together with the two previous groups, five different subfamilies were determined including the relevant Awp family (adhesin wall proteins). These adhesins are far related in terms of N-ligand-binding specificity and they are still not deeply characterized (Kranefeld *et al.*, 2011).

INTRODUCTION

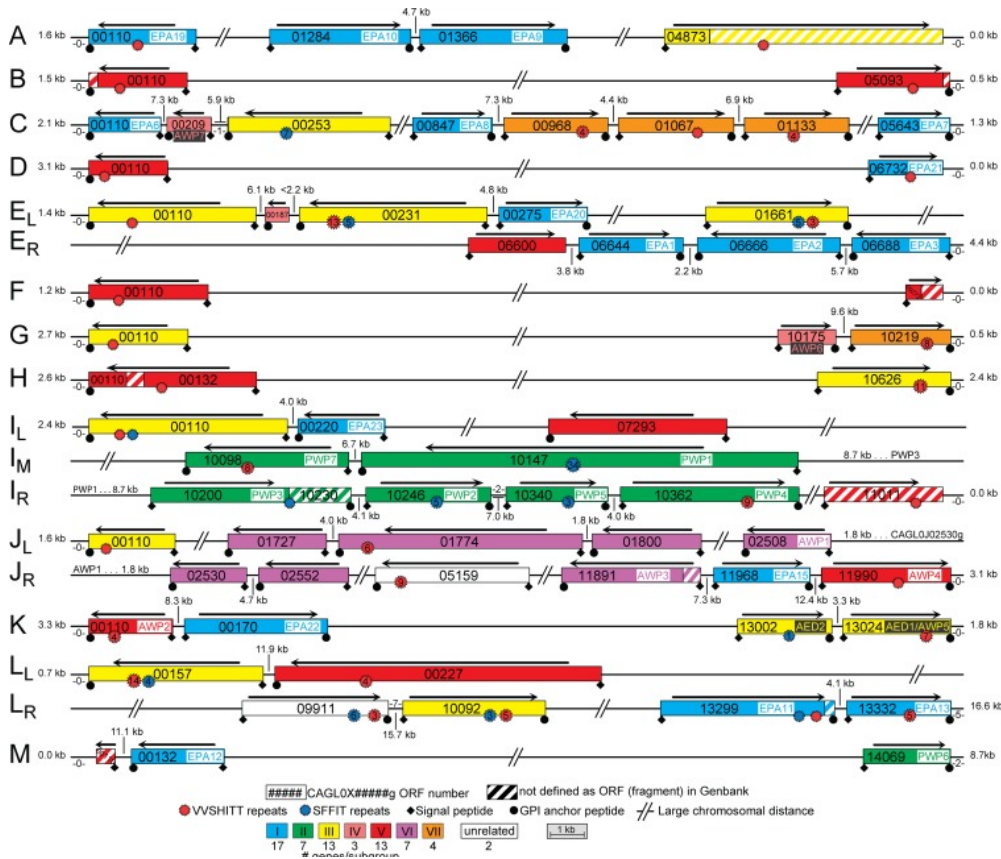
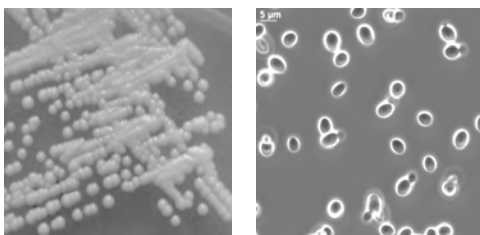


Figure 9. Chromosomal distribution of putative *C. glabrata* adhesins-encoding genes (de Groot *et al.*, 2013). Adhesins encoding genes are located in subtelomeric regions of 13 chromosomes (E_L, E_R; I_L, I_M, I_R; L_L, L_R). Colours represent seven subfamilies of adhesins depending on the N-terminal binding domain.

1.9 *Candida parapsilosis*

C. parapsilosis presented round yeast cells and pseudohyphae at 37 °C. (Figure 10) This nosocomial pathogen has gained importance in the last years and as it has been described for *C. albicans*, the capacity of *C. parapsilosis* to switch between morphologies implicates a variation in the infection-relevant cell properties which help *C. parapsilosis* to adapt to different host-niches (Laffey and Butler, 2005).



Candida parapsilosis CDC 317

Figure 10. *C. parapsilosis* CDC 317 morphology. Left, smooth colony morphotype on Sabouraud's agar. Right, round yeast cells from smooth morphotype in YPD liquid culture.

INTRODUCTION

The biofilm formation process in *C. parapsilosis* isolates is still not well understood. Nevertheless, variations in biofilm formation capacity between bloodstream isolates (59%) and samples isolated from skin (39%) have been remarked (Růzicka *et al.*, 2007; Shin *et al.*, 2002). Laffey and collaborators have remarked the importance or morphotypic switch and presence of farnesol mediating quorum-sensing process are, as well implicated in biofilm formation (Laffey and Butler, 2005). Lattif *et al.* (2010) have asserted that *C. parapsilosis* biofilms are composed by clusters or yeast cells attached to the surface with a minimal ECM production (Figure 11).

***in vitro* schematic model of biofilm formation to different medical devices**

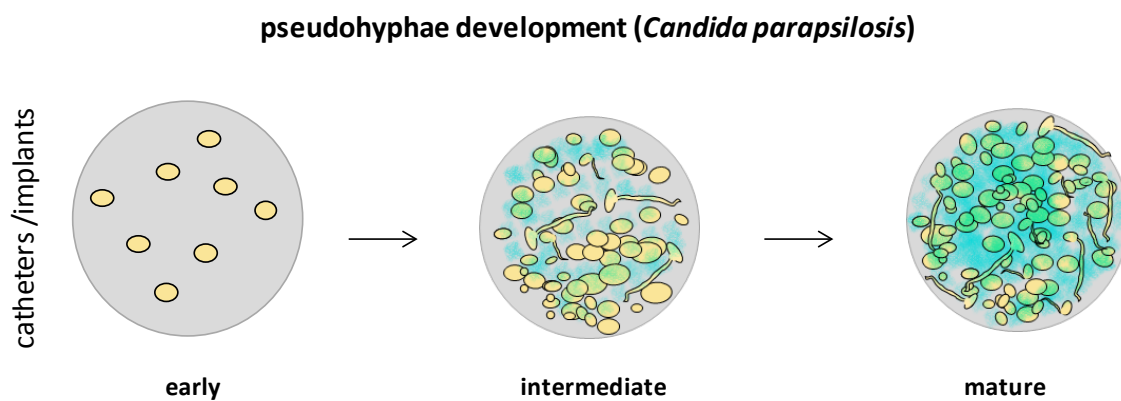


Figure 11. *C. parapsilosis in vitro* schematic model. *C. parapsilosis* biofilm formation divided in three major steps (early, intermediate and mature) on catheters and medical implants with pseudohyphae development.

1.9.1 *Candida parapsilosis* cell wall proteins

Currently, less is known about *C. parapsilosis* cell wall, the phylogenetic relation with *C. albicans* (CTG clade), has indicated a similar distribution of the cell wall components. As it has been described before for *C. albicans* and *C. glabrata*, the cell wall is also composed with sugars located in the inner layer and highly glycosylated proteins in the outer part of the cell surface (Díaz-Jiménez *et al.*, 2012). Studies based on N- and O-linked mannans have confirmed their importance in IL-1 β (O-linked mannans) and IL-6 and TNF- α (N- and O-linked mannans) stimulation in the host-immune response (Pérez-García *et al.*, 2016).

INTRODUCTION

Bioinformatic approaches performed by Butler *et al.* (2009) have remarked the presence of five *ALS* family encoding-genes and six predicted GPI-anchored protein encoding-genes (Pga 30).

Genome analyses have remarked small variations in lysophospholipases and peptidases between clinical isolates, thus, broad distribution of adhesion-encoding genes have been analyzed (Hoyer, 2001). A detectable variation in the presence of adhesins encoding genes has been found between *C. parapsilosis* isolates, indicating an unequal presence of *ALS* genes, involving deletion and recombination of genes (e.g. CPAR2_404800 and CPAR2_404780) or divergence events (CPAR2_404790) among *C. parapsilosis* strains (Pryszcz *et al.*, 2013).

1.10 *Candida* species interaction in host invasion

Cell surface *Candida* proteins are important for colonization and invasion of human epithelia, adherence to epithelia human cells have been studied in the last years in Caco-2 cells and also in fibroblast pointing the importance of the large cell surface proteins function for this purpose (Gabaldón *et al.*, 2013b; Hoyer and Cota, 2016) focusing on the interaction between human epithelia and the N-terminal binding domain of the adhesins like proteins (lectin domain). In case of *C. albicans* the presence of the Als3 is known to be crucial for the penetration through the epithelia host barrier. According to the review by (Kühbacher *et al.*, 2017), there two possible mechanism, remarking a passive endocytosis or an active penetration in which *C. albicans* *ALS3* and *HWP1* genes are clearly involved (Dieterich, *et al.*, 2002). In agreement with this, more recently it has been shown the functionality of the secreted aspartyl protease and well as the gen *ECE1* secreted a peptide toxin (Candidalysin) able to produce pores and damage the tissue under hyphal condition during the epithelia invasion (Moyes *et al.*, 2016; Richardson *et al.*, 2018). In case of *C. glabrata*, several studies pointed the possibility of a co interaction between *C. glabrata* and *C. albicans* (Alves *et al.*, 2014). In case of NCAC species, the invasion process is still under investigation. Tati *et al.* (2016) has interestingly proposed that *C. albicans* may interact with *C. glabrata* during epithelia invasion. According to the authors, *C. glabrata* CWP will be responsible for the adhesion of yeast to *C. albicans* hyphae, allowing *C. glabrata* cells to reach the bloodstream. These changes in *Candida* morphology will be

INTRODUCTION

beneficial during the colonization and host-invasion. Regarding *C. parapsilosis*, differential functionality of chitinases, dehydrogenases or phosphatases, have been described in yeast form. Contrary, the pseudohyphal stage mainly presents proteins similar to a cell surface mannoprotein Mp65, chitinase and GPI-anchored or the Rbt1 cell wall protein. Nevertheless, cell wall proteins identification and cell-surface protein encoding genes are still under studied (Karkowska-Kuleta *et al.*, 2015).

1.11 Aims of the study

C. glabrata and *C. parapsilosis* are the two most common causes of non-*Candida albicans* *Candida* (NCAC) infections in the human host. The capacity to form biofilms on abiotic and biotic surfaces encased in extracellular polymeric matrix is thought to be a prerequisite for successful host colonization. Previous works have focussed on few laboratory strains.

Therefore, with a focus on *C. glabrata* and *C. parapsilosis* clinical isolates, the major aim of this study was to further elucidate if and how phenotypic and morphological differences between and within clinical isolates are reflected on genome and proteome levels and how these differences correlate with the host infection process.

Specifically, we sought to build and phenotypically classify *C. glabrata* and *C. parapsilosis* strain collections, attending to the cell surface-related properties and the capacity to form biofilms on abiotic surfaces. It is known that biofilm formation capacity can reduce antimycotic susceptibility, therefore, antifungal drugs susceptibility tests of a morphologically and phenotypically characterized clinical isolates were to be performed to confirm if phenotypic variations would predetermine MIC towards azoles, echinocandins, or polyenes.

Furthermore, in this study, we sought to characterize variations between biofilm-forming clinical isolates and their virulence in the *G. mellonella* animal model as part of the still understudied mechanism of pathogenicity in *C. glabrata* and *C. parapsilosis* clinical isolates. It is known that genomic variability in genes encoding cell wall proteins in pathogenic *Candida* species is present. Therefore, in order to deeply investigate the importance of gene variation and cell wall proteins incorporation in both species as strategy associated with virulence, genome sequencing analyses and MS/MS spectrometry analyses of selected *C. glabrata* and *C. parapsilosis* clinical isolates were to be conducted to better understand variations as future diagnostic tools.

2. Materials and Methods

2.1 Materials

General materials, chemicals and disposables, unless specified in Table 1, were purchased from Carl Roth GmbH (Karlsruhe, Germany), Eppendorf AG (Hamburg, Germany), Sigma-Aldrich Chemie (Steinheim, Germany), Sarstedt AG & Co. KG (Nümbrecht, Germany), Merck KGaA (Darmstadt, Germany), Sartorius AG (Göttingen, Germany), and Thermo Fisher Scientific, GmbH (Darmstadt, Germany).

Table 1. Chemicals and disposables used in this study

materials	company
5-Brom-4-chlor-3-indoxyl- β -D-galactopyranosid	Sigma-Aldrich Chemie, Steinheim, Germany
12-well microtiter plates	Greiner Bio-One, Frickenhauser, Germany
96-well microtiter plates	Greiner Bio-One, Frickenhauser, Germany
α -cyano-4-Hydroxycinnamic acid (C ₁₀ H ₇ NO ₃)	Sigma-Aldrich GmbH, Steinheim, Germany
Acetonitrile LC –MS Chromasolv [®]	Fluka Analytical, Sigma-Aldrich GmbH, Steinheim, Germany
AdvanDX <i>C. albicans</i> / <i>C. glabrata</i> DNA FISH [®] identification Kit	AdvanDX A/S, Hvidovre, Denmark
Ampicilin	Sigma Aldrich Chemie GmbH, Steinheim, Germany
Amphotericin B (C ₄₇ H ₇₃ NO ₁₇)	SERVA-Feine Biochemica, Heidelberg, Germany
Bacto [™] Peptone	BD, Becton Dickinson and Company, Le-Pont de-Claix, France
Bacto [™] Yeast Extract	BD, Becton Dickinson and Company, Le-Pont de-Claix, France
BBL [™] CHROMagar [™] <i>Candida</i>	BD, Becton Dickinson and Company, Le-Pont de-Claix, France
BBL [™] Corn Meal Agar	BD, Becton Dickinson and Company, Le-Pont de-Claix, France
Blankophor P	Prechel GmbH, Schwetzingen, Germany
Caspofungin (C ₅₂ H ₈₈ N ₁₀ O ₁₅)	Merck KGaA, Darmstadt, Germany

Continued from previous page

Columbia agar + 5 % sheep blood plates	BioMèrieux Germany GmbH, Nürtingen, Germany
----------------------------------------	---------------------------------------------

MATERIALS AND METHODS

Commercial Sabouraud agar plates + glucose with gentamicin and chloramphenicol	Oxoid™ Germany GmbH, Wesel, Germany
Crystal Violet	Sigma-Aldrich GmbH, Steinheim, Germany
D + Glucose Monohydrate	Carl Roth GmbH, Karlsruhe, Germany
Difco™ Antibiotic Medium 3	BD, Becton Dickinson and Company, Le-Pont de-Claix, France
Dimethyl sulfoxide (C ₂ H ₆ OS)	Sigma-Aldrich GmbH, Steinheim, Germany
DNA Gel Loading Dye 6X	Thermo Fisher Scientific, GmbH, Darmstadt, Germany
Ethylenediaminetetraacetic acid (C ₁₀ H ₁₆ N ₂ O ₈)	Sigma-Aldrich GmbH, Steinheim, Germany
Fluconazole (C ₁₃ H ₁₂ F ₂ N ₆ O)	Discovery Fine chemicals, Wimborne, UK
Flucytosine (C ₄ H ₄ FN ₃ O)	Sigma Aldrich Chemie GmbH, Steinheim, Germany
Formic acid Rotipuran® 98 % (CH ₂ O ₂)	Carl Roth GmbH, Karlsruhe, Germany
GelRed®, 10000X	Genaxxon Bioscience, Ulm, Germany
Glass beads, 0.5 mm	BioSpec Products, Carl Roth GmbH, Karlsruhe, Germany
HotStar Taq® DNA polymerase Kit	Qiagen GmbH, Hilden, Germany
Isavuconazole	Discovery Fine Chemicals, Wimborne, UK
Mast Cryobanks™	Mast Diagnostica GmbH, Reinfeld, Germany
Micafungin (C ₅₆ H ₇₁ N ₉ O ₂₃ S)	Astellas Pharma GmbH, München, Germany
Midori ^{Green} Advance	Nippon Genetics Europe GmbH, Düren, Germany
MSP 96 polished steel BC targets	Bruker Daltonics, Bremen, Germany
N-lauroylsarcosine sodium salt (C ₁₅ H ₂₉ NO ₃)	Sigma-Aldrich GmbH, Steinheim, Germany
Nucleospin® Gel and Clean-up Kit	Macherey-Nagel, Düren, Germany
PCR grade nucleotide Mix (dATP, dCTP, dGTP, dTTP)	Roche Pharma AG, Grenzach-Wyhlen, Germany
PCR reaction buffer + Mg (10X)	Roche Pharma AG, Grenzach-Wyhlen, Germany
Phloxine B	Sigma-Aldrich GmbH, Steinheim, Germany

MATERIALS AND METHODS

Continued from previous page

Posaconazole (C ₃₇ H ₄₂ F ₂ N ₈ O ₄)	Discovery Fine chemicals, Wimborne, UK
Potassium dihydrogen phosphate 99.8% (KH ₂ PO ₄)	Calbiochem, Merck KGaA, Darmstadt, Germany
Proteinase K	PanReac AppliChem GmbH, Darmstadt, Germany
RNase (10 U/L).	Thermo Fischer Scientific GmbH, Darmstadt, Germany
RPMI-1640 w L-glutamine w/o NaHCO ₃	Biochrom GmbH, Berlin, Germany
Sabouraud's agar plates + gentamicin and chloramphenicol	Oxoid™ GmbH, Wesel, Germany
Silicone non-reinforced sheets	AMT Aromando Medizintechnik GmbH, Düsseldorf, Germany
Taq DNA polymerase, 0.5 U	Hoffmann-La Roche, Basel, Switzerland
Voriconazole (C ₁₆ H ₁₄ F ₃ N ₅ O)	Discovery Fine chemicals, Wimborne, UK
Zymolyase® 20T 20 U/mg	Carl Roth GmbH, Karlsruhe, Germany

Table 2. Media used in this study

media	components
AM3	2X AM3 commercial medium + 2% (w/v) glucose D + monohydrate in dH ₂ O
CAC	1.5% (w/v) Chromagar™ Agar, 1.02% (w/v) peptone, 2.2% (w/v) chromogenic mix, 0.05% (v/v) chloramphenicol (pH = 6.1 ± 0.2)
CMA	1.7% (w/v) commercial Corn Meal agar in dH ₂ O (pH = 6 ± 0.2)
LB	0.5% (w/v) tryptone, 1% (w/v) yeast extract, 0.5% (w/v) NaCl
modified 2X RPMI	2.08% (w/v) RPMI-1640 w glutamine w/o bicarbonate, 6.90% (w/v) MOPS, 3.6% (w/v) glucose in dH ₂ O (pH = 7. with NaOH)
RPMI	RPMI-1640
SAB/SDA	6.5% (w/v) Sabouraud's agar in dH ₂ O (pH = 5.6 ± 0.2)
YPD agar	1% (w/v) bacto yeast extract, 2% (w/v) bacto peptone, 2% (w/v) glucose and 2% (w/v) agar

MATERIALS AND METHODS

Continued from previous page

YPD medium	1% (w/v) bacto yeast extract, 2% (w/v) bacto peptone, 2% (w/v) glucose in dH ₂ O
YPD + Phloxine B	1% (w/v) bacto yeast extract, 2% (w/v) bacto peptone, 2% (w/v) glucose, 2% (w/v) agar and 0.5% (w/v) Phloxine B (filter sterilized) in dH ₂ O

Table 3. Solutions used in this study

general solutions	components
PBS 10X	0.8% (w/v) NaCl, 0.02% (w/v) KCl, 0.14% (w/v) Na ₂ HPO ₄ , 0.24% (w/v) KHPO ₄ in a final volume of 1 liter (pH = 7.4)
SDS/EtOH	1 % SDS (w/v), 50 % (v/v) ethanol in 500 ml dH ₂ O
TAE 50X	0.024% Tris base, 5.71% (v/v) glacial acetic acid, 500 mM EDTA (pH 8.0) in a final volume of 1 liter. Working solution: TAE 1X (49:1) (filter sterilized)

Table 4. Solutions used in this study

specific solutions	components
lysis buffer (genomic DNA isolation)	100 mM Tris-HCl (pH = 8), 50 mM EDTA, 1% (w/v) sodium dodecyl sulfate (SDS)
matrix (MALDI-TOF)	(l) HCCA in 50% (v/v) acetonitrile and 0.125% (v/v) TFA acid
PFGE washing buffer	20 mM Tris-Hcl (pH = 8.0) and 50 mM EDTA in a final volume of 1 liter.
proteinase K reaction solution	100 mM EDTA (pH = 8.0), 0.2% Na deoxycholate 97%, 1% N-lauroylsarcosine sodium salt and 1 mg/ml proteinase K
zymolyase solution	10 mM Tris-HCl (pH = 7.2), 50 mM EDTA, 0.1 mg/ml zymolyase 20T

All media and general solutions used in this study were sterilized for 15 min. at 121°C. The RPMI and AM3 used in the antifungal susceptibility as well as specific solutions with thermolabile additives (e.g. enzymes) tests were filter sterilized.

2.1.1 Synthetic oligonucleotides

MATERIALS AND METHODS

Synthetic oligonucleotides used for Polymerase Chain Reaction (PCR) amplification and gene sequencing were purchased from Sigma-Aldrich (Steinheim, Germany) and detailed in Table 5.

Table 5. oligonucleotides used for PCR amplification

name	amplifies	primer sequence (5'-3')
CPAR2_404800-ALS7-F	central region	5'-CCAACCACCACAGTCACAACATCT-3'
CPAR2_404800-ALS7-R	central region	5'-GGAGACAGTAGATGATAATTGC-3'
CPAR2_403520-HWP1-F1	central region	5'-CTTGCTCGAATGGTGGATGC-3'
CPAR2_403520-HWP1-R1	central region	5'-ACCGTTGTTGTCTTGATCGA-3'
CPAR2_404790-F1	5' region	5'-CACCACCGCATTGGACTG-3'
CPAR2_404790-R1	5' region	5'-CACCTTCCCCAGTCCAGAAC -3'
CPAR2_303740-ERG11-F1	5' region	5'-TAGTGGGATCGGTGGATCTT -3'
CPAR2_303740-R-ERG11-R1	5' region	5'-CTTTATCTAAATCAGCATACAATTGAG-3'
CPAR2_303740-ERG11-F2	3' region	5'-TCTAGATCCTTATTAGGAGAAGCAATG-3'
CPAR2_303740-ERG11-R2	3' region	5'-ACTGACTCCTGCCCTCAGATT-3'
CPAR2_807270-MRR1-F1	5' region	5'-CTGTATGGAGAGAGTGAGATTTTAGGTT -3'
CPAR2_807270-R-MRR1- R1	5' region	5'-TCCTTGGTTACCTCATTGCTC -3'
CPAR2_807270-F-MRR1-F2	central region	5'-GGTGATGGGGCTGACTCAAA -3'
CPAR2_807270-R-MRR1-R2	central region	5'-GCTCCACCTTGCCAATTTGG-3'
CPAR2_807270-F-MRR1-F3	3' region	5'-ATGGAGACCATTAATTTTTTTGACA-3'
CPAR2_807270-R-MRR1-R3	3' region	5'-GAATGACTTCATTGAAATGTAATGCT-3'

2.1.2 *Candida spp.* clinical isolates

The *C. glabrata*, *C. parapsilosis* and *C. albicans* clinical strains isolated during the course of this study are detailed in the appendix (Appendix).

2.1.3 *Candida spp.* reference strains

Table 6. List of *C. parapsilosis* reference strains used in this study

MATERIALS AND METHODS

clinical isolate	genotype, source of isolation and origin	collection	reference	provider
CDC 317	ATCC [®] MYA-4646 [™] , CDC 317, health care worker's hand, unknown	(1) American Type Culture Collection, ATCC [®] , Manassas, USA	(Kuhn <i>et al.</i> , 2004)	(1)
ATCC 22019	ATCC [®] 22019 [™] , CBS 604, DSMZ-5784, case of sprue, Puerto Rico	(2) German Collection of Microorganisms and Cell Cultures, DSMZ, Leibniz Institute, Braunschweig, Germany	Ashford, 1928	(2)
CBS 1954	ATCC [®] 28474 [™] environmental, olive fruit, Italy	American Type Culture Collection, ATCC [®] , Manassas, USA		CRG, Barcelona, Spain
CBS 6318	ATCC [®] 7330 [™] , man healthy skin, USA	American Type Culture Collection, ATCC [®] , Manassas, USA	Meyer, 1994	CRG, Barcelona, Spain
GA-1	SZMC 8110, clinical isolate, human blood, Hamburg, Germany	University Clinic Hamburg-Eppendorf, Hamburg, Germany	(Gácsér <i>et al.</i> , 2005, 2007)	CRG, Barcelona, Spain

Table 7. List of *C. glabrata* reference strains used in this study

CBS-138	ATCC [®] 2001 [™] , CBS 138, JCM 3761, NBRC 0622, NRRL Y-65, man feces, unknown	(3) Westerdijk Fungal Biodiversity Institute, CBS-KNAW, Utrecht, The Netherlands	Anderson, 1917	(3)
ATCC90876-CRIB	ATCC [®] 90876 [™] , human blood, Essen, Germany*	Regional Centre for Biomedical Research, Albacete, Spain	Dermoumi, 1994	(4)

Table 8. List of *C. albicans* reference strains used in this study

SC5314	ATCC [®] MYA-2876 [™] , clinical human specimen, unknown	American Type Culture Collection, ATCC [®] , Manassas, USA	(Gillum <i>et al.</i> , 1984; Fonzi and Irwin, 1993)	(1)
WT (SC5314)-GFP	P _{eno1} -EGFP _{NAT} ^{R*}		(Wheeler <i>et al.</i> , 2008)	VBC, Vienna, Austria

2.2 Methods

2.2.1 Routine diagnostic procedures

In order to routinely analyze clinical specimen for fungal growth, samples were provided from the diagnostic laboratory, where they were plated onto Sabouraud's GC agar in addition to other agars and these incubated at 35°C overnight. Yeast species were restricted in order to ensure single pure cultures and identified using MALDI-TOF (MALDI Biotyper, Bruker Daltonics, Bremen, Germany) using the YOTL database (Bernhard *et al.*, 2014). Routinely susceptibility testing was performed on a VITEK2 system (BioMérieux, Nürtingen, Germany).

2.2.2 *Candida spp.* strain maintenance and growth conditions

Once transferred to the research laboratory, mixed cultures were further differentiated on YPD agar, *C. parapsilosis* clinical isolates (n = 220) plus the *C. parapsilosis* reference strains (n = 5) (Table 6) were replated onto Sabouraud's GC, YPD agar (1% yeast extract, 2% peptone, 2% glucose, 2% agar) and YPD agar plus 5 mg/ml Phloxine B and subsequently incubated at 30°C and 37°C for pseudohyphae induction (Appendix).

In contrast, all *C. glabrata* clinical isolates (n = 488) plus *C. glabrata* (n = 2), (Table 7) and *C. albicans* (n = 2), (Table 8) reference strains were plated onto SAB's GC agar and Columbia (COS) blood agar and incubated at 37°C (mimicking human body temperature), (Appendix 1).

Individual lineages obtained were long-term preserved at -70°C in cryovials. Independent *Candida* colonies from both species were routinely grown in 3 ml of liquid YPD (1% yeast extract, 2% peptone and 2% glucose) at 37°C and 220 rpm. Before each experiment, cells were replated at least twice to confirm proper growth and pure cultures.

2.2.3 MALDI-TOF analyses species-identification

Patient isolates were classified and plated in selected media, after a previous susceptibility test (VITEK[®]2, BioMérieux, Nürtingen, Germany), clinical samples were quickly characterized using species identification YOTL (Yeast On-Target-Lysis) preparation was conducted. Briefly, single colonies were streaked onto a steel MALDI target and one μl of 70% formic acid Rotipuran[®] was added to lyse the cells. After drying, 1 μl matrix solution (α -cyano-4-hydroxycinnamic acid in 50% acetonitrile, 0.125% trifluoroacetic acid) was added and left to crystalize at room temperature. When no accurate identifications were obtained, full extractions of proteins were performed following the protocol provided by the manufacturer (Bruker Daltonics, Bremen, Germany). Several colonies from pure cultures were dissolved in 200 μl of milli-Q water. Nine hundred μl of absolute 100% ethanol were added to the cell suspension. Cells were mixed and 200 μl of the solution were centrifuged at 12000 rpm for 2 min. The supernatant was discarded and the pellet was dried out for 10-15 minutes. Between 25-50 μl of formic acid Rotipuran[®] $\geq 98\%$ were added to the suspension. Cell solution was incubated for 10 min. at RT. Equal amount of MS-grade acetonitrile as formic acid was added and centrifuged for 2 min. at 12000 rpm. One μl of the proteins presented in the supernatant were dispensed on the target before adding the MATRIX solution. All sample preparations were done in duplicate and the spectra automatically analyzed by MALDI Biotyper 3.1 software on an Autoflex III mass spectrometer (both from Bruker Daltonics, Bremen, Germany). *C. parapsilosis* and *C. glabrata* reference strains spectra were already incorporated in the system and established as baseline for new specie-identification. Standard settings defined by the automated acquisition mode were used during the measurements. A recommended cut-off of log score value of ≥ 2.000 was used to discriminate false positives and valid identifications.

2.2.4 *C. glabrata* biofilm formation capacity to polystyrol

To analyze the capacity of *C. glabrata* clinical isolates to form biofilms in abiotic surfaces used in nosocomial environments, a modified quantitative CV-biofilm formation assay was

MATERIALS AND METHODS

performed (Figure 12) (Gómez-Molero *et al.*, 2015; Kuhn *et al.*, 2002; Ramage *et al.*, 2001). *C. glabrata* clinical isolates (Appendix) plus the *C. glabrata* reference stains (Table 7) were cultured as detailed in 2.2.2. The optical density was measured (A_{600}), (Smart Spec 3000; Bio-Rad) and adjusted to an OD = 2. Cell suspensions were diluted 1+3 to a total volume of 200 μ l YPD into the 96-well plates (Greiner Bio-One, Frickenhausen, Germany) and incubated at 37°C for 24h. Medium was removed putting the plates upside down. Planktonic cells were discarded tapping the plate gently and washing once with 200 μ l of milli-Q water. Attached biofilms were stained for 30 min with 100 μ l 0.1% (w/v) CV solution.

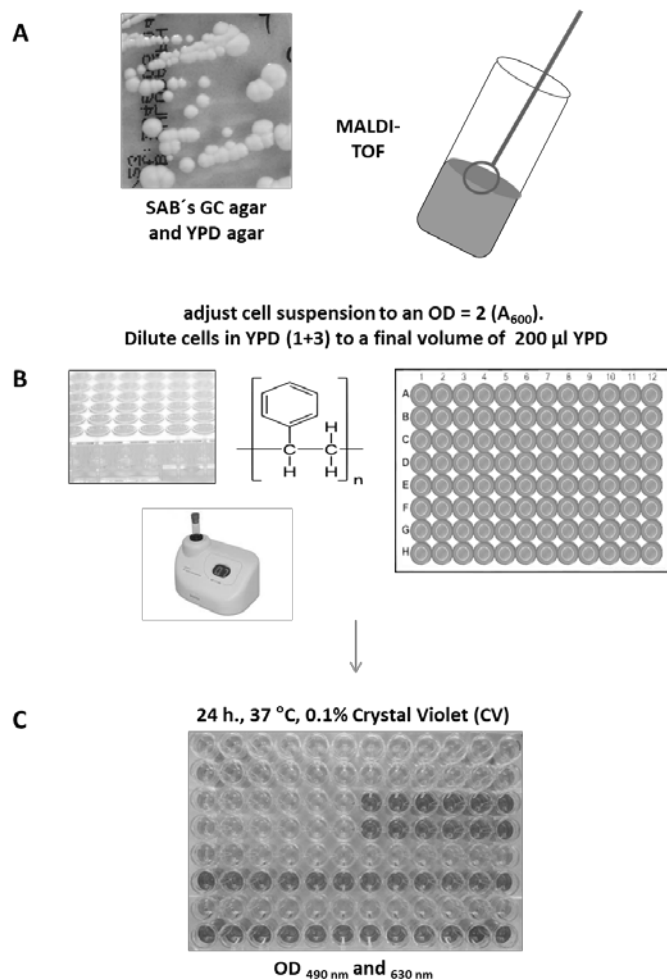


Figure 12. Schematic *C. glabrata* biofilm formation to polystyrol. (A) *C. glabrata* incubation and species-determination using MALDI-TOF Biotyper. (B) Cells adjustment to OD_{600nm} = 2. (C). Biofilm quantification by CV staining method. Total biofilm formation capacity to polystyrol was measured at (A_{490}) and (A_{630}).

MATERIALS AND METHODS

Excess dye was washed away once with 200 μ l milli-Q water. Biofilms were disrupted by carefully mixing in 200 μ l 1% (w/v) SDS in 50% (v/v) ethanol. Crystal violet staining intensity was measured at OD_{490nm} and OD_{630nm} (MRX-TC Revelation, Dynex Technologies GmbH, Denkendorf, Germany). All data shown is the average of two independent experiments with four biological replicates, classified in three different categories as LBF, IBF and HBF. Statistical unpaired t-test (Welch's t-test) analyses compared with the CBS-138 were performed for all the clinical isolates of the study.

2.2.5 *C. glabrata* biofilm formation capacity to silicone elastomers

To analyze biofilm formation capacity to silicone elastomers (Gómez-Molero *et al.*, 2015), *C. glabrata* clinical isolates (detailed in the Appendix) were incubated in SAB'GC agar and YPD agar section 2.2.2. Liquid cultures were grown overnight at 37 °C. The isolates were adjusted to an OD of 0.8 McFarland in 4 ml of NaCl_{physiol.}. One hundred μ l of the solution were added to 15 ml glass tubes containing 1 piece of a 1cm X 1cm silicone squares cut from larger non-reinforced sheets (AMT Aromando Medizintechnik GmbH, Düsseldorf, Germany). The cells plus the piece of silicone were incubated in 4 ml of YPD medium in an orbital shaker at 37 °C overnight. The silicone pieces were deposited in a 12-well plate (Greiner Bio-One, Frickenhausen, Germany) and unbound cells were washed out with 1 ml of PBS 1X, the pieces of silicone were transferred to a new plate containing 1 ml of fresh PBS. The silicone was scratched to remove the *Candida* biofilms bound to the entire surface. Biofilm production was quantified by measuring optical density of a cells/PBS solution (1:100) on the MRX-TC Revelation microplate reader (Dynex Technologies GmbH, Denkendorf, Germany) at OD_{600nm}. The data shown were performed in duplicate and the average and standard deviation of each biological replicate calculated (Figure 13).

MATERIALS AND METHODS

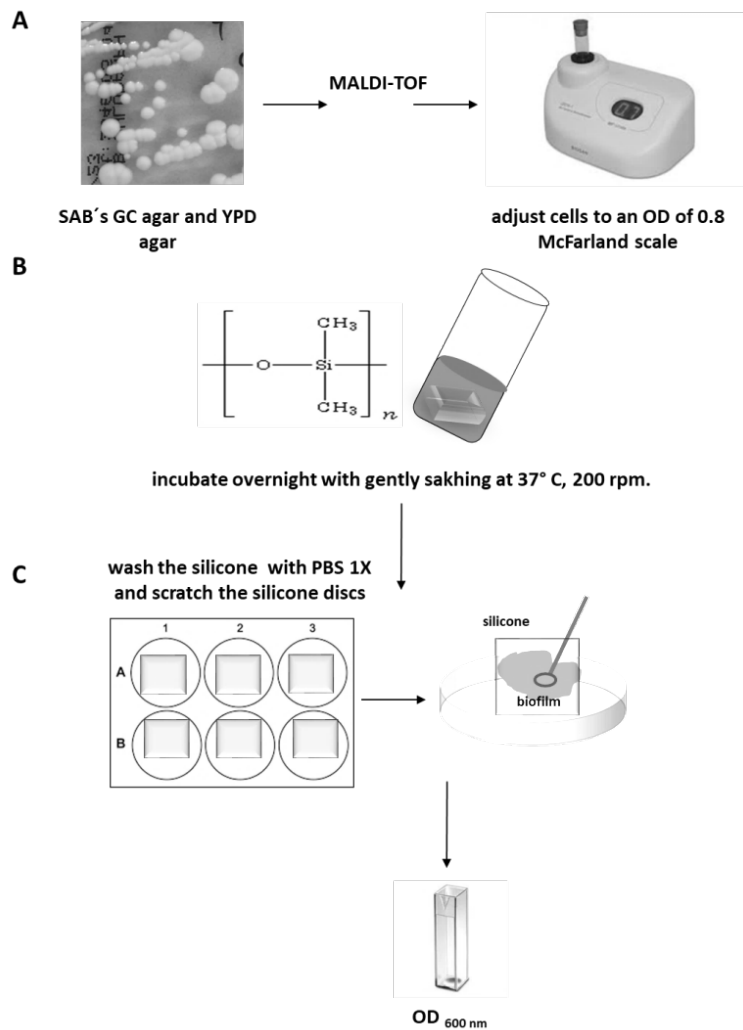


Figure 13. Schematic *C. glabrata* biofilm formation to silicone. (A) *C. glabrata* incubation and species-determination using MALDI-TOF Biotyper. (B) Cells adjustment to and OD of 0.8 McFarland. (C) Silicone pieces were scratched and cells suspension quantified at (A₆₀₀).

2.2.6 *C. parapsilosis* biofilm formation capacity to polystyrol

To assess *C. parapsilosis* biofilm quantification, stable morphotypes and phenotypic switch have to be determined (Anderson and Soll, 1987 ; Laffey and Butler, 2005). Colonies were plated and incubated on selective media (2.2.2) at 30 °C for 96 h. After four days of incubation, independent colonies presented defined morphotypes (e.g. “smooth”, “crater”, “concentric” or “crepe”). Biofilm production of *C. parapsilosis* clinical isolates to plastic materials (polystyrol) was quantified by CV staining as described before for *C. glabrata* (2.2.4). The clinical isolates used in this study are detailed in the (Appendix). Statistical analyses using unpaired t-test (Welch’s t-test) were conducted and all data shown is the average of at least two independent biological experiments with four technical replicates

MATERIALS AND METHODS

each (Figure 14). A modified biofilm quantification assay was performed to increase accuracy in colony-morphotype biofilm quantification. The optical density of single colonies was determined using a McFarland standard n° 4 ($A_{600 \text{ nm}} = 0.431$ with a Compact Benchtop Densitometer, DEN 1A, SIA BioSan, Riga, Latvia) dissolved in 4 ml of $\text{NaCl}_{\text{physiol}}$. The cell suspension was measured again at (A_{600}) (Ultrospec 1000) and adjusted to a value of 2 using sterile $\text{NaCl}_{\text{physiol}}$. The cells were diluted 1+3 to a final volume of 200 μl YPD in 96-well microtiter plates. Biofilms were incubated ON at 37°C (pseudohyphae induction temperature) and biofilms were measured as detailed before for *C. glabrata*. The data shown is the average of at least two independent biological experiments with four technical repeats each.

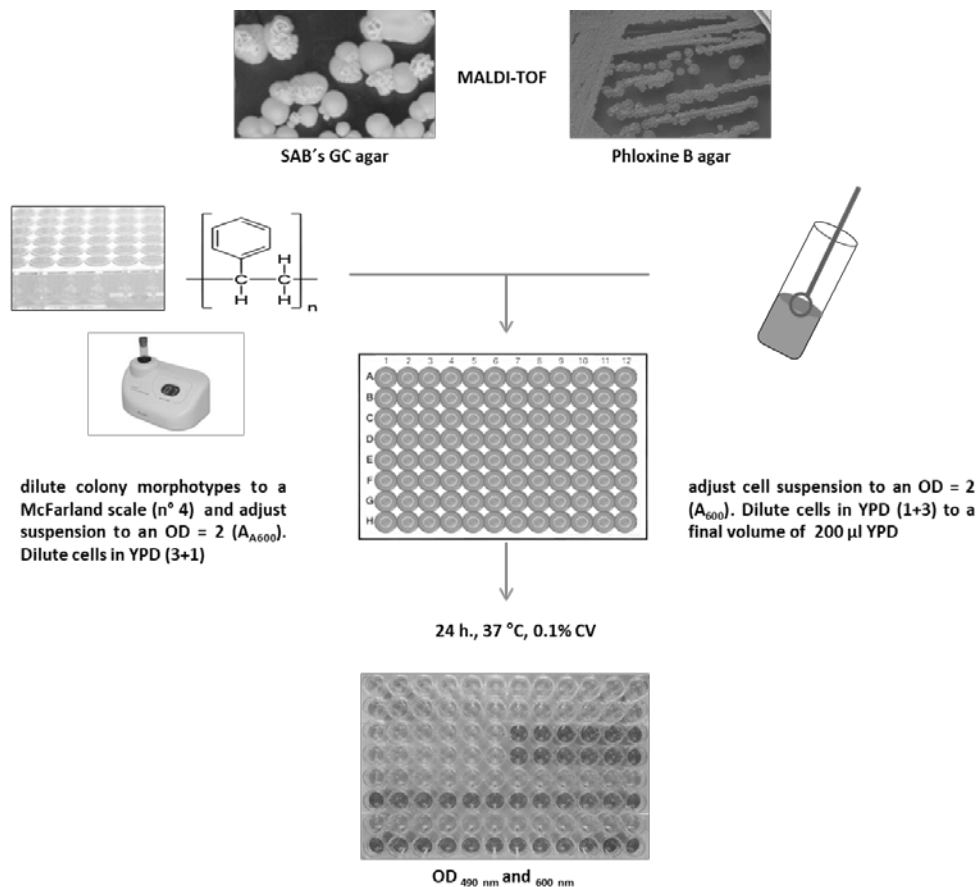


Figure 14. Schematic *C. parapsilosis* biofilm formation capacity to polystyrol. Top row: MALDI-TOF identification of *C. parapsilosis* colony morphotypes. Middle row, cell adjustment to an initial OD = 0.5 in non-treated 96-well microtiter plates. Bottom row: cell incubation for 24 h. at 37°C and biofilm quantification by CV staining. Colorimetric determination on MRX-TC Revelation microplate reader at 490 nm and 600 nm.

2.2.7 Antifungal susceptibility test

To determine the minimal inhibitory concentration towards FLU, ISA, VOR, POS, MICA, CAS, 5FC, AMB for *C. glabrata* and *C. parapsilosis* in our clinical strain collection (Appendix), antifungal susceptibility tests were performed based on the protocols previously described by (Arendrup *et al.*, 2012) and determined according to EUCAST EDef 9.0 method. Prior to analysis, the clinical isolates were replated overnight onto SAB's GC agar plates (Oxoid™ GmbH, Wesel, Germany). Cells were adjusted to a target value of 0.5 McFarland with NaCl_{physiol.}. A 10 fold dilution was prepared and 100 µl of the suspension were added to 96-well microtiter plates that already contained serial antifungal dilutions as defined by EUCAST standardized broth microdilution (Table 9) method v 9.0 The antifungal stocks solutions of 5FC, CAS, and MICA were dissolved in mQ water, the FLU was dissolved in 75 % methanol and the DMSO was the solvent selected to dilute VOR, ISA, and AMB. Antifungal dilutions were resuspended in 2X RPMI-1640 medium (FLU, ISA, VOR, POS, MICA, CAS, 5FC) and AM3 (AMB). Plates were incubated 24 and 48h. at 37°C and cell density was read at A₅₃₀ (MRX-TC Revelation microplate reader). The MIC values were calculated according to EUCAST guidelines (*). Clinical isolates were classified as susceptible isolates, when the minimal inhibitory concentration (MIC) was equal or lower than the clinical breakpoints and non-susceptible or resistant isolates, when the minimal inhibitory concentration values were higher than the EUCAST breakpoints (Orasch *et al.*, 2014). Cross-resistance is defined by non-susceptibility for at least two drugs in the same classification group (azoles or echinocandins) and multi-resistance species presented values higher than the clinical breakpoints for, at least, two kinds of antifungals at the same time.

Table 9. Description of antimycotic dilutions used in antifungal susceptibility test

antimycotic		serial inhibitory concentrations (µg/µl)										
AMB	polyene	4	3	2	1.5	1	0.750	0.500	0.375	0.250	0.188	0.125
5FC	nucleoside	32	16	8	4	2	1	0.500	0.250	0.125	0.063	0.031
FLU	triazole	256	128	64	32	16	8	4	2	1	0.500	0.250
POS	triazole	4	2	1	0.5	0.250	0.125	0.063	0.031	0.016	0.008	0.004
VOR	triazole	32	16	8	4	2	1	0.500	0.250	0.125	0.063	0.031
CAS	echinocandin	4	2	1	0.500	0.250	0.125	0.063	0.031	0.016	0.008	0.004
MICA	echinocandin	4	2	1	0.500	0.250	0.125	0.063	0.031	0.016	0.008	0.004

2.2.8 Agar invasion capacity

Agar invasion capacity of *C. parapsilosis* colony morphotypes was tested based on the protocols described by (Laffey and Butler, 2005). Cells taken from colonies with distinct morphotypes were plated on commercial SAB's GC agar plates (control) and YPD agar plates supplemented with 5 mg/ml of Phloxine B (2.2.2). Plates were incubated for 10 days at 30°C, recording the morphotype once per day, starting from day 4, recording the state photographically for selected plates. Plates were finally scored before and after wash cells out the agar plate under running water on day 10. Morphotypically mixed plates were also checked determining different gradients of invasion on agar depending on the morphotype observed. Ranked classification of agar invasion used was defined as: low invasion (1), low-medium (2), medium (3), medium-high (4), high (5) and very high (6, cells could not be removed after the plate were rinsed).

2.2.9 Optical and phase-contrast microscopy

To visualize variations in cell morphology between different clinical morphotypes, independent colony-phenotypes were routinely prepared as detailed in 2.2.2. Cells were adjusted to an OD = 2 (A_{600}) and washed two times with PBS. For aggregation analyses, cells from defined colony-types were grown ON in 3 ml YPD and YPD medium plus 2.5 mg/ml Phloxine B in an orbital shaker. Cell density was adjusted to an $OD_{600} = 2$ and washed twice with PBS. Aggregation was observed at 10X magnification (Axiovert 200M, Carl Zeiss AG, Oberkochen, Germany). For an accurate determination of cell morphologies, ON cultures were adjusted to the exponential phase in fresh YPD and stained with 200 μ l of 0.1% Blankophor P solution for 20 min. at RT. Cells were washed with PBS and fixed with 200 μ l 100% methanol for 5 min. After washing the cells twice with PBS, cells were embedded in Mowiol® 4-88 and observed at 100X magnification with immersion oil. Cell-morphology variability between morphotypes was analyzed by the imaging software Axiovision 2.05 (Carl Zeiss, Oberkochen, Germany).

2.2.10 Sedimentation assay of clinical morphotypes

To analyze the sedimentation speed of *C. parapsilosis* strains with different morphotypes, the protocol previously published for *C. glabrata* (Gómez-Molero *et al.*, 2015) was used. Strains selected were grown as described in section 2.2.2. Colonies were inoculated into 3 ml YPD medium and grown ON at 37 °C. The cultures were pelleted and washed with PBS and the optical density was measured (A_{600}), the experiment was performed in duplicate and the samples were adjusted to the lowest OD per replicate. The initial optical density was measured and calculated as $T=0$, and the cell suspensions were regularly measured (Smart Spec 3000; Bio-Rad) (A_{600}) with an interval of 15 minutes until the final time point $T=120$ was achieved. The capacity (%) of sedimentation of each colony morphotype was calculated using $(OD_{600t=1}/OD_{600t=0}) * 100$. The sedimentation percentage of each isolate at each time point is the average of two biological replicates and two technical repetitions.

2.2.11 Electrophoretic karyotyping of colony morphotypes

Intact chromosomes were separated by pulsed-field gel electrophoresis (PFGE) as described before by (Bader *et al.*, 2012; Carreté *et al.*, 2018). *C. parapsilosis* and *C. glabrata* cells were prepared as detailed in 2.2.2. Equal amount of cell suspension and 2% agarose (1:1) both preheated to 60°C were mixed and cast in a 1 x 0.5 x 0.1 casing cell. The blocks were left to solidify at 4°C for approximately 30 minutes and then transferred into 5 ml of a zymolyase solution (10 mM Tris-HCl (pH = 7.2), 50 mM EDTA and 0.1 mg/ml zymolyase 20T). The samples were incubated ON at room temperature (RT) with gentle shaking. Plugs were washed four times with 5 ml washing buffer (20 mM Tris-HCl (pH = 8.0) and 50 mM EDTA) and transferred to fresh tubes. Five ml of proteinase K reaction solution (100 mM EDTA (pH = 8.0), 0.2% Na deoxycholate 97%, 1% N-lauroylsarcosine sodium salt and 1 mg/ml proteinase K) were incubated with gentle shaking for 24 hours. The blocks were washed four times with washing buffer solution (20 mM Tris-HCl, pH = 8.0 and 50 mM EDTA) and stored at 4°C. Agarose blocks containing *C. parapsilosis* and *C. glabrata* DNA were cut in pieces of approximately 0.25 cm (“plugs”) and cast in a 1% agarose gel. The gels were placed in a PFGE running chamber (CHEF-DR II Electrophoresis,

MATERIALS AND METHODS

Bio-Rad laboratories, München, Germany) containing 1X TAE buffer (40 mM Tris (pH = 7.6), 20 mM acetic acid and 1 mM EDTA). Running conditions for *C. glabrata* were adapted to using 1.2% agarose at 17°C and pulse times from 40-100 sec. for short chromosomes and 60-140 sec. for large chromosomes. In case of *C. parapsilosis*, running time was increased in 4 h. (initial pulse time 70 sec., final pulse time 140 sec., 26h run time in 1X TAE at 200V and 17°C) for better resolution. The gels were stained ON with 3 µl 10000X GelRed[®] in 30 ml of dH₂O. Chromosome distributions were analyzed by Gel Doc XR imaging software (Bio-Rad Laboratories GmbH, München, Germany).

2.2.12 Genomic DNA isolation

To analyze the variability of adhesin-encoding genes between *C. parapsilosis* clinical isolates, stable morphotypes were cultured overnight in YPD medium at 30°C. (2.2.2). Cells were harvested by centrifugation at 7168 g for 5 min in screw cap tubes. After washing the cells with 200 µl Tris-HCl, 200 µl of genomic DNA lysis buffer 100 mM Tris-HCl (pH = 8), 50 mM EDTA, 1% (w/v) SDS and 0.5 mm glass beads were added (two times the amount of pellet used). Two hundred µl of 25:24:1 phenol/chloroform/isoamyl alcohol were incorporated to the samples, and the cells were lysed by 2X fastprepping (Thermo Savant FastPrep[®] FP 120 cell homogenizer, Qbiogene, Cedex, France) at 4.5 m/s for 30 sec. After fastprepping, phases were separated by centrifugation for 5 min at 16128 g, and supernatant was collected. One ml of 100% cold ethanol was gently added in 200 µl supernatant and stored for 30 min. at -20 °C for DNA precipitation. The solution was centrifuged at 4°C for 5 min. at 16128 g and the supernatant discarded. Excess of EtOH was dried out and DNA was resuspended in 25 -30 µl TE-buffer containing RNase A. DNA quality was checked by running a 1% agarose gel, and DNA concentration was determined (Nano Drop 2000[™], Thermo Fisher Scientific, Darmstadt, Germany).

2.2.13 Polymerase chain reaction analyses of adhesin-encoding genes in clinical morphotypes

To analyze the gene variability of adhesin repeat regions within clinical morphotypes (bsc-1700, nsc-170, tsc-1702, ncc-1701, tcc-1702), PCR analyses of selected *C. parapsilosis* adhesin-encoding genes were tested including CDC 317, ATCC 22019, CBS 1954, CBS 6318 and GA-1 as reference strains. PCR reactions contained 80-100 ng of genomic DNA plus 0.2 μ M of CPAR2_404790-F1, CPAR2_404790-R1; CPAR2-404800-ALS7-F, CPAR2-404800-ALS7-R and CPAR2_403520-HWP1-F, CPAR2_403520-HWP1-R, (Table 5), 200 μ M PCR grade nucleotides (dNTPs), 1X PCR reaction buffer + Mg (5 μ l/50 μ l PCR) and 2 units/50 μ l PCR of *Taq* DNA polymerase in a final volume of 50 μ l. The reaction was run in a T100™ Thermocycler (Bio-Rad laboratories, München, Germany). PCR reaction conditions consist on a denaturation step for 1 min at 95°C, followed by 30 cycles of 30 sec. at 95°C, 4 min. at a corresponding annealing temperature of 68.2°C and an elongation step of 5 min. at 72°C with a final 5 min. extension step at 72°C.

To analyze azole-resistant genes in selected *C. parapsilosis* clinical isolates (PEU651, PEU768, PEU941, PEU950), PCR reactions were performed as the reactions specified before and amplified with CPAR2_303740-ERG11-F1, CPAR2_303740-ERG11-R1, CPAR2_303740-ERG11-F2; CPAR2_303740-ERG11-R2; CPAR2-807270-MRR1-F1, CPAR2-807270-MRR1-R1; CPAR2_807270-MRR1-F2, CPAR2_807270-MRR1-R2 and CPAR2_807270-MRR1-F3, CPAR2_807270-MRR1-R3, (Figure 5). General PCR reaction conditions for adhesin-encoding genes amplification started with a denaturation step for 1 min at 95°C, followed by 30 cycles of 30 sec. at 95°, 1 min. at a corresponding annealing temperature of 60°C and 65°C (depending on the length of the fragment), an elongation step of 3 min. at 72°C with a 5 min. final elongation at 72°C after which, the samples were cool down to 4°C.

DNA fragments were analyzed using a 1% agarose gel at 130 volts for 45 minutes. All gels were prepared in a final volume of 100 μ l and 140 μ l of TAE 1X and developed using Bio-Rad Chemidoc software (Bio-Rad Laboratories GmbH, München, Germany).

2.2.14 DNA Sanger sequencing

PCR products were purified using Nucleospin® Gel and Clean-up DNA purification Kit (Macherey-Nagel, Düren, Germany). PCR products of *C. parapsilosis* adhesin-encoding and azole's-resistant genes were sequenced applying Sanger technology by Microsynth Seqlab (Göttingen, Germany), the same set of oligonucleotides employed in Polymerase Chain Reaction were used for standard sanger sequence analyses and detailed in Table 5.

For a proper Sanger sequence, 18 ng per 100 bp of purified PCR product and 30 pmol of specific F or R CPAR2-oligonucleotides (Table 5) in a final volume of 12 µl were processed by Microsynth Seqlab, Göttingen, Germany.

2.2.15 *Candida* cell wall isolation

Prior to performing mass spectrometry analyses to identify specific cell wall proteins, *C. parapsilosis* and *C. glabrata* cell walls were isolated in collaboration with Dr. Piet de Groot (Department of Medical Mycology, Centre for Biomedical Research (CRIB), Albacete, Spain). Cell walls were prepared following the protocol previously described (Gómez-Molero *et al.*, 2015; de Groot *et al.*, 2004, 2008). Clinical isolates (Appendix) were cultured overnight in YPD medium at 37°C (2.2.2), after which the cells were harvested. The cells were washed and resuspended in 10 mM Tris-HCl at pH 7.5 in 2 ml). Glass beads, Tris buffer and protease inhibitor were added to the screw cap tubes. Six rounds of disruption for 30 seconds at 6.5 m/s in a Fastprep machine (Fast-Prep®-24, MP Biomedicals GmbH, Thüringer, Germany) were enough for cell full breakage, and this was verified under the microscope. After cell breakage, cell wall material was once washed with 1 M NaCl, and boiled twice for 5 min with SDS extraction buffer (50 mM Tris HCl, 2% SDS, 100 mM Na-EDTA, 150 mM NaCl, and 0.8% (114 mM) β-mercaptoethanol, pH 7.8). After the SDS/β-Me extraction step, the cells were washed extensively with mQ water. Finally, the cell wall material was frozen in liquid nitrogen, lyophilized and stored at -20°C.

2.2.16 *Candida spp.* genome sequencing analyses

C. parapsilosis and *C. glabrata* genome sequences were determined in collaboration with the group of Dr. Toni Gabaldón (Centre for Genomic Regulation (CRG) Barcelona, Spain). Strains were sequenced following the protocol already described by (Carreté *et al.*, 2018; Prysycz *et al.*, 2013; Carreté *et al.*, 2019) using either Illumina Genome Analyzer IIx (GA) or HiSeq 2000 (HS) sequencing platforms. All sequence data were deposited after publication in Sequence Read Archive (SRA, NCBI) (Carreté *et al.*, 2018).

2.2.17 *In vivo* infection analyses using the *Galleria mellonella* animal model

For analysis of the virulence potential of different *C. parapsilosis* and *C. glabrata* clinical isolates, the animal model *Galleria mellonella* were used (Ames *et al.*, 2017; Gácsér *et al.*, 2007; Németh *et al.*, 2013). These analyses were performed in collaboration with Dr. Attila Gácsér, Department of Microbiology, University of Szeged, Hungary. *G. mellonella* caterpillars (R.J. Mous Live Bait, Balk, The Netherlands) were selected with the same body size and previously incubated at 30°C ON. *C. parapsilosis* and *C. glabrata* clinical isolates used in this study were listed in the Appendix 1 plus the CDC 317, ATCC 22019 (both *C. parapsilosis*) and CBS-138 (*C. glabrata*), respectively. Strains were grown as described in section 2.2.2. *G. mellonella* caterpillars were inoculated with 10 µL of the *Candida spp.* suspensions diluted in PBS 1X containing 6.10^6 yeast cells injected in the last left proleg of the caterpillar using a 26 gauge needle with Hamilton® syringe. The infected caterpillars were placed in an incubator at 37 °C, and survival scored for a period of seven days. Time-dependent survival was calculated using Graphpad PRISM 7 software. Data shown is always the average of two independent biological replicates. Ten non-manipulated caterpillars were used as untreated control and another 10 caterpillars were injected with 10 µL of PBS 1X as negative control.

2.2.18 *C. albicans* and *C. glabrata* identification from patient blood cultures

Candida spp. infected blood cultures were selected from patients with a previous diagnostic of *C. glabrata* infection (Appendix). To easily determine the presence of single specie or mixed cultures (*C. albicans* and *C. glabrata*), The AdvanDX (Woburn, MA, EE.UU.) PNA FISH Kit was used. *Candida spp.*-identification in blood cultures was performed as described before by (Rigby *et al.*, 2002) according to the manufacturer guidelines. The method consists on fluorescence in-situ hybridization (FISH) labels with peptide nucleic acid (PNA) probes. The technique is based on the hybridization selected peptide nucleic acid to the specific *C. albicans* or *C. glabrata* specific ribosomal RNA (rRNA), which directly discriminate between *C. albicans* and *C. glabrata* from positive-blood-culture bottles. The *C. glabrata* blood bottles were stored at -20°C until used. Ten µl of the culture were transferred to a microscope slide that previously contained one drop of the fixation solution (phosphate-buffered saline with detergent). One drop of PNA probes (1.5 ml of PNA probes contains 30% of formamide) was added to the microscope slide that already contains the smear. The coverslip was placed on the drop avoiding bubbles in the probe and the slides were incubated for 30 minutes at 55°C in a water bath. The solution was mixed and let it dry. The smears were fixed by flame-fixation. The test (the *C. albicans* PNA FISH method) is based on a fluorescein-labeled PNA probe that targets *C. albicans* 26S rRNA. The PNA probe is added to smears made directly from the contents of the blood culture bottle and hybridized for 90 min at 55°C. Unhybridized PNA probe is removed by washing of the mixture (30 min), and the smears are examined by fluorescence microscopy

2.2.19 *C. albicans* and *C. glabrata* interaction under phase-contrast microscopy

To analyze *C. albicans/C. glabrata in vitro* cell interaction,, we adapted the protocols already described by Tati *et al.* (2016). Selected *C. glabrata* clinical isolates plus two reference strains (ATCC90876, CBS-138, PEU52, PEU45, PEU382, PEU427) were grown as detailed in section 2.2.2. *C. albicans* reference strain (SC5314) and the genetically modified

MATERIALS AND METHODS

green fluorescence *C. albicans* WT (SC5314-GFP) (Table 8) were culture in 3 ml of liquid YPD at 30°C, ON. *C. albicans* cells were adjusted to an OD_{600nm} = 0.5 and let them grow for 5 h. at 37°C to induce hyphae. Both, *C. glabrata* and *C. albicans* were adjusted to an OD_{600nm} = 1, and co-incubated at 1:1 ratio in fresh YPD for 2 h. Suspensions were filtered and washed with PBS 1X to remove unbound *C. glabrata*. Cells were stained with 200 µl of 0.1% Blankophor P solution for 20 min. at RT, washed with PBS 1X, fixed with 200 µl 100% methanol (Carl Roth Chemie GmbH, Karlsruhe, Germany) for 10 min. and finally embedded in Mowiol® 4-88 (Polyscience Europe GmbH, Hirschberg an der Bergstraße, Germany). Samples were observed at 100X magnification with immersion oil and fluorescent Cy2 filter (534 nm) and DAPI filter (409 nm) to differentiate *C. albicans* cells and hyphae using the imaging software Axiovision 2.05 (Carl Zeiss, Oberkochen, Germany). To discriminate GFP fluorescence intensities for individual yeast cells and hyphal form (*C. albicans*) from non-fluorescent cells (*C. glabrata*), experiments were performed in duplicate.

3. RESULTS

3.1 Genomic plasticity enhances phenotypic diversity in *Candida glabrata* clinical isolates from different clades

3.1.1 Changes in the genome of hyper-biofilm-forming *C. glabrata* isolates

To assess genomic plasticity and phenotypic variability between clinical isolates with respect to biofilm formation, thirty-three genome sequenced *Candida glabrata* clinical isolates from different body sites and global sources were analysed in collaboration with Dr. Toni Gabaldón (CRG, Barcelona, Spain). The study performed by the partner group (Carreté *et al.*, 2018) included genome sequence analyses to stratify differences among clinical isolates with a focus on gene copy number and single nucleotide polymorphisms. In addition, we performed phenotypic and karyotypic analyses.

The collection was composed of isolates from three different body sites. Two hyper biofilm-forming clinical isolates PEU382 (urinary tract) and PEU427 (respiratory tract) (Gómez-Molero *et al.*, 2015), and the reference strain CBS-138 were used as controls. Gastrointestinal tract isolates conformed 18% of the collection, 70% were defined as derived from invasive candidiasis, and 12%, were isolated from oral cavity. SNP-based analyses (Carreté *et al.*, 2018) classified the thirty-three isolates into seven genetic clades, again falling into two larger group sets (Figure 16). Group 1, included clusters I, II, III, and group 2 was constituted by the clusters IV, V, VI, and VII.

First, we examined if genomic and phenotypic variations corresponded with karyotypic changes. Indeed, electrophoretic karyotyping showed chromosome variability between isolates. Only short chromosomes (A-J) of isolates from the same clade follow a similar distribution pattern (Figure 15). This could be observed in certain isolates of clades VI and VII (P35-2, P35-3 = EG01004, F15021, F03013, BG2); I and II (CST34= CST35) and four isolates from clade II (EB101M=BO101S=B1012S= B1012M). Differences in the patterns of

Candida glabrata

the long chromosomes (ChrL, M, and K in CBS138) were observed in the HBF isolates. A correlate to ChrL was not detectable in isolate F15021, possibly due to a rearrangement. Together with coverage analyses (Toni Gabaldón, CRG, Barcelona), aneuploidies in chromosome E (clade differences) and G, as well as a duplication of chromosome J in F2229 were observed (Carreté *et al.*, 2018).

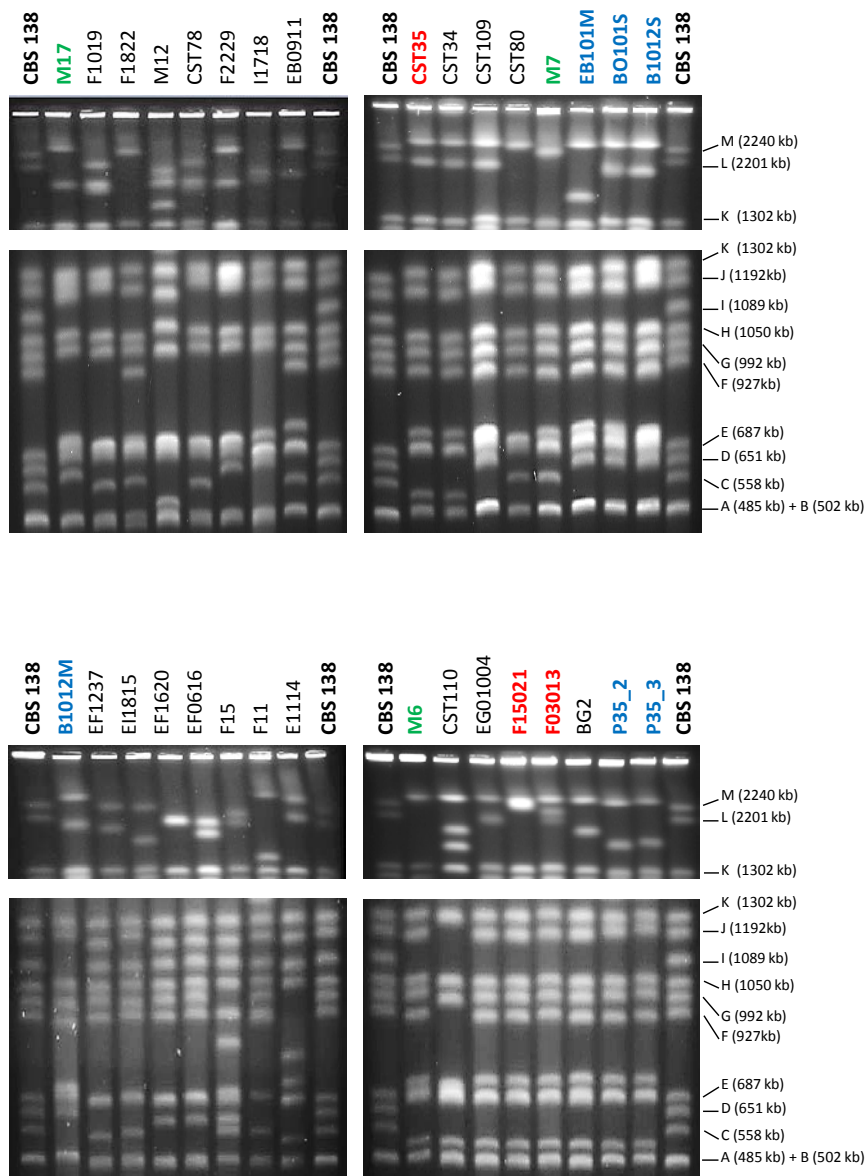


Figure 15. Electrophoretic karyotyping of *C. glabrata* clinical isolates divided in 7 different clades. PFGE of isolates including the control strains used. Top panels show large chromosomes (2240 kb – 1302 Kb). Bottom panels show small chromosomes (1302 Kb -485 Kb). Color code: red, hyper biofilm-forming isolates; green, azole resistant isolates; blue, EB101M/BO101S, B1012S/B1012M and P35_2/P35_3 represent pairs of isolates from the same patient.

Candida glabrata

To determine if karyotypic and phenotypic variations between isolates correlated with changes in MIC, susceptibility towards eight different antifungal compounds was measured. All isolates were susceptible to AMB and thirty-one isolates (31/33), including CBS-138, only showed a low to intermediate range of growth inhibition by azoles (Table 10).

However, M7, M6, and M17 showed reduced susceptibility to one (M17) and four (M7, M6) compounds out of the eight tested: They were 8-16, 32, and up to 2-fold, respectively, times less susceptible to FLU than the control CBS-138. Differential distribution of MICs among the two groups (Figure 16 and Table 10) was observed for POS, but not for the other seven antifungal drugs (AMB, 5FC, ISA, FLU, VOR, CAS, and MICA). Genome analyses indicated no mutation for the resistant-related genes *ERG6*, *FKS1* and *FKS2*, but an amino acid exchange (I390K in M6, I378T in M7, and N306S in M17) in the azole transcriptional regulator *PDR1* was identified. No global correlation between susceptibility data and source of isolation were found in this collective.

Interestingly, M7, M6, and M17 were also all isolated from blood but only classified as LBF (M7, M6) or IBF (M17) (Table 10). Isolates M7 and M6 were highly resistant to azoles (FLU, VOR, POSA, ISA), but had echinocandin MIC values similar to CBS-138. Isolate M17 was partially resistant to FLU (8 µg /µl), but no differences for CAS and MICA were observed. Despite low MIC values, HBF isolates F15021 and F03013 were on the borderline of clinical resistance to MICA (0.032-0.064 µg/µl). Both LBF and IBF isolates varied with respect to susceptibility towards VOR, ISA, and MICA and no azole-susceptibility differences between IBF isolates and HBF were found. (Table 10).

Next, we determined biofilm formation capacity in this isolate set (Figure 16). Only 3 isolates other than controls, showed high (F03013, 0.6205 ± 0.054) or intermediate-high ability to form biofilms on polystyrol (F15021, 0.33 ± 0.066 and CST35, 0.2841 ± 0.045). All these three were obtained from blood cultures. The biofilms formed by three HBF/IBF isolates were 3- to 6.7-fold larger than those formed by CBS-138. Still, this was between 1.3- to 3-fold smaller than those of the two positive controls. However, 22 isolates (22/35) were still significantly different (Figure 16) from the reference strain, but not at levels that were considered HBF.

Table 10. Distribution of MIC values of the eight antifungal drugs in the total number of isolates and selected multi resistant clinical isolates.

µg/ml	AMB		5FC ^c	FLU		VOR ^c	POS ^c	ISA ^c	MICA ^d		CAS ^c
	^a MIC 90	S/I/R	^a MIC 50	MIC 50	S/I/R	MIC 50	MIC 50	MIC 50	MIC 50	S/I/R	MIC 50
M17^b-IBF*	0.004	S	>64	4 – 8	I	0.125	0.500-1	0.032-0.064	0.032-0.064	I-R	0.064-0.125
F1019-LBF**	0.004	S	0.032-0.064	2 – 4	I	0.125	0.500-1	0.032-0.064	0.032	S	0.032-0.125
F1822-LBF	0.004-0.008	S	0.032-0.064	8	I	0.125-0.500	0.500-1	0.064-0.250	0.008-0.032	S	0.064-0.125
M12-LBF	0.004	S	0.032-0.064	8	I	0.064-0.250	0.500-2	0.125	0.016-0.032	S	0.064-0.125
CST78-LBF	0.004	S	0.032	4 – 8	I	0.125	0.500-1	0.064	0.008-0.032	S	0.064-0.125
F2229-LBF	0.004	S	0.032-0.064	4	I	0.125	1	0.064-0.250	0.032-0.064	I-R	0.064-0.125
I1718-LBF	0.004	S	0.032	1	I	0.125-0.250	0.500-1	0.032-0.064	0.004-0.032	S	0.064-0.125
EB0911-IBF**	0.004	S	0.032-0.064	4 – 8	I	0.032-0.125	0.500-1	0.032-0.125	0.016-0.032	S	0.125
<u>CST35^e-HBF***</u>	0.004	S	0.064	8 – 16	I	0.32-1	0.500-2	0.064-0.125	0.032	S	0.032-0.125
CST34-LBF	0.004	S	0.032-0.064	4 – 16	I	0.250-0.500	1	0.064-0.250	0.032	S	0.064-0.125
CST109-LBF	0.004-0.032	S	0.032-0.125	4	I	0.064-0.125	0.250-0.500	0.032	0.032-0.064	I-R	0.064-0.125
CST80-LBF	0.004	S	0.032-0.064	1 – 8	I	0.125	0.500-1	0.032-0.064	0.008-0.032	S	0.064-0.125
M7^b-LBF	0.004	S	0.032-0.064	32-64	R	2	>8	0.250-1	0.032	S	0.064-0.125
EB101M-LBF	0.004-0.008	S	0.032-0.125	1 – 8	I	0.125-0.250	1	0.125	0.032-0.064	I-R	0.064-0.125
BO101S-LBF	0.004-0.008	S	0.032-0.064	4 – 8	I	0.064-0.125	0.500-1	0.032-0.064	0.008-0.064	S	0.064-0.125
B1012S-LBF	0.004	S	0.032-0.064	1 – 4	I	0.064-0.250	0.500-1	0.032	0.032-0.064	I-R	0.032-0.125
B1012M-LBF	0.004	S	0.032-0.064	2 – 4	I	0.125	0.500-1	0.032	0.032-0.064	I-R	0.064-0.250
EF1237-LBF	0.004	S	0.032-0.064	1 – 8	I	0.064-0.125	0.500-1	0.032-0.064	0.0032	S	0.064-0.125
EI1815-LBF	0.004-0.008	S	0.064-0.125	2 – 4	I	0.032-0.064	0.250-0.500	0.032-0.250	0.032-0.064	I-R	0.064-0.125
EF1620-LBF	0.004	S	0.032-0.064	4 – 8	I	0.064-0.250	0.500-1	0.032-0.064	0.032	S	0.064-0.125
EF0616-LBF	0.004-0.008	S	0.032-0.064	8	I	0.125-0.500	0.500-1	0.032-0.064	0.032-0.064	I-R	0.064-0.125

Candida glabrata

Continued from previous page

µg/ml	AMB		5FC ^c	FLU		VOR ^c	POS ^c	ISA ^c	MICA ^d		CAS ^c
	^a MIC 90	S/I/R	MIC 50 ^a	MIC 50	S/I/R	MIC 50	MIC 50	MIC 50	MIC 50	S/I/R	MIC 50
F15-LBF	0.004-0.008	S	0.032-0.064	4 – 8	I	0.125-0.250	1	0.064	0.008-0.032	S	0.064-0.125
F11-IBF	0.004-0.008	S	0.032-0.064	1 – 4	I	0.064-0.125	0.500-1	0.032-0.064	0.032-0.064	I-R	0.064
E1114-LBF	0.004	S	0.032-0.125	4 – 8	I	0.032-0.250	0.250-2	0.032-0.125	0.032	S	0.064-0.125
M6^b-LBF	0.004	S	0.032-0.064	128	R	4	>8	2 – 4	0.032-0.064	I-R	0.032-0.125
CST110-LBF	0.004	S	0.032-0.064	4 – 8	I	0.125	0.500-1	0.032-0.064	0.008-0.032	S	0.064-0.125
EG01004-LBF	0.004	S	0.032-0.064	4 – 16	I	0.25	1-2	0.064-0.250	0.032	S	0.064-0.125
<i>F15021^e</i> -HBF	0.004	S	0.032-0.064	4 – 8	I	0.125	0.500-1	0.032	0.032-0.064	I-R	0.064-0.250
<i>F03013^e</i> -HBF	0.004	S	0.032	4 – 8	I	0.125	0.500-1	0.032	0.032-0.064	I-R	0.064-0.125
BG2-LBF	0.004-0.008	S	0.032-0.064	16	I	0.125-0.250	1	0.064-0.250	0.032	S	0.064-0.125
P35_2-LBF	0.004	S	0.032-0.064	4 – 16	I	0.25	1-2	0.064-0.250	0.032	S	0.064-0.125
P35_3-LBF	0.004	S	0.064	4 – 16	I	0.5	1-2	0.125-0.250	0.032	S	0.064-0.125
CBS138-LBF/IBF	0.004	S	0.032	4	I	0.064	0.5	0.032	0.016-0.032	S	0.064

^a broth microdilutions MIC 50 and MIC 90 of corresponding antifungal drugs compared with EUCAST values. ^b boldfaced: names and values of isolates with MIC values deviating from the wild type distribution breakpoint interpretations according to EUCAST breakpoints, Table v. 9.0, valid from February 2018. ^c no species-specific clinical breakpoints for 5FC, VOR, POS, ISA and CAS. ^d measured MIC range in most isolates (three technical repeats) encompasses both “susceptible” and “resistant” interpretations according EUCAST clinical breakpoint definition: S≤0.032, R>0.032 for MICA. ^e isolates in italics are the three HBF isolates to polystyrol. * Low biofilm-forming isolates to polystyrol, ** IBF and HBF ***.

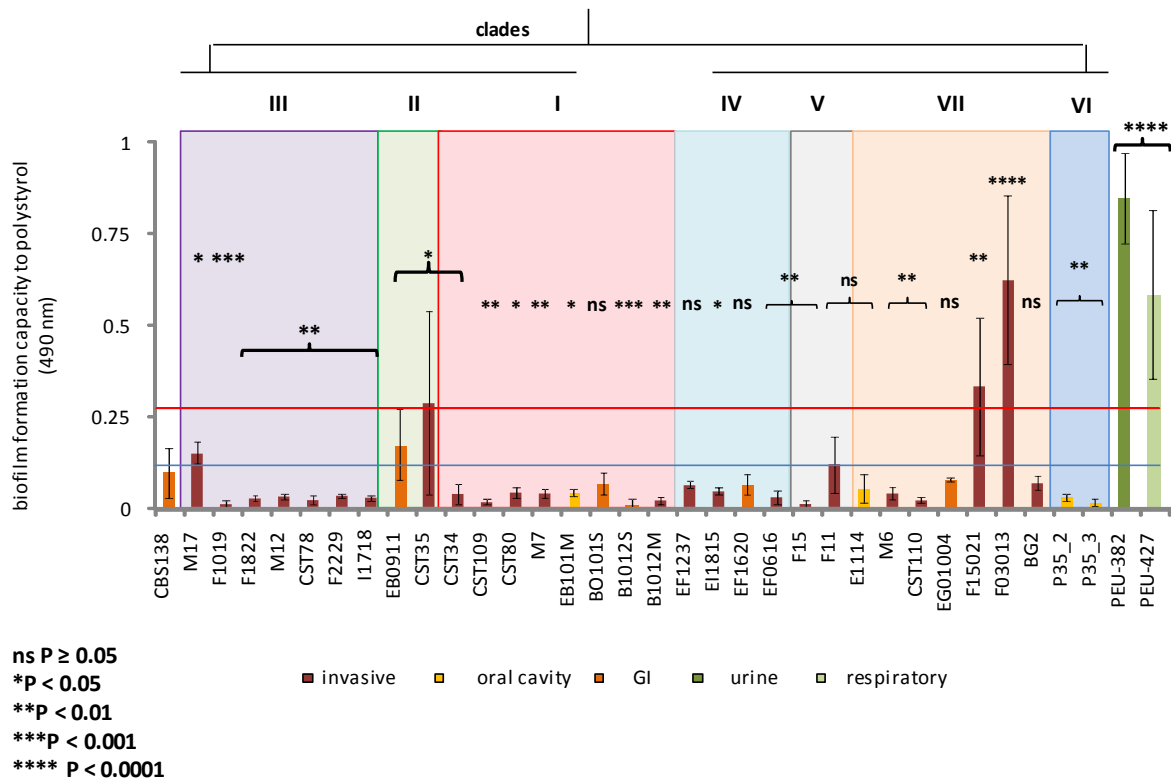


Figure 16. Biofilm formation capacity to polystyrol of thirty-three clinical isolates. Displayed are average biofilm formation values representing three biological with four technical replicates each. Source of isolation: red, blood (invasive); yellow, oral cavity; dark green, urine; bright green, respiratory tract. Colored panels represent the seven *C. glabrata* clades, described in Carreté *et al.*, 2018 The seven clades were subsequently divided in group 1: I, II, III and group 2: IV, V, VI, VII. CBS-138, PEU382 (urinary), and PEU427 (respiratory tract) were used as controls. Asterisks represent isolates significantly different compared to CBS-138. Biofilm formation capacity was classified as: low biofilm formers, $0 \leq X < 0.1392$; intermediate, $0.1392 \leq X < 0.2785$ and high, $X \geq 0.2785$. Red and blue lines, cut-off: 0.2785 and 0.1392.

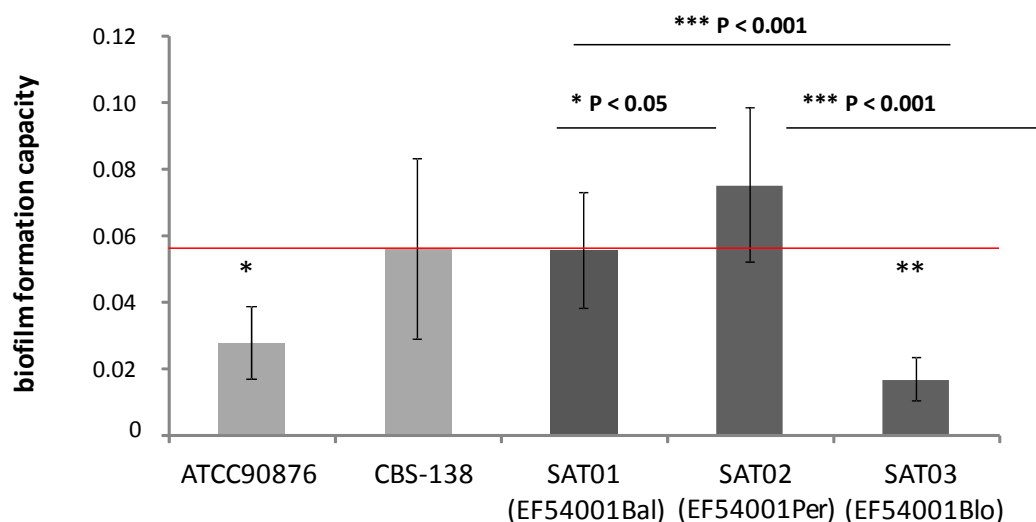
When these biofilm formation data were eventually correlated with cell wall-protein encoding gene copy numbers from the above genome analyses, all three hyper-adherent isolates F03013, F15021, and CST35 showed independent duplications of the *PWP4* gene, and deletions of the gene encoding adhesin wall protein *AWP13*. This puts Pwp4 into focus when attempting to explain the capability of these isolates to create biofilms in the colonization process.

3.1.2 Genomic changes between time-resolved *C. glabrata* isolates

Next, we analyzed how genomic properties varied between isolates obtained from the same patient with respect to biofilm formation. Three independent genome sequenced isolates from a patient with acute myeloblastic leukaemia and subsequent candidiasis obtained from bronchiolo-alveolar secrete (SAT01, EF54001Bal), peritoneal liquid (SAT02, EF54001Per), and blood culture (SAT03, EF54001Blo) were again provided by the group of Toni Gabaldón (CRG, Barcelona). The three isolates were from in the same clade and separated only by a low number of SNPs. Mutations were accumulative, remarking a significant degree of genetic variation in the host (Carreté *et al.*, 2019). Using this information as a starting point, we analyzed phenotypic properties.

Biofilm quantification classified all three isolates as LBF (CBS-138 = 0.060 ± 0.03), however significant quantitative differences between the source of isolation were seen ($P < 0.05$ and $P \leq 0.0001$): EF54001Blo displayed the lowest adherence capacity compared to the CBS-138 ($P \leq 0.01$) and both other matched isolates (Figure 17A). Indeed, EF54001Blo carried a non-synonymous mutation in *SIR4* that may correspond with differences in adherence capacity and subtelomeric silencing (Iraqi *et al.*, 2005). No differences regarding azoles susceptibility were found (Table 12B). Three additional pairs of isolates already discussed in section I1 (BO101S/EB101M, B1012S/B1012M and the P35-2/P35-3), did not show notable phenotypic variation (Figure 16) (Carreté *et al.*, 2018, 2019).

A



B

MIC of three clonal *C. glabrata* clinical isolates

	MIC (µg/ml)	AMB	5FC	FLU	VOR	POS	CAS	MICA
SAT01	24 h.	0.125	0.0625	4	0.125-0.250	0.5	0.25	0.031
EF54001Bal	48 h.	0.125	0.0625	8	0.125-0.25	0.5	0.25	0.031
SAT02	24 h.	0.125	0.0625	2-4	0.125	0.5	0.25	0.031
EF54001Per	48 h.	0.125	0.0625	4	0.125	0.250-0.5	0.25	0.031
SAT03	24 h.	0.125	0.0625	8	0.125-0.25	0.250-0.5	0.25	0.031
EF54001Blo	48 h.	0.125	0.0625	8	0.25	0.5	0.25-0.500	0.031
CBS-138	24 h.	0.125	0.032-0.064	2-4	0.125	0.125	0.032-0.064	0.016
PEU382 (c*)	24 h.	0.125	0.032	4-8	0.250-0.500	0.250	0.016-0.125	0.016-0.032
PEU427 (c)	24 h.	0.125	0.032-0.064	8-16	0.500-1	0.250-0.500	0.032	0.016-0.125

* (Gómez-Molero *et al.*, 2015)

Figure 17. *C. glabrata* phenotypic analyses of three clonal clinical isolates. (A) Biofilm formation capacity to polystyrol. Light grey bars: reference strains. Red line: CBS-138 biofilm formation capacity ($A_{490} \sim 0.060$), EF54001Bal (SAT01), EF54001Per (SAT02) and EF54001Blo (SAT03). (B) Minimal Inhibitory Concentration (MIC) towards seven antifungal drugs.

3.2 Phenotypic variability in *C. glabrata* clinical isolates correlates with variations in cell wall proteome and infection-relevant parameters

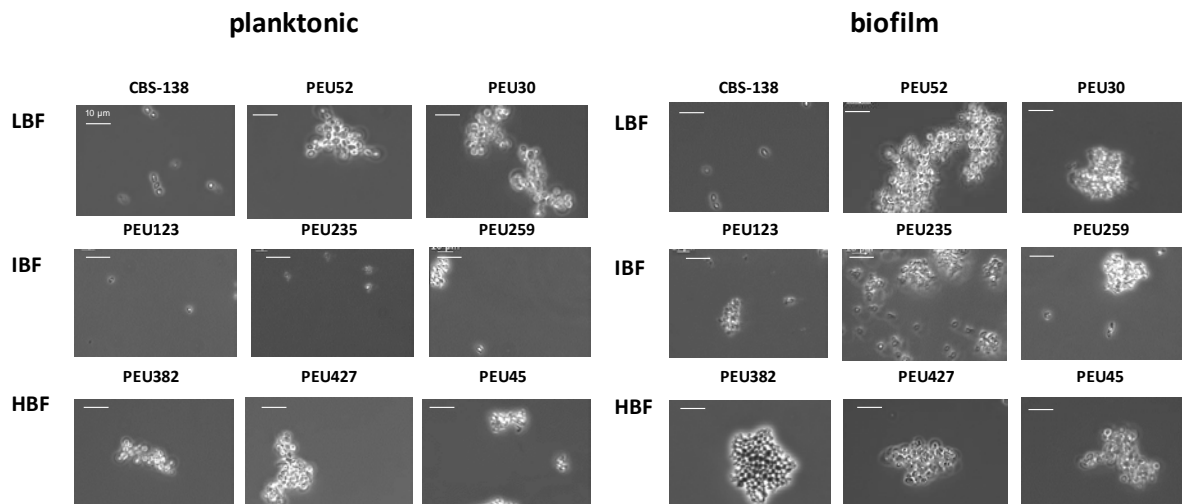


Figure 18. Cell aggregation capacity of selected biofilm-forming *C. glabrata* clinical isolates under planktonic and biofilm conditions. Isolates were categorized depending on their biofilm formation capacity (LBF, IBF, HBF).

Next, we sought to confirm the above findings in larger isolate cohorts. In a first approach we further characterized a set of strains which were previously selected for such purposes randomly, with a focus on the cell aggregation capacity (Figure 18) and biofilm formation capacity to polystyrol (Figure 19). Qualitative cell aggregation analyses indicated that isolates with LBF and IBF tended to flocculate less compared with HBF isolates, except for the clinical isolate PEU52 which presents an aggregation capacity comparable with the HBF PEU382 and PEU427. Then, the facility of the cells to form clumps apparently contribute to sediment faster and it was better detectable under biofilm conditions than the planktonic stage, (Figure 18), therefore, we proposed a possible correlation between biofilm formation capacity and cell aggregation observed in A.

In order to use these strains as controls for further downstream experiments, these eight clinical isolates were qualitatively (Figure 19A) and quantitatively (Figure 19B) characterized towards biofilm formation capacity to polystyrol. These isolates were classified in three different categories as LBF (PEU52, PEU30), IBF-HBF (PEU235, PEU259,

Candida glabrata

PEU123) and HBF (PEU45, PEU382, PEU427). Based on these results, isolates PEU45, PEU382 and PEU427 quantitatively presented strong capacity to produce biofilms on polystyrol (Figure 19B) being approximately 7-fold more adherent than the CBS-138 ($P \leq 0.0001$). No statistical differences regarding polystyrol biofilm formation intra-categories were remarked ($P \geq 0.05$).

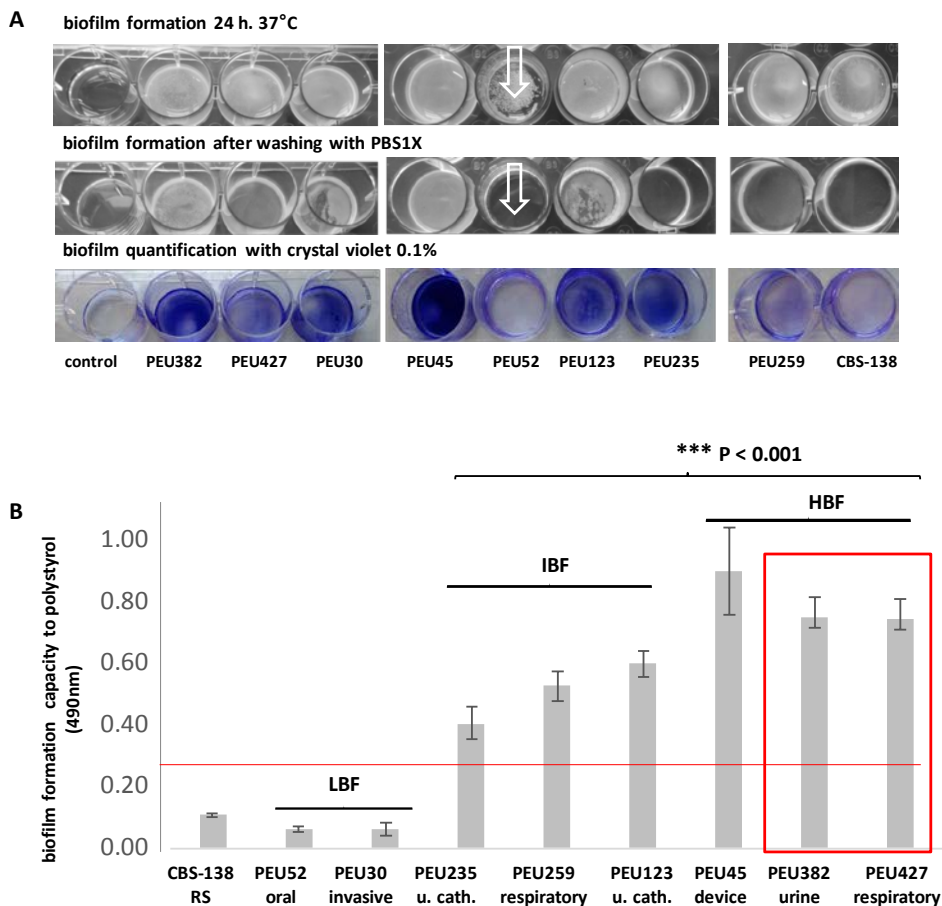


Figure 19. Biofilm formation analyses of eight selected clinical isolates + CBS-138. (A) Qualitative biofilm formation capacity of selected LBF (PEU30, PEU52), IBF (PEU123, PEU235, PEU259) and HBF (PEU45, PEU382, PEU427). Arrows indicate cell aggregates formed by the LBF PEU52 isolate removed after washing unbound cells out. (B) Quantitative biofilm formation analyses to polystyrol. Results shown are the average of two independent biological tests with four technical replicates. Red line, two-fold mean cut-off: 0.222. Red square, selected two HBF isolates for subsequent analyses of cell surface-related properties.

CBS-138, PEU382, and PEU427 were then used to assess variations in cell sedimentation, antifungal susceptibility against seven major antifungal drugs and virulence properties between hyper-adherent isolates *in vivo*, in *G. mellonella* caterpillars. Cell surfaces properties analyses of these clinical isolates were detailed in Figure 19 and Figure 20.

Candida glabrata

Susceptibility testing against seven major antifungals drugs indicated differences between the two HBF and the CBS-138 for FLU, VOR, and POS ($P < 0.05$), but no MIC differences for echinocandins, ISA and 5FC were observed (Figure 19C).

Sedimentation capacity partially correlated with cell aggregation in the PEU382 (Figure 20A) showing that HBF isolate PEU382 (64.2%) was different compared to PEU427 (43.5%) and CBS-138 (36%) ($P \leq 0.01$). The PEU382 settled approximately 1.80 and 1.47-fold faster than CBS-138 or PEU427, respectively (Figure 19B).

With respect to virulence capacity of these selected isolates, statistically significant ($P < 0.0001$) differences between the three isolates tested were indeed observed (Figure 6D). Nevertheless, Only the HBF PEU382 showed significant variations in virulence capacity compared to the reference strain CBS-138 (80%). The isolate PEU382 (100%) were more virulent than the PEU427 (90%) showing no *G. mellonella* survival at day 3 post-infection.

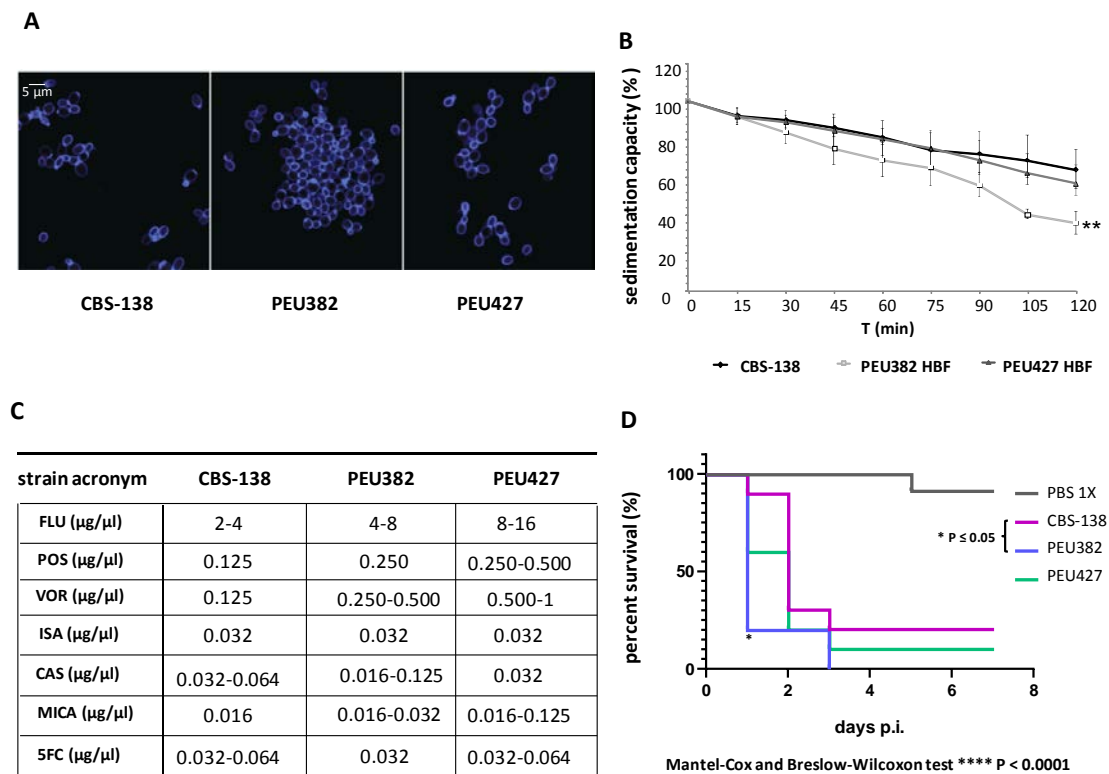


Figure 20. Cell surface analyses of reference isolates. (A) Qualitative cell aggregation of selected PEU382 and PEU427 under confocal microscopy. Cell walls are detectable with CFW staining remarking chitin distribution along the cell wall and budding yeast cells (Gómez-Molero *et al.*, 2015). (B) Cell sedimentation after 120 minutes (C) MIC values of PEU382 and PEU427 against seven major antifungal drugs. Table sums up the average of two independent experiments. (D) Kaplan-Meier survival curve of *G. mellonella* infected with the HBF isolates PEU382 and PEU427.

3.2.1 Biofilm formation capacity to polystyrol of a large *C. glabrata* clinical strain collection

We next systematically collected *C. glabrata* isolates from routine diagnostic procedures, a process that was previously initiated and established in our laboratory (Ichsan *et al.*, 2014). Isolates were grouped into nine different classes depending on the source of isolation (Figure 21A, B).

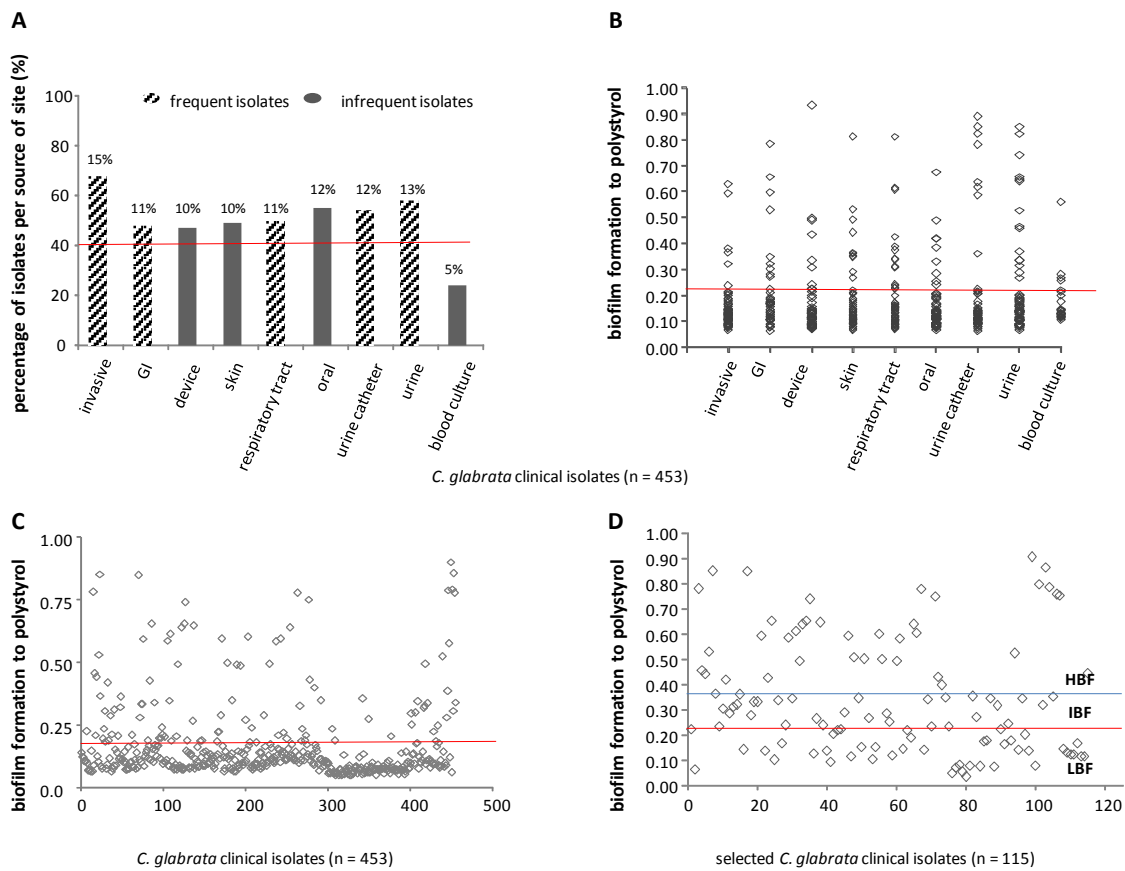


Figure 21. *C. glabrata* clinical isolates stratified according to body sites of isolation and quantitative biofilm formation capacity to polystyrol. (A) Percentage of *C. glabrata* isolates per source of isolation. Isolates were divided into nine different specimen groups. Dark grey bars represent infrequent source of isolation and black and white bars correspond with frequently-collected isolates. Red line indicates the minimal number of clinical isolates collected per source of site. (B) Biofilm formation distribution per source of site among the collection of 453 clinical isolates. (C) Biofilm formation capacity to polystyrol of the entire collection (n=453). Isolates above the cut-off represent IBF and HBF isolates, and isolates below the cut-off correspond with LBF isolates. (D) Biofilm formation capacity of 115 clinical isolates selected for downstream experiments with respect to their ability (IBF, HBF) or incapacity (LBF) to form biofilms on polystyrol surfaces. Red line in (B-D): cut-off at 2-fold median adhesion values ($A_{490nm} = 0.222$) and blue line ($A_{490nm} = 0.324$).

Candida glabrata

In total, 453 isolates were included in the collection with the goal to accumulate at least 40 isolates per group. Once 40 isolates were achieved, systematic inclusion of further isolates into that particular group was reduced, but not stopped. With the exception of category 9 (blood culture), this was achieved after a collection time frame of ~4 years (Figure 21A, B). Isolates from primary sterile sites (invasive), gastrointestinal tract, respiratory tract, urine catheters, and urinary tract were collected more frequently compared with samples isolated from general devices, skin, or epithelia and blood cultures.

3.2.2 Virulence of *C. glabrata* isolates in the *Galleria mellonella* model

We next investigated the existence of virulence differences between isolates as a function of their adherence capacity. Therefore, 47 LBF and 30 HBF isolates from 8 different site groups were selected (Figure 21A, except from blood isolates, which were not available at the time) and the virulence potential assessed using *G. mellonella* caterpillars as a systemic animal infection model (Ames *et al.*, 2017; Borghi *et al.*, 2014; Junqueira *et al.*, 2011).

Within both the LBF and HBF groups, differences between individual isolates were observed. Out of the 47 LBF-group clinical isolates tested, only twelve (24%) had a killing rate less than 100% at day seven. Isolates PEU531 (50%), PEU294 (60%) and PEU523 (60%) had the lowest killing rate on day 7. Eight out of these twelve (Figure 22A) were isolated from urine catheters (PEU531, PEU523, PEU364, PEU494, PEU541, PEU29, PEU519, PEU527), the other four were isolated from oral cavity (PEU52), respiratory tract (PEU322), GI tract (PEU1274) and only one was invasive, being isolated from a punctate (PEU294).

Candida glabrata

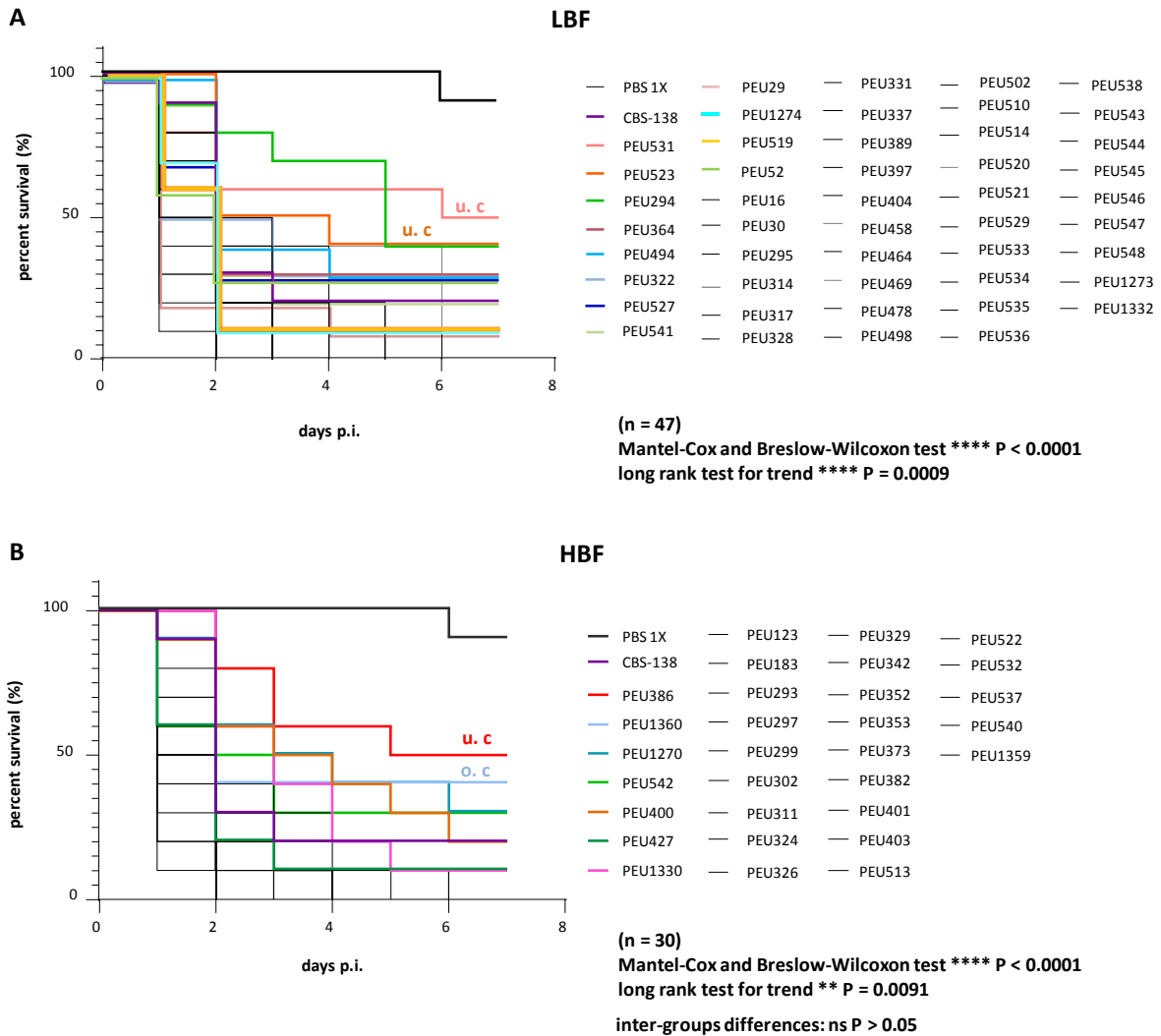


Figure 22. Kaplan-Meier *G. mellonella* survival curves infected with 77 *C. glabrata* clinical isolates + CBS-138 classified attending to their biofilm formation capacity. (A) LBF *C. glabrata* clinical isolates to polystyrol. (B) HBF clinical isolates to polystyrol. Colored lines represent isolates with survival rate equal or higher than 10% on day 7. Reference strain CBS-138/ATCC 2001 is highlighted in purple. Colored boldfaced u.c and o.c represent urine catheter and oral cavity respectively.

In case of HBF isolates, seven of thirty isolates analyzed presented a killing rate lower than 100% after a seven-days experiment. Out of these, isolates PEU386 (50%), PEU1360 (60%), PEU1270 (70%), and PEU542 (70%) had the lowest killing rate at day 7. Three isolates out of seven were isolated from oral cavity (PEU1360, PEU1270 and PEU542) and the other four were, respectively, isolated from urine catheter (PEU386), urinary tract (PEU400) and respiratory tract (PEU427 and PEU1330) (Figure 22B). Comparing both groups depending on their capacity to adhere to polystyrol, both categories approximately presented a similar percentage of isolates with a killing rate lower than 100%, (23%-25%) (Figure 22).

Table 11. Virulence capacity of *C. glabrata* isolates stratified by adherence capacity and site of isolation

origin	total isolates		% survival	LBF		HBF	
	% from n = 77	n	% per group	%	n	%	n
urine catheter	16%	12	75	75	9	25	3
device	10%	8	0	63	5	38	3
GI	16%	12	9	67	8	33	4
invasive	18%	14	7	79	11	21	3
oral cavity	9%	7	57	57	4	43	3
respiratory	12%	9	33	44	4	56	5
skin	4%	3	0	33	1	67	2
urine	15%	12	8	42	5	58	7

To conclude, intra-groups differences towards virulence capacity in *C. glabrata* clinical isolates were described. High variations in virulence capacity were found in isolates with LBF and HBF capacity to polystyrol. Samples isolated from urine catheters and oral cavity presented the highest level of survival rate in both groups independently to their capacity to form biofilms (Figure 22), In contrast, samples isolated from invasive candidiasis, medical devices, urinary tract and GI were, on average, more virulent. A partial correlation between non-adherence capacity and high survival rate was only remarkably observed in strains isolated from urine catheters (Table 11).

Although statistical differences within the two adherence categories were observed, no differences were detected inter-groups ($P > 0.05$). No global correlation between hyper-adherent clinical isolates and virulence capacity was significantly remarkable but a partial correlation was detected in strains isolated from skin, but these parameter has to be deeply analyzed increasing the study population. We proposed that virulence capacity is strain specific and partially correlated with the site of isolation. However, no apparent correlation between the ability to form biofilms on polystyrol and virulence capacity were seen amongst the 77 clinical isolates tested ($P > 0.05$) (Figure 23).

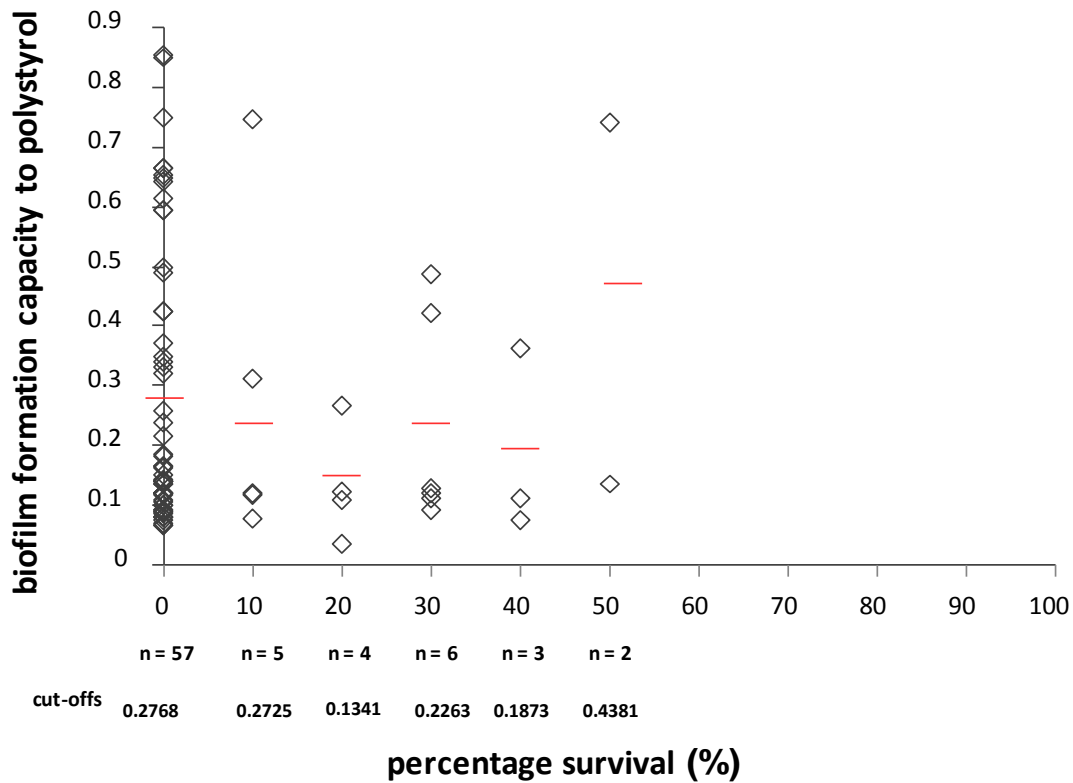


Figure 23. *C. glabrata* correlation analyses between virulence capacity and adherence to polystyrol. Isolates were tested in the *in vivo* *G. mellonella* infection model.

3.2.3 Variations in *C. glabrata* biofilm formation capacity to silicone elastomers

On the reference material polystyrol, a total of 83% isolates had quantitative biofilm formation values lower than what was considered as elevated (2-fold median of the whole cohort 0.222), leaving only 17% of the isolates to produce strong biofilms on this material (Figure 21C), and this independently of the body site of isolation. Isolates from the three categories previously detailed were subsequently analyzed using silicone elastomers as a model substrate to reflect biofilm development on urine catheters, prostheses, parenteral nutrition or such (Trofa *et al.*, 2008). From the collection of 453 isolates, a total of 115 were selected based on their high ability or disability to form biofilms on polystyrol (Figure 21D). Out of these, 22% formed biofilms only on silicone elastomers, 44% only on polystyrol, 19% on both materials, and 15% of the isolates did not adhere to either material (Figure 24).

Candida glabrata

Again, no correlation between body site of isolation and biofilm formation on either material tested was observed. The widest distribution of biofilm sizes was seen among isolates from urinary tract and urine catheters as compared to the other seven categories (Figure 21B). From this we concluded, that the formation of biofilms was independent for each material and only strain-dependent factors determine either phenotype.

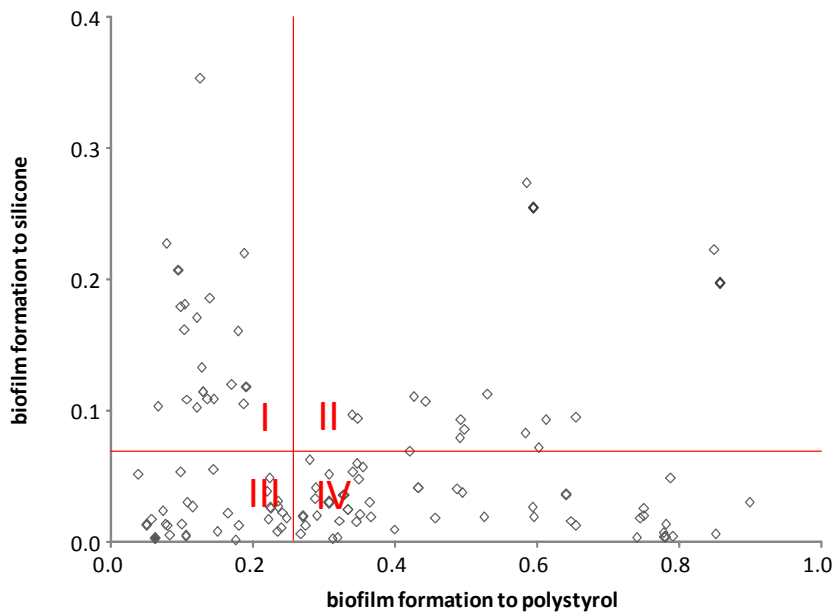


Figure 24. Correlation between biofilm formation capacity to silicone and polystyrol from 115 selected *C. glabrata* clinical isolates. (I) Isolates adherent only to silicone. (II) Isolates adherent to both materials. (III) Isolates that do not adhere to any material and (IV) Isolates that only formed biofilms on polystyrol.

In order to further investigate biofilm formation capacity to medical devices on the genome level, thirty-two clinical isolates were, once more, selected to reflect these subgroups, and sent for subsequent genome sequencing (ongoing collaboration with Dr. Toni Gabaldón). The isolates were selected according to the degree of adherence to silicone and polystyrol as well the site of isolation. Statistical differences between biofilm formation capacity to both materials were confirmed ($P \leq 0.01$). Within the group, nineteen of them, presented LBF capacity to polystyrol ($\text{abs.} \leq 0.222$) and fourteen were HBF isolates to polystyrol ($\text{abs.} \geq 0.222$). Twenty-eight isolates displayed intermediate- to high adhesion capacity to silicone (Figure 25).

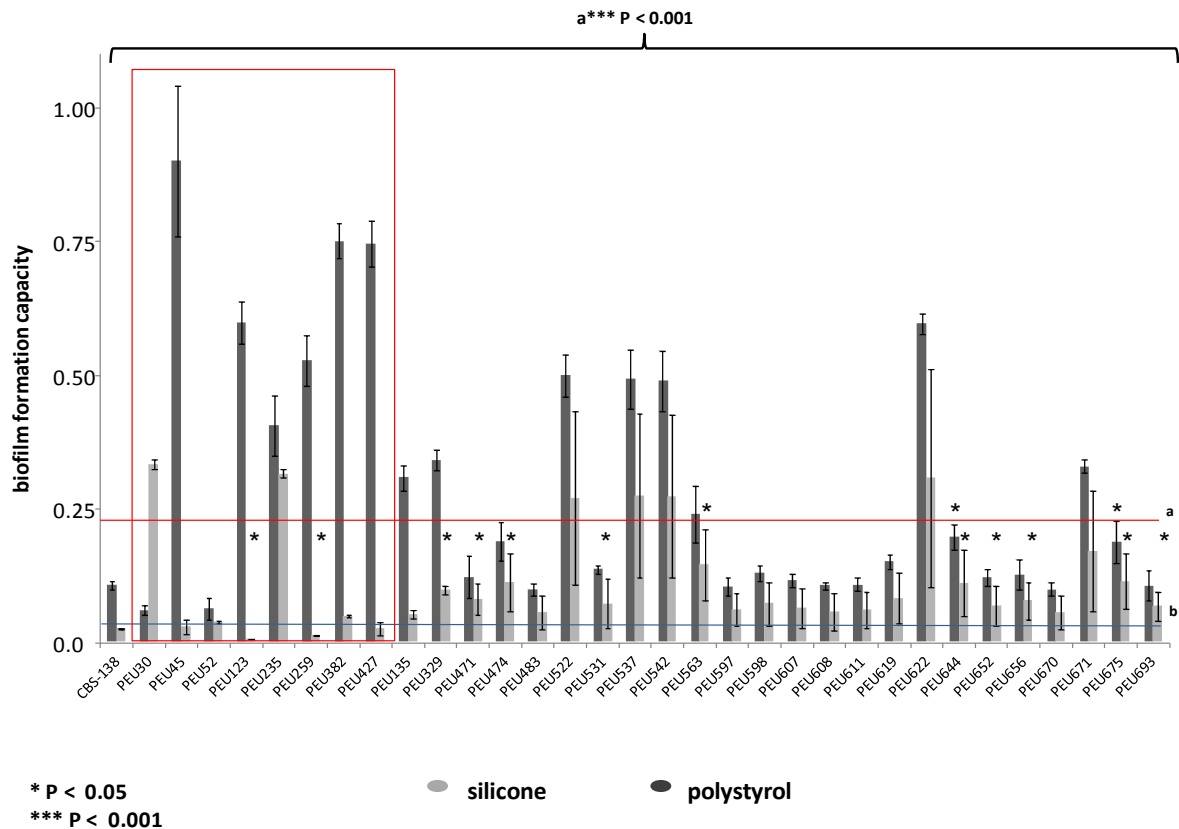


Figure 25. Biofilm formation capacity to abiotic surfaces of selected thirty-two *C. glabrata* clinical isolates + CBS-138. Red boldfaced line represents the cut-off mean for polystyrol (0.222) and blue line represents cut-off mean for silicone (0.054 nm). Isolates above lines a (polystyrol) and b (silicone) were considered strong biofilm-forming isolates for each material. Red square, selected *C. glabrata* clinical isolates for MS/MS analyses.

3.2.4 Different adhesins are present in hyper biofilm-forming clinical isolates

It is generally accepted that at the basis of linkages needed to form biofilms cell wall proteins are found. We therefore characterized the cell wall proteome in selected isolates from our study, namely of the eight phenotypically best characterized HBF isolates PEU382 and PEU427, PEU30, PEU45, PEU52, PEU123, PEU235, and PEU259. MS/MS analyses of isolated cell walls (in collaboration with Dr. Piet de Groot, Regional Center for Biomedical Research, CRIB, Albacete, Spain) identified a total of 35 authentic GPI-CWPs. Ninety-nine percent of these peptides belonged to covalently linked cell wall proteins, indicating achievement of sufficient purity during the cell wall isolation procedure. A total of 20

Candida glabrata

proteins (Table 13) were consistently identified in the nine isolates tested. This core proteome was mainly composed of proteins from the Gas/Phr (Gas 1, Gas2, Gas4 and Gas5) family with β -1, 3-glucanosyltransferase activity. Putative structural glucan-crosslinking proteins were Pir proteins (Pir1, Pir2, Pir3 and Pir4), the GPI-linked cell wall proteins Cwp 1.1, Cwp 1.2, and the mannoprotein Tir1. Pir proteins are lacking a GPI-anchor and were observed in HBF PEU382, PEU427 and PEU45; however, Pir1 was detected in six isolates, excluding the hyper-adherent PEU382 and the CBS-138 (Gómez-Molero *et al.*, 2015). Proteins with phospholipase activity were represented by Plb1 (not present in CBS-138 and PEU-52) and Plb2. Four other proteins with unknown function were also detected, namely proteins belonging to Ecm33 family (Ecm33 and Pst1), the GPI-CWP Ssr1 and the Srp/Tir family protein Tir2.

In contrast, a total of twenty GPI-CWPs proteins were not unanimously identified among the isolates. This variable proteome differed between the nine isolates, ranging between three (PEU30) and eleven (PEU45) adhesins in the cell wall (Table 12). The adhesin proteins expressed under biofilm conditions to abiotic materials (polystyrol), were mainly represented by the Epa family (Epa3, Epa6, Epa7 and Epa22) and the Awp family. Inside this family, twelve adhesins including Awp1, Awp2, Awp3, Awp4, Awp6 (de Groot *et al.*, 2008; Kraneveld *et al.*, 2011; Weig *et al.*, 2004), and six newly identified proteins Awp8, Awp9, Awp10, Awp11, Awp12 and Awp13 (Gómez-Molero *et al.*, 2015) were detected. From the ten CWPs identified here for the first time by proteomic analyses, the four proteins CAGL0L00227g (PEU52, PEU45), CAGL0F09273g (PEU123), CAGL0A04873g (PEU45), and CAGL0H00132g (PEU45) are still not classified into a protein family group.

On a global scale, increased numbers of different adhesins wall proteins were found in IBF and HBF isolates as compared to the reference strains CBS-138 (six) and ATCC90876 (one) and the LBF PEU30 (five proteins) (Table 13), with the one exception of LBF PEU52 (five proteins). In the LBF PEU30, PEU52, and the controls mainly adhesins belonging to the Epa family (Epa3, Epa6, Epa7 and Epa22), Awp1, and the newly described CAGL0L00227g were observed. Among these, CAGL0L00227g, a putative GPI-protein with glycine and serine rich tandem repeats of unknown function was found only in the two most flocculent isolates PEU52 and PEU45 indicating a possible involvement in this process. In contrast, Awp family proteins were mostly contained in IBF and HBF isolates' walls. Isolates with intermediate

Candida glabrata

and high biofilm formation capacity to polystyrol contained between six and eleven adhesins in the cell wall, with PEU235 and PEU382 (eight), PEU123 (nine), PEU427 (eleven), and PEU45 (eleven proteins) being the isolates with highest number of GPI-CWPs.

Looking only at results from analyses under biofilm-formation conditions, isolates with low degree of adherence to polystyrol (isolates highly flocculent or adherent to silicone), and thus remaining mainly in their planktonic state, presented both lower number of adhesins and core proteins (e.g. Plb1, Tir1, Gas5, Tir2). In contrast, hyper-adherent *C. glabrata* isolates contained a high number of different adhesins as well as core proteins in the cell wall. The newly described adhesins (Awp8, Awp9, Awp10, Awp12, Awp13, CAGLOF09273g, CAGLOA04873g, and CAGLOH00132g) were mainly present in isolates with high adherence capacity.

These results underlined that the core proteome (Table 13) is quite consistent and stable among *C. glabrata* clinical isolates, including GPI-phospholipases, putative glucan-crosslinkers and GPI-carbohydrate-active enzymes. In contrast, the adhesin set is highly diverse and strain-specific, conferring a unique and exclusive cell-surface proteome, which positively increases the number of proteins with increasing biofilm formation capacity.

Table 12. Variable proteome of selected hyper biofilm-forming isolates under biofilm conditions in this study

clinical isolates		ATCC90876 ^a	CBS-138 ^a	CBS-138 ^b	PEU52 ^c	PEU30 ^c	PEU123 ^c	PEU235 ^c	PEU259 ^c	PEU382 ^b	PEU427 ^b	PEU45 ^c
biofilm formation capacity polystyrol		LBF	LBF	LBF	LBF	LBF	IBF	IBF	IBF	HBF	HBF	HBF
biofilm formation capacity silicone		LBF	LBF	LBF	LBF	HBF	LBF	HBF	LBF	IBF	LBF	IBF
source of site		RS	RS	RS	oral cavity	invasive	urine catheter	urine catheter	respiratory	urine	respiratory	device
protein	cluster and protein type											
Epa3/ CAGL0E06688g	cluster I; GPI ^d	-	+	+	+	+	+	-	+	+	+	+
Epa6/ CAGL0C00110g	cluster I; GPI	-	+	+	+	+	+	+	+	+	+	+
Epa7/ CAGL0C05643g	cluster I; GPI	-	-	-	+	-	+	+	+	+	+	+
Epa22/ CAGL0K00170g	cluster I; GPI	-	-	-	+	-	-	-	-	-	-	-
Awp13/ CAGL0H10626g	cluster III; GPI	-	-	-	-	-	-	-	-	-	+	-
Aed1 (Awp5)/ CAGL0K13024g	cluster III; GPI	-	+ ^e	-	-	-	-	-	-	-	-	-
Awp6/ CAGL0G10175g	cluster IV; GPI	-	+	+ ^f	-	-	-	-	+	+	+	-
Awp2/ CAGL0K00110g	cluster V; GPI	-	+	+	-	-	-	-	+	+	+	-
Awp4/ CAGL0J11990g	cluster V; GPI	-	+	+	-	-	+	+	+	+	+	+
Awp8/ CAGL0B00110g	cluster V; GPI	-	-	-	-	-	+	+	+	+	+	+
Awp9/ CAGL0B05093g	cluster V; GPI	-	-	-	-	-	+	-	-	-	+	+
Awp10/ CAGL0F00110g	cluster V; GPI	-	-	-	-	-	+	+	-	-	+	+
Awp11/ CAGL0M00110g	cluster V; GPI	-	-	-	-	-	-	-	+	+	-	+
Awp1/ CAGL0J02508g	cluster VI; GPI	+	-	-	-	+	-	-	-	-	-	-
Awp3/ CAGL0J11891g	cluster VI; GPI	-	+ ^e	-	-	-	-	-	-	-	-	-
Awp12/ CAGL0G10219g	cluster VII; GPI	-	-	+	-	-	+	+	-	-	+	-
CAGL0A04873g	cluster III; GPI	-	-	-	-	-	-	-	-	-	-	+
CAGL0L00227g	cluster V; GPI	-	-	-	+	-	-	-	-	-	-	+
CAGL0F09273g	cluster V; GPI	-	-	-	-	-	+	-	-	-	-	-
CAGL0H00132g	unclassified	-	-	-	-	-	-	-	-	-	-	+

Table 13. Core proteome of selected hyper biofilm-forming isolates under biofilm conditions in this study

clinical isolates		ATCC90876	CBS-138	CBS-138	PEU52 (HF)	PEU30 (S)	PEU123	PEU235	PEU259	PEU382	PEU427	PEU45
biofilm formation capacity polystyrol		LBF	LBF	LBF	LBF	LBF	IBF	IBF	IBF	HBF	HBF	HBF
biofilm formation capacity silicone		LBF	LBF	LBF	LBF	HBF	LBF	HBF	LBF	IBF	LBF	IBF
protein	protein type	carbohydrate-active enzymes										
Crh1/ CAGL0G09449g	GH16; GPI	+	+	+	+	+	+	+	+	+	+	+
Utr2/ CAGL0C02211g	GH16; GPI	+	+	+	+	-	+	-	-	+	+	+
Gas1/ CAGL0G00286g	GH72; GPI	+	+	- ^f	+	+	+	+	+	+	+	+
Gas2/ CAGL0M13849g	GH72; GPI	+	+	- ^f	+	+	+	+	+	+	+	+
Gas4/ CAGL0F03883g	GH72; GPI	+	+	+	+	+	+	+	+	+	+	+
Gas5/ CAGL0F01287g	GH72; GPI	+	+	+	+	-	-	+	+	+	+	+
Scw4/ CAGL0G00308g	GH17	+	+	+	+	+	+	+	+	+	+	+
putative glucan crosslinkers												
Cwp1.1/ CAGL0F07601g	Pir repeat; GPI	+	+	+	+	+	+	+	+	+	+	+
Cwp1.2/ CAGL0F07579g	Pir repeat; GPI	+	+	+	+	+	+	+	+	+	+	+
Pir1/ CAGL0F07579g	8 Pir repeats	+	-	-	+	+	+	+	+	-	+	+
Pir2/ CAGL0I06182g	9 Pir repeats	+	+	+	+	+	+	+	+	+	+	+
Pir3/ CAGL0M08492g	9 Pir repeats	+	+	+	+	+	+	+	+	+	+	+
Pir4/ CAGL0I06160g	2 Pir repeats	+	+	+	+	+	+	+	+	+	+	+
Tir1/ CAGL0F01463g	Srp1/Tip1 family; Pir repeat; GPI	+	+	+	-	-	-	-	-	+	+	+
phospholipase												
Plb1/ CAGL0J11770g	GPI	-	-	-	-	+	+	+	+	+	+	+
Plb2/ CAGL0J11748g	GPI	+	+	+	-	+	+	+	+	+	+	+
unknown function												
Ecm33/ CAGL0M01826g	Ecm33 family; GPI	+	+	+	+	+	+	+	+	+	+	+
Pst1/ CAGL0E04620g	Ecm33 family; GPI	+	+	+	+	+	+	+	+	+	+	+
Ssr1/ CAGL0H06413g	GPI	+	+	+	+	+	+	+	+	+	+	+
Tir2/ CAGL0F01485g	Srp1/Tip1 family; GPI	-	+	+	-	+	-	-	-	+	+	+

^a data from de Groot *et al.*, 2008 and Kraneveld *et al.*, 2011. ^b data of CBS-138 and hyper-adherent PEU382 and PEU427 are published in (Gómez-Molero *et al.*, 2015). ^c proteomic data from HBF and LBF clinical isolates identified in this study were performed in ongoing collaboration with Dr. Piet de Groot (CRIB, Albacete, Spain) (unpublished data); these isolates were initially selected and partially phenotypically characterized by Mr. Ichsan (UMG, Göttingen, Germany). ^d adhesin cluster classification was detailed by de Groot *et al.*, 2008 and 2013. ^e data compiled from Groot *et al.*, 2008 and Kraneveld *et al.*, 2011, Awp3 were only identified in cell walls harvested under log. phase at 30 °C, and Aed1 was identified in stationary phase cells. ^f non-unique peptides identified. ^g positive Mascot determination of unique peptides presented in CWP 1.1 and CWP 1.2. Red boldfaced, novel adhesins identified in hyper-adherent clinical isolates not described before in previous studies (Gómez-Molero *et al.*, 2015). Blue boldfaced, novel adhesins not previously identified in CBS-138 were detected in LBF, IBF and HBF isolates. ND, not determined.

3.2.5 Hyper biofilm-forming *C. glabrata* clinical isolates' adherence to *C. albicans*.

Based on interaction studies performed by (Tati *et al.*, 2016) between *C. albicans* and *C. glabrata*, we hypothesized a correlation between biofilm formation capacity/presence of cell wall adhesins and capacity to adhere to *C. albicans* hyphae would be present among our isolates. To determine the relation between the abundance of identified cell wall adhesins in HBF isolates and interaction with *C. albicans* hyphae, isolates PEU52, PEU45, PEU382 and PEU427 were co-incubated with GFP-tagged *C. albicans* SC5314 and examined by fluorescence microscopy.

The attachment of *C. glabrata* yeast cells to *C. albicans* hyphae was quantified showing an increased number of *C. glabrata* yeast cells adhered to *C.a*-GFP-SC5314 hyphae (expressed as *C. glabrata* cells/ μm *C. albicans* hyphae) in the HBF clinical isolates and the highly flocculent strains PEU52, as compared to the two LBF reference strains (CBS-138 and ATCC90876) (Figure 26). *C. glabrata* cell aggregation capacity was significantly higher in PEU382 ($P < 0.012$, 0.068 ± 0.038), PEU427 ($P \leq 0.038$, 0.068 ± 0.047) and the HF PEU52 ($P < 0.0091$, 0.116 ± 0.078). A qualitative intermediate degree of interaction was described in the lower biofilm-forming HF-PEU52. The control PEU52 was extremely flocculent and tended to adhere to the edges of *C. albicans* hyphae and surrounding *C. albicans* freshly germinated cells as big aggregates, leaving the longer *C. albicans* hyphae free of *C. glabrata* cells (Figure 26, intermediate row, left panel).

Among the selected *C. glabrata* clinical isolates, the HBF PEU382 ($P \leq 0.001$) and PEU427 ($P \leq 0.05$) presented significantly higher adherence to *C. albicans* hyphae compared to the CBS-138 and the ATCC90876 (Figure 26). The range of *C. glabrata* adherence capacity to *C. albicans* hyphae was ATCC90876 > CBS-138 > PEU52 > PEU45 > PEU382 and PEU427) (Table 14).

Candida glabrata

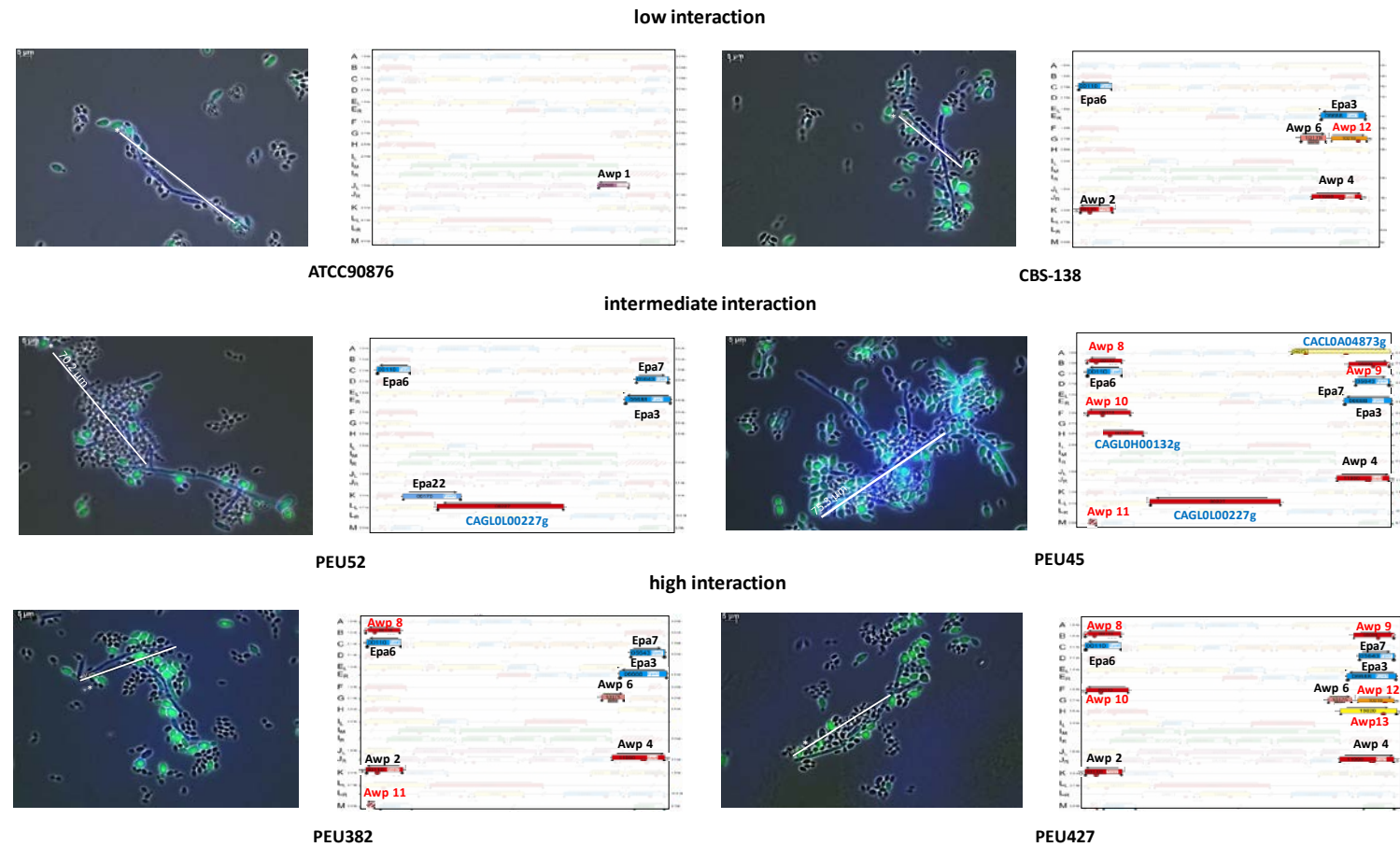
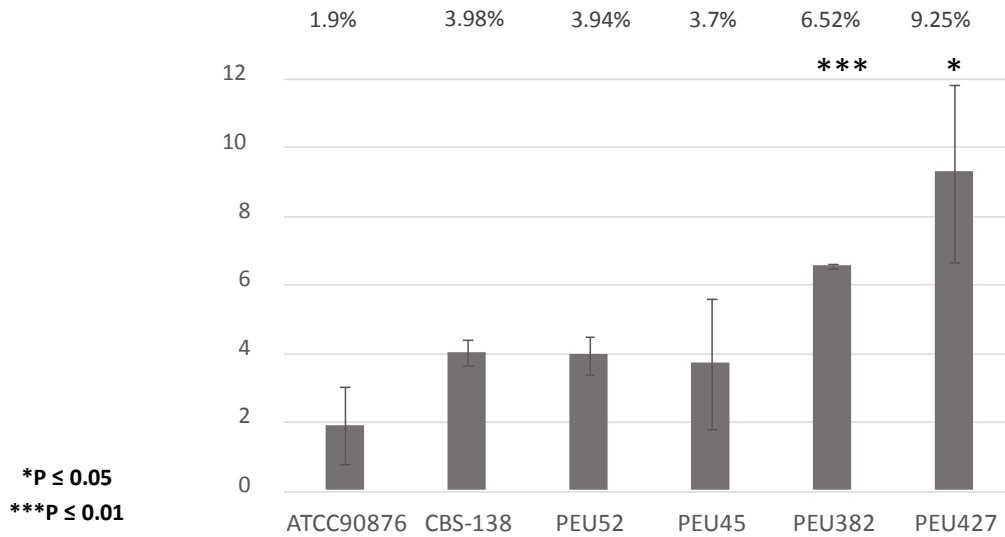


Figure 26. *C. glabrata*: *C. albicans*-GFP-SC5314 interaction *in vitro* model. Left panels, fluorescence microscopy quantification of *C. glabrata* cells adhesion to *C. albicans* hyphae. DAPI (blue) and CY2 (green) fluorescence was used for a better differentiation of *C. albicans* germinated structures (bright green), hyphae forms (light cyan) and *C. glabrata* yeast cells (dark grey). * indicates the hyphae length: ATCC90876, 68.07 μ m; CBS-138, 40.34 μ m; PEU52, 70.21 μ m; PEU45, 75.3 μ m; PEU382, 48.17 μ m and PEU427 55.52 μ m. Right panels, cell wall adhesins identification in LBF, IBF and HBF clinical isolates. The variable proteome was represented based on genomic distribution previously described for the *C. glabrata* reference strain CBS-138 (de Groot *et al.*, 2013). Red boldfaced, adhesins newly identified in this study that belongs to the Awp family (Gómez-Molero *et al.*, 2015). Blue boldfaced, adhesins newly described not yet categorized (CAGL0L00227g, CAGL0A04873g and CAGL0H00132g). Adhesin proteins distribution is mainly located in subtelomeric regions. Cell wall protein genes color code corresponds with family clusters distribution according to the cluster classification published by de Groot *et al.*, 2008 and 2013. Blue, cluster I; yellow, cluster III; pink, cluster IV; red, cluster V; purple, cluster VI and orange, cluster VII.

Candida glabrata

Table 14. Percentage of *Candida spp.* interaction between selected *C. glabrata* clinical isolates and GFP-SC5314 *C. albicans* reference strain

	ATCC90876	CBS-138	PEU52	PEU45	PEU427	PEU382
cell aggregation	-	-	++	+	+	++
biofilm formation polystyrol	-	-	-	++	++	++
biofilm formation silicone	-	-	-	+/-	+/-	+/-
number of adhesin CWPs	1	6/7	5	11	11	8



% of interaction *C. g.*: *C. a.*-GFP-SC5314, (n° *C. glabrata* yeast cells/*C. albicans* hyphae length /10 µm).

3.2.6 *C. albicans* and *C. glabrata* mixed culture analysis

Following the hypothesis, that attachment of *C. glabrata* to *C. albicans* aids *C. glabrata* in penetration into tissues and subsequently into the bloodstream (Tati *et al.*, 2016), we searched medical records for further evidence. Between 2010 and 2016 we found n =

Candida glabrata

15532 specimen processed in the microbiology lab of the University Medical Hospital in Göttingen from which either *C. glabrata*, *C. albicans* or both were cultured (Table 15).

Table 15. Frequency of *C. glabrata* and *C. albicans* infections (n = 15532) per source of isolation.

source	<i>C. albicans</i>	<i>C. glabrata</i>	mixed	ratio ^a	% <i>C. glabrata</i> in mixed cultures ^b
invasive	1805	415	53	0.139	11%
GI	500	245	55	0.144	18%
device	884	213	33	0.086	13%
skin	1720	227	19	0.049	8%
respiratory	3597	818	128	0.335	14%
oral	1339	182	37	0.097	17%
urine catheter	840	318	26	0.068	8%
urine	1084	398	21	0.055	5%
blood culture	423	143	9	0.023	6%
total	12192	2959	381		11%

* Mixed cultures diagnosed as *C. glabrata* infection were represented as total % (right column). Isolates were categorized nine different categories. ^a absolute value of *C. glabrata* identified in mixed cultures per source of site. Cut-off value: 0.110 ± 0.04 . *C. glabrata*. Bolded percentages represent the most frequent source of isolation identified as *C. glabrata* in mixed cultures.

Out of these, 78.5% had only *C. albicans*, 19.0% *C. glabrata*, and 2.5% contained both. The highest number of mixed cultures was obtained from the respiratory tract (33.0%), while the lowest number was obtained from blood cultures (Figure 27). Next, we wanted to corroborate if the frequency of mixed cultures was increased relative to the total number of *C. glabrata* findings in those specimen groups, where *C. glabrata* was expected not to penetrate without the help of *C. albicans* (blood cultures and invasive isolates). However, this was not the case. No statistical differences between the source of isolation and the presence of *C. glabrata* infections in mixed cultures were found ($P > 0.05$) (Table 15).

Candida glabrata

Table 16. *C. glabrata* blood cultures identification in CHROMagar

isolate	CHROMagar	isolate	CHROMagar	isolate	CHROMagar	isolate	CHROMagar
bc 1035	<i>c. g</i>	bc 1046	<i>c. g</i>	bc 1056	<i>c. g</i>	bc 1066	<i>c. g</i>
bc 1036	<i>c. g</i>	bc 1047	<i>c. g</i>	bc 1057	<i>c. g</i>	bc 1067	<i>c. g</i>
bc 1037	<i>c. g</i>	bc 1048	<i>c. g</i>	bc 1058	<i>c. g</i>	bc 1068	<i>c. g</i>
bc 1038	<i>c. g</i>	bc 1049	<i>c. g</i>	bc 1059	<i>c. g</i>	bc 1069	<i>c. g</i>
bc 1039	<i>c. g</i>	bc 1050	<i>c. g</i>	bc 1060	<i>c. g</i>	bc 1070	<i>c. g</i>
bc 1040	<i>c. g</i>	bc 1051	<i>c. g</i>	bc 1061	<i>c. g</i>	bc 1071	<i>c. g</i>
bc 1041	<i>c. g</i>	bc 1052	<i>c. g</i>	bc 1062	<i>c. g</i>	SC5314 ^a	<i>c. a</i>
bc 1042	<i>c. g</i>	bc 1053	<i>c. g</i>	bc 1063	<i>c. g</i>	CBS138 ^a	<i>c. g</i>
bc 1043	<i>c. g</i>	bc 1054	<i>c. g</i>	bc 1064	<i>c. g</i>	bc 395 ^a	<i>c. g+c. a</i>
bc 1044	<i>c. g</i>	bc 1055	<i>c. g</i>	bc 1065	<i>c. g</i>	bc 494 ^a	<i>c. g+c. a</i>

^a CBS-138 and SC5314 were used as *C. glabrata* and *C. albicans* reference strains, respectively. Bc-395 and bc-494 were used as positive control with mixed infections previously identified.

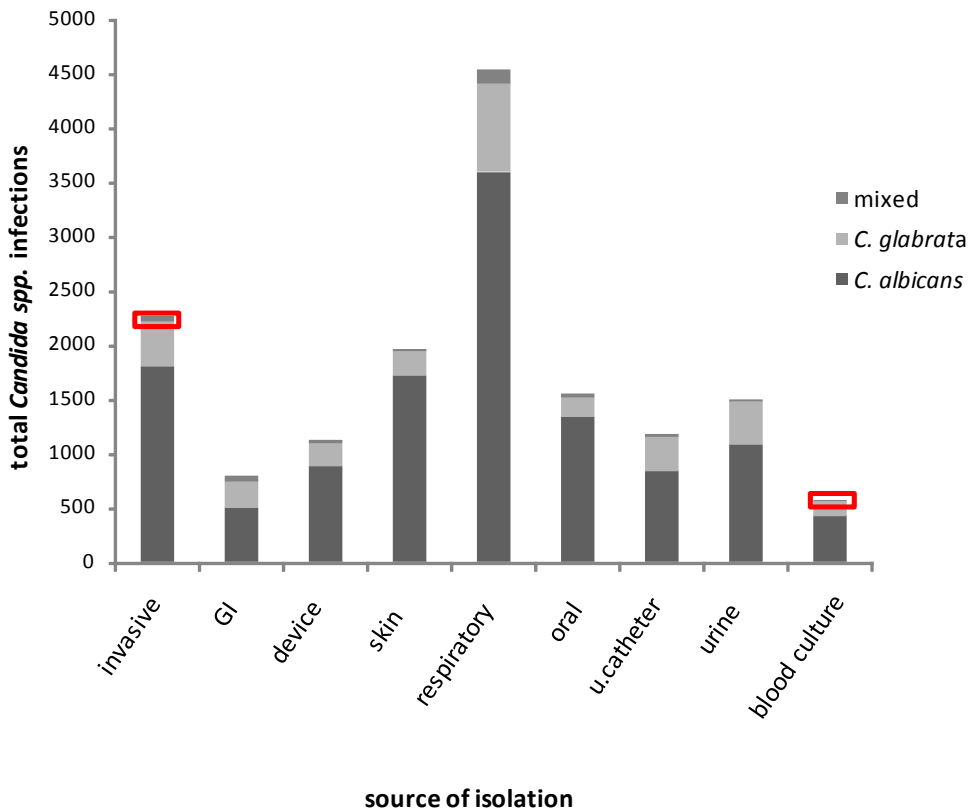


Figure 27. General distribution of single and mixed *Candida spp.* infections caused by *C. albicans* and *C. glabrata*. Red squares, mixed infections identified in cultures isolated from invasive infections (e.g. sterile primary sites) and blood cultures.

Candida glabrata

There is the possibility that *C. albicans* was simply not detected in plates inoculated from blood cultures due to overgrowth of *C. glabrata* in the liquid culture. For example, when we spiked *C. glabrata* into blood culture bottles (CBS-138) were detected after approximately 20h. Meanwhile, *C. albicans* (SC5314) was positively determined around 17 h. after incubation. We therefore took 36 blood cultures plus two reference strains and two mixed cultures (controls) which had been stored for quality control purposes and plated these on selective chromogenic agar (CHROMagar, Oxoid) for quick determination of *C. albicans* (green) and *C. glabrata* (red). All thirty-six blood cultures tested were identified as *C. glabrata* (Table 16) with no apparent identification of *C. albicans* green colonies in the samples (Figure 28A). To increase the accuracy of mixed cultures determination, selected bottles were investigated using direct PNA-FISH (Figure 28B). Indeed, the specimen *C. g-bc-PEU1038*, previously diagnosed as *C. glabrata* infection (Figure 28B) was the only blood cultures identified as a mixed culture. However, blood culture bottles from isolates *C. g-bc-PEU1035*, *C. g-bc-PEU1036*, *C. g-bc-PEU1037* and *C. g-bc-PEU1039* were only found to contain as *C. glabrata* infections. In summary, no evidence of remarkably increased identification of *C. albicans* in mixed cultures was observed and remarkable differences between the origin of the culture and the presence of *C. glabrata* is evident, but nevertheless the percentage of finding *C. glabrata* in cultures is slightly more frequent in samples isolated primary sources, gastrointestinal tract, medical devices, respiratory tract and oral cavity than variations between (Table 15).

Candida glabrata

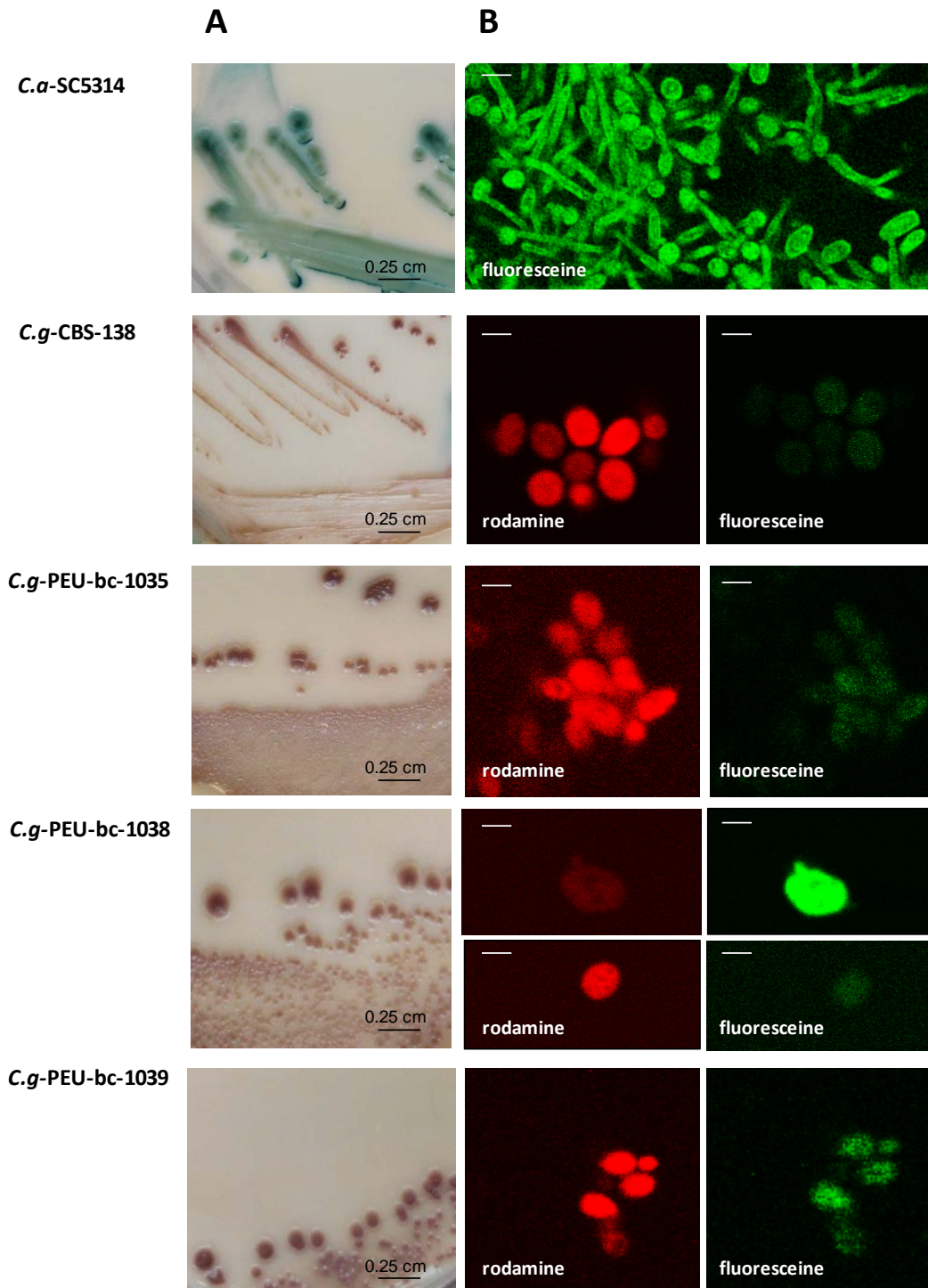


Figure 28. *C. albicans* and *C. glabrata* identification from infected-patient's blood cultures. (A) CHROMagar species determination. Green colonies *C. albicans*, dark red colonies, *C. glabrata*. (B) Fluorescence in-situ hybridization (PNA-FISH). Fluoresceine stains *C. albicans* yeast cells and rodamine detects *C. glabrata*.

3.3 Pheno- and genotypic analyses of *Candida parapsilosis* clinical isolates

3.3.1 Establishing a classification reference

Candida parapsilosis' morphology-switching is proposed to be involved in this organism adherence and pathogenicity processes. In order to analyze *C. parapsilosis* phenotypic and genotypic divergences within a large clinical strain collection, we initially classified different colony morphotypes according to the existing nomenclature proposed in the literature (Enger *et al.*, 2001; Laffey and Butler, 2005; Lott *et al.*, 1993).

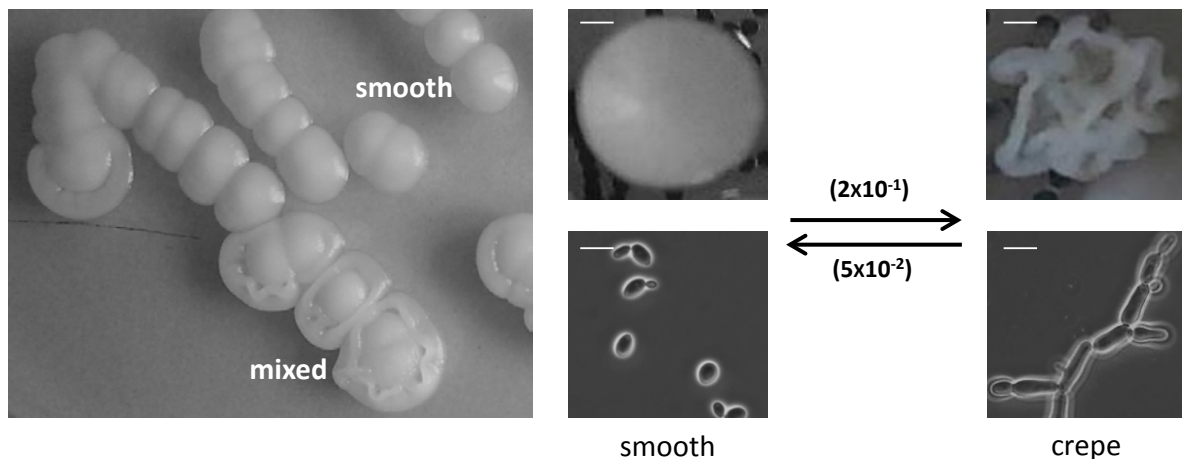


Figure 29. Morphogenic switching in a *C. parapsilosis* non-biofilm forming clinical isolate (PEU582). Left, colony morphology on SAB agar. Right, morphotypic switch on SAB's agar and exponential phase liquid cultures showing frequency changes between smooth and crepe I morphotypes. The phenotypic switch from "smooth-glossy" to "crepe I" was 4 times faster (2×10^{-1}) than the switch observed from "crepe I" to "smooth-glossy", (5×10^{-2}).

In the example from our collection shown here (Figure 29A), the phenotype smooth was comparable with those described by (Lott *et al.*, 1993) and (Nosek *et al.*, 2009), presenting initially as round glossy colonies with delimited border. The final crepe colony morphology (clearly defined from day 4 of incubation on) presented an irregular colony border and

Candida parapsilosis

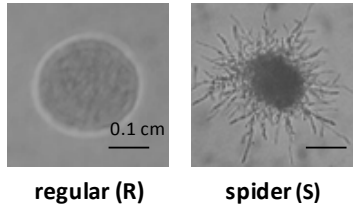
matte surface with “crepe” wrinkles, but no concentric distribution. Smooth colony morphotypes correlate with round yeast cells in liquid YPD media; in contrast, crepe colony morphologies develop long pseudohyphae (Figure 29B).

While working with increasing numbers clinical *C. parapsilosis* isolates and prolonged incubation times, numerous intermediate and novel colony forms were observed. Therefore, a new classification key chart was developed, incorporating colony border, surface color, as well as microcolony shape on agar- and cell shape in liquid cultures. Microcolony morphology on Corn meal agar (Figure 30B) varied between defined round structures (regular) and filamentous microcolonies (spider). Biofilm formation capacity and cell aggregation were classified as “low”, “intermediate” and “high”, (Figure 30B). Cell shape morphology under exponential phase growth conditions were grouped into three different categories prevailing yeast cells (0), elongated pseudohyphae (2) or mixed cultures (1) including a combination of yeast and/or pseudohyphae development (Figure 30C).

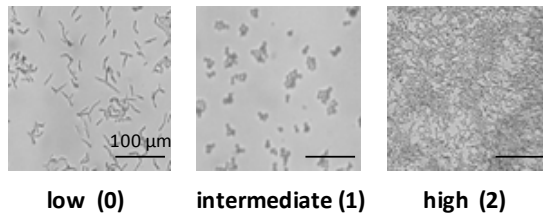
Additionally, agar invasion capacity of each colony type (A) was ranked between “low” (1 and 2) with no clear agar imprint detectable after flushing the plates with water, “medium” (3 and 4) with slightly colony border imprints on agar, and “high” with detectable concentric rings on the agar (5) as well as occasional resistance of the colony to removal with flushing water(6), a feature used to further discriminate “crepe I” and “crepe II” colonies (Figure 30D).

In total this resulted in definition of eleven different observed colony types of varying frequency during this work (Figure 31).

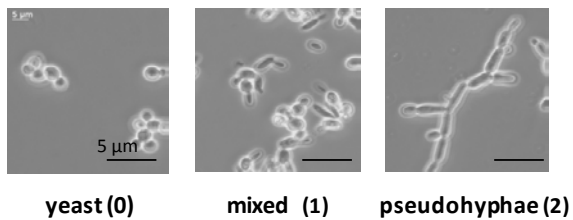
A Microcolony morphology on Corn meal agar



B Biofilm formation capacity to polystyrol



C Cell shapes



D Agar invasion capacity classification

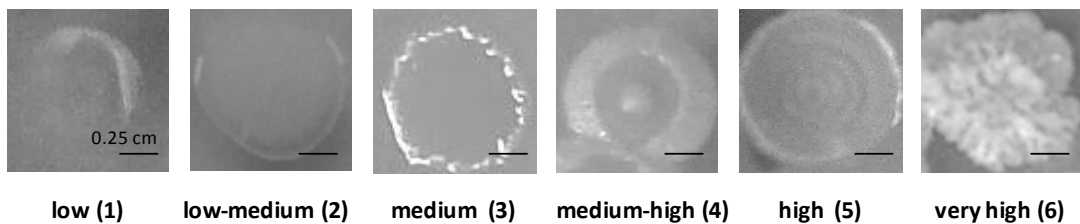
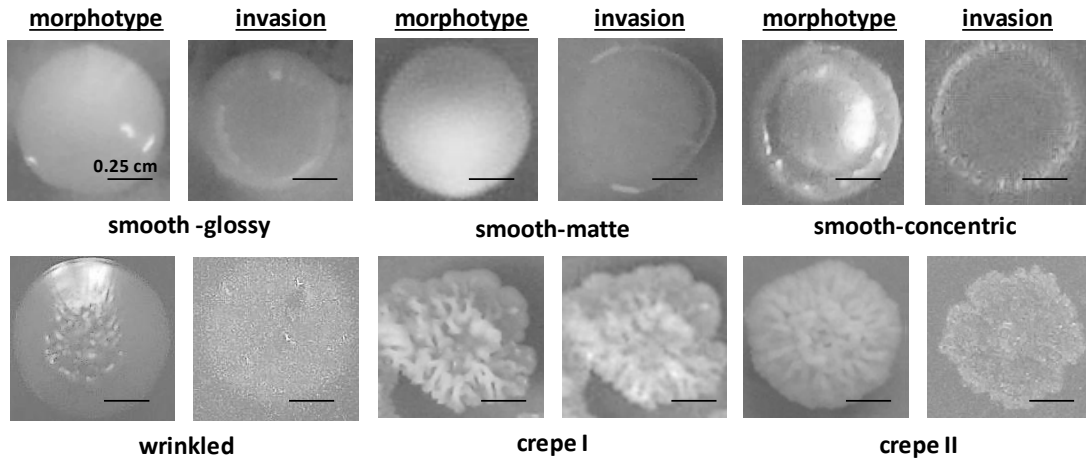


Figure 30. General characterization of *C. parapsilosis* cell-related properties. (A) Microcolony morphology on Corn meal agar: (R) regular, (S) spider. (B) Biofilm formation capacity to polystyrol: low (0), intermediate (1), high (2). (C) Cell shape morphologies associated with colony types: yeast (0), mixed (1), pseudohyphae (2). (D) Agar invasion capacity on SAB's and Phloxine B agar ranked as: low (1), low-medium (2), medium (3), medium-high (4), high (5), very high (6).

A Major colony morphologies on SAB and Phloxine B agar



B Infrequent colony morphologies on SAB and Phloxine B agar

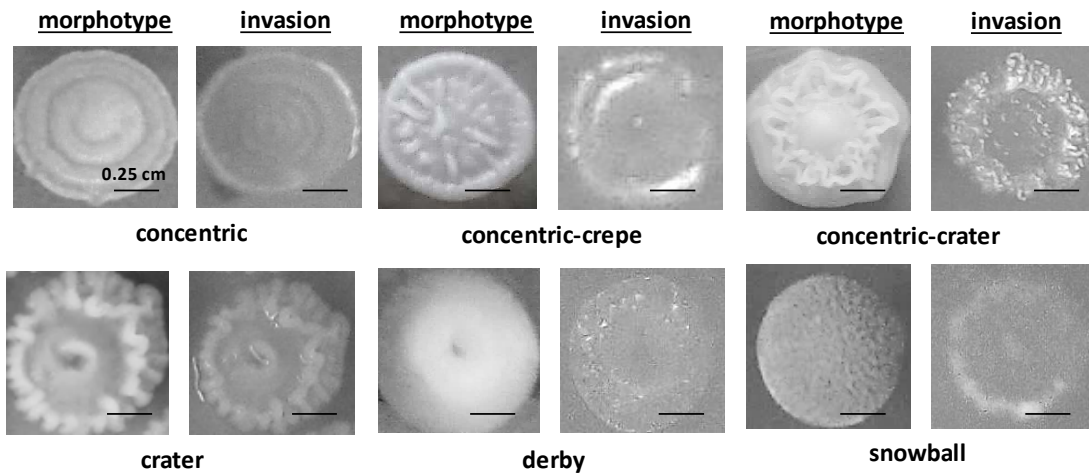


Figure 31. Classification references of *C. parapsilosis* colony morphologies on SAB's and Phloxine B agar produced in this work. (A) Major morphotypes: smooth-glossy (s-g), smooth-matte (s-m), smooth-concentric (s-cn), wrinkled (wr), crepe I and II (cr). (B) Infrequent colony phenotypes: concentric (cn), concentric-crepe (cn-cr), concentric-crater (cn-crt), crater (crt), derby (d) and snowball (sn). Left row: colony morphology after 96 h. incubation. Right row: agar imprinting on SAB's and YPD + Phloxine B agar after washing colonies with running water.

Table 17. *C. parapsilosis* colonies morphology identification key chart.

morphotype	colony border	colony color on agar		microcolony	cell shape
		YPD	Phloxine B	Corn meal	
smooth-glossy (s-g)	regular	cream, bright	bright pink	regular	yeast
smooth-matte (s-m)	regular	cream, matte	matte pink	regular	yeast
smooth-concentric (s-cn)	regular	cream, matte	magenta	regular	yeast
derby (d)	regular	cream, matte	magenta	regular	yeast
snowball (sn)	regular	cream, matte	pink velvet	regular	mixed
wrinkled (wr)	partially irregular	cream, matte	magenta	spider	mixed
crater (crt)	irregular	cream /brown, matte	magenta	spider	mixed
concentric-crater (cn-crt)	irregular	cream, matte	magenta	spider	mixed
concentric-crepe (cn-cr)	irregular	cream, matte	magenta	spider	mixed
concentric (cn)	irregular	cream, matte	magenta	spider	pseudohyphae
crepe (I and II)	irregular	cream/brown, matte	magenta	spider	mixed

3.4 *Candida parapsilosis* polymorphism drives differences at morphological and genotypic level in isolates from a single patient

After being confronted with diagnostic agar plates presenting *C. parapsilosis* with two different colony morphologies cultured from a single specimen, we investigated to what degree these phenotypic differences correlated with clinically relevant features. Several specimens from the same patient were cultured in the diagnostic laboratory, and yeast growth was obtained (in chronological order) from bronchial secrete, blood culture (BC), nose-oral swab, stool and central venous catheter (CVC). Samples from BC and swabs were collected for following studies and identified as *C. parapsilosis* sensu stricto. Early undifferentiated fungal growth from the bronchial secrete and the isolate from the CVC sample was not available for subsequent analyses; these values were taken from diagnostic facilities. Independent morphotypes were isolated from the specimen (Figure 32).

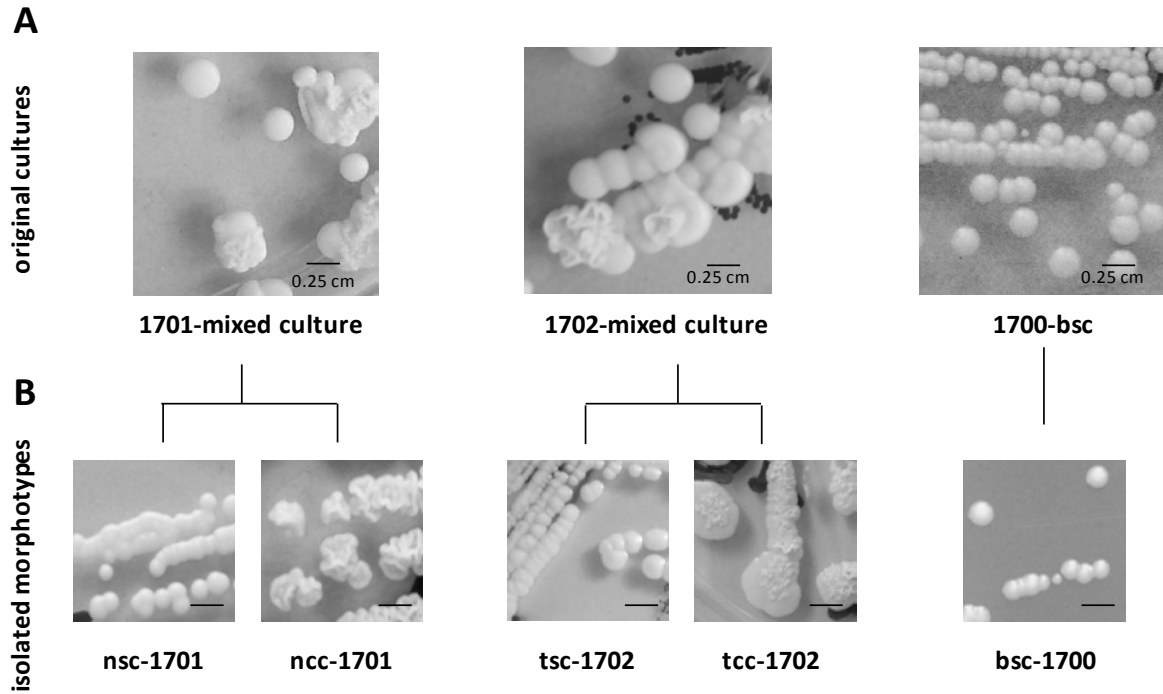


Figure 32. Colony morphology in routine culture. (A) Mixed *C. parapsilosis* growth from original routine plates from (left) nose swab (specimen 1701), (middle) throat swab (specimen 1702) and (right) blood culture (specimen 1700). (B) Isolated morphotypes from nose swab (B, left): nsc-1701 (nose swab, smooth colony) and ncc-1701 (nose swab, crepe colony), from throat swab (B, middle): tsc-1702 (throat swab, smooth colony) and tcc-1702 (throat swab, crepe colony) and bsc-1700 (blood smooth colony). All cultures were isolated on Sabouraud's agar and Columbia blood agar plates (bsc-1700).

One nasal and one oropharyngeal swab each grew colonies of two different morphotypes: cream, matte, round colonies (“smooth-matte” type) and irregular, asymmetrical, cream matte colonies (“crepe I” type); the BC isolate presented single colony morphology (smooth-glossy). As species-identification routine diagnosis, all stable morphotypes from BC and swabs were re-identified as *C. parapsilosis* by MALDI-TOF (see legend to Figure 32 for isolate naming).

After 96 h. incubation, three stable colony-types (smooth, crepe, and concentric) were produced from the five clinical isolates. Isolates from nasal and tracheal swabs appeared as both smooth and crepe I (s, cr-I) morphotype on Phloxine B agar (Figure 33, top row). Meanwhile, the isolate from blood culture (bsc-1700) only produced a smooth colony

Candida parapsilosis

type. The isolated swab samples reproducibly had two independent morphotypes (s-m and cr I) per source of isolation.

The five reference strains used at this point were CDC 317 (s-g), CBS 6318 (s-g), GA-1 (s-m), ATCC 22019 (cn-cr) and CBS 1954 (cr I). Three of the five reference strains produced only one representative phenotype per isolate, while CBS 1954 and ATCC 22019 regularly switched between morphotypes. The major colony-types in those were crepe (cr I) and concentric-crepe (cn-cr), respectively. Strain ATCC 22019 also switched to rough colony morphotype (~90%) and several infrequent smooth morphotypes (~10%, not shown). In case of the reference strain CBS 1954, the percentage of rough (cr I) morphotype was ~80% and smooth colonies ~20%, (Figure 33, top row). Microscopically, cells from smooth (s) colonies appeared round and regular shaped. In contrast, concentric (cn) and crepe (cr-I, cr-II) colony morphotypes correlated with clearly elongated pseudohyphal cells in isolates ATCC 22019-cn-cr and CBS 1954-cr-I, respectively. CBS 1954 also produced the strongest and most evident crepe colony morphotype, fully devoid of yeast-form cells. In contrast, the clinical isolates ncc-1701 and tcc-1702 produced a combination of round-shaped regular cells and incipient pseudohyphae (Figure 33, bottom row).

Candida parapsilosis

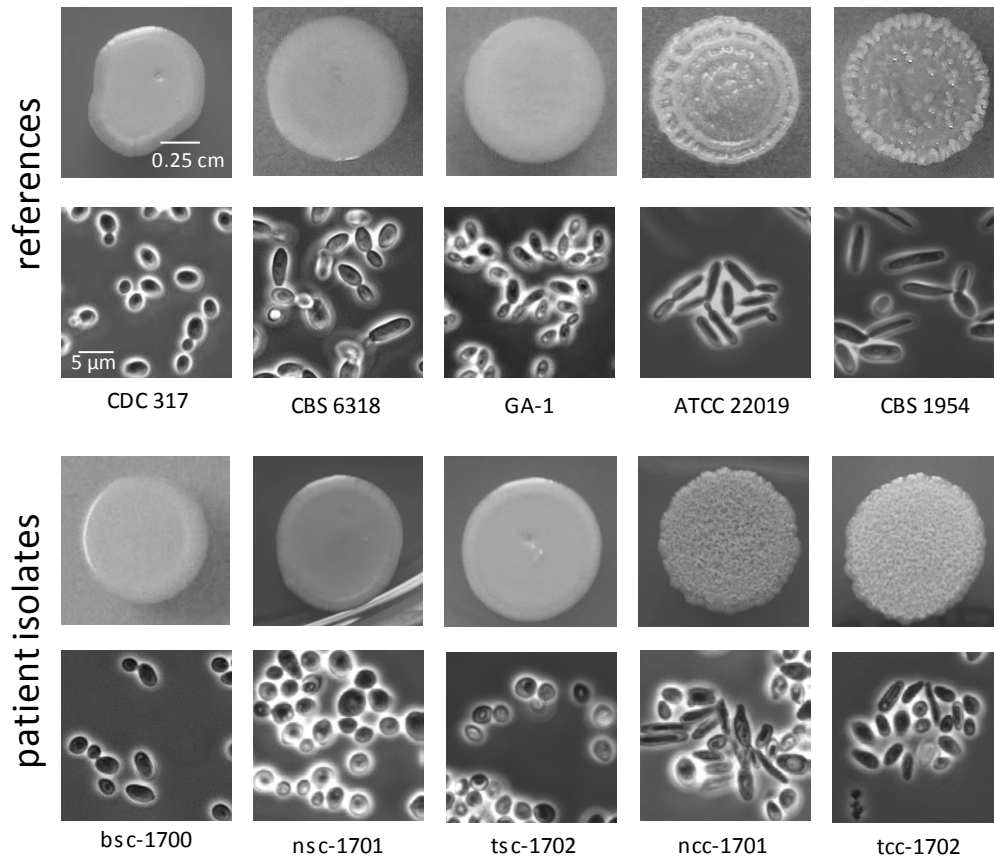


Figure 33. Morphological variations between clinical morphotypes. Top row: colony morphology on Phloxine B agar. Bottom row: cell shape and cell aggregation at 100X magnification in phase-contrast.

To analyze variations on adhesion-related properties, we tested the biofilm formation capacity to polystyrol, the cellular aggregation and agar invasion capacity of each morphotype. There was no strict correlation between biofilm formation capacity to polystyrol and colony morphotype in the five reference strains. However, among the patient isolates, only the two crepe clinical isolates (ncc-1701 and tcc-1702) showed a significantly higher capacity to form biofilms on non-charged polystyrol ($P < 0.001$), on average 50-fold higher than the control. The ranking of biofilm formation capacity to polystyrol (from least to highest capacity) was: nsc-1701 < CDC 317 < tsc-1702 < bsc-1700 < GA-1 < CBS 6318 < CBS 1954 < ATCC 22019 < ncc-1701 and tcc-1702 (Figure 34A). In addition, cell aggregation correlated with morphology, and thereby with biofilm formation capacity. Only the two isolates with hyperbiofilm-forming ability (ncc-1701 and tcc-1702)

Candida parapsilosis

also developed aggregates in YPD growth cultures. The isolate ncc-1701 produced intermediate aggregates; meanwhile the tcc-1702 developed better-defined clumps in liquid cultures. The two reference strains with concentric and crepe I morphotypes (ATCC 22019, CBS 1954) did not form aggregates in liquid media, which also correlated with an absence of biofilm formation capacity to plastic materials (Figure 34B).

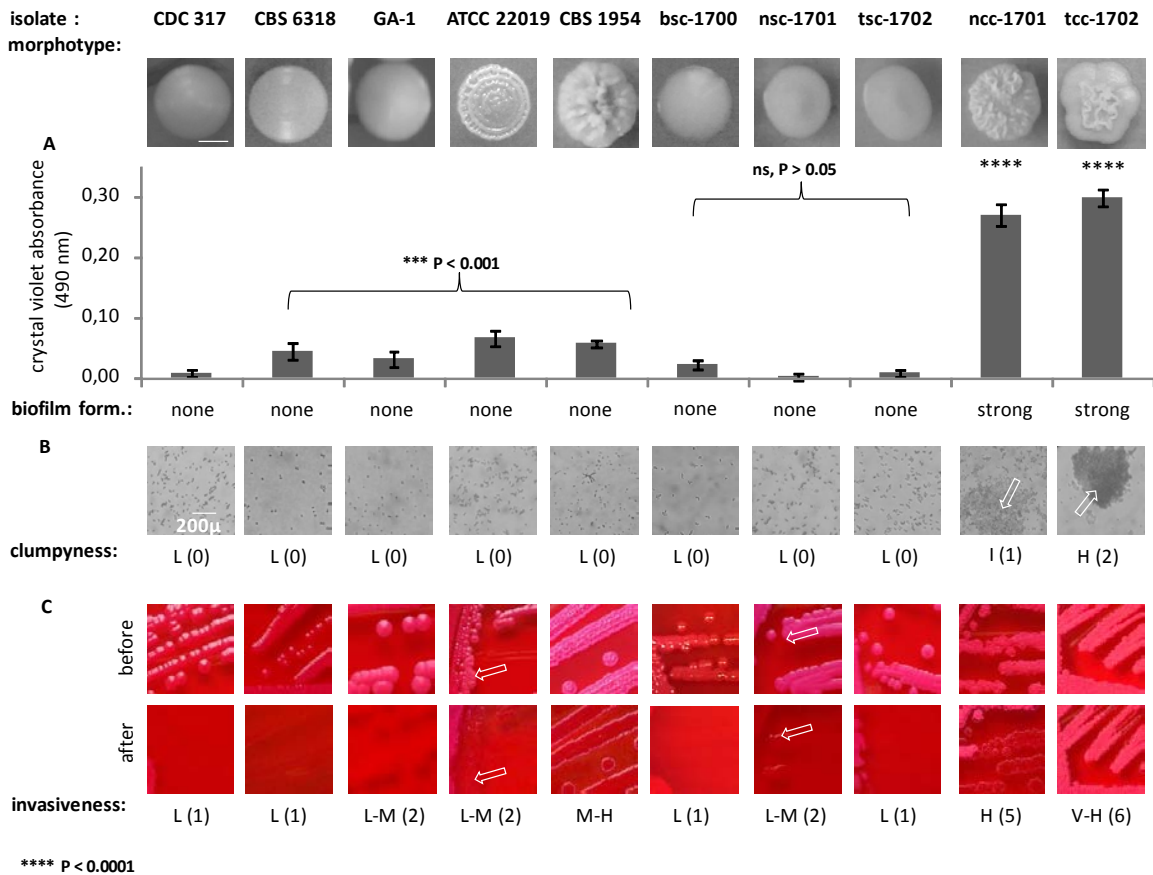


Figure 34. Biofilm formation-related phenotypes. Top row: representative colony morphologies used below (A-C). (A) Biofilm-formation capacity on polystyrol. The values are the means \pm standard deviations (error bars) of each isolate. Each experiment is the average of the absorbance of four technical measurements. Isolates were statistically compared with the CDC 317 using independent two-tail paired student T-test. The asterisks represent the 95% ($\alpha = 0.05$) confidence interval of the analyses. (B) Cell aggregation tests. Arrows indicate clumps in hyperbiofilm-forming isolates ncc-1701 and tcc-1702. (C) Agar invasion. Top row: colony growth on Phloxine B agar. Bottom row: agar invasion after washing the plates with running water. Arrows indicate partial agar imprinting corresponding with low to medium agar invasiveness. (L), low; (L-M), low-medium; (M-H), medium-high, (V-H), very-high.

Candida parapsilosis

Finally, isolates with crepe and concentric morphotypes invaded the agar better than smooth colony type. Our results showed a moderately increased agar invasion in crepe and concentric morphotypes as compared to smooth morphologies (Figure 34C). The strongest invasiveness was detected in CBS 1954, ncc-1701, and tcc-1702. A positive correlation between the three phenotypic properties (biofilm formation, aggregate formation, and invasiveness) was only evident in the two crepe clinical isolates.

Antifungal susceptibility testing showed that the reference strain CDC 317 (smooth) was intermediate against FLU (4 µg/ml), as previously reported (Grossman *et al.*, 2015). There were only slight differences between patient isolates: MIC values towards azoles in the ranged between 0.016 and 0.125 µg/ml, in case of Echinocandins the MIC values varied between 0.250 µg/ml for CAS and 2 µg/ml for MICA (Table 18). Variations in 5FC susceptibility were apparently influenced by morphotype variability and source of isolation (bsc-1700: 0.032 µg/µl and ncc-1701 and tcc-1702: 0.064-0.125 µg/µl, Table 18). All patient isolates were susceptible to the antifungal drugs tested. Only CAS MIC values for concentric (cn) morphotype in the control strain ATCC 22019 was slightly lower than values for smooth (s) and crepe (cr) colony phenotypes of the other isolates.

Candida parapsilosis

Table 18. Summary of clinically relevant properties in *C. parapsilosis* colony morphotypes

strain acronym	CDC 317	CBS 6318 ^e	GA-1	ATCC 22019	CBS 1954	bsc-1700	nsc-1701	tsc-1702	ncc-1701	tcc-1702	CVC
specimen number	ATCC®-MYA-4646™	ATCC®-7330™	SZMC 8110	CBS 604,	ATCC®-28474™	PEU-1700	PEU-1701	PEU-1702	PEU-1701	PEU-1702	not applicable ^c
				DSMZ-5784		day 16	day 20	day 20	day 20	day 20	day 31
specimen	health care worker's hand	skin	human blood	case of sprue	environmental	blood culture	nose swab	throat swab	nose swab	throat swab	central venous catheter
colony morphology on SAB-GC agar ^a	smooth	smooth	smooth	concentric	crepe	smooth	smooth	smooth	crepe	crepe	not recorded
MALDI Biotyper identification	<i>C. p</i>	<i>C. p</i>	<i>C. p</i>	<i>C. p</i>	<i>C. p</i>	<i>C. p</i>	<i>C. p</i>	<i>C. p</i>	<i>C. p</i>	<i>C. p</i>	<i>C. p</i>
log score ^b	2.09	2.19	2.09	2.05	2.03	2.07	2.02	2.07	2.05	2.10	2.20
biofilm formation capacity ^c	0.00798 ± 0.00622	0.04450 ± 0.01300	0.03265 ± 0.0055	0.06715 ± 0.0134	0.05765 ± 0.01285	0.02275 ± 0.00673	0.00285 ± 0.00535	0.00890 ± 0.00540	0.26925 ± 0.0181	0.29830 ± 0.0139	n.d. ^e
drug susceptibility^d											
FLU (µg/µl)	4	1	0.500	1	1	0.500	0.500	0.500	0.500	0.250-1	S
POS (µg/µl)	0.032	0.032	0.032	0.032-0.064	0.032	0.032	0.032-0.064	0.032	0.016-0.032	0.032	n.d.
VOR (µg/µl)	0.125	0.032	0.032	0.032	0.032	0.032	0.032	0.032	0.032	0.032	S
CAS (µg/µl)	1	0.500	1	0.500	0.500	0.500	0.250-0.500	0.250-0.500	0.500	0.25-1	n.d.
MICA (µg/µl)	2	2	2	1-2	2	2	1-2	1-2	1-2	1-2	S
5FC (µg/µl)	0.032	0.032	0.125	0.250	0.125	0.032	0.032-0.064	0.032-0.064	0.064-0.125	0.064-0.125	n.d.

^a morphology according to (Laffey and Butler, 2005); ^b obtained with YOTL-database (Bernhard *et al.*, 2014) by on-target-lysis; ^c biofilm formation capacity to polystyrol. CV absorbance measured at 490 nm. Cut-off value = 0.0771; ^d all EUCAST broth microdilution against FLU (Fluconazole), POS (Posaconazole), VOR (Voriconazole), CAS (Caspofungin), MICA (Micafungin) and 5FC (5-Fluorocytosine).

3.4.1 The five clinical isolates are distributed into three different genetic categories

Morphologically, the three smooth isolates were highly similar, differing only in bsc-1700's slightly increased biofilm formation capacity to polystyrol. Among the non-smooth types, aggregation of tcc-1702 was stronger than in ncc-1701. Despite the notable variation in their adhesion phenotypes, our hypothesis was that they represented stable forms of the same clonal population, and sought to confirm this by determining the karyotypic profile and genetic patterns.

Electrophoretic karyotyping differentiates eight somatic and the mitochondrial chromosome in the reference strain CDC 317 (Figure 35A). All were also detectable in the ten samples analyzed. However, differences in chromosome sizes were observed among patient isolates, mainly among the intermediate-sized (1-2 mbp) chromosomes with high diversity, potentially conferring to Chr. 3, 4, and 8. Low biofilm-forming isolates, nsc-1701 and tsc-1702 presented similar karyotypic pattern, visually close to tcc-1702. Conversely, the crepe isolate ncc-1701 resembled the smooth isolate bsc-1700, although they were not identical. Therefore, unexpectedly, variation between patient isolates was evident, resembling the variation range also seen between independent reference strains.

Since karyotyping results above were inconclusive, we next conducted whole genome analyses in collaboration with Dr. Toni Gabaldón Estevan (CRG, Barcelona, Spain) to clarify the genomic diversity. Whole genome sequencing indicated 3846 single nucleotide polymorphisms (SNPs) between the five strains compared to the CDC 317 (Figure 35B). The blood culture isolate bsc-1700 and nsc-1701 shared > 98.1 % SNPs (Table 19), indicating high similarity between both isolates. Meanwhile, the strain tsc-1702 was a genetic outsider (45-68% shared SNPs with the other groups). Similarly, the two hyper biofilm-forming crepe isolates ncc-1701 and tcc-1702 shared 99.2% of SNPs. In contrast, the number of shared SNPs between the bsc-1700 and the two crepe clinical isolates were less than 14%-15%. The two smooth strains isolated from swabs (nsc-1701 and tsc-1702)

Candida parapsilosis

shared close to 65% of SNPs. A PCA-based population analysis (Carreté *et al.*, 2018) including previously genome sequenced control strains (Pryszcz *et al.*, 2013) suggested a genetic distance between the three clusters similar to the independent reference strains.

Table 19. Percentage of Single Nucleotides Polymorphisms (SNPs) similarity between five clinical isolates

(% SNPs shared between clinical isolates)					
	bsc-1700	nsc-1701	tsc-1702	ncc-1701	tcc-1702
bsc-1700	NA	98.1	68.2	14.6	14.8
nsc-1701	98.1	NA	69.2	15.2	15.1
tsc-1702	68.2	69.2	NA	45.4	45.4
ncc-1701	14.6	15.2	45.4	NA	99.2
tcc-1702	14.8	15.1	45.4	99.2	NA

The percentage of shared SNPs between the bsc-1700 and nsc-1701 (99.2%) pointed to a close distance between both isolates. This was also indicated by a principal component analysis (Figure 35C) which placed bsc-1700 and nsc-1701 near clonality, as well as ncc-1701 and tcc-1702. Finally, tsc-1702 was found to be an independent genetic outlier.

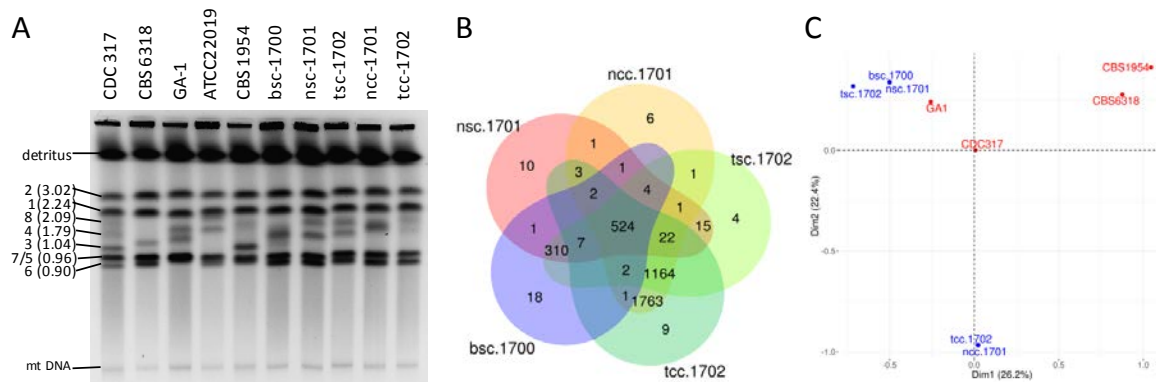


Figure 35. Genome sequencing analyses. Strain typing and genome sequencing. (A) Pulse-field gel electrophoresis suggests the isolates are not clonal. (B) Numbers of unique and shared SNPs between the 5 patient isolates and subsequent (C) PCA cluster analysis of the SNPome placing the 5 patient isolates (blue) into the context of other genome-sequenced strains (red), relative to CDC 317, indicates the presence of 3 independent clonal groups in the patient simultaneously.

3.4.2 Isolates strongly vary in their adhesion genes

To further explain the phenotypic properties, *C. parapsilosis* adhesin-encoding genes were analyzed to see if modification in gene-size and gene-presence varied between clinical morphotypes. Based on the previous analyses (3.4.1) *C. parapsilosis* clinical isolates differed in the number of SNPs shared and the morphotype they presented (Figure 35). Divergences on gene-size indicated possible deletions, duplications and recombination events involving seven adhesins. Isolates bsc-1700, nsc-1701 and tsc-1702 presented a similar tandem repeats pattern distribution compared with the two crepe reference strains (ncc-1701 and tcc-1702). Based on SNPs shared between clinical morphotypes, we remarked variations in the low complexity domain for CPAR2_500600, CPAR2_404780, CPAR2_404790, CPAR2_404800, CPAR2_403510 and CPAR2_403520. In contrast, no clear divergences in the agglutinin-like sequence *ALS3* were observed (Figure 36A). Deletions events involved CPAR2_500660 (2.2-2.7 Kb), CPAR2_404790 (2.5-4 Kb) and CPAR2_404780 (2.25-2.75 Kb) in the ncc-1701 and tcc-1702. Another possible deletion (reduced read numbers) event in the *ALS7* was observed in bsc-1700, nsc-1701 and tsc-1702. Nucleotide duplications (increase read numbers) in five adhesin-encoding genes were identified and detailed in Figure 36A. Increased number of SNPs (green panel, Figure 36A) were identified in the two crepe morphotypes in the gene encoding Hwp1 CWP protein. Genomic DNA amplification of selected CPAR2_404790, CPAR2_404800 (*ALS7*) and CPAR2_403520 (*HWP1*) confirms gene-size variations between smooth and crepe morphotypes (Figure 36C) and most strikingly in the *HWP1*.

To sum up, we associated morphotypic switch differences and variations in the degree of biofilm formation capacity to polysytyrol, with modifications in the tandem repeats copy number of seven adhesin-encoding genes (Figure 36). Correlation between the number of SNPs shared within smooth and crepe isolates positively correlates with deletion, duplication events in these adhesin genes. Variations in adhesin encoding-genes CPAR2_500660, CPAR2_404780, CPAR2_404790, CPAR2_404800, CPAR2_403510 and

Candida parapsilosis

CPAR2_403520 were observed between smooth (bsc-1700, nsc-1701 and tsc-1702) and crepe morphotypes (ncc-1701 and tcc-1702), (Figure 36A). This large plasticity in gene sequence may induced variations in adhesin's tandem repeats region length (Figure 36B). No remarkable genomic variations were observed in isolates displaying the same morphotypic switch, independently of the site of isolation.

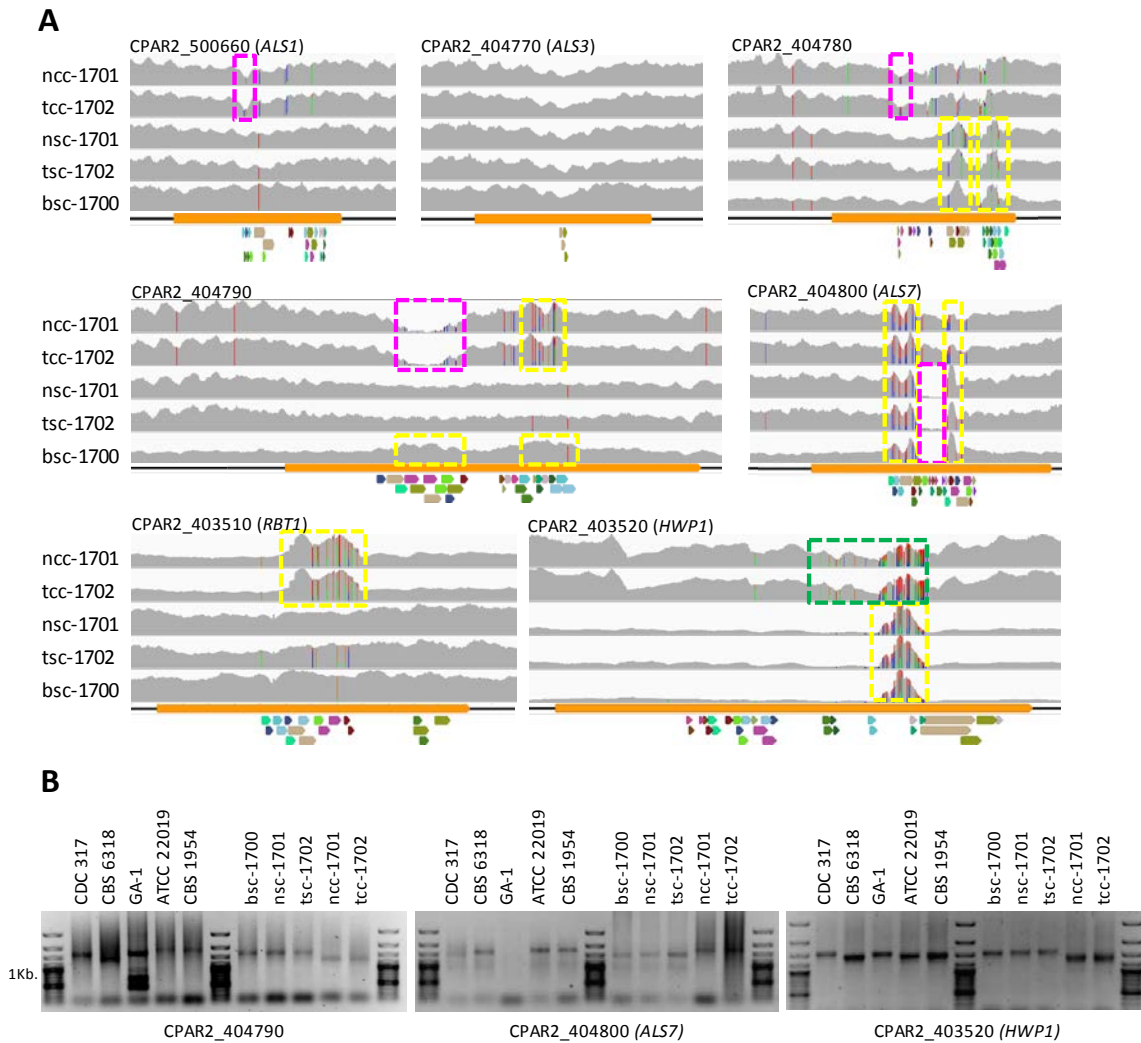


Figure 36. *C. parapsilosis* adhesin-encoding genes analyses. (A) Genome sequences of seven main adhesin-encoding genes of five different *C. parapsilosis* isolates. Raw Illumina reads mapped onto the CDC 317 reference sequence and counted (grey). SNPs are indicated by read, green, blue, or orange vertical dashes. Yellow boxes: increased read numbers, indicating repeat number extension; pink boxes: reduced read numbers indicating repeat number reduction. Colored arrows below sequence alignments, tandem repeat region (TRRs). (B) Selected PCR amplicons of repetitive regions in CPAR2_404790, CAPR2_404800, and HWP1 confirm the different lengths of the repeat regions.

3.5 *Candida parapsilosis* phenotypic cell surface variations correlate with differences at a proteomic level among isolates from a clinical strain collection

Based on the observations described above for a small set of isolates, we next created and characterized a collection of clinical *C. parapsilosis* isolates arising from the routine diagnostic laboratory. Examples of cultures with multiple phenotypes isolated on SAB's agar (s-cn-cr) are shown in Figure 37.

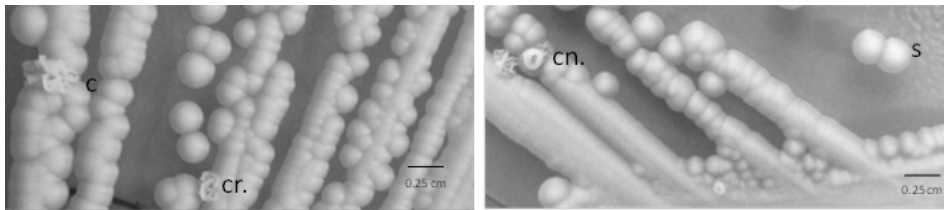


Figure 37. Colony morphology on SAB agar. Mixed cultures present (cr) crepe morphotype; (cn) concentric morphotype and (s) smooth colonies after 96 h. incubation time.

In total, 215 isolates were collected and characterized over the study period (2015-2017). Biofilm formation capacity on polystyrol surfaces were quantified and the isolates stratified into nine different groups according on the isolates' body site of isolation. The distribution of the clinical samples depending on the origin of isolation is detailed in Figure 38A. The majority of the isolates received from the diagnostic laboratory were obtained from ear-nose swabs (30%) and isolates from gastrointestinal tract or oral cavity were the least frequent (~ 2.5-3 %).

Candida parapsilosis

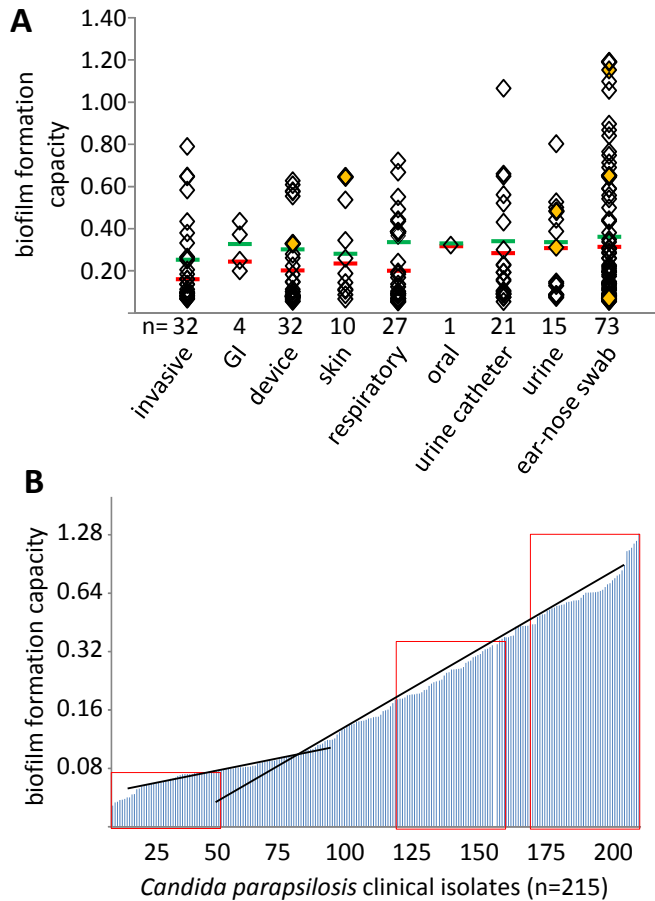
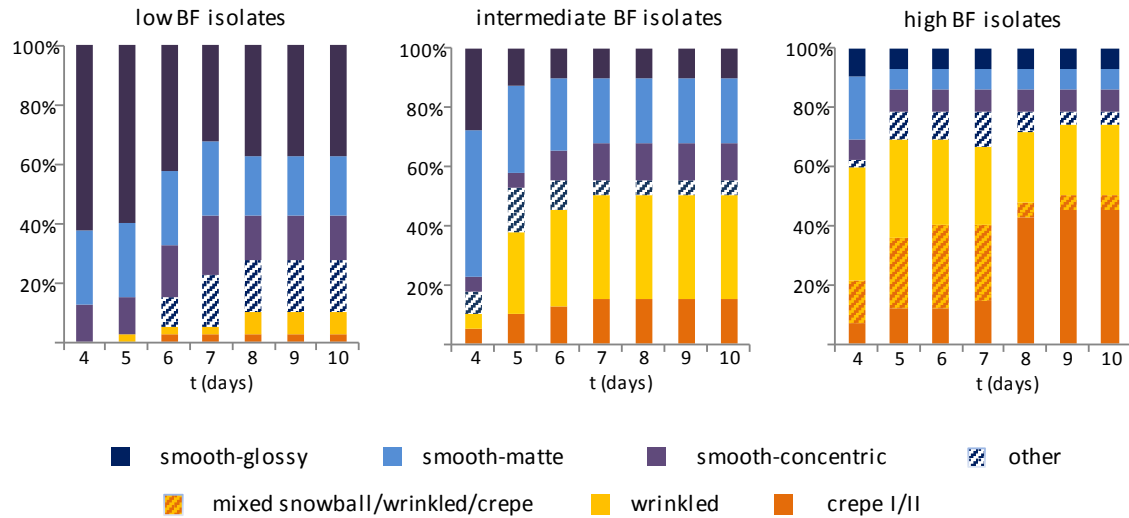


Figure 38. *C. parapsilosis* clinical isolates distribution. (A) Isolates classified according to the body site of isolation (n = 215). Green and red lines indicate the two-fold median cut-off. (B) Isolates stratified according to biofilm formation capacity to polystyrol. Three groups selected for subsequent experiments (red boxes): LBF (0.054-0.080), IBF (0.153-0.370) and HBF (0.445-1.360). Intersection of black lines: approximated cut-off.

Based on the degree of biofilm formation capacity to polystyrol, three isolate groups were selected for subsequent analyses: 39 LBF, 39 IBF and 39 HBF (Figure 38B), including two reference strains (CDC 317, ATCC 22019) to a total of 119 isolates. Predominant morphotypes in the collection were determined to estimate the correlation between adherence capacity to polystyrol, colony morphology and agar invasiveness along ten days (Figure 39).

A morphotype development



B agar invasion

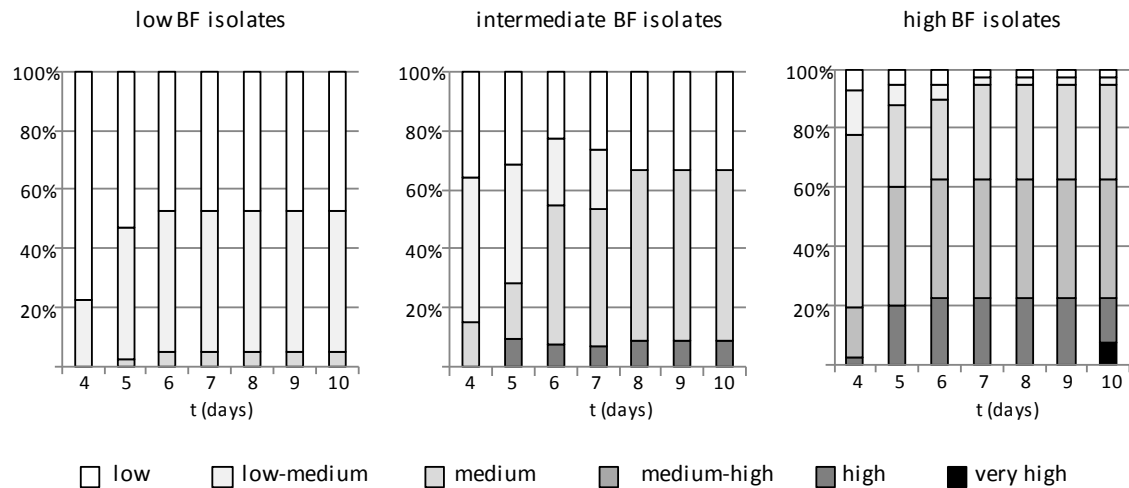


Figure 39. Clinical isolates biofilm formation capacity. (A) Colony morphology and (B) agar invasion on YPD + Phloxine B agar, tested by scraping with inoculation loop; both stratified by adhesion capacity. Distribution of colony morphotypes in a ten days experiment: isolates with low biofilm formation capacity (LBF, left), intermediate biofilm formation capacity (IBF, middle) and high biofilm formation capacity (HBF, right). Colony morphotype classification in (A): smooth-glossy (dark blue), smooth-matte (blue), smooth-concentric (purple), wrinkled (yellow), crepe I/II (orange), mixed snowball/wrinkled/crepe (yellow-orange) and mixed morphotypes (other). Color code (grayscale) in (B) represents invasiveness classification in six defined categories: low, low-medium, medium, medium-high, high and very high.

In the LBF group, all 39 isolates produced smooth (s-g, s-m and s-cn) phenotype after 96 h of incubation at 30 °C. From day 5 on, wrinkled and crepe phenotypes emerged with

Candida parapsilosis

increasing frequency up to day 10 (7.5% and 2.5%, respectively on day 10). The smooth-glossy phenotype (s-g) was the most prevalent morphotype among LBF isolates, decreasing in frequency by 30% along five days in favour of non-smooth (10%) and mixed morphotypes (20%) until day 10.

In the IBF group, smooth-matte was the most frequent (68.2%) colony morphology at day 4 (96 h), decreasing to 37.5% on day 10, surpassed by wrinkled or crepe (up to 40%).

In contrast, HBF isolates mainly produced wrinkled and crepe morphotypes (25% and 47.5%, respectively) with a decreased number of smooth strains (17.5%) right from the beginning on day 4. The majority of the isolates which display more than one morphotype presented a final crepe morphology at day 10.

Using two different strategies to test agar invasion capacity on Phloxine B we found that the LBF isolates tended to be less agar invasive than the IBF and HBF isolates. Scoring agar invasiveness along ten days with scraping a small part of the growth off the agar (strategy 1) indicated that approximately a 95% of the LBF isolates presented only low-medium invasion capacity. Almost 40% of the IBF isolates developed medium agar invasion capacity, and the HBF group isolates displayed a wider range of invasion intensity, predominantly the medium-high agar invasion category (~85%) (Figure 39B).

In accordance with the values described above (Figure 39B); the low and low-medium (cat. 1 and 2) invasion intensity in the LBF isolates was evident (37/39) when plates were washed on the final day under running water (strategy 2). In case of IBF isolates, 67.5% of the isolates previously classified as medium (cat. 3) were reclassified as medium-high (cat. 4) agar invaders, as imprints were observable here. Among HBF isolates close to ~45% of the strains were placed in subgroup 4 and another 45%, were ranked as high (cat. 5) or super high (cat. 6) as colonies remained intact after washing (Figure 40). In summary, there was a clear correlation between the capacity to form biofilms on abiotic surfaces, colony morphology, and the ability to invade into agar.

Candida parapsilosis

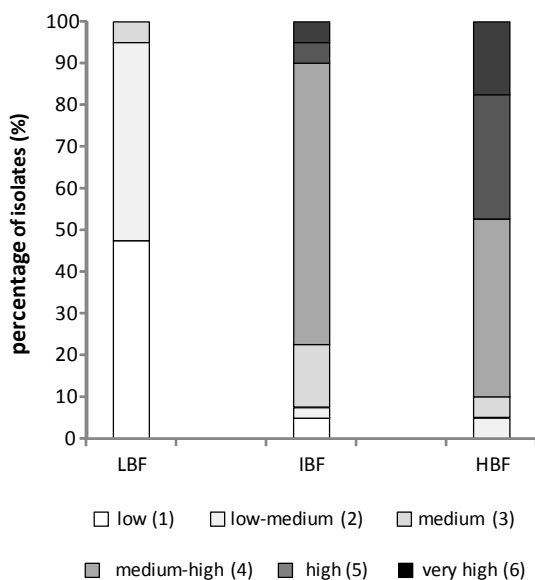


Figure 40. Correlation between agar invasion and biofilm formation capacity. Final scoring on day 10 in an agar invasion experiment (see Figure 39), removing the cells off the agar with running water instead of scraping with inoculation loop. Left, LBF (low biofilm-forming isolates); middle, IBF (intermediate biofilm-forming isolates); right, HBF (high biofilm-forming isolates). Color code (grayscale) represents invasiveness classification in six defined categories (see Figure 30D).

3.5.1 *C. parapsilosis* isolates present variations in antifungal susceptibility based on the biofilm formation capacity to abiotic surfaces

The 117 selected and 2 reference strains of the clinical collection were tested for susceptibility to selected azoles (FLU, POS, VOR), echinocandins (CAS, MICA), and one polyene (AMB). Only 4 isolates plus the reference strain CDC 317 showed highly elevated MIC values of 4-16 $\mu\text{g}/\mu\text{l}$ for FLU. These isolates originated from the IBF group, and from diverse sites of isolation, including nasal swabs (PEU768 and PEU950), medical devices (PEU651), or invasive candidiasis of the backbone (PEU941).

As it was already described by Souza *et al.*, 2015, that a point mutation, in the position 132 of the gene CPAR2_303740-*ERG11* is involved in a reduced susceptibility to FLU. In this case, the aa. tyrosine (Y) is changed to phenylalanine (F) in the *C. parapsilosis* CDC

Candida parapsilosis

317. Gene sequencing analyses of *ERG11* and *MRR1* for the selected FLU resistant isolates (4-16 µg/µl) with intermediate biofilm formation capacity were performed and no point mutation was remarked. Only in PEU651 *MRR1* contained non-synonymous SNPs (leading to amino acid exchanges). Since we could not exclude a potential influence of such mutations, PEU651 data was excluded from further analyses.

To assess the impact of morphology on drug susceptibility, the inoculum was prepared once after 24h and once after 8 days of maturation on agar, excluding the four resistant isolates mentioned above. IBF isolates showed a wider morphotypic variability; in HBF isolates the crepe I and II morphotypes (~75%) prevailed. The range of biofilm formation capacity to polystyrol of these isolates varied between 0.183 (LBF) to 0.348 (HBF), where the latter is 14-fold more adherent than the reference strain CDC 317.

After 24 h. pre-culture, LBF and HBF isolate groups differed slightly, but with statistically significance for FLU and POS susceptibility (2-3 log₂-fold differences). Also in case of echinocandins, differences between LBF-HBF against CAS were found. No apparent differences for either VOR or AMB were seen (Figure 41A). The analysis after eight days of colony development indicated significant variations only between IBF-HBF and LBF-HBF towards FLU and POS but not for VOR. No differences for CAS within the three groups were observed.

In summary, this showed that susceptibility rates of *C. parapsilosis* clinical isolates for two azoles (FLU and POS) and two type of echinocandin (CAS and MICA) were slightly influenced by morphotype and biofilm-forming capacity (Figure 41). However, in none of the cases, the observed MIC differences resulted in a major change in clinical classification (e.g. from "S" to "R")

Candida parapsilosis

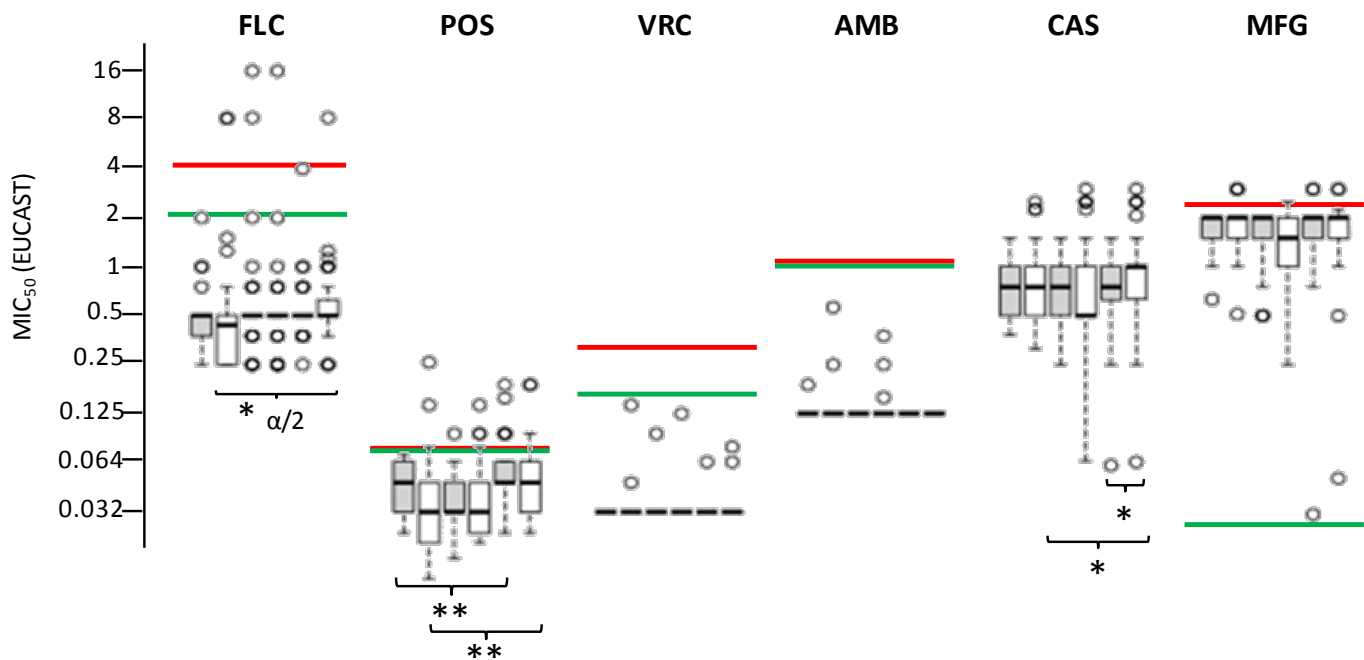
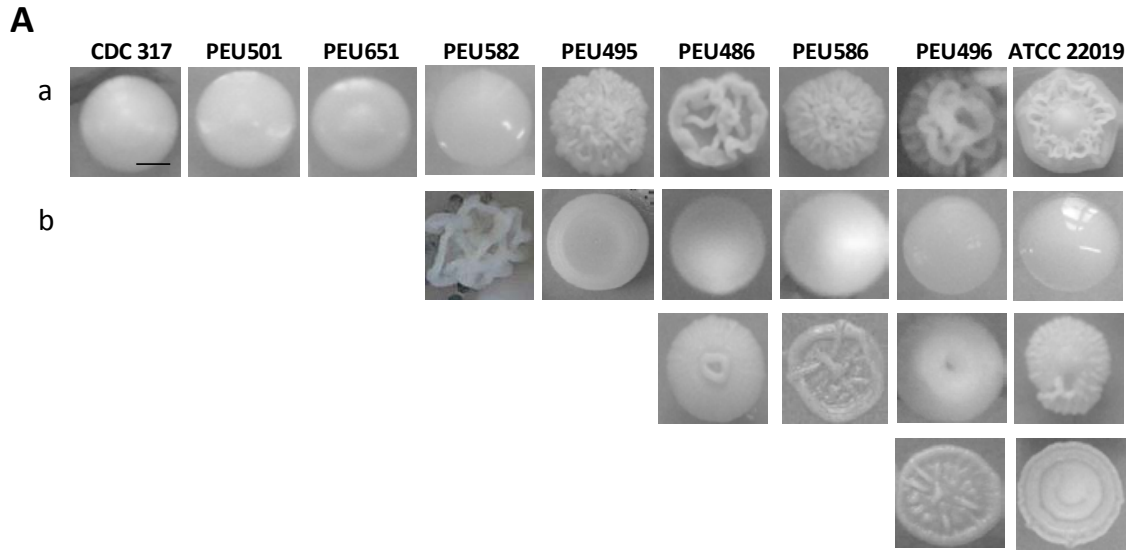


Figure 41. Drug susceptibility test of one hundred seventeen clinical isolates + two reference strains (CDC 317, ATCC 22019). Biofilm formation-phenotype dependent susceptibility testing where inoculum was prepared from cells after 1 d growth (young colonies) on SDA (grey boxes) and after 8 d growth (mature colonies), (white boxes) of the identical plates, when colonies had fully developed morphologies. Red lines: EUCAST clinical breakpoint (R>); green lines, susceptible cut-off (S ≤). MIC values were calculated after 24 h. The results are the average of two independent experiments. *, Welch T-test with unequal variances, $\alpha = 0.05/2$.

3.5.2 Morphotype generally predetermines other phenotypic properties in *C. parapsilosis* clinical isolates

To investigate *C. parapsilosis* agar invasion capacity and its correlation with morphotype switching capacity as well as cell-morphology two controls and seven isolates from the collection were selected to reflect a range of morphotypic variations (Figure 42). Three of the strains (CDC 317, PEU501, and PEU651) produced only the smooth morphotype. Two isolates (PEU495 and PEU582) produced both smooth and crepe morphotypes. Isolates PEU486 and PEU586 showed one major morphotype (crepe), but with low frequency also smooth or concentric colony types. Finally, isolates PEU496 and the ATCC 22019 reference strain frequently switched between four colony morphologies each, the crepe morphology being most frequent. When lineages derived from each isolates' morphology were tested for their ability to form biofilms on polystyrol (Figure 42B), large differences were still observed between isolates, but only less so between lineages derived from a single isolate. For example, variation in biofilm formation capacity based on the morphotypic switch significantly differ in three HBF isolates ($P < 0.01$), meanwhile the IBF isolate PEU582 did not present differences between smooth and crepe morphologies. The largest differences in biofilm formation capacity intra-strains were displayed by the isolates PEU495 (smooth <> crepe) and PEU586 (crepe <> concentric).

In summary, hyper biofilm-forming isolates were statistically different ($P < 0.01$) to the CDC 317 (s) and ATCC 22019 (s, crt, cn and cr) at all times, independently of the morphotype observed. Intra-strains differences were significantly high in HBF isolates, mostly, concentric and crepe morphotypes displayed strong biofilms compared with smooth morphologies. Nevertheless, adherence capacity is mainly influenced by strain specific properties.



B

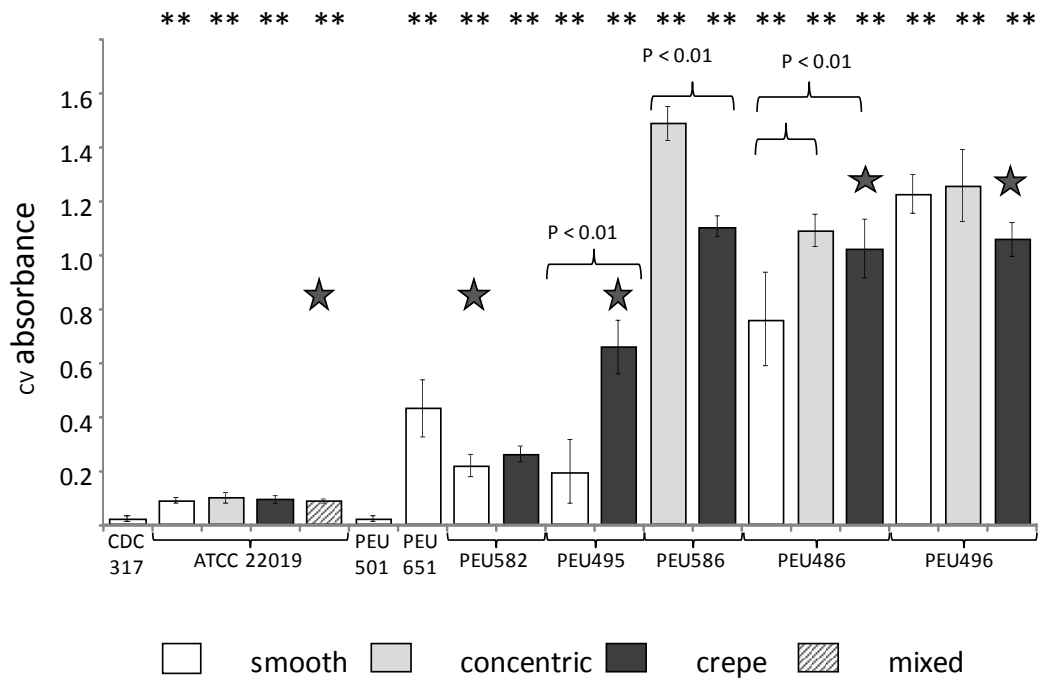


Figure 42. Morphologic variation of nine *C. parapsilosis* isolates on SAB agar plates. (Aa) Major colony morphotypes of clinical isolates selected for downstream analyses. (Ab) Less frequent morphotypic variation. (B) Biofilm formation capacity quantification assay of morphologically different lineages derived from individual isolates. Stars, “most representative” morphotype in each clinical isolate.

Candida parapsilosis

Next, we determined if the different colony morphologies in this set led to changes in drug susceptibility. No general variations on the MIC between different colony morphotypes were observed (Table 20) with the exception of the PEU486-cn which showed eight and fifteen times reduced susceptibility to VOR and POS, respectively, compared to smooth and crepe morphologies. In case of the PEU486-cr, PEU496-cr and PEU586-cr, the susceptibility against CAS was reduced between two-four times compared to smooth and concentric morphotypes (Table 20). Clinical isolates were classified sensitive to all drugs tested, with the exception of CDC 317 and PEU651, which were FLU resistant.

Table 20. Antifungal susceptibility test of the morphotypic switches (smooth<>crepe<>concentric) of nine selected *C. parapsilosis* isolates

clinical isolates	FLU (µg/ml)	VOR (µg/ml)	POS (µg/ml)	CAS (µg/ml)	MICA (µg/ml)
CDC 317s	4-16	0.125-0.250	0.125-0.250	1	1-2
ATCC 22019s	0.500-1	0.032-0.064	0.064-0.125	0.500-1	0.500-1
ATCC 22019cn	1	0.032	0.064	1	0.500
ATCC 22019cr	1	0.032	0.064	1-2	1-2
PEU501s	0.250-0.500	0.032-0.064	0.064-0.125	0.250-0.500	1-2
PEU651s	4	0.032-0.064	0.064-0.125	0.5-1	0.125-0.250
PEU582s	0.500-1	0.032	0.064-0.125	0.500-1	2
PEU582cr	2	0.064	0.064	1-2	1
PEU495s	0.500-1	0.032	0.064-0.125	1-2	2
PEU495cr	0.500-1	0.125-0.250	0.032-0.064	1-2	1-2
PEU586cr	1	0.032	0.125	2	2
PEU586cn	1	0.125	0.064-0.125	0.250-0.500	0.500-1
PEU486s	0.500-1	0.032	0.032-0.064	0.250	1-2
PEU486cr	1	0.032-0.064	0.032-0.064	1	1-2
PEU486cn	0.5	0.250	0.500	0.500	1
PEU496s	0.5	0.032	0.016	0.5	2
PEU496cr	0.5	0.032	0.064	2	2
PEU496cn	1	0.125-0.251	0.064-0.125	0.250-0.500	0.500

***Boldfaced values, isolates and morphotypes with reduced susceptibility towards specific antifungal drugs.**

Candida parapsilosis

To verify if morphotypic variations within isolates could carry chromosomal alterations, karyotypic analyses (Shin *et al.*, 2001) of one HBF clinical isolate with three different morphotypes were performed. No apparent differences between rough morphotypes were observed, in contrast, slightly differences between “smooth” and “rough” (concentric and crepe) morphotypes were identified in the intermediate chromosomes (chr. 3, 4 and 8), (Figure 43), but the data is still inconclusive, further experiment will be needed to corroborate these observations.

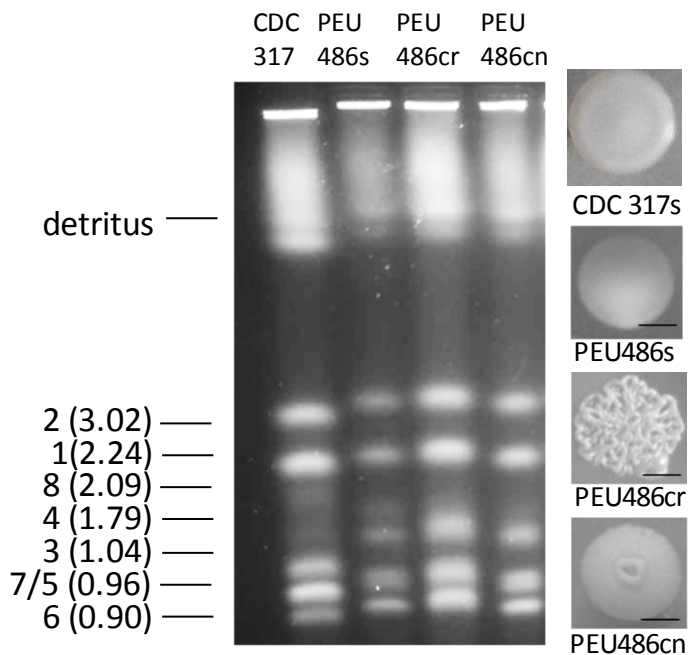


Figure 43. Electrophoretic karyotyping of *C. parapsilosis* PEU468 morphotypes. *C. parapsilosis* morphotypes produced by linages of PEU486 were analyzed and compared with *C. parapsilosis* reference strains CDC 317.

After confirmation that morphotypic differences did not correlate with gross chromosomal alterations in PEU486, the predominant colony type of each clinical isolate was selected for the subsequent analyses. Seven different phenotypic parameters of the major colony types from the nine selected isolates are summarized in Figure 44. CDC 317,

Candida parapsilosis

PEU501, PEU651, and PEU582 showed a major smooth morphology on Phloxine B agar plates, PEU486, PEU495, PEU496 and PEU586 had crepe morphotype and ATCC 22019 was frequently identified as concentric-crepe. Regular colony border was observed in the smooth morphotypes, wavy colony border was found in three crepe morphotypes, and two of the nine isolates (PEU495-cr and ATCC 22019-cn-cr) presented a rough colony border with pseudohyphae development after 24h. Microcolonies on Cornmeal agar showed the distinctive “spider” phenotype typically produced due to pseudohyphae development with crepe and concentric-crepe colony morphology. Isolate PEU582 also showed preliminary spider structures, probably explained by the dual morphotypic switch (smooth <> crepe). A qualitative biofilm formation analyses between the colony morphotype and the capacity to establish a biofilm asserted a positive relation between smooth type and absence of adherence (e.g. PEU501), and non-smooth phenotype with adhesiveness (e.g. PEU495), (Figure 44F and G). These parameters also matched with agar invasiveness, (Figure 44H and I). Cell shape morphology were classified into three groups as round yeast cells, mixed yeast and pseudohyphae in cr strains and single elongated pseudohyphae form in cn-cr morphotypes (Figure 44E).

Crepe isolates PEU486cr, PEU495cr, PEU496cr and PEU586cr showed strong capacity to establish biofilms on polystyrol after 24 h from initial YPD liquid cultures. In contrast, smooth phenotype-cells were not able to produce biofilms (Figure 44A). Smooth colonies made around 20-60 % less biofilm than the HBF crepe morphotypes, generating 70-95% less biofilm compared to the PEU-586-cr, which had the highest biofilm formation capacity in this strain subset. Isolates were ranked according to their capacity to adhere to polystyrol as PEU586-cr > PEU486-cr > PEU496-cr > PEU495-cr > PEU651-s > PEU582-s > ATCC 22019 > CDC 317 > PEU501-s (Figure 44A). Similarly, differences between adhesion (90 min.) and biofilm formation capacity to polystyrol (24 h) from independent colonies were detected ($P < 0.01$), (data not shown).

Candida parapsilosis

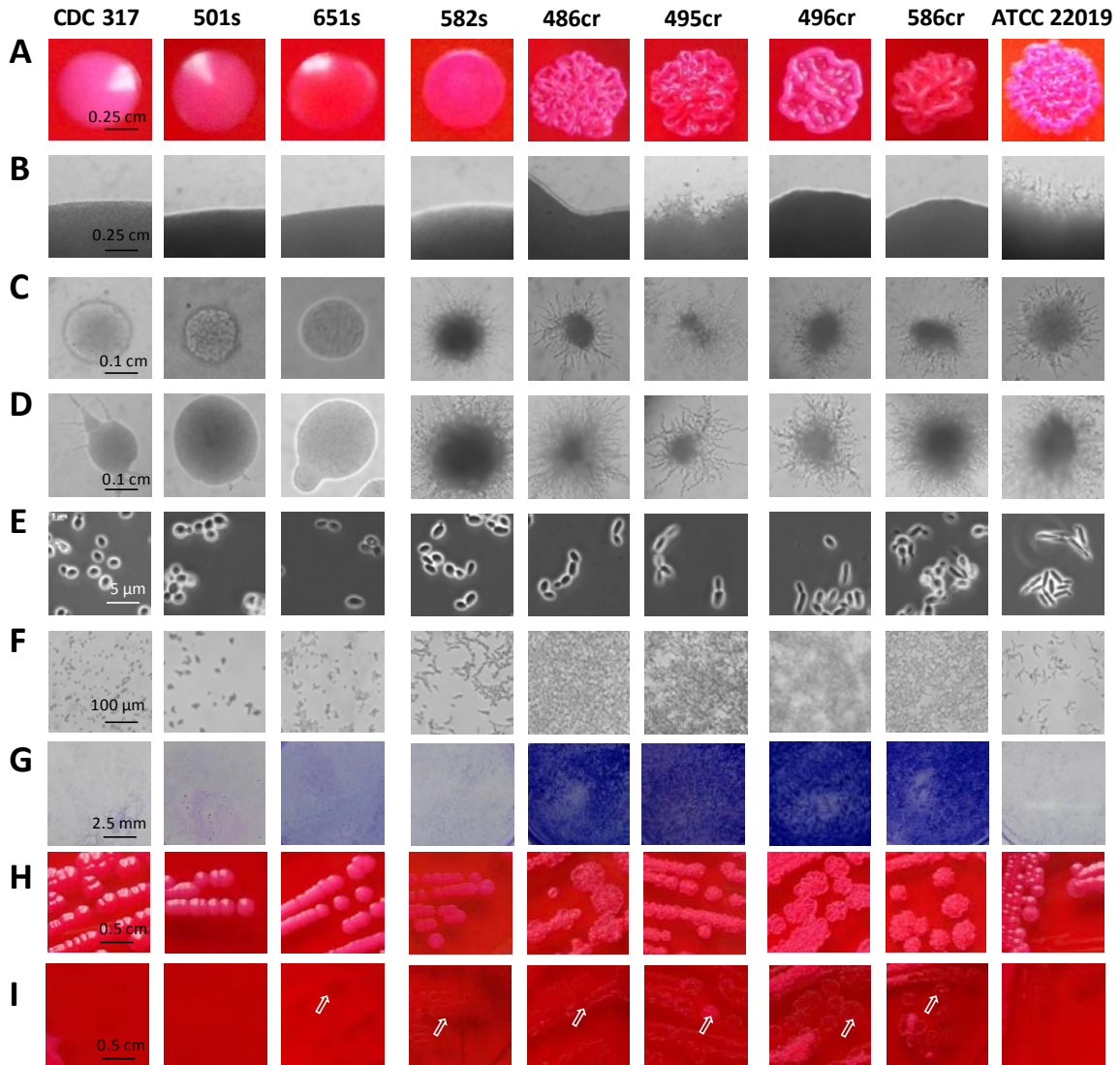


Figure 44. Phenotypic and morphological differences in nine *C. parapsilosis* clinical isolates. (A) Major colony morphotypes on YPD + Phloxine B. A1-4, smooth morphotype (s). A5-8, crepe (cr). A9, concentric-crepe. (B) Colony border under optical microscope 10X. B1-4, regular colony border. B5, B7 and B8, wavy colony border (emerging pseudohyphae formation). B6 and B9, rough colony border (pseudohyphae formation). (C) Microcolonies in corn meal after 48 h. incubation time. C1-3, regular microcolony. C4-9, spider microcolony. (D) Microcolonies in corn meal agar after 96 h. incubation time. D1, spider microcolony (incipient pseudohyphae). D2-3, regular microcolony. D4-9, spider microcolony (pseudohyphae development). (E) Cell shape under contrast-phase microscope 100X (immersion oil). E-1:E-4, round yeast cells. E-5:E-8, mixed yeast and pseudohyphae form. E9, pseudohyphal cells. (F) Biofilm formation to polystyrol. F1-2 and F9, low biofilm. F3-4, intermediate biofilm formation. F5-8, high biofilm formation. (G) Biofilm formation using crystal violet quantification assay. (H) Colony morphology on Phloxine B agar plates. (I) Invasiveness after ten days incubation on Phloxine B agar. I1-2, low agar invasion. I3-4 and I9, medium and medium-high agar invasiveness. I5-8, high agar invasion (5). Arrows indicated colony imprints on agar after removing the colonies with water at day ten.

3.5.3 Biofilm formation capacity on silicone

The importance of abiotic materials as polystyrol and silicone in terms of nosocomial infections let us to analyze variations in biofilm formation within our selected HBF isolates also on silicone. The seven clinical isolates, plus the reference strain CDC 317, were classified in four different groups (Figure 45A) depending on their adhesion capacity to these materials. Two of the eight isolates had no capacity to adhere to any material (PEU501s, CDC 317), two adhered only to polystyrol (PEU582s and PEU651s), and the other four were able to establish biofilms on both, polystyrol and silicone (PEU486-cr, PEU495-cr, PEU496-cr and PEU586-cr). The ability to form biofilms on silicone apparently correlated with the crepe morphotype but more strains should be analyzed to confirm these preliminary data. There were no isolates that adhered to silicone only. All HBF isolates attached to both materials (Figure 45B) and differences between the CDC 317 and the clinical isolates, were evident using polystyrol materials (IBF and HBF), but no differences for silicone were found within isolates with smooth morphotype ($P > 0.05$), (Figure 45B). Again, the capacity to adhere to abiotic devices varies significantly between different clinical isolates and “rough” morphotypes usually present strong capacity to form biofilms compared with “smooth” morphotypes.

Candida parapsilosis

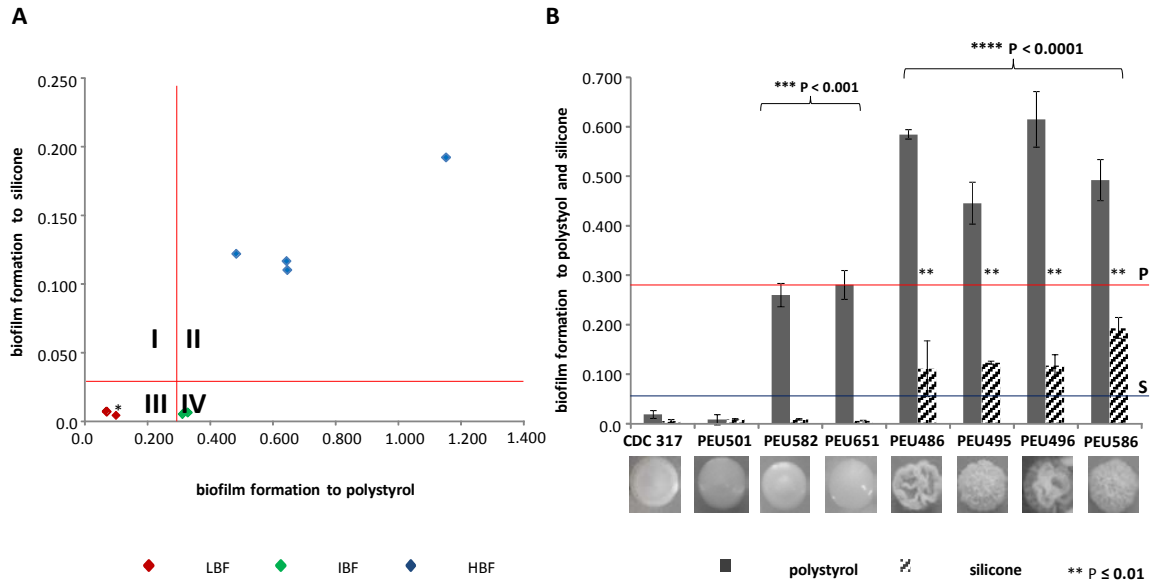


Figure 45. *C. parapsilosis* biofilm formation to polystyrol and silicone from a strain collection of clinical isolates. (A) Correlation between biofilm formation capacity to polystyrol and silicone of seven clinical isolates + CDC 317 (*). Four groups were classified as: I adherent to silicone; II, adherent to both materials; III (adherent to any material); IV, isolates adherent to polystyrol). Red diamonds, LBF; green diamonds, IBF and blue diamonds, HBF. (B) Biofilm formation to polystyrol and silicone of seven selected isolates. Results were the average of two independent biological replicates and each replicate represented the average of four technical repetitions. Red and blue lines correspond with polystyrol and silicone cut-offs ($X \sim 0.290$ and $X \sim 0.045$, respectively).

3.5.4 Sedimentation rates differ between colony morphotypes

Cell sedimentation analyses also showed variations between morphotypes and isolates. Isolates with smooth (73-80%) and crepe colony types (76-83%) were slower to sediment as compared to those producing mixed colony morphotypes and those with clear pseudohyphae development. Isolates PEU582, PEU586 and ATCC 22019 sedimented fastest after 120 min. (93%, 88 % and 80%, respectively). A correlation between the morphotype and the capacity to sediment was observed between clinical isolates. Within the same morphotype, a positive correlation between strain-sedimentation and level of aggregation was seen (PEU582 > PEU586 > ATCC 22019; PEU486 > PEU495 > PEU496; PEU501 > PEU651). Isolates with mixed morphotypes (PEU582 and PEU586) sedimented

Candida parapsilosis

significantly faster ($P < 0.05$) and sedimentation capacity of clinical isolates was most strongly associated with pseudohyphae development and cell aggregation (Figure 46), which was higher both in concentric colony types and absent in smooth colony morphologies.

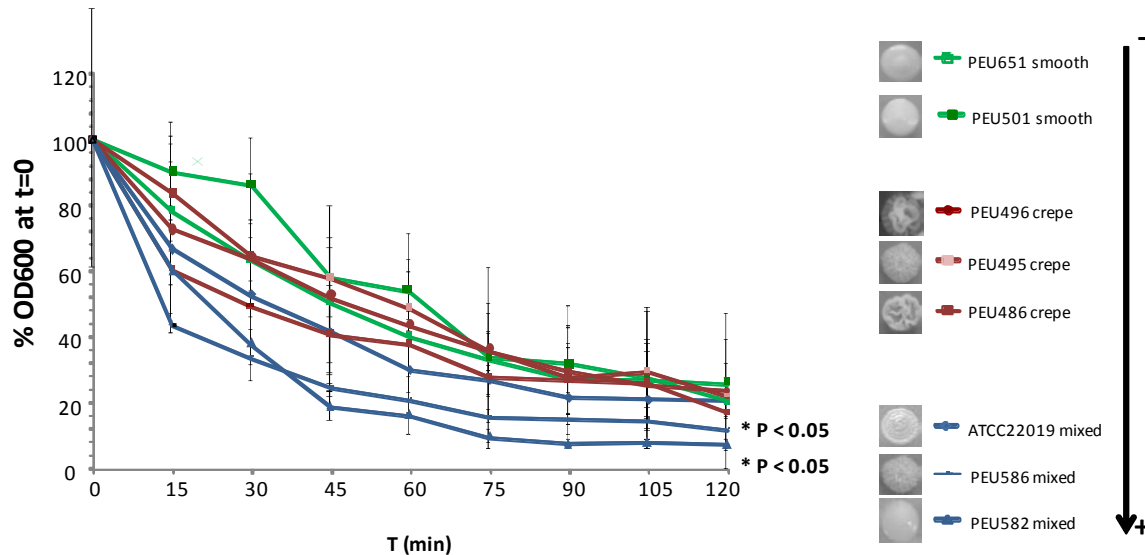


Figure 46. *C. parapsilosis* sedimentation capacity between different clinical morphotypes. Clinical morphotypes were classified in three groups, as low, intermediate and high-sedimentation capacity. Student t-test analyses were performed indicating statistically significant differences between PEU582 and PEU586 and all remaining isolates tested except PEU486-cr.

3.5.5 Clinical *C. parapsilosis* isolates show virulence differences.

Virulence differences between selected *C. parapsilosis* clinical isolates were measured using *G. mellonella* as an *in vivo* animal model for systemic infection. Isolates with HBF capacity (PEU486-cr, PEU495-cr and PEU496-cr) and LBF (PEU501-s) were tested at two different inoculum concentrations to detect differences between clinical isolates with different main morphotypes. The *C. parapsilosis* dose injected in the caterpillars was reduced from $2 \times 10^6 / 10 \mu\text{l}$ (A) to $10^6 / 10 \mu\text{l}$ (B) to increase accuracy among clinical isolates. Differences between individual isolates were observed. Smooth colony types

Candida parapsilosis

from isolates PEU501s, PEU582s and PEU651s had a killing rate of 95%, 95% and 75%, respectively, on day 9 p.i. The isolates with predominant crepe morphotype had a killing rate of 100%, and no caterpillar's survival after nine days of incubation at 37°C was observed (PEU486-cr, PEU495-cr and PEU496-cr). Surprisingly, also a single hyperbiofilm-forming isolate (PEU-586cr) was less virulent than the other three with crepe morphotypes (1.25x). Hyperbiofilm forming isolates had a killing rate of 100% (n = 20) at day 4 (PEU486), 6 (PEU495) and 7 (PEU496) respectively, correlating with a high biofilm forming capacity (HBF =2), a high agar invasiveness (5 and 6), and pseudohyphae development.

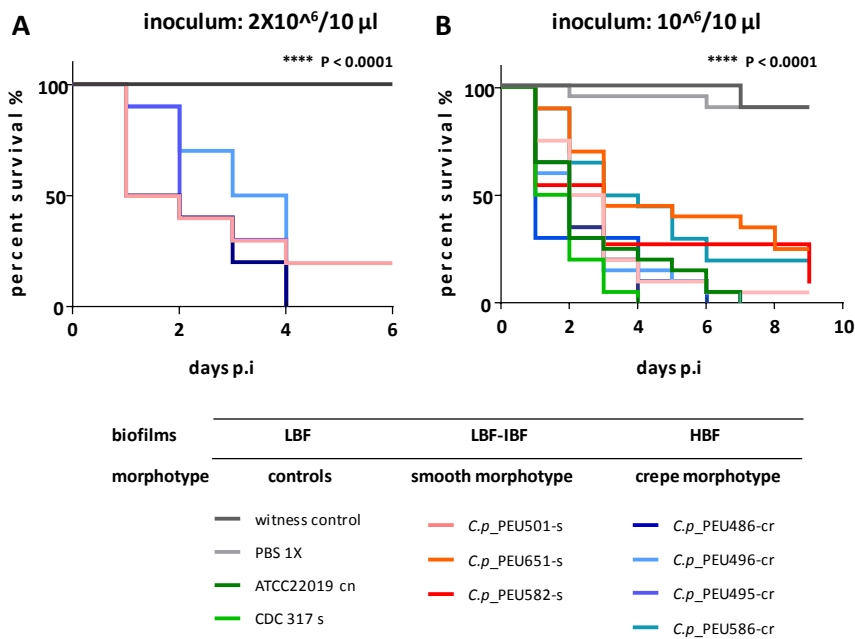


Figure 47. *Galleria mellonella* infection animal model. Survival curves. (A) first virulence assay using n = 10 *G. mellonella* caterpillars injected with $2 \times 10^6 / 10 \mu\text{l}$ cells of three HBF and one LBF *C. parapsilosis* clinical isolates. Caterpillar survival at 37° was scored for six days. (B) low inoculum of selected LBF, IBF and HBF isolates, $1 \times 10^6 / 10 \mu\text{l}$ cells were injected into n = 20 caterpillars per isolate, survival at 37°C scored along nine days.

In summary, a partial correlation between major colony morphotype and killing rate was found: Smooth isolates were less virulent than those with crepe morphotype, which apparently correlates with the capacity to form stronger biofilms on abiotic devices, as

well as the presence of pseudohyphae development on liquid cultures at human body temperature.

3.5.6 Differences in the cell wall proteome among clinical isolates

Finally, we addressed the cell wall proteome of the selected isolates, to investigate possible links between cell surface composition, cell and colony morphology, as well as biofilm formation.

The clinical isolates varied in several morphological features. Mass spectrometric analyses of the selected nine *C. parapsilosis* isolates were conducted in collaboration with Dr. Piet de Groot (CRIB, Albacete, Spain). Briefly, cells were grown into biofilms on polystyrol dishes or in planktonic culture for those that did not form biofilms, the cells harvested and the cell wall fraction extracted using hot SDS. This procedure was previously established for other *Candida* species. Cell surface proteins were classified in as previously described before for *C. albicans* and *C. glabrata* (Gómez-Molero *et al.*, 2015; de Groot *et al.*, 2013)

Principally, a core proteome (e.g. aspartyl proteases, phospholipases, and carbohydrate-active enzymes) and a variable proteome (mainly adhesin-like proteins) were found.

The core proteome, defined by its presence in nearly all samples (Table 21), was consistently present under biofilm conditions and planktonic growth. It constituted twelve different protein classes. These included the CFEM family (common in fungal extracellular matrix) involved in iron acquisition (Ding *et al.*, 2011), the Gas/Phr family, Blg2 family, and the Crh family. The chitinases belonging to the Crh family, were mainly represented by an ortholog of the CaCht2 enzyme of *C. albicans* (CPAR2_502140), which was identified in all isolates. In contrast, the CPAR2_502120 chitinase could be only identified when cells were harvested from biofilms on polystyrol or silicone, but not from the planktonic phase. At

Candida parapsilosis

least one family member each of the Sun Family, Tos Family, Pir Family (Protein with internal repeats), and the Pga 30 family were presented in all strains analyzed.

Some core proteins, were not identified in all strains or conditions, but still frequently observed. This included Sod4/Pga2 (CPAR2_213080) which was not identified in PEU582 and the hyperbiofilm-forming isolate PEU586; the aspartic protease CPAR2_702730 which was expressed in all isolates but the CPAR2_702720 was only identified in the HBF PEU486. The CPAR2_500920 ortholog of the CaSap10 was not identified in the CDC 317, the PEU-501s and three of the four hyperbiofilm forming isolates. The proteins of the Pga30 family CPAR2_200370, CPAR2_107500 and CPAR2_400900 were not identified in the LBF isolates, except in PEU501-s. The cell wall protein CPAR2_402010/RHD3 ortholog of the Pga29 of *C. albicans* was present in the hyperbiofilm-forming isolates and the LBF smooth PEU501.

Subsequently, we focused on the variable proteome, constituted by adhesins which clearly differed among strains and conditions. The most frequent cell wall GPI-linked adhesin identified in the HBF isolates only was CPAR2_806670; this ortholog of the CaYwp1 of *C. albicans* was present in all the HBF isolates including CDC 317-s.

The ortholog of the CaAls3 (orf 19.5741/*ALS1*) was identified in the PEU501-s and the four HBF isolates but not detected in either CDC 317-s, PEU582-s, or PEU651-s. In contrast, the ortholog of the cell wall protein CaAls6 (CPAR2_404790, orf 19.7414), was found in CDC 317-s, PEU582-s, PEU486-cr, PEU495-cr, and PEU496-cr, but was not identified in the LBF PEU501-s and PEU651-s and the HBF PEU586-cr.

Table 21. Summary of proteomic analyses using seven + CDC 317 of the selected *C. parapsilosis* clinical isolates

variable proteome	CDC 317	ATCC 22019	PEU501	PEU651	PEU582	PEU486	PEU495	PEU496	PEU586
origin isolate	RS	RS	ear-nose	device	urine	skin	urine	ear-nose	ear-nose
morphotypes	s	s,crt,cn,cr	s	s	s,cr	s,cn,cr	s,cr	s,crt,cn,cr	s,cn,cr
frequent morphotype	s	cn-cr	s	s	s	cr	cr	cr	cr
adhesiveness to polystyrol	LBF	LBF	LBF	IBF	IBF	HBF	HBF	HBF	HBF
adhesiveness to silicone	LBF	ND	LBF	LBF	LBF	HBF	HBF	HBF	HBF
virulence (10 ⁶ cells/10 μ) (% killing rate)	100%	100%	95%	75%	95%	100%	100%	100%	80%
Als family									
CPAR2_404790 / CaAls6_ortholog	+ (log.) ^a	ND ^b	-	-	+	+	+	+	-
CPAR2_404780 / CaAls3_like or CPAR2_404800 / CaAls7_ortholog	-	ND	+	-	-	+	+	+	+
CPAR2_404800 / CaALS7_ortholog	-	ND	-	-	-	+	+	+	+
CPAR2_404780 / CaAls3_like	-	ND	(pep.) ^c	+	(pep.)	+ ^d	+	+	+
Hwp1 family									
CPAR2_403510 / Rbt1 / CaRbt1_ortholog	-	ND	-	(pep.)	(pep.)	+	+	+	+
CPAR2_806670 / CaYwp1_ortholog	+	ND	+	+	+	+	+	+	+
CPAR2_603340 / CaPga59_ortholog	+	ND	+	-	-	-	+	+	-
Iff/Hyr family									
CPAR2_600430 / CaIff3_like_nr2	-	ND	-	-	(pep.)	+	+	+	+
CPAR2_301320 / CaIff3_like_nr1	-	ND	-	-	+	+	+	+	+

core proteome I	CDC 317	ATCC 22019	PEU501	PEU651	PEU582	PEU486	PEU495	PEU496	PEU586
CFEM family (common in fungal extracellular membrane)									
CPAR2_402910 / CFEM2/CaRbt5_like	+	ND	+	+	+	+	+	+	+
CPAR2_300120 / CFEM6/CaCsa1_ortholog	-	ND	-	-	-	+	+	-	+
Gas/Phr family CaZy^e GH72									
CPAR2_302140 / CaPhr1_ortholog	+	ND	+	+	+	+	+	+	+
CPAR2_109660 / CaPhr2_ortholog	+	ND	+	+	+	+	+	+	+
CPAR2_100110 / CaPga4_ortholog	+	ND	+	+	+	+	+	+	+
Bgl2 family CaZy GH17									
CPAR2_407410 / CaMP65/Scw1_ortholog	+	ND	+	+	+	+	+	+	+
CPAR2_401600 / CaBgl2_ortholog	+	ND	+	+	+	+	+	+	+
CPAR2_502160 / CaScw11_ortholog	+	ND	-	-	-	-	-	-	-
Crh family CaZy GH16									
CPAR2_400860 / CaCrh11_ortholog	+	ND	+	+	+	+	+	+	+
CPAR2_503190 / CaUtr2_ortholog	+	ND	+	+	+	+	+	+	+
CaZy GH18 Chitinases									
CPAR2_502140 / CaCht2_ortholog	+	ND	+	+	+	+	+	+	+
CPAR2_502130 / CaCht2_like_nr2	+	ND	+	+	+	+	+	+	+
CPAR2_502120 / CaCht2_like_nr3	-	ND	-	-	-	+(PS) ^f	+(PS)	-	+(S) ^g
Sun Family									
CPAR2_603090 / CaSun41_ortholog	+	ND	-	-	+	+	-	-	-

core proteome II	CDC 317	ATCC 22019	PEU501	PEU651	PEU582	PEU486	PEU495	PEU496	PEU586
Tos family									
CPAR2_503650 / CaTos1_ortholog	+	ND	+	+(stat)	+(stat.)	+	+	+	+(stat.)
superoxide dismutase									
CPAR2_213080 / CaSod4/Pga2_ortholog	+	ND	+	+		+	+	+	-
aspartic proteases									
CPAR2_702730 / CaSap9_like_nr4	(pep.)	ND	(pep.)	+	+	+	+	+	+
CPAR2_702720 / CaSap9_like_nr5	-	ND	-	-	-	+	-	-	-
CPAR2_102610 / CaSap9_ortholog	-	ND	-	-	-	(pep.)	(pep.)	(pep.)	(pep.)
CPAR2_500920 / CaSap10_ortholog	-	ND	-	+(PS)	+(PS)	+(PS)	-	-	-
CPAR2_702810 7 CaYps7_ortholog	-	ND	-	+	-	-	-	-	-
phospholipases									
CPAR2_804680 / CaPlb5_ortholog	+	ND	+	+	+	+	+	+	+
CPAR2_808920 / CaPlb5_like_nr2	+	ND	+	+	+	+	+	+	+
CPAR2_701130 / CaPlb3_like_nr2	-	ND	-	-	-	-	-	+(PS)	-
Pir family putative β-1,3-glucan crosslinker									
CPAR2_806490 / CaPir1_ortholog	+	ND	+	+	+	+	+	+	+

core proteome III	CDC 317	ATCC 22019	PEU501	PEU651	PEU582	PEU486	PEU495	PEU496	PEU586
Pga30 family									
CPAR2_402000/PGA30 / CaPga30_ortholog	+	ND	+	+	+	+	+	+	+
CPAR2_402010/RHD3 / CaPga29_ortholog	(stat.) ^h	ND	-	+	+	-	-	-	-
CPAR2_301540 / CaSsr1_ortholog	+	ND	+	+	+	+	+	+	+
CPAR2_200370 / CaPga1_ortholog	+ (37°C) ⁱ	ND	-	-	-	+ (stat.)	+ (stat.)	+ (stat.)	-
CPAR2_107500 / CaPga26_ortholog	+ (37°C)	ND	+	-	-	+	-	+ (stat.)	-
CPAR2_400900 / CaPga53_ortholog	-	ND	+	-		+ (PS)		+	+
GPI-CWPs with unknown function									
Ecm33 family									
CPAR2_108560 / CaEcm33_ortholog	+	ND	+	+	+	+	+	+	+
CPAR2_100710/ECM331 / CaEcm331_ortholog	+ (37°C)	ND	+	+	+	+	+	+	+

Proteomic data evaluation was performed by Dr. Piet de Groot (CRIB, Albacete, Spain), (unpublished data). MS proteomic analyses was performed using ESI-Q-TOF MS/MS. MS raw data was batched using data analysis software (Bruker, Bremen, Germany), results were processed with Mascot software (v. 2.5.1) and peptides compared with CDC 317 protein sequences provided by NCBI database as well as ORF of putative proteins. ^a(log.), adhesins were identified in cell walls isolated from cultures harvested at logarithmic phase. ^bND, not determined, ^c(pep.), only one peptide of the specific adhesins were determined. ^d“+” Peptides were identified in biofilms (polystyrol and silicone) and stationary phase growing conditions. ^eCaZy, carbohydrate active enzymes. ^fPS, adhesins were identified under biofilm conditions in abiotic surface (polystyrol). ^gS, adhesins were identified under biofilm conditions using silicone elastomers. ^h(stat.) adhesins were identified in cultures at stationary phase. ⁱ proteins were only detected in samples incubated 37°C.

4. DISCUSSION

The pathogenic capacity of *Candida spp.* is determined by the host immune response as well as pathogen cell-surface structures (reviewed by Richardson and Moyes, 2015). *Candida spp.* can invade the bloodstream leading into sepsis and the death of the patient (Pappas *et al.*, 2018). *Candida albicans* is the most frequent cause of invasive candidiasis globally, but over the last decades, non-*Candida albicans Candida* (NCAC) species have become more medically relevant. *Candida spp.* are able to exist inside the human host, having developed different pathogenicity and antifungal drug resistance strategies (reviewed by Cavaleiro and Teixeira, 2018). Most microbes live as microbial communities encased in an extracellular polymeric substance, including NCAC species, which form biofilms on abiotic and biotic surfaces, composed of only single but also mixed species. *Candida glabrata* and *Candida parapsilosis* are the two most common causes of NCAC infections. Their relevance has been attributed to the ability to form biofilms on non-living surfaces and the increased multidrug resistance capacity, together leading to different levels of pathogenicity.

Both species display superficial, mucosal and systemic infections associated with medical devices (reviewed by van Asbeck *et al.*, 2009; Rodrigues *et al.*, 2017) presenting clear morphologic and phenotypic differences between them (reviewed by Rodrigues *et al.*, 2017; Trofa *et al.*, 2008). *C. glabrata* and *C. parapsilosis* each belong to two different *Candida* clades with strong differences on genomic and pathogenic levels (Butler *et al.*, 2009). This phylogenetic distance is also reflected by variations in cell wall organization including its proteome (reviewed by Gabaldón *et al.*, 2016). The fungal cell wall is the outermost layer involved in host-pathogen recognition, cell structure, permeability, protection, and virulence. Particular differences in cell wall proteins composition between both NCAC species will be one of the focus of the study.

DISCUSSION

Thus, we here investigate cell wall molecules to be used as putative targets in NCAC infections (Rodrigues *et al.*, 2017; Silva *et al.*, 2017) or diagnostic markers. Based on this, we investigated how phenotypic and morphological differences within intra- and inter-NCAC species (*C. glabrata* and *C. parapsilosis*) are reflected in genomes and proteomes, and how these variations may reflect different pathogenic strategies during the infection process.

In addition to smaller strain sets also analyzed here, we created prospective strain collections for each as starting points to classify clinical isolates with different cell surface properties to subsequently analyze in depth the cell wall proteomes and genomes of selected isolates.

C. parapsilosis has the capacity to switch between yeast and pseudohyphal cellular morphologies as also described for *C. albicans* (Slutsky *et al.*, 1985), where this ability to switch between these and other morphologies is an important virulence factor. In *C. albicans*, the frequency of change is approximately 1.4×10^{-4} when using the absence of amino acid supplement or UV light as stimulus. This is less compared with the frequency rate described by Laffey and Butler (2005) and Lott *et al.* (1993) for *C. parapsilosis* (ranging from 10^{-1} to 10^{-3}). In *C. parapsilosis*, the change of cellular morphology is visible also as a colony phenotype. In our study, we calculated the morphotypic switch rate for one clinical isolate (PEU582), which was in the range described earlier from smooth (2×10^{-1}) colonies to crepe colonies (5×10^{-2}) with two morphotype varieties (Figure 29).

To more deeply analyze the morphotypic switch, we initially characterized five clinical *C. parapsilosis* sensu stricto isolates with different stable morphotypes (e.g. the absence of further switching on culture plates after replating) from one single patient including one from a positive blood culture. The five isolates (bsc-1700, nsc-1701, tsc-1702, ncc-1701 and tcc-1702) were isolated from nose (n=2), throat (n=2), and blood culture (Figure 32), respectively, and phenotypically represented biofilm formation capacities ranging from LBF (low biofilm-forming isolates) HBF (high biofilm-forming isolates). Based on the information of previous studies (Enger *et al.*, 2001; Laffey and Butler, 2005; Lott *et al.*,

DISCUSSION

1993) we hypothesized that lineages isolated from the same source of site were different morphotypic forms of the same strains after switching (Figure 32). To confirm the genetic relations between the five isolates, karyotypic analyses were performed; however, this remained inconclusive as variations between the isolates (Figure 35A) were in accordance with both, switched forms of the same isolate (Nosek *et al.*, 2009) (Figure 43), as well as unrelated isolates (Figure 35A).

Subsequent analyses on the genome level, surprisingly, concluded that the five isolates did not originate from a single clonal origin, but rather belonged to three independent, mostly clonal groups (Figure 35C): Within this defined set of isolates, those with “smooth” vs. “crepe” morphotypes were only distantly related. Smooth isolates were further divided into two clonal groups, one constituted by tsc-1702 and the other by bsc-1700 and tsc-1701 (Table 19, Figure 35B). These data show that the colonies originally classified as different morphotypes of a single clonal origin were indeed not representative for a morphotypic switch (Figure 33).

However, we could also show that the control ATCC 22019 produces, at least, four different morphotypes, showing a reduced-frequency of smooth morphotypes (~20%) compared with concentric-crepe (cn-cr) morphologies ($\geq 80\%$) (Figure 42A). Our data is an addition to previous analyses (Laffey and Butler, 2005) of the reference strain (ATCC 22019, there called “CLIB 214”) where a switch to a smooth morphotype was not shown.

These observations reveal two biological possibilities: the three clonal groups could have colonized and invaded the patient independently, or have diverged into different clonal subsets within the host. Our analyses show that smooth and crepe morphotypes (ncc-1701 and tcc-1702) were located at a distance of >3800 SNPs (Figure 35B), which was comparable with unrelated clinical isolates (Pryszcz *et al.*, 2013). Together, this renders the possibility of adaptive evolution within this patient unlikely, and underlines the need to consider both, switching, as well as co-occurrence of different strains within a single clinical specimen.

DISCUSSION

Stability of the observed morphotypes, e.g. the absence of switching upon replating, is important as it strongly influences the outcome of phenotypic experiments. When we followed this up in individual clinical isolates, several observations, which were in contradiction to the existing literature, were made. In our collection, we observed that around a 34% of the isolates tested along ten days present more than one morphotype and we proposed that a morphotypic switch mechanism has occurred. Most importantly, we observed that biofilm formation was a strain-specific attribute, and was less influenced by the morphotype: For example, stable lineages with different morphotypes (smooth and crepe) derived of isolate PEU582 displayed intermediate biofilm formation capacity to polystyrol. The reference strain ATCC 22019 displayed four colony morphotypes with no significant differences in the capacity to form biofilms, and HBF isolates PEU586, PEU496 and PEU486 show, at least, three (smooth and rough) colony types (Figure 42), though the capacity to form biofilms was relatively strong in all of them. To complicate matters, rare switched smooth forms of the - originally crepe - HBF isolate PEU495 displayed a LBF phenotype (Figure 42B).

The capacity to form cell aggregates has also been described to correlate with rough morphotypes and complex “spider-like” structures, which are able to produce robust biofilms (Pannanusorn *et al.*, 2013). This was also apparent among our isolates and colonies mainly constituted by mixed (yeast/pseudohyphae) or single pseudohyphae cells displayed thicker biofilms and stronger agar invasion. Isolates with round yeast cells usually correlate with smooth morphotypes and low biofilm forming capacity (Figure 44B, C, D, and E). Nevertheless, some exceptions (i.e. less than 1% of smooth colony morphotype in the present collection with high biofilm-forming capacity to polystyrene and strong agar invasion ability) were scored along ten days (Figure 39A, right, blue bars) (Pannanusorn *et al.*, 2013). These isolates would be interesting candidates for further epithelia invasion assays.

Many virulence factors are involved in *C. parapsilosis* pathogenesis, among which also biofilm formation to biotic and abiotic surfaces is a key player (Kuhn *et al.*, 2002a). One of the major complications with *C. parapsilosis* infections is the strong capacity to form

DISCUSSION

biofilms on abiotic surfaces of implants, catheters, prosthesis, or wiring for parenteral nutrition in neonates (reviewed by Trofa *et al.*, 2008). When we scored biofilm formation capacity among 215 clinical *C. parapsilosis* isolates and categorized these into LBF (0.054-0.080), IBF (0.153-0.370), and HBF (0.445-1.360) (Figure 38B), the collection represented a wide range of biofilm development, from negligible amounts of biofilm intensities to massive amounts of biomass (Figure 39A). However, the biofilm formation phenotype was independent of the isolates' source of isolation (Figure 38A) (Silva-Dias *et al.*, 2015; de Toro *et al.*, 2011).

On a phenotypic level, variation in the colony morphology as well as the capacity to invade agar (Figure 39B) was positively correlated with the biofilm formation capacity: more than 87% of the isolates with LBF capacity present smooth morphotypes, and around 45-50% of the HBF display crepe morphologies (Figure 39A). We also observed that rough colonies with HBF capacity were the best agar invaders on Phloxine B agar plates (Figure 39B and 40). A possible explanation of the morphotypic switch' link to biofilm formation capacity (Pannanusorn *et al.*, 2013) is the development of pseudohyphal growth from the basal part of the colony conferring the capacity to form thicker biofilms (Figure 31).

In addition to the colony morphologies "smooth", "snowball", "rough", "crater", "crepe", and "concentric" already described (Enger *et al.*, 2001; Laffey and Butler, 2005; Lott *et al.*, 1993), we extended this panel to twelve different morphotypes. For colony morphotype identification, our analyses followed the same procedure performed by Laffey *et al.*, 2005. These studies used YPD medium containing Phloxine B, as it is routinely used to detect white-opaque switching in *C. albicans* (Anderson and Soll, 1987). We also used Sabouraud's agar plates, rich in dextrose, which facilitate the growth and morphotypic development of *C. parapsilosis* colonies (Branchini *et al.*, 1994; Shin *et al.*, 2002) including those six already described (Enger *et al.*, 2001; Lott *et al.*, 1993; Nosek *et al.*, 2009). These fall into only two categories when stratified by observation frequency in our study: major colony morphologies (smooth-glossy, smooth-matte, smooth-concentric, wrinkled, and crepe (I, II) represented > 60% of the isolates tested and infrequent colony morphologies (concentric, concentric-crepe, concentric-crater, crater, derby and snowball) only

DISCUSSION

represented 6% of the total (Figure 31B). The remaining 34% was constituted by mixed morphotypes, e.g. frequently switching strains producing more than one colony type per plate.

Even though, while we confirmed that morphotypic switching is present in *C. parapsilosis* clinical isolates, the high frequency described in previous studies (Laffey and Butler, 2005) was not observed. In contrast, our data suggests that biofilm formation capacity is rather predetermined within the clinical isolate and the specific morphotype will only increase or decrease the biofilm formation capacity within a certain range, possibly as a survival strategy in the host.

Biofilm formation is known to reduce the effect of antifungal drugs (Katragkou *et al.*, 2008) and it was proposed as one of the major virulence factors in *C. parapsilosis* (Silva *et al.*, 2012). Despite *C. parapsilosis* producing less structured biofilms than *C. albicans*, both species easily develop reduced susceptibility especially towards azoles during the first stage of biofilm formation (Kuhn *et al.*, 2002). This type of antifungal resistance is still understudied, and only little is known about the underlying mechanism. This is especially true for *C. parapsilosis*, where biofilms are usually constituted by cells aggregates (Kuhn *et al.*, 2002) of less complexity than in *C. albicans*. They strongly vary depending on the cell density, the presence of “persister” cells, the morphotypic switch, and the strain-specific morphotype reviewed by Silva *et al.* (2017).

Together with the group of G. Quindós, we confirmed for six selected biofilm-forming isolates (two smooth IBF isolates and four crepe HBF isolates) that fungal cells embedded in preformed biofilms were reduced in susceptibility to azoles but not for echinocandins and a polyene also in our strain set (Gómez-Molero, unpublished data). Additionally, we also observed the previously reported dependency on glucose levels in echinocandin and polyene activity (Pereira *et al.*, 2015). In contrast, we confirmed that MICA and AMB inhibit their growth by antifungal concentration increment (Guillermo Quindós, personal communication). Nevertheless, azoles are the most frequent antifungals administered (van Asbeck *et al.*, 2008; Pfaller *et al.*, 2008).

DISCUSSION

Using the standard EUCAST edef 8.1 procedure we tested the three LBF, IBF and HBF sets, how this would be reflected with drug susceptibility towards commonly used azoles, echinocandins, and polyenes. Values observed for the six antifungal drugs tested were similar to the ranges previously described (Espinel-Ingroff *et al.*, 2013; Melo *et al.*, 2011; Soczo *et al.*, 2007). With the exception of minute quantitative deviations in FLU, POS and CAS (Figure 41), no substantial qualitative differences between LBF, IBF and HBF against drug susceptibility were observed. These observations are remarkably important, because while the degree of biofilm formation will not antifungal drug susceptibility for azoles, it is not predictable from EUCAST data.

For *C. albicans* it was previously shown that the visually apparent change from white to opaque phenotype can alter epithelial invasion and susceptibility against antifungal drugs (Solis *et al.*, 2018; Vargas *et al.*, 2000). We analyzed if colony morphology “maturation” of *C. parapsilosis* (Figure 39B) would affect antifungal drugs susceptibility testing using matured colonies (96h) instead of young (~16h) (Figure 41), (Pfaller *et al.*, 2005). Globally, we did not find significant differences between such young and mature colonies for any antifungal drug except for CAS, and few single isolates increasing their MIC by one log₂-fold change. These observations could indicate that antifungal drugs could be administered during the first 96 h. because no general differences between “young” and “mature” colony susceptibility rate were observed. Particularly, a positive correlation between high morphotypic switch and increased of azoles resistance was described by Vargas and colleagues for *C. albicans* supporting the idea that resistant-gene-regulation is controlled by phenotypic switch as it has been also observed in *C. tropicalis* (Moralez *et al.*, 2014).

Although we did not observe global qualitative variations between susceptibility data for young and mature colonies, we did identify small but significant MIC differences towards caspofungin for three individual HBF clinical isolates displaying rough (“crepe”) morphotypes (Table 20). These morphotypic variations correlate with the idea that biofilms are less susceptible to antifungal drugs. Nevertheless, it is striking for CAS, because as it was already shown, *Candida spp.* biofilms are usually susceptible to

DISCUSSION

echinocandins (Ferreira *et al.*, 2009). According to our observations (Figure 42A), the mean susceptibility to antifungals partially shifted with the capacity to form biofilms in three of the six compounds tested, and this is indirectly reflected in the colony morphology.

Therefore, we conclude *C. parapsilosis* clinical isolates present a high phenotypic variability with a wide range of biofilm formation intensities compared with other NCAC *spp.* (Silva-Dias *et al.*, 2015). This heterogeneity was already described for “slime” production by Branchini *et al.* (1994) and Pfaller *et al.* (1995). We observe a general correlation between colony morphotype and adhesion properties and biofilm formation capacity would usually reduce azole’s susceptibility independently on the biomass produced.

Cell surface phenotypic properties are strongly strain-specific in *C. parapsilosis* clinical isolates. Following the same hypothesis, we wanted to analyze phenotypic variants in *C. glabrata* and how such properties are reflected at genome and proteome level. *C. glabrata* belongs to the only distantly related Nakaseomyces group and is one of the few pathogens present in this clade (Kurtzman and Robnett, 2003). It has been described as close relative to *Saccharomyces cerevisiae* for the incapacity to develop hyphae, and having evolved from a common origin with a whole genome duplication event along the time (Kurtzman and Robnett, 1998). Initially, the first *C. glabrata* genome sequencing was published by Dujon *et al.* (2004) and was more deeply described by Gabaldón *et al.* (2013). To get a general overview over *C. glabrata* variability, karyotypic analyses of 33 selected clinical isolates indicated a high between. We observed large differences in both copy number and chromosome distribution between isolates (Figure 15). Karyotypic differences were particularly evident between the seven clades suggesting possible microevolutions or chromosome replacement as base of genetic variations (Carreté *et al.*, 2018). A large genomic and phenotypic plasticity is also observed in other collections (Müller *et al.*, 2009) and even between different stocks of the same laboratory strain (Bader *et al.*, 2012).

DISCUSSION

To investigate if genomic plasticity correlated with variations at phenotypic level, we characterized a large clinical strain collection towards the capacity of *C. glabrata* to form biofilms on polystyrol plastic and silicone. The ability of a *C. glabrata* biofilm to adhere to host surfaces is conferred yeast cells at the basal part, embedded in an extracellular matrix with high amounts of carbohydrates (Seneviratne *et al.*, 2009; Silva *et al.*, 2009). Over the course of two years a 453 clinical isolates belonging to nine different categories of source of isolation were screened for their capacity to adhere to abiotic surfaces. When the isolates were classified according to their capacity to form biofilms on polystyrene, a clear correlation of biofilm formation capacity to cell aggregation (Figure 18) was evident. In this study, we differentiated LBF, IBF and HBF (Figure 19) clinical isolates depending on the degree of biofilm produced (Fonseca *et al.*, 2014; Rodrigues *et al.*, 2014; Silva *et al.*, 2009). No correlation between the site of isolation and the capacity to adhere to silicone elastomers and polystyrol (Figure 24) was observed, and a high variability on biofilm formation intensities was identified as it has been already described by Estivill *et al.*, 2011. Only a 17% percent of the 453 clinical isolates tested presented strong capacity to form biofilms on abiotic surfaces (Figure 21) producing typical structures (Davey and O'toole, 2000; Kucharíková *et al.*, 2015) constituted by round yeast cells in the lower layer of the biofilm embedded in the EPS (Figure 19).

We used these screening analyses to mimicking the putative host-colonization capacity of a large *C. glabrata* strain collection. As in *C. parapsilosis*, these analyses again suggested strong strain-specificity and a large inter-strain variation regarding biofilm formation capacity and antifungal drugs susceptibility (Figure 16 and Figure 20). This has also been described for other isolate collections (Parahitiyawa *et al.*, 2006). A relation between biofilm formation capacity and reduced susceptibility was shown in two different HBF isolates (Figure 22) displaying MICs towards FLU; VOR and POS between 2 and 8 fold higher than the reference strain. Contrary, three LBF-IBF isolates (M6, M7 and M17, Figure 16) from blood cultures with a strongly reduced susceptibility against all the azoles (M6 and M7) and the nucleoside 5FC (M17) (Table 10), present individual point mutations in the pleiotropic drug resistant transcriptional factor *PDR1* (Carreté *et al.*, 2018; Tsai *et al.*,

DISCUSSION

2006) which gains of function (Vale-Silva *et al.*, 2013) predetermine a positive increase in host adherence and virulence.

We also observed that serial isolates from clonal populations (SAT01, SAT02 and SAT03, Figure 17B) which are susceptible to major antifungal drugs tested are lacking of non-synonymous mutations in specific genes involved in antimycotic regulation (Carreté *et al.*, 2019).

In fungi, the cell wall proteome composition is a strong influencer of biofilm formation as well as a main virulence (Cormarck *et al.*, 1999, Cabral *et al.*, 2014; Verstrepen *et al.*, 2006; Martínez-Gomariz *et al.*, 2009; reviewed by Klis *et al.*, 2009). In this study, we investigated the differences and constituents of *C. parapsilosis* and *C. glabrata* cell wall proteomes under biofilm conditions stratified by phenotypic and genomic variations. The main factors involved are GPI-anchored adhesin proteins covalently bound in the cell wall (de Groot *et al.*, 2008; Kraneveld *et al.*, 2011; Gómez-Molero *et al.*, 2015). Cell wall composition differences between *C. glabrata* and *C. parapsilosis* are evident: *C. glabrata* encodes at least 67 adhesins (Weig *et al.*, 2004; De Groot *et al.*, 2008) mainly located in subtelomeric regions. In contrast, the *C. parapsilosis* reference genome only encodes five different adhesins of the ALS family, one *RBT1*-like gene, and the *BCR1* effector (Hoyer *et al.*, 2001; Butler *et al.*, 2009; Prysycz *et al.*, 2013; reviewed by de Groot *et al.*, 2013, Rossignol, 2009).

Therefore, using a workflow already established for biofilms of *C. glabrata* (Gómez-Molero *et al.*, 2015; de Groot *et al.*, 2008; Weig *et al.*, 2004), we identified several known and novel adhesins being incorporated into the cell wall of biofilm forming *C. parapsilosis* and *C. glabrata* clinical isolates (Table 13 and Table 21). The total number of different adhesins incorporated correlate with the capacity to form biofilms either under logarithmic or stationary phase (Figure 21D and Figure 38B) on abiotic materials.

As described for *S. cerevisiae* (Groot *et al.*, 2008), a standard core- and a variable proteome can be stratified in both species (Table 13 and Table 21). A strong similarity is seen between *C. parapsilosis* and *C. albicans* core proteomes (reviewed by de Groot *et al.*,

DISCUSSION

2013) although there are important differences between both species (Butler *et al.*, 2009): The *C. parapsilosis* core proteome was observed in all the isolates tested independently on their adhesion capacity, except for CPAR2_502160, the ortholog of Scw11 of *C. albicans*. This protein is a glucanase only described in the reference strain CDC 317 that responds to different iron levels (Lan *et al.*, 2004) The core proteome of *C. parapsilosis* is mainly constituted by chitinases, aspartic proteases, superoxide dismutases, putative β -1,3-glucan crosslinkers, other carbohydrate active enzymes, and phospholipases (Table 21).

The *C. glabrata* core proteome followed the same pattern as seen for *C. parapsilosis* and phospholipases, putative glucan crosslinkers and carbohydrate-active enzymes (Table 13) mainly constitute it. Other proteins identified in *C. glabrata* core proteome were the GPI-cell wall protein Ssr1, which is also involved in iron homeostasis (Srivastava *et al.*, 2014) the phospholipase Plb1 (not identified in CBS-138 and PEU52), and Plb2, which was not present in the LBF PEU52 and the two reference strains.

Interestingly, the absence of Plb1 and Plb2 in the LBF and the highly flocculent PEU52 is associated with a low killing rate (70%) in the *G. mellonella in vivo* infection model (Figure 22A). The function of Plb1 and Plb2 is still not well investigated in *C. glabrata*. However, it is known that differential expression of phospholipase B genes are important in *C. albicans* oral and vaginal infections (Naglik *et al.*, 2003) as well as invasive candidiasis in *C. glabrata* (reviewed by Ghannoum, 2000).

As proposed by the Groot *et al.* (2008), the Cwp1.1, Cwp1.2 and tir1, identified in the *C. glabrata* core proteome, were described as possible β -1, 3-glucan- β -1, 6-glucan crosslinkers via GPI-anchors. The protein CAGL0M01826g, previously detected in *C. glabrata* reference strains and all *C. parapsilosis* clinical isolates belongs to the Ecm33 family proteins which function is not still identified but seems to be involved in cell wall integrity and biogenesis (Pardo *et al.*, 2004; Martínez-López *et al.*, 2006).

In addition to the core proteome, we observed a variable proteome whose constitution largely correlated with biofilm formation phenotypes. Remarkable differences within the

DISCUSSION

variable proteomes of *C. glabrata* and *C. parapsilosis* are detectable and can be related to their phylogenetic differences. Thus, our data suggests that the capacity of *C. glabrata* and *C. parapsilosis* clinical isolates to colonize host surfaces is mainly conferred by this variable proteome.

We observe that strong biofilm formation capacity, cell aggregation, cell sedimentation and agar invasion will usually reflect crepe or concentric (PEU486, PEU496 and PEU586) morphotypes with a high number of adhesins in the wall (Table 21). Klotz and collaborators (Klotz et al., 2007) already suggested this assumption describing that aggregation capacity affects the establishment of biofilms in *C. albicans* with a modification in the expression of adhesin-encoding genes. There, the expression of Als family proteins, like Als3, is involved in cell aggregation as the first step of the colonization process in single and mixed biofilms, and the *ALS7* adhesin-encoding gene (ortholog: CPAR2_404800) has been proved to be part in epithelial adhesion in *C. albicans* (Neale et al., 2018, Richardson et al., 2018; Bertini et al., 2016). Our proteomic studies showed that isolates with rough morphologies and HBF, usually present Als6 or Als7 in the cell wall (isolates PEU486, PEU495, and PEU496). Surprisingly, the strong biofilm-forming isolate with crepe morphotype (PEU586) was lacking of the CPAR2_404790 (ortholog of Als6 in *C. albicans*); this absence correspond with a reduction in *G. mellonella* killing rate (80%). Therefore, we propose that the Als6 would be involved, together with the extracellular lipases (Toth et al., 2014), in *C. parapsilosis* virulence. Interestingly, all hyper biofilm-forming clinical isolates analyzed in this study, presented, both, Hwp1 and Iff/hyr family proteins in their cell wall, determining their relevance in the colonization process.

Our proteomic analyses for nine selected *C. glabrata* clinical isolates identified eighteen GPI-CWPs proteins differentially expressed under biofilm conditions (Table 12). Ten out of these were previously undetected adhesin-wall proteins (de Groot, unpublished data).

The largest group of adhesins of *C. glabrata* in the variable proteome is the Epa family, known to be involved in epithelia cell adhesion. For example, Epa3 takes part in osmotic stress counter action (Roetzer et al., 2008), and Epa6 and Epa7 are present in all the

DISCUSSION

isolates analyzed excluding the Epa7 in the reference strain CBS-138. Epa6 and Epa7 are highly homologous and the N-binding site adhere to β -glucans (Epa7) and α - and β -glucans (Epa6) (Castaño *et al.*, 2005). The proteomic identification of Epa adhesins in our clinical isolates' cell walls correlates well with gene transcriptional regulation data under biofilm conditions and subtelomeric silencing (Iraqi *et al.*, 2005). Contrary, the main adhesin-encoding genes did not show a general increase in the transcription profile in the two HBF isolates PEU427 and PEU382 (Gómez-Molero *et al.*, 2015). It has previously been claimed that that Epa22 (Kraneveld *et al.*, 2011) is highly expressed in biofilms, however here it was only identified in the LBF and highly flocculent strain PEU52, suggesting a possible function in flocculation and thereby cell sedimentation.

Six *C. glabrata* proteins identified in HBF isolates belonging to clusters III (Awp13), V (Awp8, Awp9, Awp10 and Awp11) and VII (Awp12) (Gómez-Molero *et al.*, 2015) and four remaining to be categorized (de Groot, unpublished data) were previously undetected. Solely, the newly described: Awp8, Awp9, Awp10, Awp11, CAGL0L00227g and CAGL0F09273g are included in the cluster V as the Awp2-4 (de Groot *et al.*, 2008 and 2013) sharing a remarkable number of peptides with Epa family proteins. We observed that these novel adhesins were frequently present in HBF isolates and less in IBF or LBF groups. Although the molecular function of these proteins are still undetermined, they seem to have a role in cell adhesion. Awp12 is similar to the *S. cerevisiae* flocculins homologs to the Epa family (Gómez-Molero *et al.*, 2015, Weig *et al.*, 2004; de Groot *et al.*, 2008, Thierry *et al.*, 2010, Desai *et al.*, 2011; de las Peñas *et al.*, 2003) and it is only presented in the CBS-138 and IBF isolates. In contrast, Awp13 (cluster III) and Aed1 were only identified in the HBF PEU427 (Gómez-Molero *et al.*, 2015). Molecular studies on Aed1 confirmed its function in adherence to epithelia (Desai *et al.*, 2011). While the molecular role of Awp13 is unknown, genome sequence analyses corroborated by phenotypical analyses in this study (Carreté *et al.*, 2018), remarked independent deletions of *AWP13* in three IBF-HBF blood isolates CST35, F15021 and F03013. A possible outcome of the *AWP13* deletion is a reduction of the adherence capacity inside the host to facilitate the dissemination in the bloodstream. The novel adhesins and most prominently are most

DISCUSSION

frequently identified in the IBF and HBF clinical isolates with large variations between them. In contrast, Epa family proteins are quite constantly detectable in all the isolates studied. Therefore, we suggest that the Awp family is the one that will confer remarkable proteome variability.

Along our proteome subset, we identified several remarkable exceptions. Isolate PEU30 is hyper-adherent to silicone elastomers, but not able to form biofilms on polystyrol material. It only presents three adhesins in the cell wall, two of them belonging to the Epa family (Epa3 and Epa6). In addition, it is, together with the LBF reference strain ATCC90876, one of the only isolates presenting Awp1 in the cell wall. PEU30 was isolated from tissue of a catheterized patient; this allows hypothesizing that, while the capacity to adhere to catheters may be mediated by Epa3 and Epa6 (Kuchariková *et al.*, 2015), once the pathogen has colonized the host surface, a low number of adhesins in the cell wall could facilitate the invasion and dissemination inside the host.

Surprisingly, isolates with high capacity to form aggregates PEU45 (HBF) and PEU52 (LBF) present a unique adhesin not identified before in the reference strain CBS-138. The CAGL0L00227g is still understudied but we propose a possible function related to aggregation and flocculation in pre-existing biofilms or cell-cell interactions. Further studies based on adhesins mutation and overexpression should be performed to firmly confirm these observations.

The HBF isolates PEU427 and PEU45 showed the highest number of different adhesins and the strongest capacity to form biofilms on polystyrol. PEU45 also had an intermediate-high capacity to adhere to silicone, potentially conferred by the Epa family proteins (reviewed by Timmermans *et al.*, 2018). The highly hydrophobic isolate PEU427 (Gómez-Molero *et al.*, 2015) was isolated from tracheal secrete which is rich in mucin and hydrophobic constituents with serine and threonine residues which are thought to mimick the residues present in the tandem repeat regions of the CWPs (Bustamante-Marín *et al.*, 2017). In summary, we observed a clear increase in the number of different adhesins in the cell wall in hyper biofilm-forming isolates of both species.

DISCUSSION

Next to the functional N-terminal lectin domain, another structural feature of cell wall adhesins is the more C-terminal repeat region (reviewed by Hoyer *et al.*, 2008). Looking in genome sequences obtained for the five *C. parapsilosis* isolates of the single patient, we observed that a large *C. parapsilosis* genome plasticity is mainly observed in the high amplification of the repeat-encoding NH₂-terminal domain of *HWP1* (Figure 36), a gene involved in biofilm formation and epithelia adherence (Nobile *et al.*, 2006). This cell wall protein is not frequently identified in LBF clinical isolates (Table 21) and the homolog in *C. albicans* presents high similarities to small mammalian proteins used as substrate for mammalian transglutaminases (Staab *et al.*, 1999).

For *C. glabrata* it has been shown that, despite its highly clonal population structure, a remarkable amount of recombination along the evolutionary process is still ongoing (Dodgson *et al.*, 2003 and 2005; Lin *et al.*, 2007). Studies of Carreté *et al.* (2018) show that isolates from different clades seems to be more diverse than isolates that belonging to the same clade; this in line with the observation that *C. glabrata* presents a higher genomic plasticity compared with *C. albicans* populations (Hirakawa *et al.*, 2015). Approximately, nearly half of the deleted or the duplicated genes from the collection of 33 genome-sequenced *C. glabrata* clinical isolates investigated here code for CW-adhesin proteins. This suggests that variations on the adhesin repertoire together with differences in cell-adherence capacity are a main selection mechanism within the *C. glabrata* population (Carreté *et al.*, 2018).

Since both species belong to two different subclades in the *Candida spp.* phylogenetic tree, also the cell wall proteome organization varies. Our data supports the idea that *C. glabrata* and *C. parapsilosis* have developed different adaptive strategies for survival in a human host:

Looking at *C. glabrata*, the second most frequent fungal species isolated from blood cultures, and which is generally incapable to form hyphae, it is interesting to evaluate how it can cross from a colonized surface into the blood stream. One theory is that *C. glabrata* can use the hyphae of *C. albicans* to penetrate into host tissues and disseminate (Alves *et*

DISCUSSION

al., 2014; Tati *et al.*, 2016). Using our isolates, we could confirm that clinical isolates with high capacity to form biofilms and aggregates (Table 14) are also the ones that easily adhere to *C. albicans* hyphae. This correlates with the increased presence of adhesins identified in the cell wall (Figure 26). However, *C. glabrata* and *C. albicans* co-isolation from blood cultures was not frequently observed (Figure 28). A reduced presence of *C. albicans* cells in *C. glabrata* blood cultures were found could, however be explained if *C. albicans* will be only used by *C. glabrata* to invade the tissue and does not reach the bloodstream for subsequent dissemination (Table 16 and Figure 28).

Tati *et al.* (2016) identified the *EPA8*, *EPA19*, *AWP2*, *AWP7* and *CAGLOF00181* adhesins to be important in the interaction between *C. glabrata* and *C. albicans* hyphae. In addition, we could identify novel adhesins that were expressed in the strains able to bind hyphae (Figure 26) and may facilitate this interaction.

In contrast, cell aggregation capacity (Figure 20A), cell sedimentation (Figure 20 B), or biofilm formation capacity do not imperatively correlate with virulence in *G. mellonella* animal model for either species (Figure 20 D, 22, 47). Strikingly, for most isolates with high numbers of adhesins in the wall, a reduction in virulence, at least in the *G. mellonella* model, and not an increase is observed here.

No variations between murine infection model and *G. mellonella* animal model have been described previously for *C. glabrata* clinical isolates. It usually presents an only low killing rate across infection models (Rossoni *et al.*, 2013) and a high *C. glabrata* inoculum is needed to increase the virulence (Ames *et al.*, 2017). Nevertheless, we were able to observe differences among both *C. glabrata* and *C. parapsilosis* clinical isolates in the *G. mellonella* infection model, but there was no distinctiveness with respect to LBF or HBF isolates (Figure 22 and Figure 47). In case of *C. glabrata* clinical isolates, approximately 24% of the isolates had a killing rate lower than 100% and those were mainly isolated from urine catheters and oral cavity independently of the capacity to form biofilms. We propose as a possible port of entry into the host that strains from catheters or oral cavity formed biofilms there. Considering that *C. glabrata* secretes phospholipases orthologous

DISCUSSION

to those of *C. albicans*, and the enzymatic activity in *C. glabrata* invasive candidiasis (Ghannoum *et al.*, 2000) is higher compared to oral cavity (Ibrahim *et al.*, 1995), wounds or urine (Price *et al.*, 1982), only a reduced expression of phospholipase B in the oral cavity or urine tract could explain the reduced killing rate. Interestingly, the postulated absences could be observed in the avirulent *C. glabrata* LBF clinical isolate PEU52 which cell wall proteome is absent of Plb1 and Plb2 (Figure 22, table 13).

C. parapsilosis strain PEU586 was the exception to these findings: it had a high capacity to form biofilms and seven adhesins were identified in the wall, but the killing rate in *G. mellonella* was less than 100%. This seems to indicate that this isolate was a better colonizer than tissue invader. Within our *C. parapsilosis* subset, isolates with crepe morphotypes and a large number of adhesins in the cell wall generally displayed higher killing rates in *G. mellonella* animal model as compared to isolates with a reduced number of adhesins (Table 21 and Figure 47B). Strikingly, we found that two non-adherent smooth clinical isolates (CDC-317 and PEU501) each only containing three adhesins (CPAR2_404780/CPAR2_404800, CPAR2_806670 and CPAR2_603340) in their cell wall had a high killing rate (100% and 95%, respectively). Consequently, this suggests that isolates with smooth colony types and LBF capacity are more virulent while presenting fewer adhesins in the cell wall. This may represent a potential adaptive mechanism contributing towards the invasion process.

In contrast to *C. glabrata*, *C. parapsilosis* is able to switch between cellular forms and thus different colony morphotypes (Laffey *et al.*, 2005). In line with this, the capacity of *C. parapsilosis* to form strong biofilms on abiotic surfaces again suggests this as a possible entry route into the host (Reviewed by Trofa *et al.*, 2008; Ruan *et al.*, 2008), with a subsequent dissemination within the patient described above (Figure 32). Retrospectively looking at the treatment course, the patient received echinocandins (Caspofungin) once samples were positively identified as *C. parapsilosis*. Afterwards, fluconazole was administered in addition, and the treatment continued only with fluconazole after an improvement of the patient. *C. parapsilosis* biofilms are known to resist azole antifungal treatment, but are susceptible to echinocandins, a feature that we were able to confirm in

DISCUSSION

collaboration with Dr. Guillermo Quindós for several isolates of our collection. A reduction in biofilms' growth was only observed after echinocandin and amphotericin B treatment. Therefore, these observations would explain the patient's improvement. The recurrent exchanges in the catheter happened once the BAL positive culture was isolated. The first time blood culture was positive corresponded with another catheter exchange (Gómez-Molero *et al.*, unpublished data).

The different morphologies of the *C. parapsilosis* isolates isolated from this patient were however not caused by morphotypic switch, but rather represented three independent lineages. The fact that the blood culture isolate bsc-1700 was genetically closest to a throat isolate (tsc-1702) let us speculate the possible route of dissemination:

From our data, we propose that the blood stream infection was initiated during surgery, by the smooth morphotype strains spreading more easily to different tissues due to the inability to adhere to biotic and abiotic surfaces (Uppuluri *et al.*, 2010). This is in contrast to the crepe strains present in the same locations, which have strong ability to adhere and likely stay in a fixed location resulting in less likelihood to reach the bloodstream. Unfortunately, the sample isolated from central venous catheter (CVC) was not retained in the diagnostic laboratory; this would have let us know the phenotypic and genotypic properties to better analyze the whole pathogenic process.

These observations are in similarity with the report that a *C. albicans* strain isolated from a blood stream infection was incapable to form biofilms due to the lack of *EFG1* (Hirakawa *et al.*, 2015). During disseminated candidiasis with *C. albicans*, hyphae, pseudohyphae, and yeast are presented (Noble *et al.*, 2017). This is in accordance with our observations in *C. parapsilosis* that the yeast form, which is at least, partially characterized by the absence of adhesins in the *C. parapsilosis* cell wall, may facilitate the dissemination into and in the blood stream. The remaining *C. parapsilosis* smooth isolates with their low number of adhesins in the wall with high killing rates in *G. mellonella*, let us speculate about their ability to easily disseminate (Table 21) also in this model.

DISCUSSION

Consequently, this suggests that isolates with smooth colony types and LBF capacity may be more virulent while presenting fewer adhesins in the cell wall. This may represent a potential adaptive mechanism contributing towards the invasion process. In line with this, we propose that the adaptive strategy to adhere to host surfaces is mediated by the number of different adhesins present in the cell wall, along with their abundance as suggested previously for *C. glabrata* (reviewed by Timmermans *et al.*, 2018). In addition, we emphasize that the main pathogenic and immunogenic differences within clinical isolates would be represented by the variable proteome. We suggest that both species use their specific phenotypes and cell surface properties with subsequent variation of the cell wall proteome as selective pathogenic strategy.

A large genetic variability is presented in *C. glabrata* clinical isolates (reviewed by López-Fuentes *et al.*, 2018; Bader *et al.*, 2012) compare with *C. parapsilosis* (Tavanti *et al.*, 2010). However Prysycz *et al.* (2013), revealed, as well, unexpected variations between distant *C. parapsilosis* clinical isolates.

In this work, we have observed several instances of genomic variation. Within these analyses (Carreté *et al.*, 2018), *C. glabrata* isolates with duplications of adherence wall proteins *PWP4* (Desai *et al.*, 2011) and deletions of *AWP13* (Gómez-Molero *et al.*, 2015) corresponded with three hyper biofilm-forming isolates (CST35, F15021 and F03013) (Figure 16) from blood cultures. We suggest that deletions of *AWP13* could be a possible adaptive mechanism carried by the clinical isolates to easily reach the bloodstream.

The majority of the adhesin encoding genes identified in *C. glabrata* are located in subtelomeric regions (de Groot *et al.*, 2008) which are known to be controlled by subtelomeric silencing. This may be another indicator that the presence of adhesins on the cell surface may counter dissemination and therefore virulence during infections. A possible biological explanation may be that genetic modification of the adhesin-encoding genes facilitates the colonization and subsequent dissemination in the bloodstream. In different analyses (Biswas *et al.*, 2017; Vale-Silva *et al.*, 2017; Carreté *et al.*, 2018), pairs of matched *C. glabrata* isolates belonged to the same clade and shared a large number of

DISCUSSION

SNPs as compared to other strains indicating a high degree of similarity within pairs. Despite their clonality, the number of variations between isolates from the same patient is still remarkable. In case of the trio of isolates analyzed here, the number of mutations shared between the first (SAT01) and the third isolate (SAT03) indicated that the mutations did not occur during the isolation process and they were pre-existing variations in the population. One hypothesis was that independent isolates from different infections must be taken into consideration but non-synonymous variations seem to accumulate during the course of the infection (Carreté *et al.*, 2019). We observed a reduced biofilm formation capacity in the strain isolated from blood (Figure 17A) which correlates with a point mutation in *SIR4*, part of biofilm formation regulation and subtelomeric silencing pathways (Leiva-Peláez *et al.*, 2018).

The genetic variations observed in *C. glabrata* (Carreté *et al.*, 2018) complement our phenotypic analyses indicating large variability between *C. glabrata* clades, which likely reflects geographical differences and dispersion mediated by humans. The degree of phenotypic intensities correlates with a large diversity towards CWP-encoding genes (López-Fuentes *et al.*, 2018). A high genomic plasticity leads enrichment in non-synonymous mutations of cell wall encoding genes (Gabaldón *et al.*, 2013). Here, a recurrent infection from a unique external source and the low adherence capacity of SAT03 with a mutation in *SIR4* may have facilitated the dissemination in the bloodstream as we also proposed for *C. parapsilosis*.

5. Conclusion and summary

Analyzing phenotypic variations of large *Candida glabrata* and *Candida parapsilosis* strain collections, showed several differences in genome and proteome organization. The overall observation was as a very high variability between the isolate's capacities to form biofilms on abiotic surfaces for both species.

In *C. glabrata*, biofilm formation capacity positively correlates with cell aggregation and cell sedimentation. By MS/MS spectrometric analyses of selected high biofilm-forming clinical isolates, we were able to differentiate a core and a unique variable proteome. An increased number of adhesins in *C. glabrata* cell wall, including ten new adhesins for the first time detected in this study correlated with a strong capacity to colonize host surfaces as well and co-interact with *C. albicans* hyphae facilitating epithelia invasion. The inability of *C. glabrata* to form hyphae may therefore be balanced by a high number of adhesins and adhesin-encoding genes in the cell wall. Alternatively, differences in the variable proteome may also indicate a high immunogenic heterogeneity to facilitate host evasion.

A positive correlation between intermediate or high capacities to form biofilms on abiotic surfaces and an increased incorporation of adhesins in the cell wall was found also for *C. parapsilosis*. Increased biofilm formation phenotypes became visible morphologically by the appearance of "rough" colony morphotypes. While such isolates' biofilms are notoriously insusceptible to azoles, EUCAST-based antifungal susceptibility testing was not able to predict this. Therefore, non-smooth morphologies identified in patient cultures might serve as an interesting novel diagnostic indicator to initiate echinocandin-based treatment to eradicate the biofilms of *C. parapsilosis*.

We also found a wide spectrum of *C. parapsilosis* killing rates in a *G. mellonella* animal model. The lack of Als6 in the cell wall was directly related with a reduced virulence and, surprisingly, *C. parapsilosis* isolates with low biofilm-formation capacity and therefore smooth morphotype presented a notably higher virulence.

CONCLUSION AND SUMMARY

Taken together, our phenotypical data point towards the unique role of non-adhesin presenting cells during dissemination in the patient, i.e. that “smooth” *C. parapsilosis* morphotypes will disseminate easier than “rough” morphologies, and therefore be more virulent in infection models.

Genome sequence analyses of matched isolates in *C. glabrata* point to mechanisms other than the previously described subtelomeric silencing, namely deletions and duplications of cell wall adhesin-encoding genes, as an important adaptive mechanism moving on from colonization to infection and dissemination.

6. Bibliography

Alcoba-Flórez, J., Méndez-Alvarez, S., Cano, J., Guarro, J., Pérez-Roth, E., and del Pilar Arévalo, M. (2005). Phenotypic and molecular characterization of *Candida nivariensis* sp. nov., a possible new opportunistic fungus. *J. Clin. Microbiol.* *43*, 4107–4111.

Alves, C.T., Wei, X.-Q., Silva, S., Azeredo, J., Henriques, M., and Williams, D.W. (2014b). *Candida albicans* promotes invasion and colonisation of *Candida glabrata* in a reconstituted human vaginal epithelium. *J. Infect.* *69*, 396–407.

Ames, L., Duxbury, S., Pawlowska, B., Ho, H., Haynes, K., and Bates, S. (2017a). *Galleria mellonella* as a host model to study *Candida glabrata* virulence and antifungal efficacy. *Virulence* *8*, 00–00.

Anderson, J.M., and Soll, D.R. (1987a). Unique phenotype of opaque cells in the white-opaque transition of *Candida albicans*. *Journal of Bacteriology* *169*, 5579–5588.

Arendrup, M.C., and Patterson, T.F. (2017). Multidrug-Resistant *Candida*: Epidemiology, molecular mechanisms, and treatment. *J. Infect. Dis.* *216*, S445–S451.

Arendrup, M.C., Cuenca-Estrella, M., Lass-Flörl, C., Hope, W., and EUCAST-AFST (2012). EUCAST technical note on the EUCAST definitive document EDef 7.2: method for the determination of broth dilution minimum inhibitory concentrations of antifungal agents for yeasts EDef 7.2 (EUCAST-AFST). *Clin. Microbiol. Infect.* *18*, E246-247.

van Asbeck, E., Clemons, K.V., Martinez, M., Tong, A.-J., and Stevens, D.A. (2008). Significant differences in drug susceptibility among species in the *Candida parapsilosis* group. *Diagn. Microbiol. Infect. Dis.* *62*, 106–109.

van Asbeck, E.C., Clemons, K.V., and Stevens, D.A. (2009). *Candida parapsilosis*: a review of its epidemiology, pathogenesis, clinical aspects, typing and antimicrobial susceptibility. *Crit. Rev. Microbiol.* *35*, 283–309.

Bader, O., Weig, M., Taverne-Ghadwal, L., Lugert, R., Gross, U., and Kuhns, M. (2011). Improved clinical laboratory identification of human pathogenic yeasts by matrix-assisted laser desorption ionization time-of-flight mass spectrometry. *Clin. Microbiol. Infect.* *17*, 1359–1365.

Bader, O., Schwarz, A., Kraneveld, E.A., Tangwattanchuleeporn, M., Schmidt, P., Jacobsen, M.D., Gross, U., De Groot, P.W.J., and Weig, M. (2012). Gross karyotypic and phenotypic alterations among different progenies of the *Candida glabrata* CBS138/ATCC2001 reference strain. *PLoS ONE* *7*, e52218.

Baillie, G.S., and Douglas, L.J. (1999). Role of dimorphism in the development of *Candida albicans* biofilms. *Journal of Medical Microbiology* *48*, 671–679.

BIBLIOGRAPHY

- Barnett, J.A. (2004). A history of research on yeasts 8: taxonomy. *Yeast* *21*, 1141–1193.
- Beaussart, A., Alsteens, D., El-Kirat-Chatel, S., Lipke, P.N., Kucharíková, S., Van Dijck, P., and Dufrêne, Y.F. (2012). Single-Molecule imaging and functional analysis of Als adhesins and mannans during *Candida albicans* morphogenesis. *ACS Nano* *6*, 10950–10964.
- Bernhard, M., Weig, M., Zautner, A.E., Groß, U., and Bader, O. (2014). Yeast On-Target Lysis (YOTL), a procedure for making auxiliary mass spectrum data sets for clinical routine identification of yeasts. *J Clin Microbiol* *52*, 4163–4167.
- Biswas, C., Chen, S.C.-A., Halliday, C., Kennedy, K., Playford, E.G., Marriott, D.J., Slavin, M.A., Sorrell, T.C., and Sintchenko, V. (2017). Identification of genetic markers of resistance to echinocandins, azoles and 5-fluorocytosine in *Candida glabrata* by next-generation sequencing: a feasibility study. *Clin. Microbiol. Infect.* *23*, 676.e7-676.e10.
- Bodey, G.P., Mardani, M., Hanna, H.A., Boktour, M., Abbas, J., Girgawy, E., Hachem, R.Y., Kontoyiannis, D.P., and Raad, I.I. (2002). The epidemiology of *Candida glabrata* and *Candida albicans* fungemia in immunocompromised patients with cancer. *Am. J. Med.* *112*, 380–385.
- Boisramé, A., Cornu, A., Da Costa, G., and Richard, M.L. (2011). Unexpected role for a serine/threonine-rich domain in the *Candida albicans* Iff Protein Family. *Eukaryot Cell* *10*, 1317–1330.
- Borghi, E., Andreoni, S., Cirasola, D., Ricucci, V., Sciota, R., and Morace, G. (2014). Antifungal resistance does not necessarily affect *Candida glabrata* fitness. *J Chemother* *26*, 32–36.
- Branchini, M.L., Pfaller, M.A., Rhine-Chalberg, J., Frempong, T., and Isenberg, H.D. (1994). Genotypic variation and slime production among blood and catheter isolates of *Candida parapsilosis*. *J. Clin. Microbiol.* *32*, 452–456.
- Butler, G., Rasmussen, M.D., Lin, M.F., Santos, M.A.S., Sakthikumar, S., Munro, C.A., Rheinbay, E., Grabherr, M., Forche, A., Reedy, J.L., *et al.* (2009a). Evolution of pathogenicity and sexual reproduction in eight *Candida* genomes. *Nature* *459*, 657–662.
- Carreté, L., Ksiezopolska, E., Pegueroles, C., Gómez-Molero, E., Saus, E., Iraola-Guzmán, S., Loska, D., Bader, O., Fairhead, C., and Gabaldón, T. (2018). Patterns of genomic variation in the opportunistic pathogen *Candida glabrata* Suggest the existence of mating and a secondary association with humans. *Curr. Biol.* *28*, 15-27.e7.
- Carreté, L., Ksiezopolska, E., Gómez-Molero, E., Angoulvant, A., Bader, O., Fairhead, C., and Gabaldón, T. (2019). Genome comparisons of *Candida glabrata* serial clinical isolates reveal patterns of genetic variation in infecting clonal populations. *Front. Microbiol.* *10*.

BIBLIOGRAPHY

ten Cate, J.M., Klis, F.M., Pereira-Cenci, T., Crielaard, W., and de Groot, P.W.J. (2009). Molecular and cellular mechanisms that lead to *Candida* biofilm formation. *J Dent Res* 88, 105–115.

Cavalheiro, M., and Teixeira, M.C. (2018). *Candida* Biofilms: Threats, challenges, and promising strategies. *Front Med (Lausanne)* 5.

Chaffin, W.L. (2008). *Candida albicans* cell wall proteins. *Microbiol Mol Biol Rev* 72, 495–544.

Chandra, J., Kuhn, D.M., Mukherjee, P.K., Hoyer, L.L., McCormick, T., and Ghannoum, M.A. (2001). Biofilm formation by the fungal pathogen *Candida albicans*: Development, architecture, and drug resistance. *J Bacteriol* 183, 5385–5394.

Chandra, J., Mukherjee, P.K., and Ghannoum, M.A. (2008). *In vitro* growth and analysis of *Candida* biofilms. *Nature Protocols* 3, 1909–1924.

Chaudhuri, R., Ansari, F.A., Raghunandan, M.V., and Ramachandran, S. (2011). FungalRV: adhesin prediction and immunoinformatics portal for human fungal pathogens. *BMC Genomics* 12, 192.

Cleveland, A.A., Farley, M.M., Harrison, L.H., Stein, B., Hollick, R., Lockhart, S.R., Magill, S.S., Derado, G., Park, B.J., and Chiller, T.M. (2012). Changes in incidence and antifungal drug resistance in candidemia: results from population-based laboratory surveillance in Atlanta and Baltimore, 2008-2011. *Clin. Infect. Dis.* 55, 1352–1361.

Cormack, B.P., Ghori, N., and Falkow, S. (1999). An adhesin of the yeast pathogen *Candida glabrata* mediating adherence to human epithelial cells. *Science* 285, 578–582.

Cornet, M., Sendid, B., Fradin, C., Gaillardin, C., Poulain, D., and Nguyen, H.-V. (2011). Molecular identification of closely related *Candida* species using two ribosomal intergenic spacer fingerprinting methods. *J Mol Diagn* 13, 12–22.

Correia, A., Sampaio, P., James, S., and Pais, C. (2006). *Candida bracarensis* sp. nov., a novel anamorphic yeast species phenotypically similar to *Candida glabrata*. *International Journal of Systematic and Evolutionary Microbiology* 56, 313–317.

Costerton, J.W., Stewart, P.S., and Greenberg, E.P. (1999). Bacterial biofilms: a common cause of persistent infections. *Science* 284, 1318–1322.

Davey, M.E., and O'toole, G.A. (2000). Microbial biofilms: from ecology to molecular genetics. *Microbiol. Mol. Biol. Rev.* 64, 847–867.

De Groot, P.W.J., Hellingwerf, K.J., and Klis, F.M. (2003). Genome-wide identification of fungal GPI proteins. *Yeast* 20, 781–796.

De Las Peñas, A., Pan, S.-J., Castaño, I., Alder, J., Cregg, R., and Cormack, B.P. (2003). Virulence-related surface glycoproteins in the yeast pathogen *Candida glabrata* are encoded in

BIBLIOGRAPHY

subtelomeric clusters and subject to *RAP1*- and *SIR*-dependent transcriptional silencing. *Genes Dev* 17, 2245–2258.

De Las Peñas, A., Juárez-Cepeda, J., López-Fuentes, E., Briones-Martín-del-Campo, M., Gutiérrez-Escobedo, G., and Castaño, I. (2015). Local and regional chromatin silencing in *Candida glabrata*: consequences for adhesion and the response to stress. *FEMS Yeast Res* 15.

Desai, C., Mavrianos, J., and Chauhan, N. (2011). *Candida glabrata* Pwp7p and Aed1p are required for adherence to human endothelial cells. *FEMS Yeast Res.* 11, 595–601.

Díaz-Jiménez, D.F., Mora-Montes, H.M., Hernández-Cervantes, A., Luna-Arias, J.P., Gow, N.A.R., and Flores-Carreón, A. (2012). Biochemical characterization of recombinant *Candida albicans* mannosyltransferases Mnt1, Mnt2 and Mnt5 reveals new functions in O- and N-mannan biosynthesis. *Biochem. Biophys. Res. Commun.* 419, 77–82.

Ding, C., Vidanes, G.M., Maguire, S.L., Guida, A., Synnott, J.M., Andes, D.R., and Butler, G. (2011). Conserved and divergent roles of Bcr1 and CFEM proteins in *Candida parapsilosis* and *Candida albicans*. *PLoS ONE* 6, e28151.

Dujon, B., Sherman, D., Fischer, G., Durrens, P., Casaregola, S., Lafontaine, I., De Montigny, J., Marck, C., Neuvéglise, C., Talla, E., *et al.* (2004). Genome evolution in yeasts. *Nature* 430, 35–44.

Eisenhaber, B., Schneider, G., Wildpaner, M., and Eisenhaber, F. (2004). A Sensitive Predictor for Potential GPI Lipid Modification Sites in Fungal Protein Sequences and its Application to Genome-wide Studies for *Aspergillus nidulans*, *Candida albicans*, *Neurospora crassa*, *Saccharomyces cerevisiae* and *Schizosaccharomyces pombe*. *Journal of Molecular Biology* 337, 243–253.

El-Kirat-Chatel, S., Beaussart, A., Derclaye, S., Alsteens, D., Kucharíková, S., Van Dijck, P., and Dufrêne, Y.F. (2015). Force nanoscopy of hydrophobic interactions in the fungal pathogen *Candida glabrata*. *ACS Nano* 9, 1648–1655.

Ene, I.V., and Bennett, R.J. (2009). Hwp1 and related adhesins contribute to both mating and biofilm formation in *Candida albicans*. *Eukaryotic Cell* 8, 1909–1913.

d'Enfert, C., and Janbon, G. (2016). Biofilm formation in *Candida glabrata*: What have we learnt from functional genomics approaches? *FEMS Yeast Res.* 16, fov111.

Enger, L., Joly, S., Pujol, C., Simonson, P., Pfaller, M., and Soll, D.R. (2001). Cloning and characterization of a complex DNA fingerprinting probe for *Candida parapsilosis*. *J. Clin. Microbiol.* 39, 658–669.

Erb Downward, J.R., Falkowski, N.R., Mason, K.L., Muraglia, R., and Huffnagle, G.B. (2013). Modulation of Post-Antibiotic Bacterial Community Reassembly and Host Response by *Candida albicans*. *Sci Rep* 3.

BIBLIOGRAPHY

- Espinel-Ingroff, A., Chowdhary, A., Gonzalez, G.M., Lass-Flörl, C., Martin-Mazuelos, E., Meis, J., Peláez, T., Pfaller, M.A., and Turnidge, J. (2013). Multicenter Study of Isavuconazole MIC Distributions and Epidemiological Cutoff Values for *Aspergillus spp.* for the CLSI M38-A2 broth microdilution Method. *Antimicrob Agents Chemother* 57, 3823–3828.
- Estivill, D., Arias, A., Torres-Lana, A., Carrillo-Muñoz, A.J., and Arévalo, M.P. (2011). Biofilm formation by five species of *Candida* on three clinical materials. *J. Microbiol. Methods* 86, 238–242.
- Ferreira, J.A.G., Carr, J.H., Starling, C.E.F., de Resende, M.A., and Donlan, R.M. (2009). Biofilm Formation and Effect of Caspofungin on Biofilm Structure of *Candida* Species Bloodstream Isolates. *Antimicrob Agents Chemother* 53, 4377–4384.
- Finkel, J.S., Xu, W., Huang, D., Hill, E.M., Desai, J.V., Woolford, C.A., Nett, J.E., Taff, H., Norice, C.T., Andes, D.R., *et al.* (2012). Portrait of *Candida albicans* Adherence Regulators. *PLoS Pathogens* 8, e1002525.
- Fitzpatrick, D.A., Logue, M.E., Stajich, J.E., and Butler, G. (2006). A fungal phylogeny based on 42 complete genomes derived from supertree and combined gene analysis. *BMC Evolutionary Biology* 6, 99.
- Fitzpatrick, D.A., O’Gaora, P., Byrne, K.P., and Butler, G. (2010). Analysis of gene evolution and metabolic pathways using the *Candida* gene order browser. *BMC Genomics* 11, 290.
- Fonseca, E., Silva, S., Rodrigues, C.F., Alves, C.T., Azeredo, J., and Henriques, M. (2014). Effects of fluconazole on *Candida glabrata* biofilms and its relationship with ABC transporter gene expression. *Biofouling* 30, 447–457.
- Fonzi, W.A., and Irwin, M.Y. (1993). Isogenic Strain Construction and Gene Mapping in *Candida albicans*. *Genetics* 134, 717–728.
- Fox, E.P., Bui, C.K., Nett, J.E., Hartooni, N., Mui, M.M., Andes, D.R., Nobile, C.J., and Johnson, A.D. (2015). An expanded regulatory network temporally controls *Candida albicans* biofilm formation. *Mol Microbiol* 96, 1226–1239.
- Gabaldón, T., and Carreté, L. (2016). The birth of a deadly yeast: tracing the evolutionary emergence of virulence traits in *Candida glabrata*. *FEMS Yeast Res* 16.
- Gabaldón, T., Martin, T., Marcet-Houben, M., Durrens, P., Bolotin-Fukuhara, M., Lespinet, O., Arnaise, S., Boissard, S., Aguilera, G., Atanasova, R., *et al.* (2013a). Comparative genomics of emerging pathogens in the *Candida glabrata* clade. *BMC Genomics* 14, 623.
- Gabaldón, T., Naranjo-Ortíz, M.A., and Marcet-Houben, M. (2016a). Evolutionary genomics of yeast pathogens in the Saccharomycotina. *FEMS Yeast Res* 16.

BIBLIOGRAPHY

Gácsér, A., Salomon, S., and Schäfer, W. (2005). Direct transformation of a clinical isolate of *Candida parapsilosis* using a dominant selection marker. *FEMS Microbiol. Lett.* *245*, 117–121.

Gácsér, A., Schäfer, W., Nosanchuk, J.S., Salomon, S., and Nosanchuk, J.D. (2007). Virulence of *Candida parapsilosis*, *Candida orthopsilosis*, and *Candida metapsilosis* in reconstituted human tissue models. *Fungal Genet. Biol.* *44*, 1336–1341.

Ghannoum, M.A. (2000). Potential role of phospholipases in virulence and fungal pathogenesis. *Clin. Microbiol. Rev.* *13*, 122–143, table of contents.

Gillum, A.M., Tsay, E.Y., and Kirsch, D.R. (1984). Isolation of the *Candida albicans* gene for orotidine-5'-phosphate decarboxylase by complementation of *S. cerevisiae* *ura3* and *E. coli* *pyrF* mutations. *Mol. Gen. Genet.* *198*, 179–182.

Gómez-Molero, E., de Boer, A.D., Dekker, H.L., Moreno-Martínez, A., Kraneveld, E.A., Ichsan I, Chauhan, N., Weig, M., de Soet, J.J., de Koster, C.G., *et al.* (2015). Proteomic analysis of hyperadhesive *Candida glabrata* clinical isolates reveals a core wall proteome and differential incorporation of adhesins. *FEMS Yeast Res.* *15*.

Gow, N.A.R., van de Veerdonk, F.L., Brown, A.J.P., and Netea, M.G. (2012). *Candida albicans* morphogenesis and host defence: discriminating invasion from colonization. *Nat. Rev. Microbiol.* *10*, 112–122.

de Groot, P.W.J., de Boer, A.D., Cunningham, J., Dekker, H.L., de Jong, L., Hellingwerf, K.J., de Koster, C., and Klis, F.M. (2004). Proteomic analysis of *Candida albicans* cell walls reveals covalently bound carbohydrate-active enzymes and adhesins. *Eukaryot Cell* *3*, 955–965.

de Groot, P.W.J., Kraneveld, E.A., Yin, Q.Y., Dekker, H.L., Groß, U., Crielaard, W., de Koster, C.G., Bader, O., Klis, F.M., and Weig, M. (2008). The cell wall of the human pathogen *Candida glabrata*: Differential incorporation of novel adhesin-like wall proteins. *Eukaryot Cell* *7*, 1951–1964.

de Groot, P.W.J., Bader, O., de Boer, A.D., Weig, M., and Chauhan, N. (2013). Adhesins in human fungal pathogens: Glue with plenty of stick. *Eukaryot Cell* *12*, 470–481.

Grossman, N.T., Pham, C.D., Cleveland, A.A., and Lockhart, S.R. (2015). Molecular mechanisms of fluconazole resistance in *Candida parapsilosis* isolates from a U.S. surveillance system. *Antimicrob Agents Chemother* *59*, 1030–1037.

Guinea, J. (2014). Global trends in the distribution of *Candida* species causing candidemia. *Clinical Microbiology and Infection* *20*, 5–10.

Harriott, M.M., and Noverr, M.C. (2011). Importance of *Candida*-bacterial polymicrobial biofilms in disease. *Trends Microbiol* *19*, 557–563.

BIBLIOGRAPHY

Hawser, S. (1996). Comparisons of the susceptibilities of planktonic and adherent *Candida albicans* to antifungal agents: a modified XTT tetrazolium assay using synchronised *C. albicans* cells. *J. Med. Vet. Mycol.* *34*, 149–152.

Hawser, S.P., and Douglas, L.J. (1995). Resistance of *Candida albicans* biofilms to antifungal agents *in vitro*. *Antimicrob. Agents Chemother.* *39*, 2128–2131.

Hazen, K.C., Plotkin, B.J., and Klimas, D.M. (1986). Influence of growth conditions on cell surface hydrophobicity of *Candida albicans* and *Candida glabrata*. *Infect. Immun.* *54*, 269–271.

Hill, J.A., O’Meara, T.R., and Cowen, L.E. (2015). Fitness Trade-Offs Associated with the Evolution of Resistance to antifungal drug Combinations. *Cell Reports* *10*, 809–819.

Hirakawa, M.P., Martinez, D.A., Sakthikumar, S., Anderson, M.Z., Berlin, A., Gujja, S., Zeng, Q., Zisson, E., Wang, J.M., Greenberg, J.M., *et al.* (2015). Genetic and phenotypic intra-species variation in *Candida albicans*. *Genome Res* *25*, 413–425.

Hoyer, L.L. (2001). The *ALS* gene family of *Candida albicans*. *Trends Microbiol.* *9*, 176–180.

Hoyer, L.L., and Cota, E. (2016). *Candida albicans* Agglutinin-like sequence (Als) family vignettes: a review of Als protein structure and function. *Front Microbiol* *7*.

Hoyer, L.L., and Hecht, J.E. (2000). The *ALS6* and *ALS7* genes of *Candida albicans*. *Yeast* *16*, 847–855.

Hoyer, L.L., and Hecht, J.E. (2001). The *ALS5* gene of *Candida albicans* and analysis of the Als5p N-terminal domain. *Yeast* *18*, 49–60.

Hoyer, L.L., Scherer, S., Shatzman, A.R., and Livi, G.P. (1995). *Candida albicans ALS1*: domains related to a *Saccharomyces cerevisiae* sexual agglutinin separated by a repeating motif. *Mol. Microbiol.* *15*, 39–54.

Hoyer, L.L., Payne, T.L., Bell, M., Myers, A.M., and Scherer, S. (1998a). *Candida albicans ALS3* and insights into the nature of the *ALS* gene family. *Curr. Genet.* *33*, 451–459.

Hoyer, L.L., Payne, T.L., and Hecht, J.E. (1998b). Identification of *Candida albicans ALS2* and *ALS4* and localization of als proteins to the fungal cell surface. *J. Bacteriol.* *180*, 5334–5343.

Hoyer, L.L., Fundyga, R., Hecht, J.E., Kapteyn, J.C., Klis, F.M., and Arnold, J. (2001b). Characterization of agglutinin-like sequence genes from non-*albicans Candida* and phylogenetic analysis of the *ALS* family. *Genetics* *157*, 1555–1567.

Hoyer, L.L., Green, C.B., Oh, S.-H., and Zhao, X. (2008). Discovering the secrets of the *Candida albicans* agglutinin-like sequence (*ALS*) gene family—a sticky pursuit. *Med Mycol* *46*, 1–15.

BIBLIOGRAPHY

Hull, C.M., Raisner, R.M., and Johnson, E.D. Evidence for mating of the "asexual" yeast *Candida albicans* in a mammalian host.

Ichsan Ichsan, Weig, M, Groß, U, Schwarz, A, Tangwattanaachuleeporn, M, Ziebolz, D, Jacobsen, M, Odds, F, Chauchan, N, de Groot, P.W.J, Bader, O. (2014). Genotypic and Phenotypic variability in a collection of *Candida glabrata* clinical isolates. ASM conference on *Candida* and Candidiasis. New Orleans, Louisiana, EE.UU.

Ielasi, F.S., Decanniere, K., and Willaert, R.G. (2012). The epithelial adhesin 1 (Epa1p) from the human-pathogenic yeast *Candida glabrata*: structural and functional study of the carbohydrate-binding domain. *Acta Crystallogr. D Biol. Crystallogr.* 68, 210–217.

Iraqi, I., Garcia-Sanchez, S., Aubert, S., Dromer, F., Ghigo, J.-M., D'Enfert, C., and Janbon, G. (2005). The Yak1p kinase controls expression of adhesins and biofilm formation in *Candida glabrata* in a Sir4p-dependent pathway. *Molecular Microbiology* 55, 1259–1271.

Jack, A.A., Daniels, D.E., Jepson, M.A., Vickerman, M.M., Lamont, R.J., Jenkinson, H.F., and Nobbs, A.H. (2015). *Streptococcus gordonii* comCDE (competence) operon modulates biofilm formation with *Candida albicans*. *Microbiology (Reading, Engl.)* 161, 411–421.

Jackson, A.P., Gamble, J.A., Yeomans, T., Moran, G.P., Saunders, D., Harris, D., Aslett, M., Barrell, J.F., Butler, G., Citiulo, F., *et al.* (2009). Comparative genomics of the fungal pathogens *Candida dubliniensis* and *Candida albicans*. *Genome Res* 19, 2231–2244.

Jacobsen, I.D., and Hube, B. (2017). *Candida albicans* morphology: still in focus. *Expert Review of Anti-Infective Therapy* 15, 327–330.

Jahagirdar, V.L., Davane, M.S., Aradye, S.C., and Nagoba, B.S. (2018). *Candida* species as potential nosocomial pathogens – A review. *Electron J Gen Med* 15.

Jouault, T., Sarazin, A., Martinez-Esparza, M., Fradin, C., Sendid, B., and Poulain, D. (2009). Host responses to a versatile commensal: PAMPs and PRRs interplay leading to tolerance or infection by *Candida albicans*. *Cellular Microbiology* 11, 1007–1015.

Junqueira, J.C., Fuchs, B.B., Muhammed, M., Coleman, J.J., Suleiman, J.M.A.H., Vilela, S.F.G., Costa, A.C.B.P., Rasteiro, V.M.C., Jorge, A.O.C., and Mylonakis, E. (2011). Oral *Candida albicans* isolates from HIV-positive individuals have similar *in vitro* biofilm-forming ability and pathogenicity as invasive *Candida* isolates. *BMC Microbiol.* 11, 247.

Kapteyn, J.C., Hoyer, L.L., Hecht, J.E., Müller, W.H., Andel, A., Verkleij, A.J., Makarow, M., Van Den Ende, H., and Klis, F.M. (2000). The cell wall architecture of *Candida albicans* wild-type cells and cell wall-defective mutants. *Mol. Microbiol.* 35, 601–611.

Karkowska-Kuleta, J., Zajac, D., Bochenska, O., and Kozik, A. (2015). Surfaceome of pathogenic yeasts, *Candida parapsilosis* and *Candida tropicalis*, revealed with the use of cell surface shaving method and shotgun proteomic approach. *Acta Biochimica Polonica* 62, 807–819.

BIBLIOGRAPHY

Katragkou, A., Chatzimoschou, A., Simitsopoulou, M., Dalakiouridou, M., Diza-Mataftsi, E., Tsantali, C., and Roilides, E. (2008). Differential activities of newer antifungal agents against *Candida albicans* and *Candida parapsilosis* biofilms. *Antimicrob Agents Chemother* 52, 357–360.

Kaur, R., Ma, B., and Cormack, B.P. (2007). A family of glycosylphosphatidylinositol-linked aspartyl proteases is required for virulence of *Candida glabrata*. *Proc. Natl. Acad. Sci. U.S.A.* 104, 7628–7633.

Kim, J., and Sudbery, P. (2011). *Candida albicans*, a major human fungal pathogen. *J. Microbiol.* 49, 171–177.

Klis, F.M., de Groot, P., and Hellingwerf, K. (2001). Molecular organization of the cell wall of *Candida albicans*. *Med. Mycol.* 39 Suppl 1, 1–8.

Klis, F.M., Sosinska, G.J., de Groot, P.W.J., and Brul, S. (2009). Covalently linked cell wall proteins of *Candida albicans* and their role in fitness and virulence. *FEMS Yeast Res.* 9, 1013–1028.

Kraneveld, E.A., de Soet, J.J., Deng, D.M., Dekker, H.L., de Koster, C.G., Klis, F.M., Crielaard, W., and de Groot, P.W.J. (2011). Identification and differential gene expression of adhesin-like wall proteins in *Candida glabrata* biofilms. *Mycopathologia* 172, 415–427.

Krcmery, V., and Barnes, A.J. (2002). Non-*albicans* *Candida* spp. causing fungaemia: pathogenicity and antifungal resistance. *J. Hosp. Infect.* 50, 243–260.

Kucharíková, S., Neirinck, B., Sharma, N., Vleugels, J., Lagrou, K., and Van Dijck, P. (2015). *In vivo* *Candida glabrata* biofilm development on foreign bodies in a rat subcutaneous model. *Journal of Antimicrobial Chemotherapy* 70, 846–856.

Kühbacher, A., Burger-Kentischer, A., and Rupp, S. (2017). Interaction of *Candida* Species with the skin. *Microorganisms* 5.

Kuhn, D.M., George, T., Chandra, J., Mukherjee, P.K., and Ghannoum, M.A. (2002). Antifungal susceptibility of *Candida* biofilms: Unique efficacy of amphotericin B lipid formulations and echinocandins. *Antimicrob Agents Chemother* 46, 1773–1780.

Kuhn, D.M., Mukherjee, P.K., Clark, T.A., Pujol, C., Chandra, J., Hajjeh, R.A., Warnock, D.W., Soll, D.R., and Ghannoum, M.A. (2004). *Candida parapsilosis* characterization in an outbreak setting. *Emerg Infect Dis* 10, 1074–1081.

Kurtzman, C.P., and Robnett, C.J. (1998). Identification and phylogeny of ascomycetous yeasts from analysis of nuclear large subunit (26S) ribosomal DNA partial sequences. *Antonie Van Leeuwenhoek* 73, 331–371.

Kurtzman, C.P., and Robnett, C.J. (2003). Phylogenetic relationships among yeasts of the “*Saccharomyces* complex” determined from multigene sequence analyses. *FEMS Yeast Res.* 3, 417–432.

BIBLIOGRAPHY

Kurtzman, C.P., and Robnett, C.J. (2013). Relationships among genera of the *Saccharomycotina* (*Ascomycota*) from multigene phylogenetic analysis of type species. *FEMS Yeast Res.* *13*, 23–33.

Laffey, S.F., and Butler, G. (2005). Phenotype switching affects biofilm formation by *Candida parapsilosis*. *Microbiology (Reading, Engl.)* *151*, 1073–1081.

Lamoth, F., Lockhart, S.R., Berkow, E.L., and Calandra, T. (2018). Changes in the epidemiological landscape of invasive candidiasis. *J. Antimicrob. Chemother.* *73*, i4–i13.

Lamster, I.B., Lalla, E., Borgnakke, W.S., and Taylor, G.W. (2008). The relationship between oral health and diabetes mellitus. *J Am Dent Assoc* *139 Suppl*, 19S-24S.

Lan, C.-Y., Rodarte, G., Murillo, L.A., Jones, T., Davis, R.W., Dungan, J., Newport, G., and Agabian, N. (2004). Regulatory networks affected by iron availability in *Candida albicans*. *Mol. Microbiol.* *53*, 1451–1469.

Lattif, A.A., K. Mukherjee, P., Chandra, J., Swindell, K., Lockhart, S.R., Diekema, D.J., Pfaller, M.A., and Ghannoum, M.A. (2010). Characterization of biofilms formed by *Candida parapsilosis*, *C. metapsilosis*, and *C. orthopsilosis*. *International Journal of Medical Microbiology* *300*, 265–270.

Leiva-Peláez, O., Gutiérrez-Escobedo, G., López-Fuentes, E., Cruz-Mora, J., De Las Peñas, A., and Castaño, I. (2018). Molecular characterization of the silencing complex *SIR* in *Candida glabrata* hyperadherent clinical isolates. *Fungal Genet. Biol.* *118*, 21–31.

Li, L., Redding, S., and Dongari-Bagtzoglou, A. (2007). *Candida glabrata*, an Emerging Oral Opportunistic Pathogen. *J Dent Res* *86*, 204–215.

Lindsay, A.K., Morales, D.K., Liu, Z., Grahl, N., Zhang, A., Willger, S.D., Myers, L.C., and Hogan, D.A. (2014). Analysis of *Candida albicans* Mutants Defective in the Cdk8 Module of Mediator Reveal Links between Metabolism and Biofilm Formation. *PLOS Genetics* *10*, e1004567.

Lo, H.J., Köhler, J.R., DiDomenico, B., Loebenberg, D., Cacciapuoti, A., and Fink, G.R. (1997). Nonfilamentous *C. albicans* mutants are avirulent. *Cell* *90*, 939–949.

Lockhart, S.R., Wagner, D., Iqbal, N., Pappas, P.G., Andes, D.R., Kauffman, C.A., Brumble, L.M., Hadley, S., Walker, R., Ito, J.I., *et al.* (2011). Comparison of *in vitro* susceptibility characteristics of *Candida* species from cases of invasive candidiasis in solid organ and stem cell transplant recipients: Transplant-Associated Infections Surveillance Network (TRANSNET), 2001 to 2006. *J. Clin. Microbiol.* *49*, 2404–2410.

Lockhart, S.R., Iqbal, N., Cleveland, A.A., Farley, M.M., Harrison, L.H., Bolden, C.B., Baughman, W., Stein, B., Hollick, R., Park, B.J., *et al.* (2012). Species identification and antifungal susceptibility testing of *Candida* bloodstream isolates from population-based surveillance studies in two U.S. cities from 2008 to 2011. *J. Clin. Microbiol.* *50*, 3435–3442.

BIBLIOGRAPHY

- López-Fuentes, E., Gutiérrez-Escobedo, G., Timmermans, B., Van Dijck, P., De Las Peñas, A., and Castaño, I. (2018). *Candida glabrata's* genome plasticity confers a unique pattern of expressed cell wall proteins. *J Fungi (Basel)* 4.
- Lott, T.J., Kuykendall, R.J., Welbel, S.F., Pramanik, A., and Lasker, B.A. (1993a). Genomic heterogeneity in the yeast *Candida parapsilosis*. *Curr. Genet.* 23, 463–467.
- Luo, G., and Samaranayake, L.P. (2002). *Candida glabrata*, an emerging fungal pathogen, exhibits superior relative cell surface hydrophobicity and adhesion to denture acrylic surfaces compared with *Candida albicans*. *APMIS* 110, 601–610.
- Lyon, G.M., Karatela, S., Sunay, S., and Adiri, Y. (2010). Antifungal susceptibility testing of *Candida* isolates from the *Candida* surveillance study. *J Clin Microbiol* 48, 1270–1275.
- Malani, A.N., Psarros, G., Malani, P.N., and Kauffman, C.A. (2011). Is age a risk factor for *Candida glabrata* colonisation? *Mycoses* 54, 531–537.
- Martin, D.S., and Jones, C.P. (1940). Further studies on the practical classification of the Monilias 1. *J Bacteriol* 39, 609–630.
- McCarty, T.P., and Pappas, P.G. (2016). Invasive Candidiasis. *Infect. Dis. Clin. North Am.* 30, 103–124.
- McCullough, M.J., Ross, B.C., and Reade, P.C. (1996). *Candida albicans*: a review of its history, taxonomy, epidemiology, virulence attributes, and methods of strain differentiation. *Int J Oral Maxillofac Surg* 25, 136–144.
- Melo, A.S., Bizerra, F.C., Freymüller, E., Arthington-Skaggs, B.A., and Colombo, A.L. (2011). Biofilm production and evaluation of antifungal susceptibility amongst clinical *Candida spp.* isolates, including strains of the *Candida parapsilosis* complex. *Med Mycol* 49, 253–262.
- Meyer, E., Geffers, C., Gastmeier, P., and Schwab, F. (2013). No increase in primary nosocomial candidemia in 682 German intensive care units during 2006 to 2011. *Euro Surveill.* 18.
- Moralez, A.T.P., França, E.J.G., Furlaneto-Maia, L., Quesada, R.M.B., and Furlaneto, M.C. (2014). Phenotypic switching in *Candida tropicalis*: association with modification of putative virulence attributes and antifungal drug sensitivity. *Med. Mycol.* 52, 106–114.
- Moyes, D.L., Wilson, D., Richardson, J.P., Mogavero, S., Tang, S.X., Wernecke, J., Höfs, S., Gratacap, R.L., Robbins, J., Runglall, M., *et al.* (2016). Candidalysin is a fungal peptide toxin critical for mucosal infection. *Nature* 532, 64–68.
- Mukherjee, P.K., Zhou, G., Munyon, R., and Ghannoum, M.A. (2005). *Candida* biofilm: a well-designed protected environment. *Med. Mycol.* 43, 191–208.

BIBLIOGRAPHY

Müller, H., Thierry, A., Coppée, J.Y., Gouyette, C., Hennequin, C., Sismeiro, O., Talla, E., Dujon, B., Fairhead, C. (2009). Genomic polymorphism in the population of *Candida glabrata*: Gene copy-number variation and chromosomal translocations. *Fungal Genet. and Biol.* *46*, 264-276.

Naglik, J.R., Challacombe, S.J., and Hube, B. (2003). *Candida albicans* secreted aspartyl proteinases in virulence and pathogenesis. *Microbiol. Mol. Biol. Rev.* *67*, 400–428, table of contents.

Nather, K., and Munro, C.A. (2008). Generating cell surface diversity in *Candida albicans* and other fungal pathogens. *FEMS Microbiology Letters* *285*, 137–145.

Neji, S., Hadrach, I., Trabelsi, H., Abbes, S., Cheikhrouhou, F., Sellami, H., Makni, F., and Ayadi, A. (2017). Virulence factors, antifungal susceptibility and molecular mechanisms of azole resistance among *Candida parapsilosis* complex isolates recovered from clinical specimens. *Journal of Biomedical Science* *24*, 67.

Németh, T., Tóth, A., Szenzenstein, J., Horváth, P., Nosanchuk, J.D., Grózer, Z., Tóth, R., Papp, C., Hamari, Z., Vágvölgyi, C., *et al.* (2013). Characterization of virulence properties in the *C. parapsilosis sensu lato* species. *PLOS ONE* *8*, e68704.

Nett, J., Lincoln, L., Marchillo, K., Massey, R., Holoyda, K., Hoff, B., VanHandel, M., and Andes, D. (2007). Putative role of beta-1,3 glucans in *Candida albicans* biofilm resistance. *Antimicrob. Agents Chemother.* *51*, 510–520.

Nett, J.E., Zarnowski, R., Cabezas-Olcoz, J., Brooks, E.G., Bernhardt, J., Marchillo, K., Mosher, D.F., and Andes, D.R. (2015). Host contributions to construction of three device-associated *Candida albicans* biofilms. *Infect. Immun.* *83*, 4630–4638.

Nobbs, A.H., Vickerman, M.M., and Jenkinson, H.F. (2010). Heterologous expression of *Candida albicans* cell wall-associated adhesins in *Saccharomyces cerevisiae* reveals differential specificities in adherence and biofilm formation and in binding oral *Streptococcus gordonii*. *Eukaryotic Cell* *9*, 1622–1634.

Nobile, C.J., and Johnson, A.D. (2015). *Candida albicans* Biofilms and Human Disease. *Annu. Rev. Microbiol.* *69*, 71–92.

Nobile, C.J., Andes, D.R., Nett, J.E., Smith, F.J., Yue, F., Phan, Q.-T., Edwards, J.E., Filler, S.G., and Mitchell, A.P. (2006). Critical role of Bcr1-dependent adhesins in *C. albicans* biofilm formation *in vitro* and *in vivo*. *PLoS Pathog* *2*.

Nobile, C.J., Schneider, H.A., Nett, J.E., Sheppard, D.C., Filler, S.G., Andes, D.R., and Mitchell, A.P. (2008). Complementary adhesin function in *C. albicans* biofilm formation. *Curr Biol* *18*, 1017–1024.

BIBLIOGRAPHY

Nobile, C.J., Nett, J.E., Hernday, A.D., Homann, O.R., Deneault, J.-S., Nantel, A., Andes, D.R., Johnson, A.D., and Mitchell, A.P. (2009). Biofilm matrix regulation by *Candida albicans* Zap1. *PLoS Biol.* 7, e1000133.

Noble, S.M., Gianetti, B.A., and Witchley, J.N. (2017). *Candida albicans* cell-type switching and functional plasticity in the mammalian host. *Nat. Rev. Microbiol.* 15, 96–108.

Nosek, J., Holesova, Z., Kosa, P., Gacser, A., and Tomaska, L. (2009). Biology and genetics of the pathogenic yeast *Candida parapsilosis*. *Curr. Genet.* 55, 497–509.

Odds, F.C. (1988). *Candida* and candidosis (London; Philadelphia: Baillière Tindall).

Orasch, C., Marchetti, O., Garbino, J., Schrenzel, J., Zimmerli, S., Mühlethaler, K., Pfyffer, G., Ruef, C., Fehr, J., Zbinden, R., *et al.* (2014). *Candida* species distribution and antifungal susceptibility testing according to European Committee on Antimicrobial Susceptibility Testing and new vs. old clinical and laboratory standards institute clinical breakpoints: a 6-year prospective candidaemia survey from the fungal infection network of Switzerland. *Clinical Microbiology and Infection* 20, 698–705.

Otoo, H.N., Lee, K.G., Qiu, W., and Lipke, P.N. (2008). *Candida albicans* Als adhesins have conserved amyloid-forming sequences. *Eukaryotic Cell* 7, 776–782.

Pannanusorn, S., Fernandez, V., and Römling, U. (2013). Prevalence of biofilm formation in clinical isolates of *Candida* species causing bloodstream infection. *Mycoses* 56, 264–272.

Pappas, P.G., Rex, J.H., Lee, J., Hamill, R.J., Larsen, R.A., Powderly, W., Kauffman, C.A., Hyslop, N., Mangino, J.E., Chapman, S., *et al.* (2003). A prospective observational study of candidemia: epidemiology, therapy, and influences on mortality in hospitalized adult and pediatric patients. *Clin. Infect. Dis.* 37, 634–643.

Pappas, P.G., Lionakis, M.S., Arendrup, M.C., Ostrosky-Zeichner, L., and Kullberg, B.J. (2018a). Invasive candidiasis. *Nat Rev Dis Primers* 4, 18026.

Parahitiyawa, N.B., Samaranayake, Y.H., Samaranayake, L.P., Ye, J., Tsang, P.W.K., Cheung, B.P.K., Yau, J.Y.Y., and Yeung, S.K.W. (2006). Interspecies variation in *Candida* biofilm formation studied using the Calgary biofilm device. *APMIS* 114, 298–306.

Patel, R., Grogg, K.L., Edwards, W.D., Wright, A.J., and Schwenk, N.M. (2000). Death from inappropriate therapy for lyme disease. *Clin Infect Dis* 31, 1107–1109.

Pathak, A.K., Sharma, S., and Shrivastva, P. (2012). Multi-species biofilm of *Candida albicans* and non-*Candida albicans* *Candida* species on acrylic substrate. *J Appl Oral Sci* 20, 70–75.

Peleg, A.Y., Hogan, D.A., and Mylonakis, E. (2010). Medically important bacterial–fungal interactions. *Nature Reviews Microbiology* 8, 340–349.

BIBLIOGRAPHY

Percival, S.L., McCarty, S.M., and Lipsky, B. (2014). Biofilms and wounds: An overview of the evidence. *Advances in Wound Care* 4, 373–381.

Pereira, L., Silva, S., Ribeiro, B., Henriques, M., and Azeredo, J. (2015). Influence of glucose concentration on the structure and quantity of biofilms formed by *Candida parapsilosis*. *FEMS Yeast Res.* 15, fov043.

Pérez-García, L.A., Csonka, K., Flores-Carreón, A., Estrada-Mata, E., Mellado-Mojica, E., Németh, T., López-Ramírez, L.A., Toth, R., López, M.G., Vizler, C., *et al.* (2016). Role of protein glycosylation in *Candida parapsilosis* cell wall integrity and host interaction. *Front Microbiol* 7.

Pfaller, M.A., and Diekema, D.J. (2007). Epidemiology of invasive candidiasis: a persistent public health problem. *Clin. Microbiol. Rev.* 20, 133–163.

Pfaller, M.A., Messer, S.A., and Hollis, R.J. (1995). Variations in DNA subtype, antifungal susceptibility, and slime production among clinical isolates of *Candida parapsilosis*. *Diagnostic Microbiology and Infectious Disease* 21, 9–14.

Pfaller, M.A., Messer, S.A., Boyken, L., Tendolkar, S., Hollis, R.J., and Diekema, D.J. (2004). Geographic Variation in the Susceptibilities of Invasive Isolates of *Candida glabrata* to seven systemically active antifungal agents: a global assessment from the ARTEMIS antifungal surveillance program conducted in 2001 and 2002. *J Clin Microbiol* 42, 3142–3146.

Pfaller, M.A., Boyken, L., Hollis, R.J., Messer, S.A., Tendolkar, S., and Diekema, D.J. (2005a). *In vitro* activities of anidulafungin against more than 2,500 clinical isolates of *Candida spp.*, including 315 isolates resistant to fluconazole. *J. Clin. Microbiol.* 43, 5425–5427.

Pfaller, M.A., Boyken, L., Messer, S.A., Tendolkar, S., Hollis, R.J., and Diekema, D.J. (2005b). Comparison of results of voriconazole disk diffusion testing for *Candida* species with results from a central reference laboratory in the ARTEMIS global antifungal surveillance program. *J. Clin. Microbiol.* 43, 5208–5213.

Pfaller, M.A., Diekema, D.J., and Sheehan, D.J. (2006). Interpretive breakpoints for fluconazole and *Candida* revisited: a blueprint for the future of antifungal susceptibility testing. *Clinical Microbiology Reviews* 19, 435–447.

Pfaller, M.A., Boyken, L., Hollis, R.J., Kroeger, J., Messer, S.A., Tendolkar, S., and Diekema, D.J. (2008). *In vitro* susceptibility of invasive isolates of *Candida spp.* to anidulafungin, caspofungin, and micafungin: six years of global surveillance. *J. Clin. Microbiol.* 46, 150–156.

Pfaller, M.A., Diekema, D.J., Gibbs, D.L., Newell, V.A., Ellis, D., Tullio, V., Rodloff, A., Fu, W., Ling, T.A., and Global Antifungal Surveillance Group (2010). Results from the ARTEMIS DISK global antifungal surveillance study, 1997 to 2007: a 10.5-year analysis of susceptibilities of *Candida* species to fluconazole and voriconazole as determined by CLSI standardized disk diffusion. *J. Clin. Microbiol.* 48, 1366–1377.

BIBLIOGRAPHY

- Pfaller, M.A., Castanheira, M., Lockhart, S.R., Ahlquist, A.M., Messer, S.A., and Jones, R.N. (2012). Frequency of decreased susceptibility and resistance to echinocandins among fluconazole-resistant bloodstream isolates of *Candida glabrata*. *J Clin Microbiol* 50, 1199–1203.
- Pryszcz, L.P., Németh, T., Gácsér, A., and Gabaldón, T. (2013). Unexpected genomic variability in clinical and environmental strains of the pathogenic yeast *Candida parapsilosis*. *Genome Biol Evol* 5, 2382–2392.
- Puig-Asensio, M., Padilla, B., Garnacho-Montero, J., Zaragoza, O., Aguado, J.M., Zaragoza, R., Montejo, M., Muñoz, P., Ruiz-Camps, I., Cuenca-Estrella, M., *et al.* (2014). Epidemiology and predictive factors for early and late mortality in *Candida* bloodstream infections: a population-based surveillance in Spain. *Clin. Microbiol. Infect.* 20, O245-254.
- Quindós, G. (2014). Epidemiology of candidaemia and invasive candidiasis. a changing face. *Rev Iberoam Micol* 31, 42–48.
- Ramage, G., Vandewalle, K., Wickes, B.L., and López-Ribot, J.L. (2001). Characteristics of biofilm formation by *Candida albicans*. *Rev Iberoam Micol* 18, 163–170.
- Ramage, G., Bachmann, S., Patterson, T.F., Wickes, B.L., and López-Ribot, J.L. (2002). Investigation of multidrug efflux pumps in relation to fluconazole resistance in *Candida albicans* biofilms. *J. Antimicrob. Chemother.* 49, 973–980.
- Richardson, J.P., and Moyes, D.L. (2015). Adaptive immune responses to *Candida albicans* infection. *Virulence* 6, 327–337.
- Rigby, S., Procop, G.W., Haase, G., Wilson, D., Hall, G., Kurtzman, C., Oliveira, K., Von Oy, S., Hyldig-Nielsen, J.J., Coull, J., *et al.* (2002). Fluorescence in situ hybridization with peptide nucleic acid probes for rapid identification of *Candida albicans* directly from blood culture bottles. *J. Clin. Microbiol.* 40, 2182–2186.
- Rodrigues, C.F., Silva, S., and Henriques, M. (2014). *Candida glabrata*: a review of its features and resistance. *Eur. J. Clin. Microbiol. Infect. Dis.* 33, 673–688.
- Rodrigues, C.F., Rodrigues, M.E., Silva, S., and Henriques, M. (2017b). *Candida glabrata* Biofilms: How Far Have We Come? *J Fungi (Basel)* 3.
- Romão, D., Cavalheiro, M., Mil-Homens, D., Santos, R., Pais, P., Costa, C., Takahashi-Nakaguchi, A., Fialho, A.M., Chibana, H., and Teixeira, M.C. (2017). A new determinant of *Candida glabrata* virulence: The Acetate Exporter CgDtr1. *Front Cell Infect Microbiol* 7.
- Rossoni, R.D., Barbosa, J.O., Vilela, S.F.G., Jorge, A.O.C., and Junqueira, J.C. (2013). Comparison of the hemolytic activity between *C. albicans* and non-*albicans* *Candida* species. *Braz. Oral Res.* 27, 484–489.

BIBLIOGRAPHY

Ruhnke, M. (2014). Antifungal stewardship in invasive *Candida* infections. *Clinical Microbiology and Infection* 20, 11–18.

Ruiz-Herrera, J., Elorza, M.V., Valentín, E., and Sentandreu, R. (2006). Molecular organization of the cell wall of *Candida albicans* and its relation to pathogenicity. *FEMS Yeast Research* 6, 14–29.

Růzicka, F., Holá, V., Votava, M., and Tejkalová, R. (2007). Importance of biofilm in *Candida parapsilosis* and evaluation of its susceptibility to antifungal agents by colorimetric method. *Folia Microbiol. (Praha)* 52, 209–214.

Saballs, P., Torres-Rodríguez, J.M., Salvadó, M., Sales, P., Gimeno-Bayón, J.L., Knobel, H., López Colomé, J.L., Serrano, C., and Drobnic, L. (2000). Candidemia in AIDS. A retrospective study of nine cases. *Revista Iberoamericana de Micología* 17, 2–5.

Santos, M.A.S., Gomes, A.C., Santos, M.C., Carreto, L.C., and Moura, G.R. (2011). The genetic code of the fungal CTG clade. *C. R. Biol.* 334, 607–611.

Schaller, M., Borelli, C., Korting, H.C., and Hube, B. (2005). Hydrolytic enzymes as virulence factors of *Candida albicans*. *Mycoses* 48, 365–377.

Schauer, F., and Hanschke, R. (1999). [Taxonomy and ecology of the genus *Candida*]. *Mycoses* 42 Suppl 1, 12–21.

Seidler, M., Salvenmoser, S., and Müller, F.-M.C. (2006). *In vitro* effects of micafungin against *Candida* biofilms on polystyrene and central venous catheter sections. *Int. J. Antimicrob. Agents* 28, 568–573.

Seneviratne, C.J., Silva, W.J., Jin, L.J., Samaranayake, Y.H., and Samaranayake, L.P. (2009). Architectural analysis, viability assessment and growth kinetics of *Candida albicans* and *Candida glabrata* biofilms. *Arch. Oral Biol.* 54, 1052–1060.

Shepherd, M.G., Poulter, R.T.M., and Sullivan, P.A. (1985). *Candida albicans*: Biology, Genetics, and Pathogenicity. *Annual Review of Microbiology* 39, 579–614.

Shin, J.H., Shin, D.H., Song, J.W., Kee, S.J., Suh, S.P., and Ryang, D.W. (2001). Electrophoretic karyotype analysis of sequential *Candida parapsilosis* isolates from patients with persistent or recurrent fungemia. *J. Clin. Microbiol.* 39, 1258–1263.

Shin, J.H., Kee, S.J., Shin, M.G., Kim, S.H., Shin, D.H., Lee, S.K., Suh, S.P., and Ryang, D.W. (2002b). Biofilm production by isolates of *Candida* species recovered from nonneutropenic patients: Comparison of bloodstream isolates with isolates from other sources. *Journal of Clinical Microbiology* 40, 1244–1248.

BIBLIOGRAPHY

Silva, A.P., Miranda, I.M., Guida, A., Synnott, J., Rocha, R., Silva, R., Amorim, A., Pina-Vaz, C., Butler, G., and Rodrigues, A.G. (2011). Transcriptional profiling of azole-resistant *Candida parapsilosis* strains. *Antimicrob Agents Chemother* 55, 3546–3556.

Silva, S., Henriques, M., Oliveira, R., Azeredo, J., Malic, S., Hooper, S.J., and Williams, D.W. (2009a). Characterization of *Candida parapsilosis* infection of an *in vitro* reconstituted human oral epithelium. *Eur. J. Oral Sci.* 117, 669–675.

Silva, S., Henriques, M., Martins, A., Oliveira, R., Williams, D., and Azeredo, J. (2009b). Biofilms of non-*Candida albicans* *Candida* species: quantification, structure and matrix composition. *Med. Mycol.* 47, 681–689.

Silva, S., Negri, M., Henriques, M., Oliveira, R., Williams, D.W., and Azeredo, J. (2012). *Candida glabrata*, *Candida parapsilosis* and *Candida tropicalis*: biology, epidemiology, pathogenicity and antifungal resistance. *FEMS Microbiol. Rev.* 36, 288–305.

Silva, S., Rodrigues, C.F., Araújo, D., Rodrigues, M.E., and Henriques, M. (2017). *Candida* Species biofilms' antifungal resistance. *J Fungi (Basel)* 3.

Silva-Dias, A., Miranda, I.M., Branco, J., Monteiro-Soares, M., Pina-Vaz, C., and Rodrigues, A.G. (2015). Adhesion, biofilm formation, cell surface hydrophobicity, and antifungal planktonic susceptibility: relationship among *Candida spp.* *Front Microbiol* 6.

Slutsky, B., Buffo, J., and Soll, D.R. (1985). High-frequency switching of colony morphology in *Candida albicans*. *Science* 230, 666–669.

Slutsky, B., Staebell, M., Anderson, J., Risen, L., Pfaller, M., and Soll, D.R. (1987). “White-opaque transition”: a second high-frequency switching system in *Candida albicans*. *J Bacteriol* 169, 189–197.

Sóczó, G., Kardos, G., McNicholas, P.M., Falusi, E., Gergely, L., and Majoros, L. (2007). Posaconazole susceptibility testing against *Candida* species: comparison of broth microdilution and E-test methods. *Mycoses* 50, 178–182.

Solis, N.V., Park, Y.-N., Swidergall, M., Daniels, K.J., Filler, S.G., and Soll, D.R. (2018). *Candida albicans* white-opaque switching influences virulence but not mating during oropharyngeal candidiasis. *Infect. Immun.*

Souza, A.C.R., Fuchs, B.B., Pinhati, H.M.S., Siqueira, R.A., Hagen, F., Meis, J.F., Mylonakis, E., and Colombo, A.L. (2015). *Candida parapsilosis* resistance to fluconazole: Molecular mechanisms and *in vivo* Impact in infected *Galleria mellonella* larvae. *Antimicrob Agents Chemother* 59, 6581–6587.

Srivastava, V.K., Suneetha, K.J., and Kaur, R. (2014). A systematic analysis reveals an essential role for high-affinity iron uptake system, haemolysin and CFEM domain-containing protein in iron homeostasis and virulence in *Candida glabrata*. *Biochem. J.* 463, 103–114.

BIBLIOGRAPHY

Sudbery, P., Gow, N., and Berman, J. (2004). The distinct morphogenic states of *Candida albicans*. *Trends in Microbiology* *12*, 317–324.

Tati, S., Davidow, P., McCall, A., Hwang-Wong, E., Rojas, I.G., Cormack, B., and Edgerton, M. (2016). *Candida glabrata* binding to *Candida albicans* hyphae enables its development in oropharyngeal candidiasis. *PLoS Pathog.* *12*, e1005522.

Tavanti, A., Hensgens, L.A., Mogavero, S., Majoros, L., Senesi, S., and Campa, M. (2010). Genotypic and phenotypic properties of *Candida parapsilosis sensu strictu* strains isolated from different geographic regions and body sites. *BMC Microbiol* *10*, 203.

Timmermans, B., De Las Peñas, A., Castaño, I., and Van Dijck, P. (2018). Adhesins in *Candida glabrata*. *J Fungi (Basel)* *4*.

Tortorano, A.M., Peman, J., Bernhardt, H., Klingspor, L., Kibbler, C.C., Faure, O., Biraghi, E., Canton, E., Zimmermann, K., Seaton, S., *et al.* (2004). Epidemiology of candidaemia in Europe: results of 28-month European Confederation of Medical Mycology (ECMM) hospital-based surveillance study. *Eur. J. Clin. Microbiol. Infect. Dis.* *23*, 317–322.

Toth, R., Toth, A., Vagvolgyi, C., and Gacser, A. (2017). *Candida parapsilosis* secreted lipase as an important virulence factor. *Curr. Protein Pept. Sci.* *18*, 1043–1049.

Tournu, H., and Van Dijck, P. (2012). *Candida* Biofilms and the Host: Models and New Concepts for Eradication.

Tragiannidis, A., Fegeler, W., Rellensmann, G., Debus, V., Müller, V., Hoernig-Franz, I., Siam, K., Pana, Z.-D., Jürgens, H., and Groll, A.H. (2012). Candidaemia in a european paediatric university hospital: a 10-year observational study. *Clin. Microbiol. Infect.* *18*, E27-30.

Trofa, D., Gácser, A., and Nosanchuk, J.D. (2008). *Candida parapsilosis*, an emerging fungal pathogen. *Clin. Microbiol. Rev.* *21*, 606–625.

Tsai, H.-F., Krol, A.A., Sarti, K.E., and Bennett, J.E. (2006). *Candida glabrata PDR1*, a transcriptional regulator of a pleiotropic drug resistance network, mediates azole resistance in clinical isolates and petite mutants. *Antimicrob. Agents Chemother.* *50*, 1384–1392.

Uppuluri, P., Chaturvedi, A.K., Srinivasan, A., Banerjee, M., Ramasubramaniam, A.K., Köhler, J.R., Kadosh, D., and Lopez-Ribot, J.L. (2010). Dispersion as an important step in the *Candida albicans* biofilm developmental cycle. *PLoS Pathog* *6*.

Uppuluri, P., Zaldívar, M.A., Anderson, M.Z., Dunn, M.J., Berman, J., Ribot, J.L.L., and Köhler, J.R. (2018). *Candida albicans* dispersed cells are developmentally distinct from biofilm and planktonic Cells. *MBio* *9*, e01338-18.

Vale-Silva, L.A., and Sanglard, D. (2015). Tipping the balance both ways: drug resistance and virulence in *Candida glabrata*. *FEMS Yeast Res.* *15*, fov025.

BIBLIOGRAPHY

Vale-Silva, L., Ischer, F., Leibundgut-Landmann, S., and Sanglard, D. (2013). Gain-of-function mutations in *PDR1*, a regulator of antifungal drug resistance in *Candida glabrata*, control adherence to host cells. *Infect. Immun.* *81*, 1709–1720.

Vale-Silva, L., Beaudoin, E., Tran, V.D.T., and Sanglard, D. (2017). Comparative genomics of two sequential *Candida glabrata* Clinical Isolates. *G3 (Bethesda)* *7*, 2413–2426.

Vargas, K., Messer, S.A., Pfaller, M., Lockhart, S.R., Stapleton, J.T., Hellstein, J., and Soll, D.R. (2000). Elevated phenotypic switching and drug resistance of *Candida albicans* from human immunodeficiency virus-positive individuals prior to first thrush episode. *J. Clin. Microbiol.* *38*, 3595–3607.

Verstrepen, K.J., and Klis, F.M. (2006). Flocculation, adhesion and biofilm formation in yeasts. *Mol. Microbiol.* *60*, 5–15.

Weig, M., Jansch, L., Groß, U., De Koster, C.G., Klis, F.M., and De Groot, P.W.J. (2004). Systematic identification in silico of covalently bound cell wall proteins and analysis of protein–polysaccharide linkages of the human pathogen *Candida glabrata*. *Microbiology* *150*, 3129–3144.

Whaley, S.G., Berkow, E.L., Rybak, J.M., Nishimoto, A.T., Barker, K.S., and Rogers, P.D. (2016). Azole antifungal resistance in *Candida albicans* and emerging non-*albicans* *Candida* species. *Front Microbiol* *7*, 2173.

Wheeler, R.T., Kombe, D., Agarwala, S.D., and Fink, G.R. (2008). Dynamic, morphotype-specific *Candida albicans* beta-glucan exposure during infection and drug treatment. *PLoS Pathog.* *4*, e1000227.

Whiteway, M., and Bachewich, C. (2007). Morphogenesis in *Candida albicans*. *Annu. Rev. Microbiol.* *61*, 529–553.

Yapar, N. (2014). Epidemiology and risk factors for invasive candidiasis. *Ther Clin Risk Manag* *10*, 95–105.

Yarrow, D., and Meyer, S.A. (1978). Proposal for Amendment of the Diagnosis of the Genus *Candida* Berkhout nom. cons. *International Journal of Systematic Bacteriology* *28*, 611–615.

Zarnowski, R., Westler, W.M., Lacmbouh, G.A., Marita, J.M., Bothe, J.R., Bernhardt, J., Lounes-Hadj Sahraoui, A., Fontaine, J., Sanchez, H., Hatfield, R.D., *et al.* (2014). Novel entries in a fungal biofilm matrix encyclopedia. *MBio* *5*, e01333-01314.

Zervou, F.N., Zacharioudakis, I.M., Kurpewski, J., and Mylonakis, E. (2017). T2 Magnetic resonance for fungal diagnosis. *Methods Mol. Biol.* *1508*, 305–319.

BIBLIOGRAPHY

Zheng, X.-D., Lee, R.T.H., Wang, Y.-M., Lin, Q.-S., and Wang, Y. (2007). Phosphorylation of Rga2, a Cdc42 GAP, by CDK/Hgc1 is crucial for *Candida albicans* hyphal growth. *EMBO J.* 26, 3760–3769.

Zilberberg, M.D., Shorr, A.F., and Kollef, M.H. (2008). Secular trends in candidemia-related hospitalization in the United States, 2000-2005. *Infect Control Hosp Epidemiol* 29, 978–980.

Zupancic, M.L., Frieman, M., Smith, D., Alvarez, R.A., Cummings, R.D., and Cormack, B.P. (2008). Glycan microarray analysis of *Candida glabrata* adhesin ligand specificity. *Mol. Microbiol.* 68, 547–559.

7. Appendix

Sets of strains used in this study

Five *C. parapsilosis* isolates from the same patients used in this study case report

clinical isolate	source of isolation	clinical isolate	source of isolation
bsc-1700	blood culture-smooth	tsc-1702	throat swab-smooth
nsc-1701	nose swab-smooth	tcc-1702	throat swab-crepe
ncc-1701	nose swab-crepe		

***Isolates used in this study were provided by University Medical Centre (UMG), Göttingen, Germany**

One hundred seventeen *C. parapsilosis* clinical isolates used in biofilm formation capacity to polystyrol, agar invasion and antifungal susceptibility analyses

clinical isolate	source of isolation		clinical isolate	source of isolation	
PEU307	nose swab	9	PEU876	oral	6
PEU308	skin	4	PEU881	nose swab	9
PEU317	respiratory	5	PEU882	invasive	1
PEU320	nose swab	9	PEU883	invasive	1
PEU336	nose swab	9	PEU884	respiratory	5
PEU356	nose swab	9	PEU885	device	3
PEU357	skin	4	PEU886	invasive	1
PEU358	urine	8	PEU887	urine	8
PEU385	nose swab	9	PEU890	invasive	1
PEU391	invasive	1	PEU891	respiratory	5
PEU506	device	3	PEU893	GI	2
PEU525	respiratory	5	PEU894	invasive	1
PEU555	invasive	1	PEU898	GI	2

APPENDIX

Continued from previous page

PEU583	nose swab	9	PEU811	nose swab	9
PEU584	invasive	1	PEU899	nose swab	9
PEU589	nose swab	9	PEU913	nose swab	9
PEU596	respiratory	5	PEU915	urine catheter	7
PEU617	urine catheter	7	PEU916	invasive	1
PEU623	respiratory	5	PEU918	urine catheter	7
PEU628	device	3	PEU924	device	3
PEU630	invasive	1	PEU935	urine catheter	7
PEU647	nose swab	9	PEU937	nose swab	9
PEU648	nose swab	9	PEU940	nose swab	9
PEU649	nose swab	9	PEU941	invasive	1
PEU650	urine catheter	7	PEU944	urine catheter	7
PEU660	device	3	PEU950	nose swab	9
PEU663	device	3	PEU960	respiratory	5
PEU674	nose swab	9	PEU961	urine catheter	7
PEU681	nose swab	9	PEU-963	device	3
PEU682	nose swab	9	PEU965	urine	8
PEU688	nose swab	9	PEU968	nose swab	9
PEU689	nose swab	9	PEU969	nose swab	9
PEU707	respiratory	5	PEU971	urine catheter	7
PEU709	nose swab	9	PEU972	nose swab	9
PEU720	nose swab	9	PEU974	device	3
PEU724	device	3	PEU975	device	3
PEU732	urine catheter	7	PEU976	invasive	1
PEU738	device	3	PEU981	nose swab	9
PEU750	respiratory	5	PEU984	skin	4
PEU751	device	3	PEU990	respiratory	5
PEU752	urine catheter	7	PEU991	respiratory	5

APPENDIX

Continued from previous page

PEU760	nose swab	9	PEU997	skin	4
PEU761	invasive	1	PEU1001	urine catheter	7
PEU762	invasive	1	PEU1010	urine catheter	7
PEU763	respiratory	5	PEU1013	nose swab	9
PEU768	nose swab	9	PEU1019	device	3
PEU769	skin	4	PEU1020	device	3
PEU772	device	3	PEU1021	device	3
PEU776	nose swab	9	PEU1023	device	3
PEU781	nose swab	9	PEU1024	nose swab	9
PEU783	nose swab	9	PEU1026	urine	8
PEU784	nose swab	9	PEU1028	nose swab	9
PEU808	nose swab	9	PEU1031	nose swab	9
PEU815	device	3	PEU1032	urine catheter	7
PEU850	urine	8	PEU1072	nose swab	9
PEU856	respiratory	5	PEU1077	nose swab	9
PEU-859	nose swab	9	PEU1079	respiratory	5
PEU860	nose swab	9	PEU1085	nose swab	9
			PEU1088	invasive	1

***Isolates used in this study were provided by University Medical Centre (UMG), Göttingen, Germany**

Seven *C. parapsilosis* isolates used in biofilm formation capacity assay to polystyrol, *In vivo* virulence test and biofilm formation analyses in presence of antifungal drugs

clinical isolate	source of isolation		clinical isolate	source of isolation	
PEU486	skin	4	PEU582	urine	8
PEU495	skin	4	PEU586	nose swab	9
PEU496	nose swab	9	PEU651	device	3
PEU501	nose swab	9			

***Isolates used in this study were provided by University Medical Centre (UMG), Göttingen, Germany**

APPENDIX

Thirty-two *C. glabrata* clinical isolates genetically sequenced + 2 positive controls

clinical isolate *	ID synonymous	cluster	source of isolation	country
M17	US02Bal017	3	blood	USA
F1019	EF1019Blo1	3	blood	France
F1822	EF1822Blo1	3	blood	France
M12	US01BG2Blo	3	blood	USA
CST78	US003NY078	3	blood	USA
F2229	EF2229Blo1	3	blood	France
I1718	EF1718Blo1	3	blood	Italy
EB0911Sto	EB0911Sto	2	stool (GI)	Belgium
CST35	US003NY035	2	blood	USA
CST34	US000NY034	1	blood	USA
CST109	US003NY109	1	blood	USA
CST80	US003NY080	1	blood	USA
M7	US02Bal007	1	blood	USA
EB101M	EB0101MouC	1	oral cavity	Belgium
BO101S	EB0101StoC	1	stool (GI)	Belgium
B1012S	EB01012StoC	1	stool (GI)	Belgium
B1012M	EB01012MouC	1	oral cavity	Belgium
EF1237Blo1	EF1237Blo1	4	blood	France
EI1815Blo1	EI1815Blo1	4	blood	Italy
EF1620Sto	EF1620Sto	4	stool (GI)	France
EF0616Blo1	EF0616Blo1	4	blood	France
F15	F15035, EF1535Blo1	5	blood	France
F11	F11017, EF1117Blo1	5	blood	France
E1114	EB1114Mou (O)	7	oral cavity	Belgium
M6	US02Bal006	7	blood	USA
CST110	US003NY110	7	blood	USA
EG01004Sto	EG01004Sto	7	stool (GI)	Germany
F15021	EF1521Blo1	7	blood	France
F03013	EF0313Blo1	7	blood	France
BG2	US01BG2Blo	7	blood	USA
P35_2	P35_2	6	oral cavity	Taiwan
P35_3	P35_3	6	oral cavity	Taiwan
PEU382	positive control	-	urine	Germany
PEU427	positive control	-	respiratory	Germany

***Isolates used in this study were provided by Toni Gabaldón Estevan, Centre for Genomic Regulation (CRG) Barcelona, Spain. Genome data published by (Carreté *et al.*, 2018).**

APPENDIX

Three *C. glabrata* isolates used for biofilm formation capacity to polystyrol and azoles susceptibility

clinical isolate	source of isolation
SAT01BAL-EF54001Bal	bronchiolo-alveolar lavage
SAT02PL-EF54001Per	peritoneal fluid
SAT03BC-EF54001Blo	blood culture

*Isolates used in this study were genetically sequenced provided by Toni Gabaldón Estevan, Centre for Genomic Regulation (CRG) Barcelona, Spain. Genome data published by (Carreté *et al.*, 2019).

Thirty-two *C. glabrata* isolates phenotypically classified used for genome sequencing

clinical isolate	source of isolation		clinical isolate	source of isolation	
<i>PEU30</i>	invasive	1	PEU542	oral	6
<i>PEU45</i>	device	3	PEU563	GI	2
<i>PEU52</i>	oral	6	PEU597	oral	6
<i>PEU123</i>	urine catheter	7	PEU598	skin	4
<i>PEU135</i>	respiratory	5	PEU607	skin	4
<i>PEU235</i>	urine catheter	7	PEU608	oral	6
<i>PEU259</i>	respiratory	5	PEU611	urine catheter	7
PEU329	respiratory	5	PEU619	GI	2
<i>PEU382</i>	urine	8	PEU622	invasive	1
<i>PEU427</i>	respiratory	5	PEU644	respiratory	5
PEU471	skin	4	PEU652	device	3
PEU474	skin	4	PEU656	urine	8
PEU483	urine catheter	7	PEU670	respiratory	7
PEU522	device	3	PEU671		
PEU531	urine catheter	7	PEU675	skin	4
PEU537	device	3	PEU693	urine	8

*Isolate CBS-138 was used as reference strain.

APPENDIX

List of daily screening *C. glabrata* clinical isolates used in biofilm formation analyses to polystyrol and silicone

isolate	source of isolation		isolate	source of isolation	
PEU69	respiratory	5	PEU532	GI	2
PEU96	urine	8	PEU537	device	3
PEU113	urine catheter	7	PEU542	urine catheter	7
PEU117	urine	8	PEU546	skin	4
PEU119	skin	4	PEU552	GI	2
PEU122	skin	4	PEU553	urine catheter	7
PEU123	urine catheter	7	PEU554	oral	6
PEU124	Invasive	1	PEU558	urine catheter	7
PEU134	respiratory	5	PEU563	GI	2
PEU135	respiratory	5	PEU587	GI	2
PEU159	oral	6	PEU597	oral	6
PEU162	urine	8	PEU598	skin	4
PEU193	respiratory	5	PEU601	GI	2
PEU209	invasive	1	PEU612	urine catheter	7
PEU210	skin	4	PEU622	invasive	1
PEU214	oral	6	PEU635	oral	6
PEU297	urine	8	PEU636	GI	2
PEU299	GI	2	PEU653	oral	6
PEU302	urine	8	PEU656	urine	8
PEU311	invasive	1	PEU668	skin	4
PEU314	invasive	1	PEU671	urine catheter	7
PEU324	respiratory	5	PEU675	skin	4
PEU326	urine	8	PEU676	skin	4
PEU328	respiratory	5	PEU686	GI	2
PEU329	respiratory	5	PEU692	urine	8
PEU330	GI	2	PEU698	device	3
PEU342	device	3	PEU706	oral	6
PEU349	urine catheter	7	PEU731	blood culture	9
PEU352	skin	4	PEU746	device	3
PEU353	respiratory	5	PEU749	device	3
PEU368	skin	4	PEU764	device	3
PEU373	urine	8	PEU777	device	3
PEU379	GI	2	PEU782	urine catheter	7
PEU386	urine	8	PEU793	urine	8

APPENDIX

Continued from previous page

PEU398	oral	6	PEU795	respiratory	5
PEU400	urine	8	PEU802	device	3
PEU401	urine	8	PEU814	urine catheter	7
PEU471	skin	4	PEU953	skin	4
PEU474	skin	4	PEU954	device	3
PEU478	device	3	PEU956	invasive	1
PEU483	urine catheter	7	PEU957	oral	6
PEU508	device	3	PEU1011	skin	4
PEU509	device	3	PEU1044	blood culture	9
PEU511	skin	4	PEU1048	blood culture	9
PEU513	GI	2	PEU1049	blood culture	9
PEU522	device	3	PEU1050	blood culture	9
PEU531	urine catheter	7	PEU1055	blood culture	9
			PEU1056	blood culture	9

*Isolates used in this study were provided by University Medical Centre (UMG), Göttingen, Germany.

Seventy-seven *C. glabrata* clinical isolates used in *Galleria mellonella* infection animal model

isolates	BF	isolates	BF	isolates	BF	isolates	BF	isolates	BF
PEU531	LBF	PEU328	LBF	PEU520	LBF	PEU386	HBF	PEU326	HBF
PEU523	LBF	PEU331	LBF	PEU521	LBF	PEU1360	HBF	PEU329	HBF
PEU294	LBF	PEU317	LBF	PEU529	LBF	PEU1270	HBF	PEU342	HBF
PEU364	LBF	PEU337	LBF	PEU533	LBF	PEU542	HBF	PEU352	HBF
PEU494	LBF	PEU389	LBF	PEU534	LBF	PEU400	HBF	PEU353	HBF
PEU322	LBF	PEU397	LBF	PEU535	LBF	PEU427	HBF	PEU373	HBF
PEU527	LBF	PEU404	LBF	PEU536	LBF	PEU1330	HBF	PEU382	HBF
PEU541	LBF	PEU458	LBF	PEU538	LBF	PEU123	HBF	PEU401	HBF
PEU29	LBF	PEU464	LBF	PEU543	LBF	PEU183	HBF	PEU403	HBF
PEU1274	LBF	PEU469	LBF	PEU544	LBF	PEU293	HBF	PEU513	HBF
PEU519	LBF	PEU478	LBF	PEU545	LBF	PEU297	HBF	PEU522	HBF
PEU52	LBF	PEU498	LBF	PEU546	LBF	PEU299	HBF	PEU532	HBF
PEU16	LBF	PEU502	LBF	PEU547	LBF	PEU302	HBF	PEU537	HBF
PEU30	LBF	PEU510	LBF	PEU548	LBF	PEU311	HBF	PEU540	HBF
PEU295	LBF	PEU514	LBF	PEU1273	LBF	PEU324	HBF	PEU1359	HBF
PEU314	LBF	PEU1332	LBF						

*Red boldfaced, isolates with killing rate lower than 100%.

